

UNSATURATED FLOW IN HYDRATING POROUS MEDIA: APPLICATION TO CEMENTED PASTE BACKFILL

by

Mandy L. Witteman

A thesis submitted to the Faculty of Graduate and Postdoctoral Affairs
in partial fulfillment of the requirements for the degree of

Master of Applied Science

in

Environmental Engineering*

Department of Civil and Environmental Engineering

Carleton University

Ottawa, Ontario

*The Master of Applied Science is a joint program with the University of Ottawa,
administered by the Ottawa-Carleton Institute for Environmental Engineering

© 2013, Mandy L. Witteman

ABSTRACT

Sustainability of hardrock mining is contingent upon delivering a high quality cemented paste backfill (CPB) that is self-sustaining during ore recovery. The integrity of CPB systems hinges on how quickly in excess pore-water pressures (PWP) dissipates. Consolidation and self-desiccation are critical factors that determine how rapid PWPs expel in hydrating CPB.

Current models characterize stress distributions in CPB based on fully saturated / undrained conditions. Recent studies suggest that such conditions are not entirely valid. This research therefore, describes PWP behaviour in CPB by using an unsaturated flow theory framework that takes into account self-desiccation.

The analyses involved capturing the experimental lower and upper bound water-retention properties of CPB. These properties are then used to solve a modified 1-D unsaturated flow equation of hydrating CPB material. Numerical predictions of PWPs in a column test were well simulated when comparing these results with the experimental measurements.

DEDICATION

*'By letting your light shine, you have graciously allowed others around you
to shine'*

– In loving memory of my grandpa, Marcel

ACKNOWLEDGEMENTS

The completion of this work would not have been possible without the advice, time and guidance of my advisor, Dr. Paul H. Simms for your unending support and opportunities that you have provided me throughout this research. Without it, my efforts would not have been realized – Thank you. To Dr. Murray F. Grabinsky, Dr. Ben Thompson, and Dr. Dragana Simon at the University of Toronto – thank you all for your time, assistance and support.

I would also like to extend my gratitude to the Cemented Paste Backfill research group at the University of Toronto, and the University of Waterloo for their collaborative efforts. Additionally, to our industry partners: Barrick Gold Corporation, Xstrata Copper Canada, and Inmet Mining Corporation, as well as the Natural Science and Engineering Research Council (NSERC) of Canada – I gratefully acknowledge their financial support for this research.

A special thanks to Carleton University's Civil and Environmental Departmental technicians and laboratory personnel, Stanley Conley, Pierre Trudel and Marie-Josée Tudoret Chow for their creative and pragmatic approach during the course of my research. I would also like to extend my appreciation to my colleagues, and faculty members for their advice, support, humor, kindness and friendship.

Lastly, to lovely friends and family for your unconditional love, patience and encouragement – Thank you.

TABLE OF CONTENTS

Abstract.....	i
Dedication.....	ii
Acknowledgements.....	iii
List of Tables	viii
List of Figures	xi
Acronyms	xvii
Nomenclature	xix
CHAPTER 1: INTRODUCTION, BACKGROUND AND OBJECTIVES	1
1.1 USE OF CEMENTED PASTE BACKFILL IN MINING	1
1.2 AN OVERVIEW OF THE CEMENTED PASTE BACKFILL PROJECT	7
1.3 SCOPE OF RESEARCH AND OBJECTIVES.....	11
1.4 ORGANIZATION OF THESIS	13
CHAPTER 2: LITERATURE REVIEW	16
2.1 UNDERGROUND MINING.....	16
2.1.1 Terminology and Methods.....	17
2.1.2 Mine Backfill.....	20
2.2 CEMENTED PASTE BACKFILL.....	22
2.2.1 Strength Properties.....	22
2.2.2 Water-Retention Properties	24
2.2.3 Effects of Curing Temperature.....	25
2.2.4 Self-Desiccation.....	27
2.2.5 In-Situ Pore-Pressures.....	30
2.2.5.1 <i>Williams Gold Mine</i>	31
2.2.5.2 <i>Kidd Copper Mine</i>	36
2.2.5.3 <i>Çayeli Copper-Zinc Mine</i>	40
2.3 SOIL SUCTION: THEORETICAL AND EXPERIMENTAL	43
2.3.1 Total Suction	43
2.3.1.1 <i>Osmotic Suction</i>	46
2.3.1.2 <i>Matric Suction</i>	47
2.3.2 Direct Measurement of Matric Suction	50
2.3.2.1 <i>Air-Entry Porous Ceramics</i>	50
2.3.2.2 <i>Phenomenon of Cavitation Nuclei</i>	52
2.3.2.3 <i>Pressure Transducer / Tensiometers</i>	55
2.3.2.4 <i>Axis Translation Technique</i>	61
2.3.3 Indirect Measurement of Osmotic Suction.....	68
2.3.4 Indirect Measurement of Total Suction.....	68

2.3.4.1	<i>Chilled-Mirror Dew Point Technique</i>	69
2.3.4.2	<i>Filter Paper Method</i>	71
2.4	FLOW IN UNSATURATED SOILS	72
2.4.1	Water Content-Suction Relationship	76
2.4.1.1	<i>Experimental Measurement of the $\Theta(\psi)$ Relationship</i>	78
2.4.1.2	<i>Equations for the Water-Retention Curve</i>	80
2.4.2	Unsaturated Hydraulic Conductivity.....	85
2.4.2.1	<i>Equations for the Hydraulic Conductivity Function</i>	85
2.5	MODELS FROM SOIL MECHANICS.....	90
2.5.1	Small-Strain Consolidation Model	91
2.5.1.1	<i>Davis and Raymond Model</i>	92
2.5.2	Large-Strain Consolidation Model	93
2.5.2.1	<i>Large-Strain, Fully Coupled with Self-Desiccation</i>	95
2.5.3	Consolidation Models and Unsaturated Flow Model	97
	CHAPTER 3: AN UNSATURATED FLOW THEORY FRAMEWORK.....	99
3.1	A MODIFIED 1-D UNSATURATED FLOW EQUATION	99
3.2	APPLICATION TO CEMENTED PASTE FILL.....	100
	CHAPTER 4: MATERIALS AND EXPERIMENTAL PROCEDURES.....	103
4.1	PHYSICAL CHARACTERIZATION OF PASTE TAILINGS	105
4.1.1	Particle-Size / Grain-Size Distribution	105
4.1.2	Atterberg Limit.....	105
4.1.3	Specific Gravity	106
4.2	PREPARATIONS: SAMPLE SPECIMENS.....	106
4.2.1	'Pumping' Water Contents	106
4.2.2	Cemented Paste Fill Recipes	107
4.3	PHASE I: CALIBRATIONS AND TREATMENT PROTOCOLS	108
4.3.1	Non-Contact Vertical Displacement / Proximity Sensor	108
4.3.2	Electrical Capacitance Sensors.....	110
4.3.2.1	<i>Williams Paste Tailings</i>	112
4.3.2.2	<i>Williams 3% and 7% Binder Material</i>	112
4.3.3	Pre-Treatment of Ceramic Discs	114
4.3.3.1	<i>Saturation Process</i>	115
4.3.3.2	<i>Saturated Hydraulic Conductivity</i>	117
4.3.4	Saturation Method: Pressure Transducers	121
4.4	PHASE II: PRE- AND POST- HYDRATION EXPERIMENTS.....	123
4.4.1	Determination of the Water-Retention Curves	123
4.4.1.1	<i>Measurement of Matric Suctions</i>	124
4.4.1.2	<i>Measurement of Total Suctions</i>	127
4.4.2	Pre-Hydrated Water-Retention Curves	128

4.4.3	Post-Hydrated Testing	129
4.4.4	Analysis and Calculations.....	132
4.5	PHASE III: HYDRATION-TIME DEPENDENT EXPERIMENTS	134
4.5.1	Self-Desiccation Tests	135
4.5.1.1	<i>Williams Paste Fill Material</i>	135
4.5.1.2	<i>Kidd's Binder Paste Material</i>	137
4.5.2	Mercury Intrusion Porosimetry	138
4.5.2.1	<i>Theory of Mercury Intrusion Porosimetry</i>	138
4.5.2.2	<i>Sample Preparations</i>	140
4.6	PHASE IV: PASTE FILLED COLUMN EXPERIMENT	141
4.6.1	Column Set-up	141
4.6.2	Backfilling.....	142
CHAPTER 5: EXPERIMENTAL RESULTS AND DISCUSSION		145
5.1	PHYSICAL PROPERTIES OF PASTE TAILINGS.....	146
5.2	PHASE I: CALIBRATION CURVES AND TREATMENT RESULTS	148
5.2.1	Vertical Displacement Sensor	148
5.2.2	ECH2O Soil-Moisture Sensors	149
5.2.2.1	<i>Williams Paste Tailings</i>	150
5.2.2.2	<i>Cemented Paste: 3% and 7% Binder Material</i>	152
5.2.3	Saturation Method: High Air-Entry Value Porous Discs.....	159
5.3	PHASE II: PRE- AND POST-HYDRATION RESULTS.....	160
5.3.1	Direct and Indirect Suction Measurements.....	160
5.3.1.1	<i>Williams Paste: Pre- and Post-Hydration</i>	161
5.3.1.2	<i>Kidd Paste: Pre- and Post-Hydration</i>	167
5.3.2	Summary: Pre- and Post-Hydration Properties	174
5.4	PHASE III: BINDER HYDRATION.....	177
5.4.1	Generation of Matric Suctions.....	177
5.4.2	Rate of Water Removal.....	182
5.4.3	Micro-Structural Changes During Paste Hydration.....	188
5.4.4	Effects of Temperature on Self-Desiccation	197
5.5	PHASE IV: PASTE FILLED COLUMN TEST	201
5.5.1	Drainage.....	201
5.5.2	Matric Suction and Water Content Profiles.....	205
CHAPTER 6: UNSATURATED FLOW MODELLING		210
6.1	FORMULATION AND GENERAL ASSUMPTIONS	210
6.2	METHODOLOGY.....	212
6.2.1	Model 'Inputs': Sink and Water-Retention Properties	212
6.2.1.1	<i>3% Binder Sink</i>	212
6.2.1.2	<i>Pre- and Post- Material Properties</i>	214

6.2.2	Generic Model of a Paste ‘Plug’	217
6.2.2.1	<i>Model Parameters, Initial and Boundary Conditions</i>	217
6.2.2.2	<i>Effects of Pre- and Post- Properties, and Sink Term</i>	218
6.2.3	Column Test Simulation	221
6.2.3.1	<i>Model Description</i>	221
6.2.3.2	<i>Assumptions and Initial Conditions</i>	222
6.2.3.3	<i>Boundary Conditions</i>	224
6.3	MODELLING RESULTS AND DISCUSSION	229
6.3.1	Solver Results and Model Verification	229
6.3.2	Distributions of Pore-Water Pressures in a CPB Column	232
6.4	LIMITATIONS	235
CHAPTER 7: SUMMARY AND CONCLUSIONS	237
7.1	RESTATEMENT OF THE PROBLEM	237
7.2	EVOLUTION OF CEMENTED PASTE FILL PROPERTIES.....	239
7.2.1	Pre- and Post-Hydrated Water-Retention Properties	239
7.2.2	Self-Desiccation and Pore-Structure.....	240
7.3	AN UNSATURATED FLOW IN A PASTE FILLED COLUMN	242
CHAPTER 8: RECOMMENDATIONS FOR FUTURE WORK	245
REFERENCES	248
APPENDIX A – WILLIAMS AND KIDD TAILINGS [RAW DATA]	263
A.1	SAMPLE PREPARATIONS AND INITIAL WATER CONTENTS.....	263
A.2	PHYSICAL PROPERTIES OF TAILINGS	266
A.3	CALIBRATION DATA	273
A.4	WATER-RETENTION CURVES	279
A.5	MERCURY INTRUSION POROSIMETRY.....	285
A.6	CHEMICAL ANALYSES	286
APPENDIX B – ÇAYELI TAILINGS [EXPERIMENTAL RESULTS]	287
B.1	PHYSICAL PROPERTIES OF ÇAYELI TAILINGS	287
B.2	SELF-DESICCATION – HEAT TESTS	288
B.3	PRE- AND POST- WATER-RETENTION CURVE	291
APPENDIX C – NUMERICAL MODELLING [DATA]	292
C.1	MODELLING ‘INPUTS’	292
APPENDIX D – SUPPORTING FILES [COMPACT DISC]	336
D.1	DESCRIPTION AND CONTENTS OF CD.....	336
D.2	ACCOMPANIED CD.....	337
GLOSSARY	338
PUBLICATION	344

LIST OF TABLES

Table 2.2.1	Summary of fill deposition in stages ('lifts'), rates-of-rise, volume and duration of each pour (Thompson et al. 2008).....	32
Table 2.3.1	Properties of commercially available high air entry porous ceramics.....	52
Table 2.4.1	Summary of suction measurement methods (adapted from Pan et al., 2010).....	79
Table 2.4.2	Water-retention curve models (Sillers and Fredlund, 2001).....	84
Table 2.4.3	Empirical equations for the unsaturated coefficient of permeability $k(\psi)$ (Fredlund et al., 1994).....	86
Table 2.4.4	Some statistical hydraulic conductivity functions based on the water-retention curves and saturated hydraulic conductivity (Ebrahimi et al., 2004; as cited by Fredlund, 2006).....	89
Table 2.5.1	Key differences between the small- and large- strain consolidation models and the unsaturated flow model	97
Table 4.2.1	Pumping water contents for Williams, Kidd Creek and Çayeli mine tailings (Simon, 2010).....	107
Table 4.2.2	CPB recipes used at Williams, Kidd Creek and Çayeli Mine (Simon, 2010).	108
Table 4.3.1	Specifications for Decagon's EC volumetric sensors (Campbell, 2002; Cobos, 2007; 2009).....	111
Table 4.3.2	Technical specifications of the 5 bar and 15 bar ceramic porous discs (SoilMoisture Equipment Corp., 2008)	115
Table 4.4.1	Sizes and initial water contents of the test specimens used in the pre-curing phase axis translation experiments	128
Table 4.4.2	Williams paste prepared with 3% binder, cured in the volumetric pressure plate extractor for 28 days prior to the axis translation test.....	129
Table 4.4.3	Kidd paste prepared with 2.2% binder, cured in the volumetric pressure plate extractor for 28 days prior to the axis translation test.....	130
Table 4.4.4	Sizes and initial water contents of the test specimens used in the post-curing phase	130

Table 4.5.1	(Trial #1) Williams CPB recipes for 3, 5 and 7% binder containing specimens.....	136
Table 4.5.2	(Trial #2) Williams CPB recipes for 3, 5 and 7% binder containing specimens.....	137
Table 4.5.3	Kidd’s CPB recipes for 2.2 and 4.5% binder containing specimens	138
Table 4.6.1	Summary of each ‘lift’ placement in the test column.....	143
Table 4.6.2	Amount of paste deposited and final conditions after settlement and drainage.....	143
Table 5.1.1	Atterberg Limits and bulk densities of the materials used in the experimental phase.....	147
Table 5.2.1	Williams Tailings: Measured volumes, water contents and averaged raw data (voltage output from Decagon’s data logger)	150
Table 5.2.2	Calibration data for Williams’ 3% and 7% binder material (Test #1): water contents, and raw data from the 10HS and EC-5 sensors.....	155
Table 5.2.3	Calibration data for Williams’ 3% and 7% binder material (Test #2): water contents, and raw data from the EC-5 and 10HS sensors.....	156
Table 5.2.4	Measured versus actual saturated hydraulic conductivity of the 5 bar and 15 bar ceramic porous discs.....	160
Table 5.3.1	Pre-water retention data for Williams paste tailings containing no binder	161
Table 5.3.2	Williams’ post-hydrated water-retention curve data (Trial #2) for specimen containing 3% binder.....	163
Table 5.3.3	Water-retention data for Kidd paste tailings containing no binder.....	170
Table 5.3.4	Water-retention data for post-hydrated Kidd paste containing 2.2% binder	171
Table 5.3.5	Summary of the pre- and post- hydration properties of Williams and Kidd paste	174
Table 5.4.1	Material compressibility as a function of hydration time.....	185
Table 5.4.2	Results of the MIP tests (threshold diameter, critical pore diameter, specific surface, total porosity, and void ratio as functions of curing time	196

Table 5.5.1	Summary of the initial conditions of each lift (prior to drainage and consolidation).....	202
Table 5.5.2	Summary of the final conditions of each lift after drainage and consolidation.....	202
Table 5.5.3	Volumetric flowrate (Q), and drainage rate (v_s), and hydraulic conductivity (k_{sat}) of each lift.....	203
Table 5.5.4	Estimated volumetric water contents of each lift compared to the measured values obtained from the calibrated EC sensors	206
Table 6.2.1	Pre- and post-hydrated input parameters	214
Table 6.2.2	Fredlund and Xing (1994) estimated material properties for Williams' paste tailings containing no binder and 3% binder	215
Table 6.2.3	Modelling scenarios: alternating between the pre- and post- properties (i.e. WRC, compressibility and permeability), and effect of self-desiccation (i.e. sink term).....	218
Table 6.2.4	Description of model(s) and settings to simulate a 1-D distribution pore-water pressures in a 1.01m length column.....	222
Table 6.2.5	Initial conditions for each model layer	224
Table 6.2.6	Estimated outflow volumes compared to experimental volumes	226
Table 6.3.1	Numerical results: water balance checks	232
Table 6.3.2	Model verification: numerical versus experimental water balances.....	232

LIST OF FIGURES

Figure 2.1.1	Underground mine development: a) generic schematic, and b) mine development plan at the Çayeli copper/zinc mine in Turkey	18
Figure 2.1.2	Schematic of a generic backfilled stope.....	20
Figure 2.2.1	Coupled effects of temperature and initial sulphate content on the 28 day of UCS of CPB containing Type I Portland cement (Fall and Pokharel, 2010)	26
Figure 2.2.2	Generation of matric suction during self-desiccation (Simms and Grabinsky, 2009).....	29
Figure 2.2.3	Alimak test stope at Williams – backfilled in 5 lifts with CPB containing 3% binder (Thompson et al., 2008)	33
Figure 2.2.4	Total pressure data from Cages 1 and 2 in the Alimak Nest (Thompson et al., 2008)	34
Figure 2.2.5	a) Total pressure and pore-water pressure data in Cages 1 and 2; and b) Effective stress results calculated from data presented during the plug pour and subsequent plug cure (Thompson et al., 2008)	35
Figure 2.2.6	Cross section view of test stope 67SL1, with locations of instrument Cages 1 through 6 (Thompson et al., 2009).....	37
Figure 2.2.7	Total and pore pressure response measured for a 4 day period following the covering of instruments in Cages 1 and 2, with temperature indicated on the secondary axis (Thompson et al., 2009)	39
Figure 2.2.8	Suction data (a) shows data from Cages 1, 2, 4 and 6 with a 10 point moving average (Thompson et al., 2009)	40
Figure 2.2.9	Temperature profiles in stopes 685(N20) and 715(N22). Observed hydration to be dependent upon tailings chemistry (Thompson et al., 2010)	42
Figure 2.3.1	Thermodynamic relationship between soil suction and relative humidity (Fredlund and Rahardjo, 1993).....	46
Figure 2.3.2	Idealized capillary tube model of a glass tube inserted into water under atmospheric pressure (Fredlund and Rahardjo, 1993)	48
Figure 2.3.3	The crevice model of heterogeneous nucleation (Marinho et al., 2008) ..	54

Figure 2.3.4	A schematic of a pressure transducer tensiometer model, T5x from UMS GmbH, Germany (2009)	56
Figure 2.3.5	Idealized conical crevice (Marinho et al., 2008).....	59
Figure 2.3.6	Capillary pore model: working principle of axis translation technique (Marinho et al., 2008)	62
Figure 2.3.7	Axis translation technique to avoid metastable states via to stable states (Marinho et al., 2008)	64
Figure 2.3.8	Schematic of the axis translation test cell	65
Figure 2.4.1	Typical desorption and adsorption curves for a fine-grain soil at its saturated water content, θ_s (Fredlund and Xing, 1994).....	78
Figure 4.3.1	Set-up of the non-contact vertical displacement sensor.....	109
Figure 4.3.2	Decagon's soil-moisture sensors: (a) ECH ₂ O EC-5 sensor, and (b) 10HS sensor	111
Figure 4.3.3	Saturation chamber for saturating porous discs and tensiometers	116
Figure 4.3.4	Reference measurements to calculate the volume of the test cell.....	119
Figure 4.3.5	Equipment set-up: volumetric pressure plate extractor system and gas line	120
Figure 4.3.6	(a) A schematic of the T5x / T5 Tensiometer; and (b) water reservoir, where the T5 body and tips are filled with de-aired water (UMS GmbH, 2009)	123
Figure 4.4.1	SWC-150 Fredlund SWCC Device (GCTS Testing Devices, 2009).....	125
Figure 4.4.2	Axis translation equipment test set-up	125
Figure 4.6.1	Design specifications of the column test	142
Figure 5.1.1	Grain-size distributions for tailings and aggregates in Williams and Kidd CPB mixtures	147
Figure 5.2.1	Calibration curve: non-contact displacement / proximity sensor	149
Figure 5.2.2	Calibration of the EC-5 sensor: (1) VWC estimate based upon measured values obtained experimentally, calibrated for Williams' tailings, and (2) Decagon's calibration for mineral soil.....	151

Figure 5.2.3	Calibration of the 10HS sensor: (1) VWC estimate based upon measured values obtained experimentally, ‘soil-specific’ calibration, and (2) Decagon’s calibration for mineral soil.....	151
Figure 5.2.4	Test #1: Volumetric water contents from grab samples prepared with 3% and 7% binder (Williams paste).....	153
Figure 5.2.5	Test #2: Volumetric water contents from grab samples prepared with 3% and 7% binder (Williams paste).....	153
Figure 5.2.6	10HS Sensor calibrated for 3% binder material (Test #1): Output data as a function of Time	154
Figure 5.2.7	EC-5 Sensor calibrated for 7% binder material (Test #1): Output data as a function of Time	155
Figure 5.2.8	10HS calibration curves that were calibrated for Williams’ paste containing 3% and 7% binder	158
Figure 5.2.9	EC-5 calibration curves that were calibrated for Williams’ paste containing 3% and 7% binder	158
Figure 5.3.1	Williams’ pre-hydrated water-retention curve data	162
Figure 5.3.2	Williams’ Trial #2, post-hydrated water-retention curve data in terms of water content and degree of saturation	162
Figure 5.3.3	Pre- shrinkage curve for Williams tailings containing no binder	165
Figure 5.3.4	Post- shrinkage curve for Williams containing 3% binder	165
Figure 5.3.5	Williams' specimen containing no binder: pre- volumetric strain curve in the positive pore-water pressure region	166
Figure 5.3.6	Williams 3% binder containing specimen: post- volumetric strain curve in the positive pore-water pressure region	167
Figure 5.3.7	Pre- water-retention curve data in terms of water content and degree of saturation (<i>S</i>) for Kidd material containing no binder	168
Figure 5.3.8	Post- water-retention curve data in terms of water content and degree of saturation (<i>S</i>) for Kidd material containing 2.2% binder	169
Figure 5.3.9	Pre- shrinkage curve for Kidd paste material with no binder	172
Figure 5.3.10	Post- shrinkage curve for Kidd paste with 2.2% binder	172

Figure 5.3.11	Kidd paste specimen containing no binder: pre- volumetric strain curve in the positive pore-water pressure region	173
Figure 5.3.12	Kidd paste containing 2.2% binder: post- volumetric strain curve in the positive pore-water pressure region	174
Figure 5.4.1	(Trial #1) Williams CPB specimens in sealed samples: induced matric suctions during 28 days of paste hydration.....	178
Figure 5.4.2	(Trial #2) Williams CPB specimens in sealed samples: induced matric suctions during 28 days of paste hydration.....	179
Figure 5.4.3	(Trial #1) Kidd CPB specimens in sealed samples: induced matric suctions during 20 days of paste hydration.....	180
Figure 5.4.4	(Trial #2) Kidd CPB specimens in sealed samples: induced matric suctions during 20 days of paste hydration.....	180
Figure 5.4.5	Kidd cemented paste specimens containing 2.2% binder (a), and 4.5% binder (b), post- self-desiccation tests (on the 22 nd day of hydration)....	181
Figure 5.4.6	Water contents of replicate samples for Williams with 3% binder, showing decrease in water content due to binder hydration.....	182
Figure 5.4.7	Rate of hydration for Williams' 3%: induced matric suctions and water consumption as a function of the hydration time.....	184
Figure 5.4.8	Estimated coefficient of compressibility(s) during paste hydration, compared with the pre- and post- values at respective air-entry values .	186
Figure 5.4.9	Rate of hydration for Kidd 2.2% binder paste	188
Figure 5.4.10	Differential pore-size distribution for 3% binder paste during binder hydration	190
Figure 5.4.11	3% binder: (a) total MIP porosity; and (b) incremental porosity as a function of pore radius	192
Figure 5.4.12	Threshold diameter and critical pore diameter for Williams 3% binder specimens cured for 2, 3, 7, 12, and 14 days	193
Figure 5.4.13	Differential pore-size distribution for 7% binder paste during binder hydration	194
Figure 5.4.14	Threshold diameter and critical pore diameter for Williams 7% binder specimens cured for 1, 5, 12, 14, and 16 days	194

Figure 5.4.15	Çayeli paste containing 4.5% binder: rate of self-desiccation as a function of temperature(s) at 24, 40 and 50 °C	199
Figure 5.4.16	Çayeli paste containing 8.5% binder: rate of self-desiccation as a function of temperature(s) at 24, 40 and 50 °C	200
Figure 5.5.1	Cumulative volume of leachates collected after placement of each paste layer.....	202
Figure 5.5.2	Permeabilities of 3% Williams CPB as a function of curing age, obtained from a compressive test with a normal stress of 250 kPa (Veenstra, 2010)	204
Figure 5.5.3	Initial and final height of each CPB layer after settlement and drainage	204
Figure 5.5.4	Measured matric suction values for a multi-layered deposition of Williams 3% CPB material in a 30 by 30 cm square column	205
Figure 5.5.5	Water content data from the 10HS soil-moisture sensors.....	208
Figure 5.5.6	Water content data from the EC-5 soil-moisture sensors	208
Figure 5.5.7	Column test filled in 4 ‘lifts’: 15 cm ‘Plug’ paste and 3 main pours, each with 30 cm thick layer.....	209
Figure 6.2.1	Rate of water removal from the experimental data (generic rate for a 1.0 m thick layer)	213
Figure 6.2.2	Water removal rate incorporated into SVFlux for the modelling regions – plug and main layers, expressed in cubic meters per day per unit area (m/day).....	213
Figure 6.2.3	Water-retention curve of Williams’ pre-hydrated tailings containing no binder	215
Figure 6.2.4	Water-retention curve of Williams’ post-hydrated cemented paste containing 3% binder	216
Figure 6.2.5	Unsaturated hydraulic conductivity function of Williams’ pre-hydrated paste tailings containing no binder	216
Figure 6.2.6	Unsaturated hydraulic conductivity function of Williams’ post-hydrated cemented paste containing 3% binder.....	217
Figure 6.2.7	Simulation of pore-water pressure drawdown after 24 hours varying the coefficient of volume compressibility	220

Figure 6.2.8	Simulation of pore-water pressure drawdown after 24 hours, showing relative contributions of drainage and self-desiccation	221
Figure 6.2.9	Cumulative water volumes collected after each paste pour	226
Figure 6.2.10	Simulation #1: bottom boundary condition assigned to the plug layer ..	227
Figure 6.2.11	Simulation #2: bottom boundary condition assigned to the Main_1 layer	227
Figure 6.2.12	Simulation #3: bottom boundary condition assigned to the Main_2 layer	228
Figure 6.2.13	Simulation #4: bottom boundary condition assigned to the Main_3 layer	228
Figure 6.3.1	Finite element solver results using the pre-WRC	230
Figure 6.3.2	Finite element solver results using the pre-HCF.....	230
Figure 6.3.3	Finite element solver results using the post-WRC.....	231
Figure 6.3.4	Finite element solver results using the post-HCF	231
Figure 6.3.5	Simulated distribution of pore-water pressures in a cemented paste filled column.....	234
Figure 6.3.6	Experimentally measured pore-water pressure distribution in a cemented paste filled column.....	234
Figure 6.4.1	Alternating between pre- and post-WRC properties when defining a ‘new initial condition’ based on the results of a previous ‘final condition’	236

ACRONYMS

AEP	Air-entry pressure
AEV	Air-entry value
AMD	Acid mine drainage
ARD	Acid rock drainage
BFS	Blast-furnace slag
CPB	Cemented paste backfill
CPD	Critical pore diameter
DAS	Data acquisition system
DTA	Differential thermal analysis
EC	Electrical capacitance
EM	Electromagnetic
FA	Fly ash or pulverized fly ash
GSD	Grain-size distribution
GWC	Gravimetric water content
HAEV	High air-entry value
HCF	Hydraulic conductivity function
IPM	Instantaneous profile method
IRH	Internal relative humidity

LL	Liquid limit
MIP	Mercury intrusion porosimetry
PAP	Pore-air pressure
PC	Portland cement
PI	Plastic index
PL	Plastic limit
POI	Point of inflection
PSD	Particle-size distribution
PWP	Pore-water pressure
-PWP	Negative pore-water pressure (or suction)
+PWP	Positive pore-water pressure
RH	Relative humidity
SATP	Standard atmospheric temperature and pressure (i.e. 25°C; 100 kPa)
SG	Specific gravity
SL	Shrinkage limit
SWCC	Soil-water characteristic curve
THD	Threshold diameter
UCS	Uniaxial / Unconfined compression strength
VWC	Volumetric water content
WRC	Water-retention curve

NOMENCLATURE

SYMBOL	PARAMETER	UNITS
e	Void ratio	cm^3/cm^3
g	Gravity	9.81 m/s^2
h_C	Capillary head rise	m
h_z	Elevation head	m
h_p	Pressure head	m
h	Hydraulic head or total head ($h = h_p + h_z$)	m
k_s	Saturated hydraulic conductivity (coefficient of water permeability)	m/s, m/d
$K(\psi, \theta)$	Unsaturated hydraulic conductivity as a function of either suction or volumetric water content	m/s, m/d
k_r	Relative coefficient of permeability function	dimensionless
m_w, m_2^w	Coefficient of volume change	kPa^{-1}
m_v	Coefficient of compressibility	kPa^{-1}
M_S	Mass of dry solids	g, kg
M_w	Mass of water	g, kg
M_T	Total mass ($M_T = M_w + M_S$)	g, kg

SYMBOL	PARAMETER	UNITS
P_{atm}	Absolute atmospheric pressure at SATP	100 kPa
Q	Vertical flow of water per unit area of a medium (Darcy's flux)	$m^3/d/m^2$
R	Radius	mm
R	Universal molar gas constant	8.31432 J/mol·K
R_s	Radius of curvature	mm
S	Degree of saturation	%
SG	Specific gravity of solids	$g/cm^3, kg/m^3$
S_K	Sink term	m/day
S_s	Specific storage ($S_s = -\gamma_w m_2^w$)	m^{-1}
T	Temperature	$^{\circ}C, K$
T_s	Surface tension	N/m
V_a	Volume of air	cm^3
V_s	Volume of solids	cm^3
V_w	Volume of water	cm^3
V_T	Total volume ($V_T = V_v + V_s$)	cm^3
w	Gravimetric water content (Geotechnical)	%
w_m	Gravimetric water content (Mining / pumping)	%
SYMBOL	PARAMETER	UNITS

w'	Normalized gravimetric water content	%
ΔP	Pressure differential	kPa
γ_w	Specific weight of water at SATP ($\gamma_w = \rho_w g$)	9.18 kN/m ³
ϕ	Contact angle	°
ρ_b	Density of a bulk material (bulk density)	kg/m ³
ρ_w	Density of water	1000 kg/m ³
θ_V	Volumetric water content	%
\bar{u}_v	Partial pressure of pore-water vapour	kPa
v_b	Specific volume of a bulk material ($v_b = 1/\rho_b$)	m ³ /kg
v_{wo}	Specific volume of water ($v_{wo} = 1/\rho_w$)	m ³ /kg
u_a	Pore-air pressure	kPa
u_w	Pore-water pressure	kPa
$(u_a - u_w), \psi_m$	Matric suction or capillary pressure	kPa
π	Osmotic suction	kPa
ψ	Total suction ($\psi = \pi + [u_a - u_w]$)	MPa
y, z	Vertical direction	m

CHAPTER 1

1 INTRODUCTION, BACKGROUND AND OBJECTIVES

1.1 USE OF CEMENTED PASTE BACKFILL IN MINING

Mineral and metal mining is a vital part of the Canadian and global economy. Canada is one of the world's leading producers and exporters of more than 60 mineral and metal products (NRCAN, 2011), which makes a significant contribution to Canada's international trade, accounting for \$81.4 billion dollars (or 21.8%) of Canada's gross domestic exports in 2010 (Stothart, 2011). With these economic benefits however, comes the risk of severe environmental impacts. Rather than viewing this as a trade-off, these risks require mitigation and interception to ensure the future sustainability of the mining industry.

Mining can be defined as the process or industry of excavating subsurface material to extract valuable ores or minerals. Mineral extraction is dictated by the type of mineral or class of mineral that is in question: soft rock mining or hardrock mining. Underground hard rock mining, or simply, hard rock mining refers to various underground mining techniques used to excavate metallic ore (or hard minerals), mainly those containing economic value, such as ore containing gold, silver, iron, copper, zinc, tin and lead (de la Vergne, 2003). Similar techniques are also used for mining kimberlite and other gem-containing ore that cannot be accessed, through surface excavation techniques, such as

surface or open pit mining. In contrast, soft rock mining refers to excavation of softer minerals (e.g., limestone, salt, coal, or potash, etc.), through surface mining techniques, such as an 'Open-cast' procedure. Surface mines normally extend to depths of less than 200 meters, and are usually less expensive to develop than from underground mines (The Mining Industry's Weekly Newspaper, 2010).

Ore production on average generates 1Mt of mine waste for every tonnage of recoverable material. For instance, in Canada, an average of 99 tonnes of waste material is produced for every tonne of copper extracted, while the amount of gold extracted per tonne of waste material is even less (Safe Drinking Water Foundation, 2004). Mine waste is a by-product of all aspects of mine development, from quarrying, excavation and ore/mineral processing. It is defined as waste rock (quarried rock) and tailings (milled rock and processed water). Milled rock particles typically have grain sizes ranging from 100 to 2 microns. Many ore minerals contain acid generating sulphides (or pyrite); heavy metals and other contaminants are problematic when leached into the environment. Pyrite (FeS_2) containing minerals are chemically stable in low oxygen environments; however, when exposed to above ground conditions, normally as waste, they may become acid generating. In the presence of oxygen and water, pyrite containing waste becomes unstable, dissolving into an aqueous solution (characterized by a pH of less than 4), and producing what is commonly referred to as acid mine drainage (AMD) and/or acid rock drainage (ARD). Proper disposal and management of such wastes are challenging and problematic as it is further amplified by the amount generated throughout the operational mine life and thereafter. In 2004, it was estimated that the Canadian mineral industry

alone generated 1Mt of waste rock and 950,000 tonnes of tailings per day, totaling, 650 million tonnes of waste annually (SDWF, 2004). The ongoing economic and environmental sustainability of selective and bulk mining at whole, in today's mining industry has become extremely challenging to improve, not just in Canada, but also worldwide.

Reducing mine expenditures while increasing ore recovery rates relies on proper scheduling of the mine development phase and ore production phase. After a thorough assessment of the geomechanical characteristics of the host rock as well as its surroundings, the decision making process begins by selecting mining techniques that maximize mine safety and productivity. During this phase, underground access configurations and routes are mapped out for both workers (e.g. air ventilation) and machinery. Vertical shafts, tunnels and sub-level channels are also planned and designed to minimize pre-production development (i.e. top-down versus bottom-up mining), and to minimize production development as well as its operational costs (i.e. selective extraction versus bulk mining). Next, the production phase is initiated once safe access and routes are established, where local masses and host rock are blasted, and then excavated by mining from the top-down and from the bottom-up. Safe working conditions are provided with the construction and placement of underground supports in access shafts, tunnels and rooms. Fractured material and unstable rock slabs from the channel sidewalls and roofs are quarried to the surface.

Hard rock mining techniques (almost) always involves a blast-sequencing-removal process, called stoping or stope development. Successive drilling and blasting of the host rock allows for relatively easy access and recovery by creating large underground voids (up to 100 meters deep), called stopes. The excavated materials from these stopes are hauled to the surface to a milling facility. Once a stope is completely harvested, barricades are constructed and placed at the foot of the stope, and then, backfilled with slurry material (e.g., alluvial sands and/or waste material) to provide local support from ground relaxations that have been produced from mined out stopes. However, between successive stoping and backfilling cycles, a downtime is required. This is called, ‘stope turn around’ time (or cycle), which includes drilling, loading, blasting, backfilling, setting, etc. (de la Vergne, 2003). The length of the turn-around time depends upon whether or not the fill material acquires enough strength to be self-supporting to facilitate removal of adjacent rock. Therefore, a good quality backfill that offers smaller gaps between stopes and faster excavation rates may proffer optimization in ore recovery, and in turn, increase the overall productivity of a mine.

One of the earliest backfills – hydraulic fill, is comprised of the coarse fraction of tailings (from the processing plant) to facilitate vertical drainage. In most cases, hydraulic fill is mixed with a hydraulic binder (e.g. Portland cement, furnace slag, etc.,) to gain sufficient strength. Slow vertical drainage rates (and delayed hydration rates – if binder is added) have resulted in lengthy turn-around cycles (Jung and Biswas, 2002), and self- and blast-induced liquefaction (Mitchell, 1989a; Belem et al., 2010). Hydraulic fills have been known to perform poorly in achieving the desired mechanical strength and operational

performance (Grice, 1998; Mitchell, 1989a; Jung and Biswas, 2002). To improve overall mine safety and productivity, many mines worldwide have adopted the use of CPB, or simply paste fill. CPB is composed of a mixture of highly dewatered tailings (75-85% wt. solids), binding agent (2-8% dry wt.), and processed mine water (wastewater). CPB also uses the total tailings stream. For many types of mining, the high content of fines and low pumping requirements facilitates the transport of CPB. At this solid concentration of CPB, the material will typically have a yield stress of between 100 to 250 kPa (Grabinsky, 2010).

Over the last decade, CPB technology has gained popularity in the mining industry worldwide (e.g. Barrsotti, 1978; Stone, 1993; Bodi et al., 1996) and in Canada (e.g. Viles and Davis, 1989; Landriault and Lidkea, 1993; Naylor et al., 1997). The acceptance of paste fill as a viable alternative did not truly occur until the mid-to-late 1990s with the construction and successful operation of several CPB systems in Canada and Australia (Jung and Biswas, 2002; Sivakugan et al., 2004). The use of paste backfill has become an increasingly common practice in underground hard rock mining. A survey conducted on 32 mines in the year 2003 showed that 44% (or 13) of the surveyed underground mines in Canada, USA and Australia use CPB systems (Benzaazoua et al., 2004a). The attractiveness of CPB technology is owed to its numerous advantages over traditional hydraulic fills, because it affords a wide range of opportunities and solutions to unique problem sets in both the operational and environmental planning process of mine design.

CPB systems have numerous benefits, such as, the use of total tailings (both coarse and fine fractions), the ability to fill stopes faster and to achieve the desired strength quickly and thus, increase mine productivity and mine safety, minimize the risk of contamination and a breach associated with tailing impoundments, etc. Unfortunately, due to the relatively undeveloped understanding of the geotechnical behaviour and material properties of paste fill systems, much of its design applications are highly conservative. One of the difficulties with paste fill is that it is a complex material that is continuously evolving from the moment of preparation in the paste plant to underground delivery through pipelines, via disposal point; and, setting in the stope until short- and long-term strength and hardening takes place (Benzaazoua et al., 2004). Conservative design assumptions have resulted in binder content and curing times in excess of what is actually required as well as perhaps overly designed containment barriers.

Current designs of CPB systems significantly affect operating costs of a mine. Cemented paste fill alone, accounts for 10 – 20% of total mine operating cost, with binder agents, currently varying from \$2 to \$20 Canadian dollars per cubic meter (Belem and Benzaazoua, 2008), accounting for up to 75% of the backfilling costs (Grice, 1998; Fall and Benzaazoua, 2003). The cost of mining operations is substantially affected by both binder content and curing time. Lack of uncertainty of paste fill design has undoubtedly contributed to at least some of the 12 known barricade failures that occurred between 2003 and 2006, as well as resulted in production delays and overly conservative filling schedules (Helinski et al., 2011).

1.2 AN OVERVIEW OF THE CEMENTED PASTE BACKFILL PROJECT

The sustainability of bulk underground hardrock mining is dependent upon rapid delivery of high quality backfill that is self-supporting, and capable of achieving and maintaining regional ground stability of surrounding rock mass (Grabinsky, 2007). Several mine design situations require critical improvement and understanding of the geotechnical behaviour and properties of CPB systems, such as the potential for self-weight liquefaction during filling; and, the time required for paste backfill to harden and strengthen before nearby production blasting resumes, in order to prevent blast-induced liquefaction of the fill; hence, reduce the risks of barricade failures (Grabinsky, 2007; 2010). Thus, in order to better understand and manage the risks associated with the geomechanical mine design of CPB systems, a collaborative research project between three Universities and three mining companies was initiated in January 2007, called *The Cemented Paste Backfill Project* or simply *The CPB Project*.

The CPB project involves the University of Waterloo, Carleton University, and coordinated by the University of Toronto, with industrial partners, Barrick Gold Corporation, Xstrata Copper Canada and Inmet Mining Corporation, in partnership at three different mines: (1) Barrick Gold Corporations' Williams Mine in Hemlo, Ontario, (2) Xstrata Copper Canada's Kidd Creek Mine in Sudbury, Ontario, and (3) Inmet Mining Corporation's Çayeli Mine in Çayeli, Turkey.

The CPB project was geared towards addressing the ambiguities that exist with current methodologies in the geomechanical mine design of CPB systems. To address these

shortcomings, the primary goal of the project was to undertake field measurements in test stopes, operated by the three mines, from the moment the stopes were filled to subsequent cement hydration. Field instrumentations included total stress cells, pore pressure and matric suction sensors, thermocouples, and deflection gauges measured at the bottom barricades of various test stopes. This data was to serve as the basis for designing a number of laboratory investigations on specific components of CPB behaviour, such as the rate of hydration, the dissipation of pore-water pressure, the influence of arching on stress distribution, and the temperature effects on strength acquisition.

As a whole, the CPB project has intended to provide a coherent understanding of the geotechnical behaviour and geomechanical properties (i.e. discussed in Grabinsky, 2007), by determining the: (i) internal stresses on filled barricades, mainly the total stresses and hydraulic stresses, as inputs to rationale barricade design; (ii) potential for self-weight liquefaction during backfilling, and therefore limit fill-rise rates, and/or the need for “paste plugs” to protect the barricades; and (iii) time required for backfill to harden and strengthen before nearby production to take place, in order to prevent blasting-induced liquefaction of the fill. This research work studied two different paste fill streams from Williams and Kidd Mine with different physical and chemical compositions. The intent of this study is to serve as an exemplified model for planning and optimizing mine design and performance.

The research goals of the CPB project at whole have been related into ten (10) major Milestones. As per the NSERC CRD Proposal (Grabinsky, 2007):

- *Milestone 1: Fieldwork* – measuring the in situ performance of paste backfill at three different mines with different geometries to assess the arching effects.
- *Milestone 2: Analysis of electromagnetic (EM) and bulk property data* – calibrating an EM probe that will determine paste's void ratio, degree of saturation, and conductivity, which can then be related to the stage of binder hydration;
- *Milestone 3: Binder hydration Analysis* – using scanning electron microscopy (SEM) technology to show how hydration products are formed in paste backfill;
- *Milestone 4: Static and dynamic triaxial strength testing* – determining the development of static and dynamic paste strength with time;
- *Milestone 5: Dynamic strength testing using Hopskin Bar* – quantifying dynamic strength of backfill at very high strain rates and examine its' temporal and compositional effects;
- *Milestone 6: Ultrasonic hydration analysis* – correlating the development of suction and elastic wave velocity as CPB hydrates;
- *Milestone 7: Resonant column testing* – using Resonant Column tests to help interpret non-destructive and destructive test results;
- *Milestone 8: Unsaturated property testing of paste backfill* – capturing paste's transient unsaturated water retention properties and unsaturated hydraulic properties as a function of paste hydration;

- *Milestone 9: Blast testing* – using controlled blast testing in a laboratory chamber to better understand paste’s dynamic behaviour at very large strain amplitudes and rates; and,
- *Milestone 10: Synthesis and Reporting* – synthesizing all test results and develop a generalized framework for undertaking future analysis of CPB operations.

The ultimate deliverable is expected to be a handbook that summarizes the framework in optimization of geomechanical design of CPB systems and to demonstrate its application using the case studies from the three mines. This thesis entitled, “*Unsaturated Flow in Hydrating Porous Media: Application to Cemented Paste Backfill,*” aims to support the CPB project goals, thereby imparting the research work described in Milestone 8. It is expected that capturing CPB’s hydraulic properties during and after premature-aged curing will provide a better understanding of pore-water pressure (PWP) behaviour and perhaps making it possible to estimate its distribution in a CPB stope. Understanding how PWPs develop and dissipate under drained conditions can provide both quantitative and qualitative information about the liquefaction potential under static and dynamic loading, and hence the risk of failure of a bottom barricade. This next subsection (Section 1.2) describes the aim of this research work, *Milestone 8*, in the context of the overall goals of the CPB project.

1.3 SCOPE OF RESEARCH AND OBJECTIVES

Performance of CPB systems is contingent upon how quickly the material gains sufficient strength to be self-standing after initial deposition and subsequent cement hydration. One serious concern at many mines is the liquefaction potential and risk of bottom barricade failures of paste fill. Much of this concern is well documented, in which fill barricades are breached, with the fluidized fill flooding into the mine workings, where excess pore-water pressures (PWP) do not properly dissipate (Thompson et al., 2008). To illustrate the importance of PWPs, consider the stress experienced by a containment barrier – if the pressure remains hydrostatic; the barrier would have to hold back columns of water more than 30 meters high (or ~ 300 kPa). And, for freshly deposited paste fill, the theoretical hydrostatic loading acting on a containment barrier would be more than twice of that of water (i.e., > 600 kPa). The internal stresses and loads acting on these systems are a function of the complex relationships involving the geometry of the stope and the barricade(s) and the time scale associated with consolidation, cement hydration, and filling rates (Helinski et al., 2011).

Depending upon the adopted mining strategies (i.e. rate of pour, backfilling in stages or ‘lifts’ rather than continuous filling) the initial hydrostatic loading on fill barricades may be alleviated if significant consolidation occurs (Belem et al., 2002; 2010; Grabinsky and Simms, 2006; Simms and Grabinsky, 2009). Although, very little water, if any, has been observed to drain out the bottom of CPB stopes (le Roux, 2004; le Roux et al., 2005), because of its low permeability. The combination of poor drainage and high fill rates would suggest that consolidation occurs relatively slowly. However, consolidation may

be accelerated by self-desiccation. The phenomenon of self-desiccation has been known to facilitate +PWP drawdown in CPB material, and in some instances, induce matric suction or -PWPs, such as observed by (Helinski et al., 2007a) and (Grabinsky and Simms, 2006; Simms and Grabinsky, 2009).

Self-desiccation is a phenomenon, in which water is removed internally through chemical consumption. This occurs in hydrating concrete, where it is alternately defined as “chemical shrinkage” or “self-desiccation” (Hua et al., 1995; Kim and Lee, 1999; Acker, 2004; Helinski et al., 2007a). Self-desiccation generally causes a volume change, such that the total volume of the hydrated products is less than the combined volume of the unhydrated constituents (Helinski et al., 2007). Helinski and co-workers have integrated self-desiccation into a large-strain consolidation model that assumes fully saturated conditions (Helinski et al., 2006; 2007a, b, c; 2011; Fourie et al., 2007). Whereas this research, by contrast, considers the scenario where CPB becomes unsaturated during hydration, which may occur during plug placement, or when a relatively high concentration of binder or low fill rate is employed. This work, therefore studies the material properties used to define unsaturated flow behaviour; namely, the water-retention curve (WRC), saturated hydraulic conductivity, and material stiffness, change with time due to hydration. This thesis also proposes a means to quantify the amount of water consumed by hydration, and investigates how to incorporate this effect in an unsaturated flow model using a sink term.

This research consists of two main parts. The first part is comprised of the experimental work to determine the required material properties of CPB before, during and after cement hydration. At the end of the first part, the pre-and post- properties as well as hydration induced matric suctions and internal water consumption changes are incorporated into a finite element solver as ‘inputs’. The second part of this study, evaluated the use of the modified 1-D unsaturated flow model by conducting a series of numerical simulations by interchangeably using the pre- and post-hydration properties of CPB material to simulate PWP profiles of a 1-D vertical column.

The central goals of this study in its entirety, aims to: (1) study how hydration continuously alters the material properties of paste fill material under these imposed conditions; and (2) assess the suitability of the modified 1-D unsaturated flow equation to estimate PWP profiles in a generic cemented paste backfilled stope.

1.4 ORGANIZATION OF THESIS

This manuscript is organized hereafter, into seven (7) Chapters.

- *Chapter 2: Literature Review* – delivering an overview on: underground mining methods (Section 2.1); laboratory studies conducted on cemented paste material; field investigations conducted at Williams, Kidd and Çayeli Mine (Section 2.2); theoretical and experimental soil suction (Section 2.3); principles related to unsaturated flows through porous media (Section 2.4); and a review of models used for cemented paste (Section 2.5). All topics presented in this Chapter are to

serve as a basis and rationale to conduct this research using an unsaturated flow theory framework.

- *Chapter 3: Theoretical Framework* – presenting a: modified 1-D unsaturated flow model (Section 3.1); and methodology to delineate the distribution of PWP in CPB material (Section 3.2).
- *Chapter 4: Materials and Experimental Procedures* – describing the experimental designs of four (4) experimental phases, plus physical characterization testing of the paste materials (Section 4.1) and sample batch preparations (Section 4.2). Phase I, includes the equipment calibration methods and pre-laboratory treatment protocols (Section 4.3). Phase II, consists of the experiments of paste tailings before curing / pre- hydration, and paste tailings after 28 days of early-age curing / post- hydration (Section 4.4). Phase III, incorporates different test methods to capture the effects of binder hydration (Section 4.5). Lastly, Phase IV involves a column test that takes into account paste deposition in stages and subsequent fill hydration (Section 4.6).
- *Chapter 5: Experimental Results and Discussion* – presenting the results and evaluating the implications of those findings from each experimental phase. These results are then incorporated into an unsaturated flow model as parameter ‘inputs’.
- *Chapter 6: Unsaturated Flow Modelling* – presenting an application and methodology of the unsaturated flow theory framework to estimate the

distribution of PWPs in a CPB column, by using a finite element solver, and results and discussion.

- *Chapter 7: Summary and Conclusion* – restating the purpose of this research (Section 7.1), summarizing key findings from the experimental portion (Section 7.2), and the numerical modelling portion (Section 7.3) of this research.
- *Chapter 8: Recommendations for Future Work* – to this end, some final recommendations for future work that may compliment and/or improve this study.

CHAPTER 2

2 LITERATURE REVIEW

The literature review comprises: (i) a brief background in underground mining and current mine practices (Section 2.1); (ii) advancements and contributions made in CPB technology as well as preliminary field studies (Section 2.2); (iii) theoretical and experimental measurement of soil suction; and (Section 2.3); (iv) a background in the unsaturated flow theory framework (Section 2.4); and (v) a description of models used for cemented paste material (Section 2.5).

2.1 UNDERGROUND MINING

Mineral exploitation, in which ore extraction are carried out beneath the earth's surface, is termed *underground mining* (Hustrulid and Holmberg, 1991). Underground mining methods involve subsurface excavation of tunnels and rooms. Compared to surface mining, underground mining is more expensive and precarious. Therefore, it is used primarily in situations where high-valued ores (e.g. gold, copper, zinc, etc.,) are concentrated in narrow veins or other unusually rich deposits. Due to the uniqueness of each ore deposit, mining techniques are nearly unlimited, and hinge mainly upon determining the appropriate form of underground support; access configuration or opening; and, extraction sequence designed to the spatial characteristic of ore deposits (Hartman, 1992).

2.1.1 TERMINOLOGY AND METHODS

Ore deposits have been extracted using underground mining techniques for more than a century (e.g. Hustrulid and Holmberg, 1991), during which common mining terminologies have been developed. For instances, an *access drive* is an excavated opening along the horizontal, vertical and incline (or ramp) to allow accessibility to working areas near ore deposits. Vertical passages that are excavated from the top down are called *shafts*, whereas *raises* and *winzes* are vertical passages excavated upward and downward, respectively, between horizontal workings beneath the surface. A horizontal passage excavated into a hillside is called an *adit*, while an *incline* is a sloping passage excavated inward from a hillside. Horizontal underground passages that follow the trend of an ore body are known as *drifts*. An open room created through ore-pillar-removal is a *stope* and its roof is known as the *back*. Additional terminologies that have not been defined here but often used in reference to underground mining can be found in the beginning of this manuscript in the Glossary (page 338).

Subsurface mining methods that are used in today's industry include, the room-and-pillar method, where large open rooms are created and supported by pillars, whereas an open-stope is created without the support of pillars. The open-stope method is employed only if the ore body is small, or the rock is strong enough to withstand collapsing into the stope (Hustrulid, 1991). Other methods include sub-level caving, block caving and long-hole stoping by excavation of vertical chutes and horizontal passages beneath an ore body, which is then allowed to collapse into the openings under its own weight (Hartman, 1992; Straskraba and Abel, 1994). An illustration of an underground mine site is

presented in Figure 2.1.1a, while Figure 2.1.1b is an example of an actual mine plan developed at the Çayeli Mine in Turkey (provided by Inmet Mining Corporation).

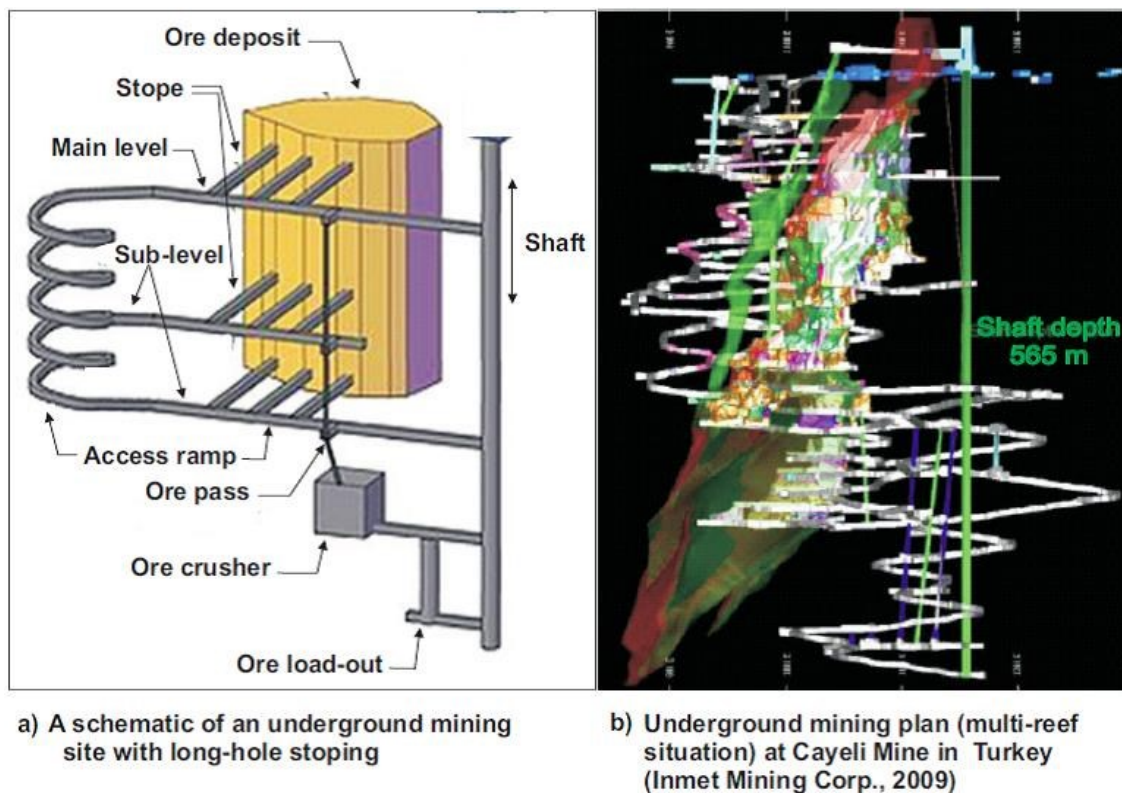


Figure 2.1.1 Underground mine development: a) generic schematic, and b) mine development plan at the Çayeli copper/zinc mine in Turkey

Underground mining techniques have been adapted and developed over the years to improve ore productivity, as well as minimizing geotechnical failures (e.g., surface subsidence, and collapsing of a hanging wall) associated with underground hard rock mining (as discussed by Ran, 2007). For example, the undercut-and-fill method was developed by Inco Ltd. (in 1989) at the Inco Copper- Zinc Mine in Sudbury, Ontario, Canada, to deal with abnormal ground conditions encountered in ore pillar recovery

(Murray, 2001). The undercut-and-fill method recovers ore deposits by extracting blocks of ore by mining successive cuts and backfilling open stopes, working from the top down. Variations of such methods (e.g. cut-and-fill, room-and-pillar, etc.) have been used in cases where ore deposits are located at extended depths. Difficulties however, tend to arise in the presence of *multi-reef* situations, where the need for service shafts are positioned in the *hanging wall* of the ore bodies, in which case, additional support is needed by backfilling (Murray, 2001; Jung and Biswas, 2002). The development of stress concentrations in regional bulk rock at whole has been minimized by leaving numerous pillars while backfilling underground stopes.

Mining methods employing successive stoping and backfilling operations renders problematic issues, especially concerning the material that is used as backfill. For example, pillars that are left behind tend to fail gradually as stoping progresses causing most pillars to completely de-stress and collapse by the time successive recovery commences (Murray, 2001). Further, if the backfill material lacks the required strength properties it too will fail. A well designed backfill however, can minimize liabilities during and after mine undertaking, additionally improving regional ground support. Ground stability has been and continues to be for the most part, a major concern in ore productivity, as it is contingent upon mining conditions (e.g. drilling, blasting, and ore-sequence removal) that exist in the workplace. Therefore, backfilling methods have become an increasingly important component of underground mining operations around the world.

2.1.2 MINE BACKFILL

In mining applications, backfilling is referred to as emplacing or filling waste material in mined-out stopes to enhance the engineering performance of mine design applications while additionally, minimizing surface waste disposal requirements. Mine waste includes waste rock, deslimed and whole mill tailings, quarried and crushed aggregate and alluvial sand (Grice, 1998). Commonly used backfill are comprised of waste ranging from boulders to silty-clay particles to make up sand fills, hydraulic fills, rock fills and cemented paste backfill (CPB), also referred to as paste fill. These backfill systems comprise of either waste material alone, or include very lean amounts of cement or other hydraulic binders to improve the mechanic strength properties (e.g. reduce the liquefaction potential). The fill material is contained from entering the mine workings by a containment barrier called a barricade. Barricades are engineered to be permeable barriers made out of waste rock and concrete aggregate mixtures (e.g., *shotcrete*) for preferential drainage. A schematic of a backfilled stope is presented in Figure 2.1.2.

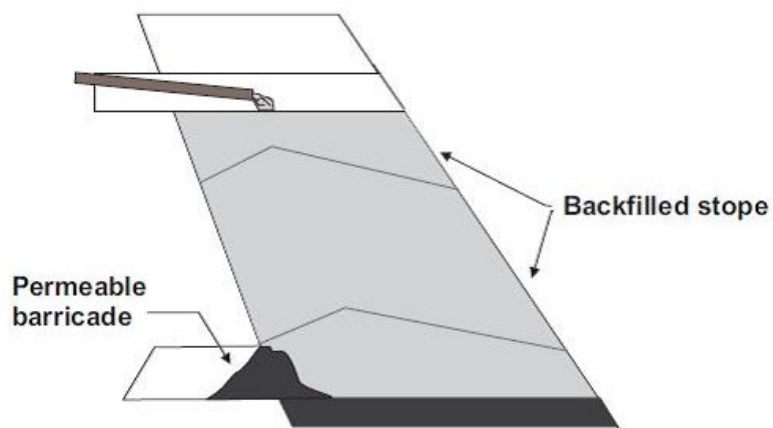


Figure 2.1.2 Schematic of a generic backfilled stope

As early as the nineteenth century, underground mining practices employed backfilling technologies. According to Jung and Biswas (2002), in 1864, an anthracite coal mine at Shenandoah, Pennsylvania was the first mine site to utilize a hydraulic backfill. Hydraulic fills are comprised of 50 to 70% of classified tailings (i.e., classified as ML or SM under the Unified Soil Classification System) (Grice, 1998; Sivakugan et al., 2004) ranging from sand to silt size aggregates (without the clay fraction), water and usually (but not always) some type of binder. The small silty-clay fraction of milled tailings, (referred to as slime) is separated, pumped and disposed of in a surface tailings facility. The solids concentration (or pulp density) of hydraulic fills are generally between 55 to 72%. The primary advantage of hydraulic backfill is the simplicity and low cost production and delivery (e.g. transported by gravity through boreholes). Non-cemented hydraulic fill can be placed for less than \$2 per cubic meter (Grice, 1998). Its heterogeneous behaviour upon placement (i.e., separation of air, water and classified tailings and/or sand) makes it inadequate as an underground support system in deeper mines (Jung and Biswas, 2002). This is mainly due to the time required for significant hydration to occur. Grice (1998) reported a number of failures in Australia, where hydraulic fills were employed.

Disadvantages of the use of hydraulic backfills are, the: (i) increased capital expenditures for the design and construction of permeable barricades (Grice, 1998; Jung and Biswas, 2002) to retain the backfill and permit free drainage of excess transport water; (ii) time it takes to construct a barricade where it occurs at a critical path activity between the completion of production in a stope and the commencement of filling (Grice, 1998); (iii)

management of large quantities of on-site mine water – pumping excess water out of the mine, followed by a wastewater treatment (le Roux, 2004); (iv) lengthy time required in between blasting and sequencing activities, due to excess pore-water in mine fill, which can cause liquefaction and barricade failures under static and dynamic conditions (Grice, 1998; Murray, 2001; Jung and Biswas, 2002; Sivakugan et al., 2004); and (v) leaching of heavy metals into groundwater, and contaminating the environment (Baker, 1986; Benzaazoua et al., 2002b; Benzaazoua et al., 2002c; Ouellet et al., 2006).

2.2 CEMENTED PASTE BACKFILL

Early research and development efforts (e.g. by Wayment, 1978; and Arioglu, 1983; as cited by Belem and Benzaazoua, 2008) focused primarily on issues of paste production and delivery, and to a lesser extent on binder-mix design (Grabinsky, 2007). In practice, it has been recommended that CPB is to be designed to have compressive strength indices ranging from approximately 0.1 MPa to 5 MPa (Belem and Benzaazoua, 2008) so that the liquefaction potential is avoided, although, a target strength of 1 MPa is commonly adopted (le Roux et al., 2002). It has been suggested by Belem et al. (2000) that CPB should be designed so that it will reach its target compressive strength value at of 28 days of early-age curing and beyond (Belem et al., 2000).

2.2.1 STRENGTH PROPERTIES

Many authors (e.g., Bernier et al., 1999; Fall et al., 2004; Kesimal et al., 2004; Kesimal et al., 2005; Yilmaz et al, 2003) demonstrated that strength properties of CPB are dependent upon its physical characteristics (e.g., particle-size distribution, solids concentration) and

chemical properties (e.g., sulphur content), binder type and dose. These studies, in short, have found that the UCS strength of CPB depended on the amount of binder used, and that short- and long-term mechanical integrity hinged upon the chemical composition of tailings in conjunction with the type of binder that is used. Belem et al. (2000, 2001, 2008), Belem and Benzaazoua (2008), and Benzaazoua et al. (2004a) made huge contributions into understanding the hardening process and strength acquisition of hydrating paste fill. Benzaazoua et al. (2004a) investigated the hardening process of paste hydration and strength developing in hydrating CPB. The author(s) also found that the hardening process was attributed to, not only through direct hydration of the binder reagents, but also the formation of hydrates from the pore-water chemistry of the tailings. The presence of calcium sulphate aided in the hardening phenomena (Benzaazoua et al., 2004). It is well known that strength properties evolve during the course of curing.

Benzaazoua et al. (2002b; 2004), Fall et al. (2004), and Ouellet et al. (2006) have successfully track the evolution of such properties using UCS test on hydrating paste specimens. The investigators have found that tailings with higher sulphur contents (e.g., > 39%) acquired greater short-term strength, due to an increased bulk density, and hence increased binder hydration. However, over the long-term, strength was affected by the higher sulphur contents, which lead to strength loss caused by sulphate attacks (Fall et al., 2004). The presence of sulphate species have been known to have an effect on the saturated hydraulic conductivity during different stages of curing.

2.2.2 WATER-RETENTION PROPERTIES

Godbout et al. (2007) and Fall et al. (2009) undertook studies to track the evolution of the saturated hydraulic conductivity through flexible wall permeability and rigid wall permeability tests, respectively. In both studies, authors found that (1) the proportion of binder directly impacted the reduction of water permeability (Godbout et al., 2004), and (2) slag-Portland cement based paste during hydration lower the permeabilities compared to Portland-fly ash mixes. It is thought that slag-based binders when reacting with Portland cement improved the pore structure by increasing the solid volume of the hydration products (i.e. calcium-silicate-hydrate gel) led to a reduction in capillary porosity, and denser packing within the cement matrix, and thus, decreasing the permeability (Fall et al., 2009).

Evolution of the saturated hydraulic conductivity in the presence of sulphate, curing time and curing temperatures were also investigated by Fall and co-workers (Fall et al., 2009; Fall and Pokharel, 2010). The authors found that the presence of sulphate resulted in two opposing effects (Fall et al., 2009): a reduction in permeability can occur due to the formation of secondary precipitates, or it can inhibit hydration, to which may result in the formation of more porous cemented matrix, and hence increased the permeability. The relationship between curing time and curing temperatures were studied by increasing each variable to: (1) assess the rate of hydration, facilitated by the increase in curing temperatures, and (2) track changes / evolution of the saturated conductivity as a function of binder hydration. The authors observed that the permeability decreased with curing time, and increased in curing temperature. More significant changes (or decreases) in

permeability was exhibited in early-age cured samples (i.e. up to 7 days). This conferred with mercury intrusion porosimetry (MIP) results. Additionally, it was found that slag-based binders produced a finer cement matrix, and hence smaller permeabilities (Fall et al., 2009). The authors also observed that the threshold diameter also decreased for samples containing higher %wt. binder, as did Deschamps et al. (2008) for early-aged cured CPB samples, albeit, no noticeable differences over long-term curing. Deschamps et al. (2008) observed with higher %wt. binder contents, the specific surface area also increased (i.e. for $1.8 \text{ m}^2/\text{g}$ to $5 \text{ m}^2/\text{g}$ for paste containing 2wt% binder). An increase in specific surface corresponds to an increase in material fineness due to the binder and its hydration products, which in turn, increases stiffness and thus, the UCS value of the material (Deschamps et al., 2008). Increased stiffness, coupled with reduced saturated hydraulic conductivities in hydrating paste fill is advantageous in the field, because pore-pressure dissipation throughout a backfilled stope is highly dependent upon the rate of consolidation, which in turn, is dependent on the rate of self-desiccation. Temperature effects in normal concrete and cement pastes are known to affect the rate and degree of hydration (i.e., maturity concept).

2.2.3 EFFECTS OF CURING TEMPERATURE

In these same studies by Fall and co-workers (Fall and Samb, 2008; 2009; Fall et al., 2009; Fall and Pokharel, 2010), the effects of curing temperatures were also observed. At higher temperatures, the authors observed an overall increase in rate of hydration, and decrease in permeability as well as a reduction in porosity and pore-connectivity. Results of the MIP tests also exhibited a reduction in threshold diameter and % fineness of the

material when samples were cured above room temperatures, coupled with the presence of sulphates. This concurred with the UCS tests at 28 days of curing (provided in Figure 2.2.2). It is evident that a relationship exists between the sulphate and curing temperature, where strength is of concern: As discussed in Fall et al. (2009), the presence of sulphate species may affect the permeability of CPB by either increasing it or decreasing it. Similarly, presence of sulphate will either increase or decrease the ultimate strength after early-age curing. As observed at all curing temperature ranges, the lower and upper sulphate concentrations (0 and 25,000 ppm, respectively) produced the lowest strengths, compared to specimens containing 5,000 and 15,000 ppm. However, regardless of the sulphate concentration, higher curing temperatures resulted in an overall strength increase (Fall and Pokharel, 2010).

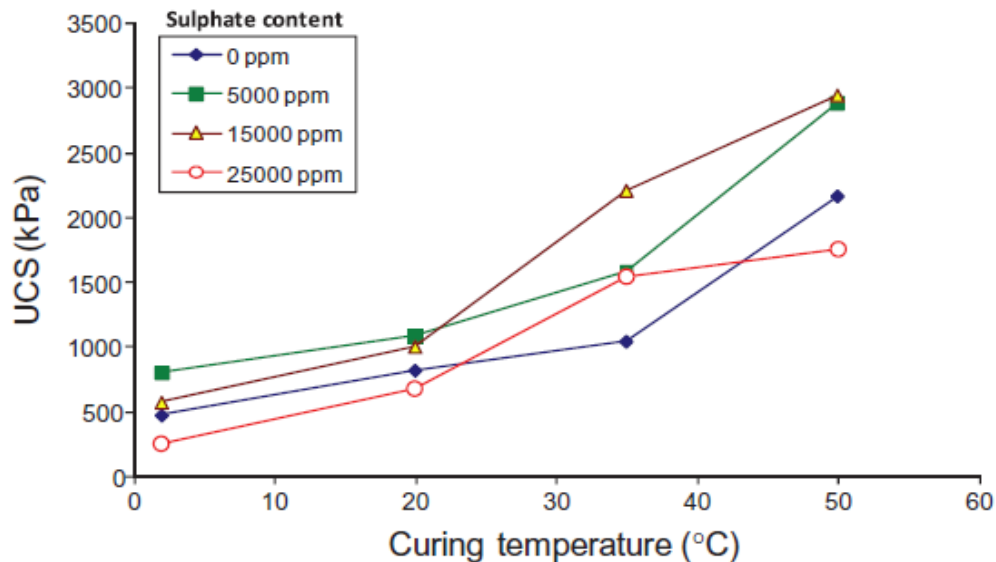


Figure 2.2.1 Coupled effects of temperature and initial sulphate content on the 28 day of UCS of CPB containing Type I Portland cement (Fall and Pokharel, 2010)

Numerous differential thermal analysis (DTA) were also conducted by Fall and Samb (2008; 2009) to quantify the heat changes of paste fill at different curing temperatures. The authors found that increased curing temperatures lead to higher amount of hydration products for early-aged (~28 days) cured CPB samples.

2.2.4 SELF-DESICCATION

Grabinsky and Simms (2006) examined self-desiccation in CPB by inserting T5 tensiometer into sample mixtures under controlled conditions. Sample test results indicated suction development peaking over 100 kPa in 6 days (Grabinsky and Simms, 2006). In addition, a 1-D compression test also showed matric suction development of CPB under applied vertical loads, which corresponded to a prescribed rate of rise used in stope filling (Grabinsky and Simms, 2006). This study demonstrated that the induced suctions in CPB under self-desiccation and vertical load rates might have implications in the design of these systems.

Helinski et al. (2006; 2007*c*) have demonstrated that barricade loads are highly dependent on the degree of consolidation and extent to which effective stress develops in backfill during placement. Helinski and co-workers (Helinski et al., 2007*a*; 2007*b*; 2007*c*; 2011; Fahey et al., 2009; Fourie et al., 2007) developed a small-strain consolidation model that takes account paste hydration (i.e. stiffness, strength), drainage and self-desiccation, fully coupled with consolidation strain. They also examined the process of self-desiccation in CPB by modelling the reduction of PWPs in CPB under undrained conditions, because the combination of rapid loading rate and fine-grain tailings commonly used in paste fill

operations can result in self-weight loading conditions, which are closely related to undrained conditions (Helinski et al., 2007a). Helinski et al. (2007) and (Fourie et al., 2007) reported that for under undrained conditions (i.e. high filling rate and low permeability), the self-desiccation mechanisms dominated the PWP changes that occurred during, and immediately following, the filling process. Whereas, Simms and Grabinsky (2009) found that +PWPs dissipate through the self-desiccation phenomenon is affected by the: (1) initial rate or facilitation of self-desiccation/matric suction generation can be delayed for samples containing high initial water contents or slow dissipation of +PWPs; (2) rate of matric suctions produced during hydration is dependent upon the amount of binder, where high binder contents increase the generation rate of matric suctions; and (3) generation of matric suctions stabilize as ‘consumable pore water’ becomes the limiting factor (Simms and Grabinsky, 2009). Evidence of self-desiccation in the absence of drainage and evaporation for cemented paste for specimens containing 1.5%, 3%, 5% and 7% binder (50% fly ash and 50% ordinary Portland Cement) are shown in Figure 2.2.2.

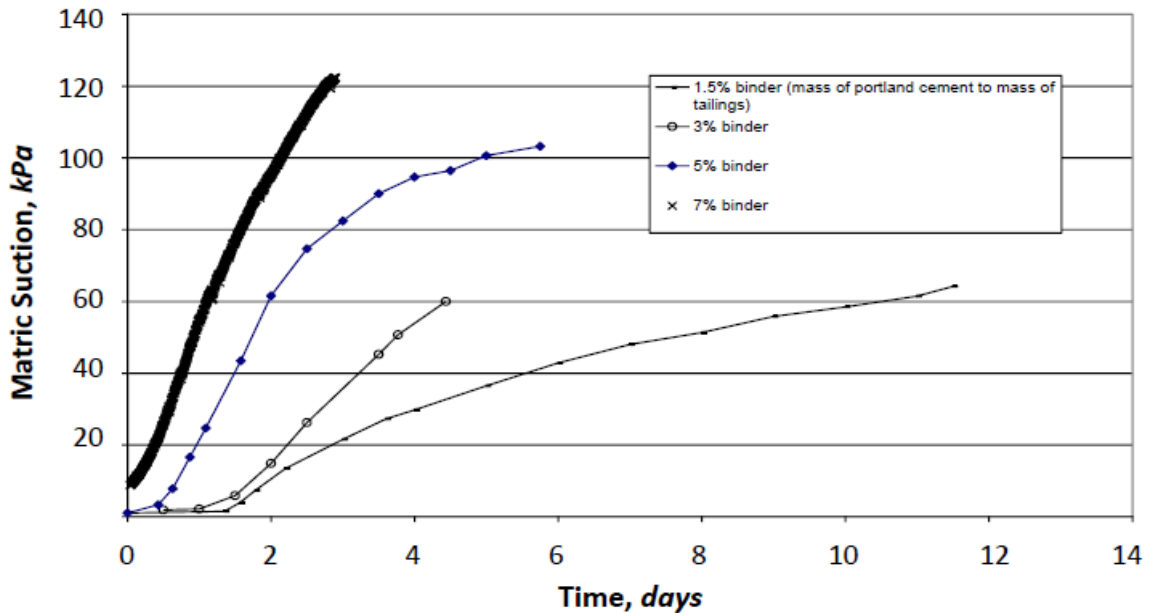


Figure 2.2.2 Generation of matric suction during self-desiccation (Simms and Grabinsky, 2009)

Helinski and co-workers (Helinski et al., 2007a, b, c; 2011; Fahey et al., 2009) have found subtle variations in material properties, such as the hydraulic conductivity can have significant influences on barricade loads. For example, an increase in material hydraulic conductivity can actually increase the pore-pressures, and hence increase barricade stresses, whereas low permeability when combined with a high degree of self-desiccation actually result in low pore-pressures during and for some time following hydration (Helinski, et al., 2007c).

Persson (2005) investigating the effects of temperature on self-desiccation for conventional concrete pastes. The author found that an increase in curing temperature by a few degrees during the early stages of curing resulted in a porous skeleton that had a lower specific surface area, which is an indicator that material was coarser, compared to

pastes cured at room temperatures. Self-desiccation is thought to be the cause of a material to gain more 'fineness' compared to paste materials cured at temperatures 10 degrees centigrade. More, Persson (2005) found that an increase in curing temperature also suppressed self-desiccation, which resulted in less rigid cement bonds. At present knowledge, such studies have yet to be conducted on self-desiccating cemented paste fill material.

2.2.5 IN-SITU PORE-PRESSURES

Mine workings near a stope have correlated pressure changes within CPB stopes, where overloading was experienced in the paste fill as well as at the bottom barricades. Fieldwork conducted by Thompson et al. (2008) have shown the importance of measuring both total pressures and pore pressures in order to properly interpret the nature of the loadings experienced in CPB stopes. For instance, increases in total pressure were shown to be caused entirely by the increase in pore pressures during water flushes into the stope, or by hanging wall relaxation that had no corresponding increase in the PWP distribution. The presence of pore-pressures in a stope defines the liquefaction risk; without these pore-pressure measurements, both situations would have appeared as increases in total stress; and thus, would have made it more challenging to interpret pore-pressure changes as potential failure modes (Thompson et al., 2010).

Preliminary field investigations conducted at Williams, Kidd and Çayeli Mines have shown that upon fill placement the distribution of PWPs change rapidly through self-weight consolidation and cement hydration. Additionally, each of these studies has

provided valuable information regarding pore-pressure behaviour by (Thompson et al., 2011):

- 1) Backfilling in stages / lifts at Williams Mine provide evidence that significant pore-pressure dissipation can occur with low rise-rates.
- 2) Pressure increases were caused by thermal expansion during paste plant shut-down at Kidd Mine. Pressure increases were also correlated with paste fill containing a higher percentage of binder. The effect of thermal expansion may suppress pore-pressure dissipation.
- 3) Factors that affect backfill and barricade pressures (i.e. rise-rates, rate of hydration and tailings composition).

Field results at all three mines are discussed in the following subsections.

2.2.5.1 WILLIAMS GOLD MINE

The Williams mine is one of the largest gold-producing mines in Canada. It is located in Northern Ontario's Hemlo mining region. The underground mine is accessed by a 1,300 metre production shaft, where mining is carried out by longhole stoping with cemented paste backfill (Barrick Gold Corporation, 2004). The test stope (stope 55) was of an Alimak type stope. The test stope was approximately 149 m down dip length and backfilled in 5 stages (or lifts). A summary of these backfilling stages are provided in Table 2.2.1.

Table 2.2.1 Summary of fill deposition in stages ('lifts'), rates-of-rise, volume and duration of each pour (Thompson et al. 2008)

Stage	Lift	Duration (hour)	Start height (meter)	End height	Fill rate (m/h)	Flow rate (m ³ /h)	Volume (m ³)
1	Plug	22.4	0	8	0.4	99	2215
2	Main	57.7	8	82	1.3	96	5539
3	Main	16.6	82	104	1.3	90	1492
4	Fill	4.8	104	112	1.7	84	404
5	Fill	4.6	112	149	8.0	87	401
Total		106.1					10051

The Alimak stope presented in Figure 2.2.3 was instrumented with two wired cages (cage dimension of 74 x 60 x 54 cm). These cages were then attached to an external cage for physical protection (dimensions 1 x 1 x 1 m) (Thompson et al., 2008). Each cage was equipped with sensors to measure PWP (piezometers), total stress (total earth cells – TEPC), matric suctions (heat dissipation sensors – HDS), and temperature changes (conductivity probes). Two cages were placed in the Alimak Nest – Cages 1 and 2. TEPCs 1 through 4 have been used to record the three principal stresses in the vertical direction (TEPC_1); the horizontal direction perpendicular to the plane of the stope (TEPC_2) and along the strike of the stope (TEPC_3); and the stress into the plane of the footwall at a 70 degree dip angle (TEPC_4) (Thompson et al., 2008). Total pressure data from Cages 1 and 2 are shown in Figure 2.2.4. During the plug pour, the hydrostatic pressure induced by the ~ 5 meter CPB overburden is theoretically 114 kPa, which is significantly higher than the maximum pressures measured in the undercut (>25 kPa), indicating that the CPB does not behave hydrostatically and provides evidence that arching mechanisms reduces the applied load (Thompson et al., 2008). PWP data as well

as the effective stresses in Cages 1 and 2 are shown in Figure 2.2.5a and Figure 2.2.5b, respectively. The effective stresses are calculated from the total stresses minus the pore pressures. Field measurements during plug paste pour and subsequent hydration for Cages 1 and 2, respectively, observed +PWPs to dissipate to approximately -8 kPa and -12 kPa. Preliminary findings and data interpretations from Williams mine, found that there were no significant temperature changes during paste hydration. Effective stress changes were small in the Alimak nest, and hence the bottom barricade. Arching effects appeared significant, which enhanced the rate of strength gained. During production blasts, very small stress changes were observed, even in freshly deposited paste layers. Rate of consolidation facilitated +PWP dissipation, to which -PWPs (suctions) developed. This Negative PWPs developed during the paste pour.

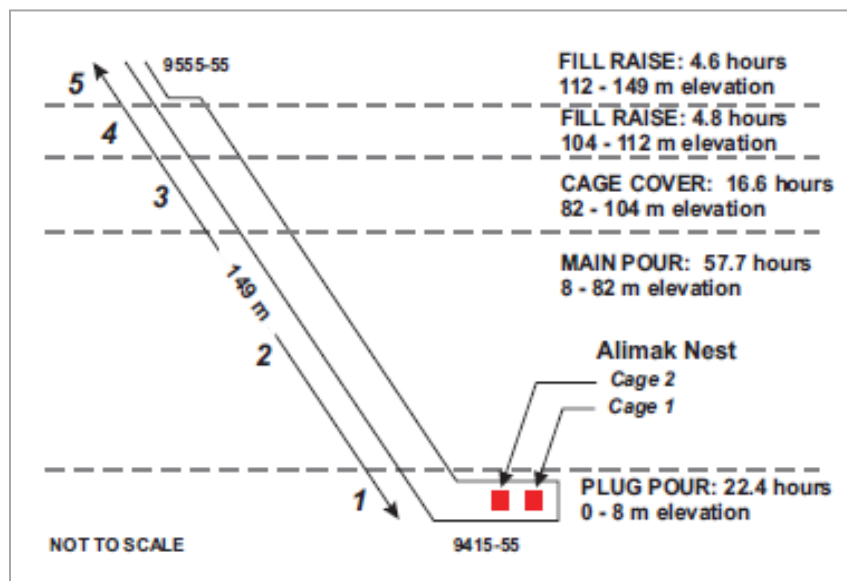
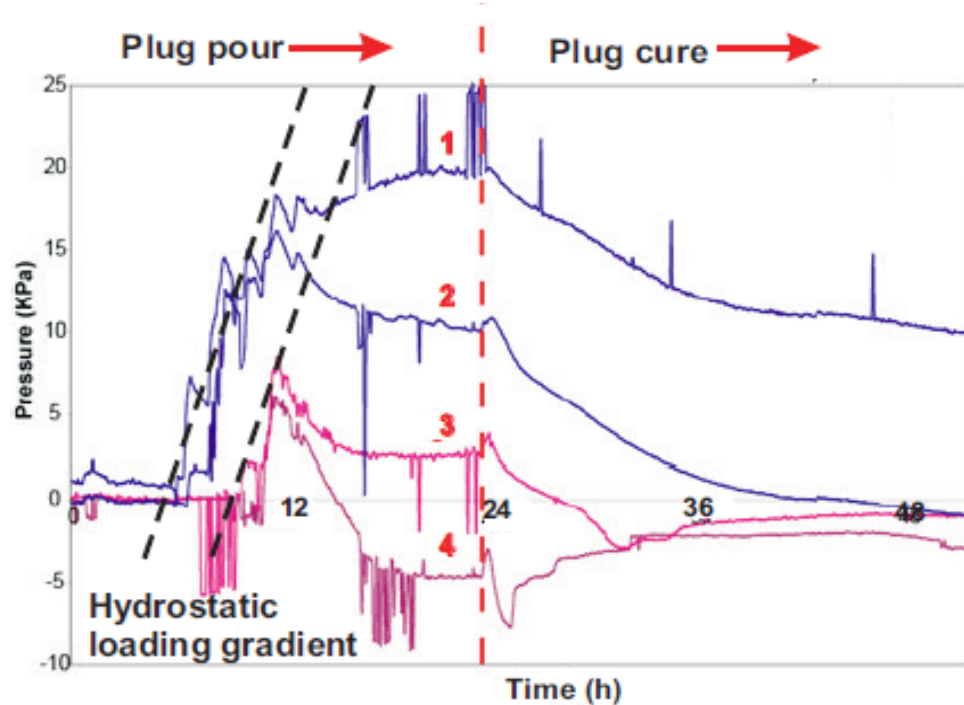
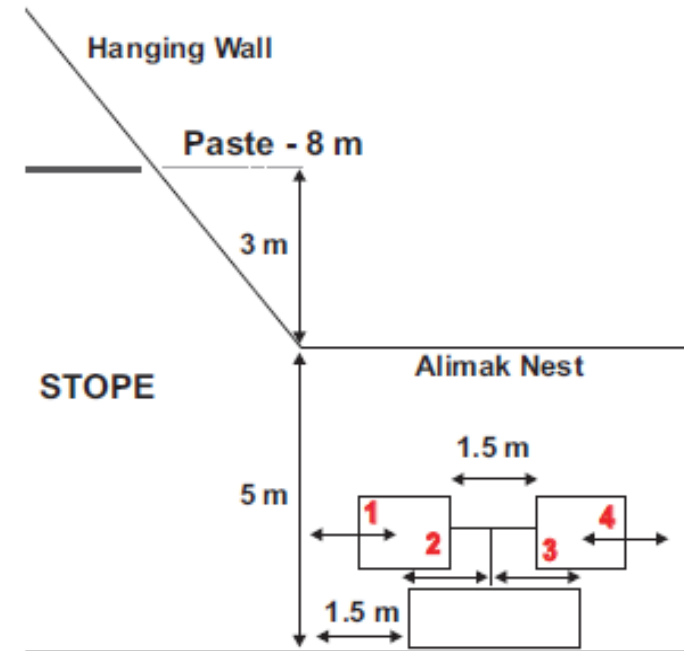


Figure 2.2.3 Alimak test stope at Williams – backfilled in 5 lifts with CPB containing 3% binder (Thompson et al., 2008)



a) Total pressure data in Cages 1 and 2, as shown in b) during the plug pour (8 m thick) and subsequent cement hydration



b). Alimak Nest backfilled with an 8 m paste plug containing 3% binder (50% PC and 50% FA)

Figure 2.2.4 Total pressure data from Cages 1 and 2 in the Alimak Nest (Thompson et al., 2008)

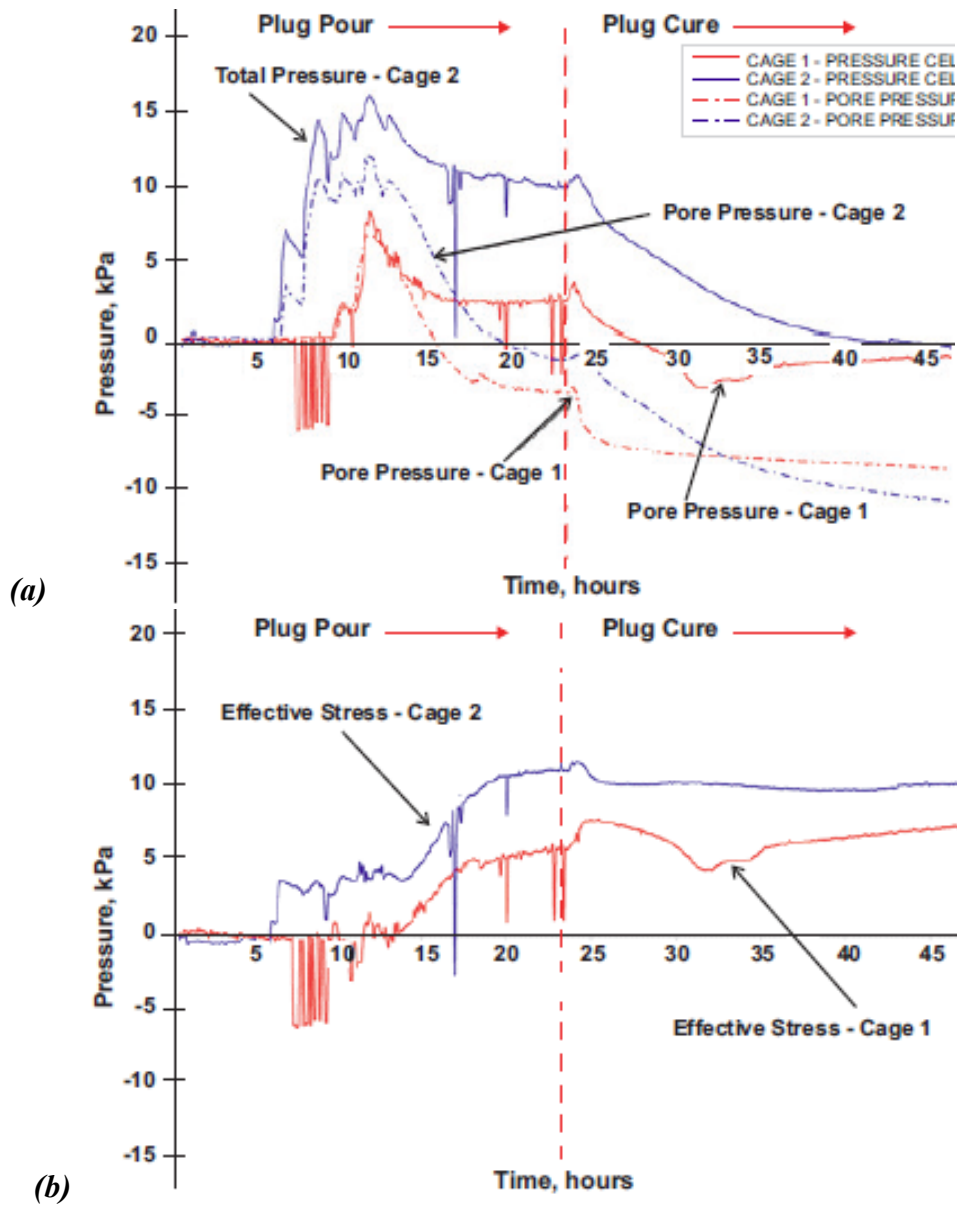


Figure 2.2.5 a) Total pressure and pore-water pressure data in Cages 1 and 2; and b) Effective stress results calculated from data presented during the plug pour and subsequent plug cure (Thompson et al., 2008)

2.2.5.2 KIDD COPPER MINE

The Kidd copper mine is located in Timmins, Ontario. It is owned and operated by Xstrata Copper Canada. Production operations reach a depth of 2,800 meter below grade, making the operation the deepest base metal mine in the world (Thompson et al., 2009). Mining is carried out by long-hole stoping.

The test stope, 67SL1 was 32 m in height, with a length and width of 28 m and 12 m, respectively (Figure 2.2.6). The CPB material was comprised of 45% tailings and 55% alluvial sand, by mass, with a solids concentration of 82% and 18% mine processing water (i.e. 22% mining water content). The binder mix was pre-mixed with 90% blast furnace slag, and 10% ordinary Portland cement. The approximate density of the paste fill material was 2100 kg/m^3 - which is based on the stope volume ($15,560 \text{ m}^3$) and mass of paste fill. The mean pour rate was 248.4 tonne per hour with a rise rate of 0.26 meter per hour (Thompson et al., 2009). A paste plug was employed; which was made up with a dose of 4.5% binder. The paste plug lasted for 27 hour, after which the paste plant switched directly to the main stope mix, comprised of 2.2% binder. The total pour time was 128 hours of continuous pouring.

Field results showed that peak pore pressures in the brow (Cages 1 and 2) reached approximately 25 kPa after 0.3 days after the initial instrumentation response, after this pore pressures dropped to 0 kPa after 1.9 days. In Cage 3, a peak pore pressure of 48 kPa was experienced 0.8 days after the first response (in Cages 1 and 2), and declined in 3.6

days (Thompson et al., 2009). In Cage 4, a peak pressure of 145 kPa was achieved, and Cages 5 and 6 experienced peak pore pressures of 281 kPa and 214 kPa, respectively.

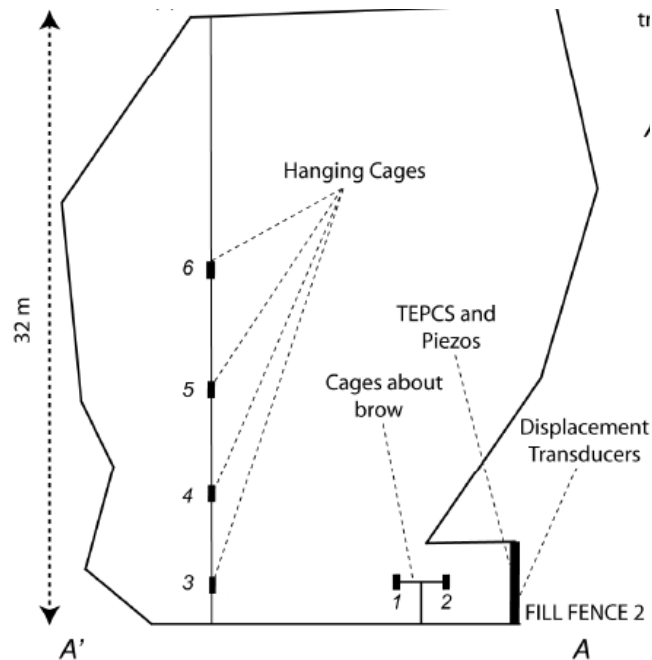


Figure 2.2.6 Cross section view of test stop 67SL1, with locations of instrument Cages 1 through 6 (Thompson et al., 2009)

Three different trends in PWP behaviour were observed (Thompson et al., 2009):

- 1) Cages 1 and 2: loading was observed for less than 12 hours; similar trends manifested in total pressures. This translated to slower seepage rates as fill increased. +PWPs took longer to dissipate during increased fill rise.
- 2) Cage 4: loading on this cage was hydrostatic for approximately 1 day.
- 3) Cage 5 and 6: loading was hydrostatic for around 2.5 days.

Temperatures were observed to increase after the initial covering of Cages 1 and 2 (Figure 2.2.7). The plant was shut down on the 4th day. Thermal expansion is thought as the mechanism for driving pressures to increase within the stope (Thompson et al., 2009). Initially, the temperatures are low, representing the ambient air temperature in the stope. Peak temperatures in Cages 1, 2 and 3 were between 36 to 37 degrees Celsius at the end of the pour. Cage 4, the peak temperature was 34 degrees Celsius, and in Cages 5 and 6, the peak temperature was 27 degrees Celsius. The temperature gradient progressed vertically upwards in the CPB; the lower brow having the % binder content and longer curing time presumably generated more heat. Suction data was also recorded during this study (Figure 2.2.8). Suctions developed shortly after the 3rd day. Maximum suction was observed in the brow (Cages 1 and 2), approximately 400 kPa. Higher suction recorded in the brow is most likely due to the higher binder content of the paste plug. However, higher temperatures were also observed in there as well.

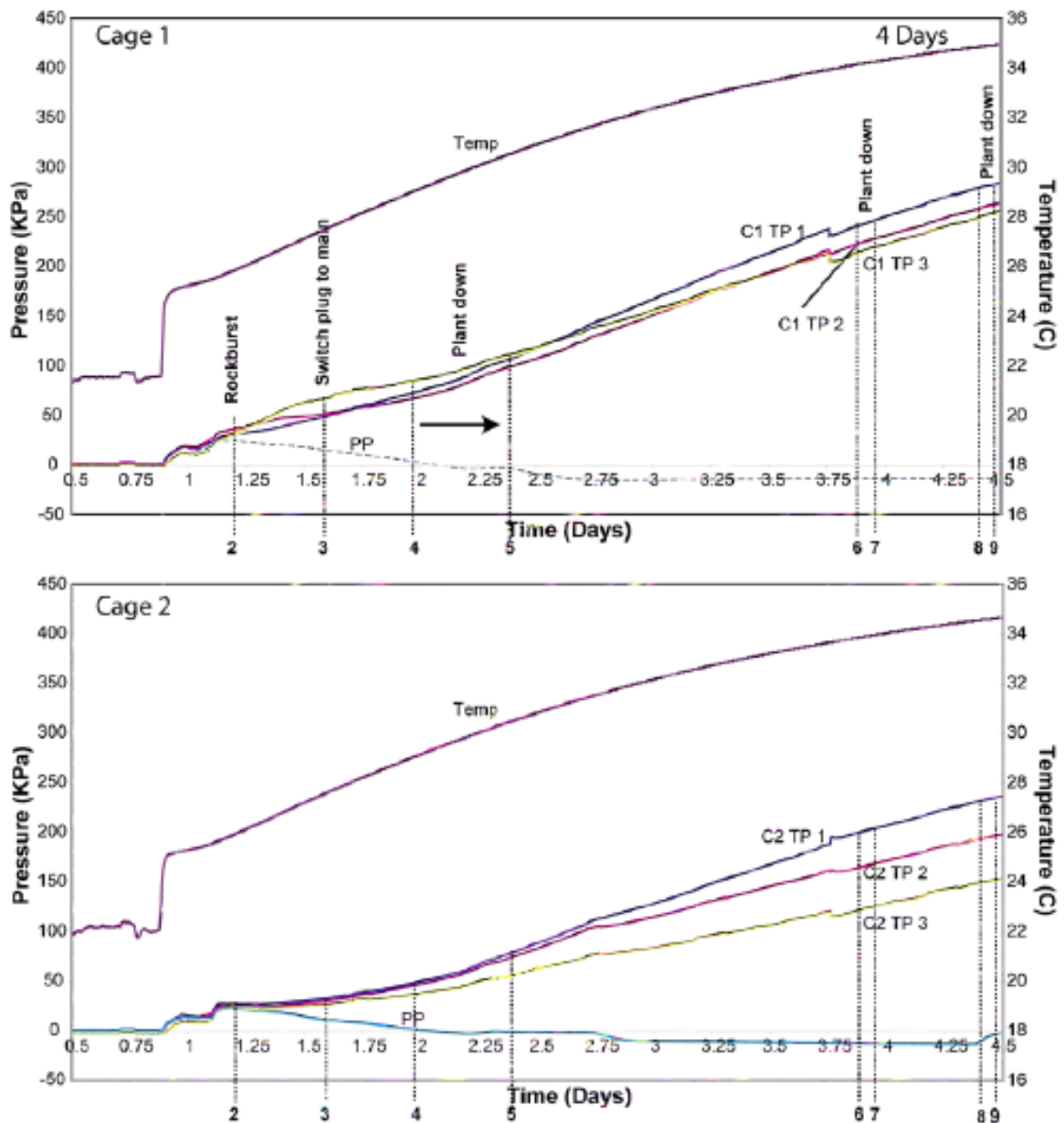


Figure 2.2.7 Total and pore pressure response measured for a 4 day period following the covering of instruments in Cages 1 and 2, with temperature indicated on the secondary axis (Thompson et al., 2009)

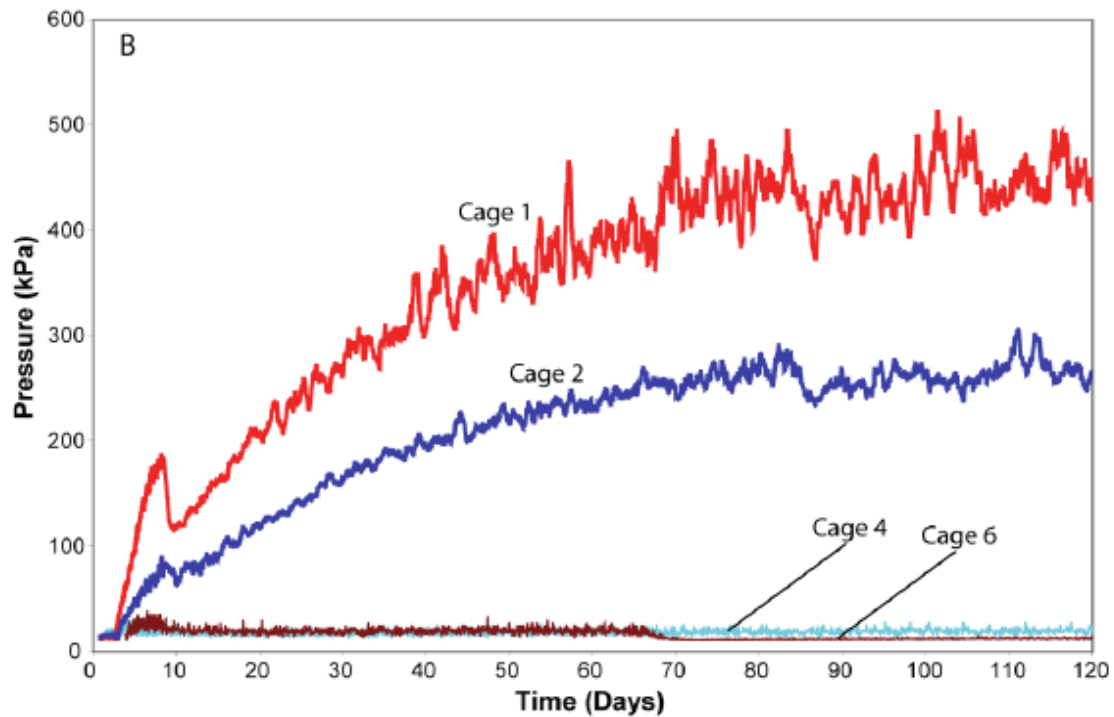


Figure 2.2.8 Suction data (a) shows data from Cages 1, 2, 4 and 6 with a 10 point moving average (Thompson et al., 2009)

2.2.5.3 ÇAYELI COPPER-ZINC MINE

Çayeli mine is an underground copper and zinc mine, located in Turkey. It is owned and operated by Inmet Mining Corporation. Production is carried out using sub-level stoping, 550 m below grade (Thompson et al., 2010).

Two test stopes were studied at this site, both using different types of tailings. Test stope 680(N20) was backfilled with non-clastic / spec- tailings. While test stope 715(N22) was slightly smaller, and was backfilled with clastic / non spec- tailings (finer particles). The binder-mixed used on-site comprised of 100% cement from Ünye Cement (Type CEM 11/A 42.4 R) and is a blend of Portland cement and a natural pozzolana (Thompson et al.,

2010). Both were backfilled with a bulk volume of paste containing 6.5% binder, and a paste plug containing 8.5% binder, followed by a 3 day curing period. Initial mining water contents of the fill material were approximately 23 – 28%. Pressure data was networked to the surface of each stope, and used to define if the stope could be poured continuously, until a barricade threshold pressure of 100 kPa was reached (Thompson et al., 2011).

Initial pressures (hydrostatic loading) increased linearly to 100 kPa in stope 715(N22) within the first 18 hours. Backfilling operations were shut-down, and a 3 day curing period was required. After curing, the remainder of the stope was poured without further interruptions. During the curing period, pressures initially decreased, albeit, subsequent pressures began to increase during the 3rd day of curing. This was interpreted or cause of thermal expansion of hydrating CPB. After completion of backfilling, peak pressures of 120 – 226 kPa were observed, respectively, in the brow and undercut of the stope. Pressure increases were also dependent on rise-rate. Thompson et al. (2011), observed that the rate of pressure increases were observed for higher rise-rates, and thus, increases in barricade pressures. Stope 680(N20) was backfilled continuously, without a paste plug. Peak pressures at the barricade reached 55 kPa (5 m overburden height), which was well below the shut-down pressure. Pressures initially increased hydrostatically. This pattern persisted for approximately 14 hours, before the rate of horizontal pressures and pore-pressures declined. This demonstrated that backfill is gaining shear strength and pressures are arching (Thompson et al., 2011). Horizontal pressures did not significantly increase during the remainder of the pour, albeit, vertical pressures increased to peak

pressures of 116 – 194 kPa at the end of backfill, in the brow and in the undercut, respectively. In Figure 2.2.9, rapid temperature increases were observed to in stope 680(N20), whereas, temperature data for 715(N22) indicated a 2.5 day delay had occurred before temperatures began to increase. This indicating that hydration was delayed by 2.5 days in stope 715(N22) (Thompson et al., 2011). The results of these two test stopes differ significantly (e.g. peak pressures). Both stopes contained 6.5% binder for the upper volume of the stope.

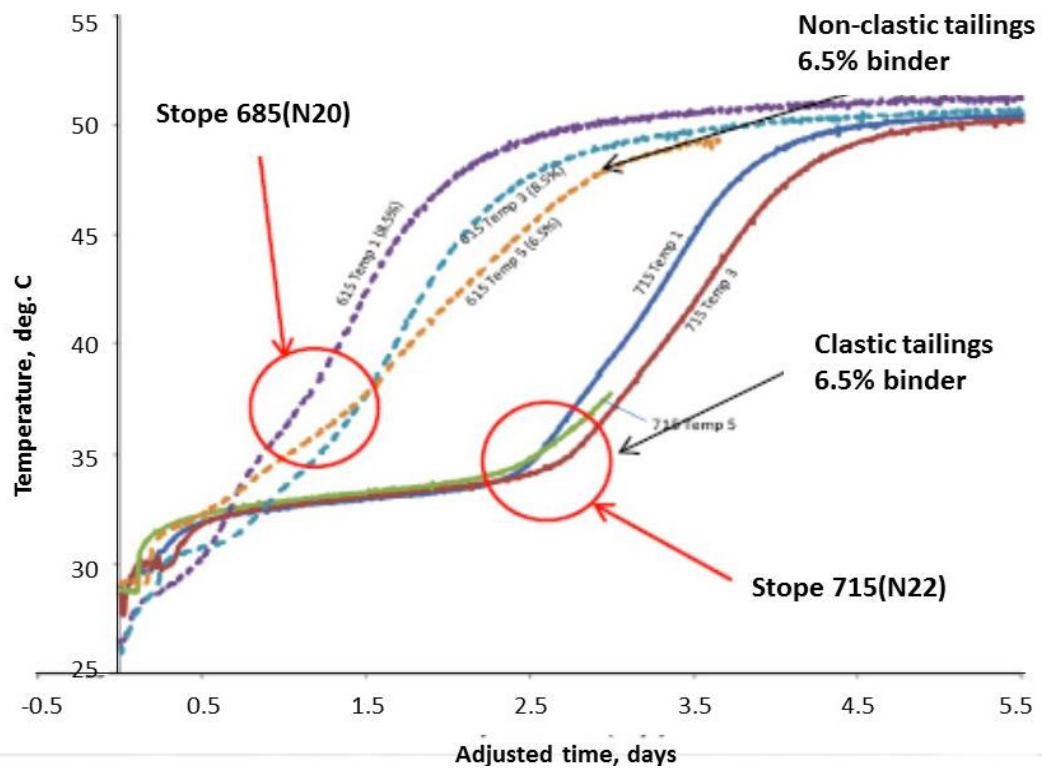


Figure 2.2.9 Temperature profiles in stopes 685(N20) and 715(N22). Observed hydration to be dependent upon tailings chemistry (Thompson et al., 2010)

The only difference was the tailings stream. Non-clastic tailings were used at stope 685(N20), while clastic tailings were used at stope 715(N22) (Thompson et al., 2011). This would imply that tailings chemistry effects the rate of hydration, where clastic tailings delayed thermal expansion (Thompson et al., 2010). Similar to Kidd results, binder content was shown to be an important variable in controlling the rate of hydration and the time of non-hydrostatical loading.

2.3 SOIL SUCTION: THEORETICAL AND EXPERIMENTAL

2.3.1 TOTAL SUCTION

The concept of soil suction was first developed in the early 1900's by Buckingham (1907) and followed by others (e.g., Briggs and McLane, 1907; Gardner et al., 1922; as cited by Richards, 1931; Narasimhan, 2005), mainly in agronomy development in relation to understanding soil-water-plant systems, and applied later to geotechnical sciences to gain a quantitative understanding of the mechanical behaviours of partially saturated soils.

Soil suction, or total suction, is defined as the potential energy of liquid water per unit volume relative to pure water, at its reference state (i.e., atmospheric pressure, temperature and elevation). This potential, quantifies the tendency of water to move from one area to another due to gravitational potential, solute potential and capillary potential (Richards, 1931).

The total suction of liquid water can be related to the relative humidity (RH) of the pore-air, using the Kelvin equation (Edlefsen and Anderson, 1943; Richards, 1965):

$$\psi = -\frac{RT}{v_{wo}\omega_v} \ln\left(\frac{\bar{u}_v}{\bar{u}_{vo}}\right) \quad [2.3.1]$$

where, ψ is the total suction, [kPa]; \bar{u}_v/\bar{u}_{vo} is the relative humidity, RH index (or percentage); v_{wo} is the specific volume of water (i.e. $1/\rho_w$) at $T^\circ C$, [m^3/kg]; ω_v is the molar mass of water vapour, [18.016 kg/kmol]; \bar{u}_v is the partial pressure of pore-water vapour, [kPa]; \bar{u}_{vo} is the saturation vapour pressure of pure water over a flat surface at $T^\circ C$, [kPa]; R is the universal molar gas constant, [8.31432 J/mol·K]; and, T is the absolute temperature ($T = 273 + T^\circ C$), [K]. A plot of equation 2.3.1 is shown in Figure 2.3.1, and illustrates that the RH of the pore-water does not change appreciably for total suctions less than 4 MPa or so.

The total suction of a soil is comprised of two components – matric suction and osmotic suction. Soil suction is defined by (Aitchison, 1965a):

- i. *Total suction* – the free energy of soil water. It is the equivalent suction derived from the measurement of the partial pressure of the water vapour in equilibrium with a solution identical in composition with the soil-water, relative to the partial pressure of water vapour in equilibrium with free pure water.

- ii. *Matric suction* – the capillary component of free energy. It is the equivalent suction derived from the measurement of the partial pressure of the water vapour in equilibrium with the soil water, relative to the partial pressure of the water vapour in equilibrium with a solution identical in composition with the soil.
- iii. *Osmotic suction* – the solute component of free energy. It is the equivalent suction derived from the measurement of the partial pressure of the water vapour in equilibrium with a solution identical in composition with the soil water, relative to the partial pressure of water vapour in equilibrium with free pure water.

Thus, the definition of total suction (ψ) corresponds to the free energy contributions of the capillary component and the solute component of free energy:

$$\psi = (u_a - u_w) + \pi \quad [2.3.2]$$

where, $(u_a - u_w)$ is the capillary suction, [kPa]; π is osmotic suction, [kPa]; u_a is the pore-air pressure, [kPa]; and, u_w is the pore-water pressure (PWP), [kPa].

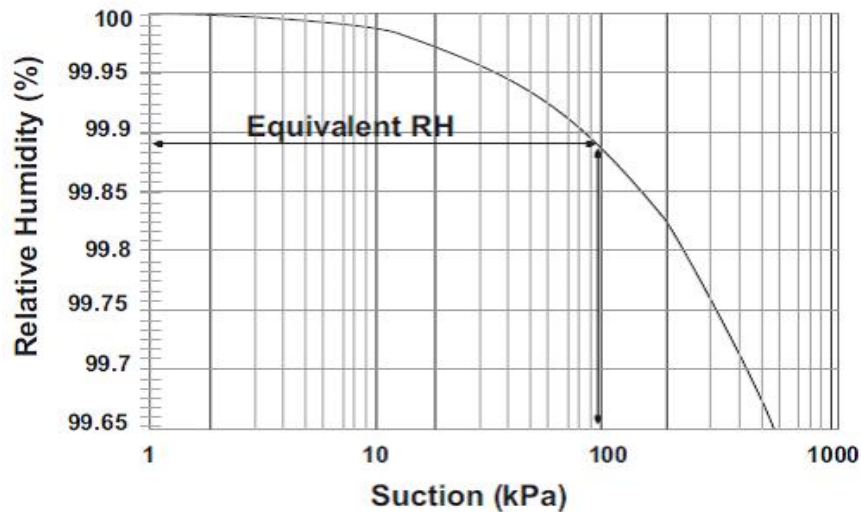


Figure 2.3.1 Thermodynamic relationship between soil suction and relative humidity (Fredlund and Rahardjo, 1993)

2.3.1.1 OSMOTIC SUCTION

The solute component of free energy is called osmotic suction. The presence of dissolved ions (or impurities) in soil-water (or pore-water) decreases the equilibrium soil vapour pressure, and thus decreases the RH (Fredlund and Rahardjo, 1993). Thus, dissolved ions can alter the total suction of soil-water independently of the pore-water pressure as would be measured by a tensiometer. Osmotic suction contributes a significant portion of the overall soil suction as compared to matric suction. It has been reported (e.g., Olson and Langfelder, 1965) that the vapour portion of soil-water for different types of soil, can produce suctions that range from 10^4 to 10^6 kPa, whereas the liquid portion of pore-water can produce suctions that range from 1 to 7000 kPa.

2.3.1.2 *MATRIC SUCTION*

Matric suction is the capillary component of free energy in soil-water. It is fundamentally related to the surface tension along the air-water interface and the pore geometry of a partially saturated soil. This relationship is defined by a capillary tube model, in which soil grains or the pore geometry of a soil is analogous to a capillary tube. By considering a cross-sectional circular capillary, a general relation between pressures in the vapour phase and liquid phase, give rise to a pressure gradient across the fluid boundary at equilibrium. This pressure differential between the two fluid phases is described by the Young – Laplace equation:

$$\Delta u = (u_a - u_w) = \frac{2T_s \cos \theta}{R_s} \quad [2.3.3]$$

where, the surface tension of liquid water, T_s , is the force per unit length acting along a curved meniscus of a radius, R_s , in contact with its own vapour, resulting from an unsymmetrical force field, and, θ is the contact angle between a solid surface and gas-liquid interface at the three-phase line contact, measured through the liquid (Marinho et al., 2008). The contact angle is a result of a balance between the cohesive forces in the liquid phase and the adhesive forces between the solid and the liquid phase (Marinho et al., 2008).

A liquid with a contact angle less than 90° , such as water is said to be ‘wetting’ such that, a drop of liquid tends to spread when placed on a solid surface. The phenomenon of capillarity occurs in a fluid-surface system where the contact angle is less than 90° , which

causes the liquid to rise in within the capillary pores (Marinho et al., 2008). This phenomenon is called capillarity rise, and in terms of matric suction – capillarity head rise. To illustrate this phenomenon (Figure 2.3.2), consider a small glass tube is inserted into water under atmospheric conditions.

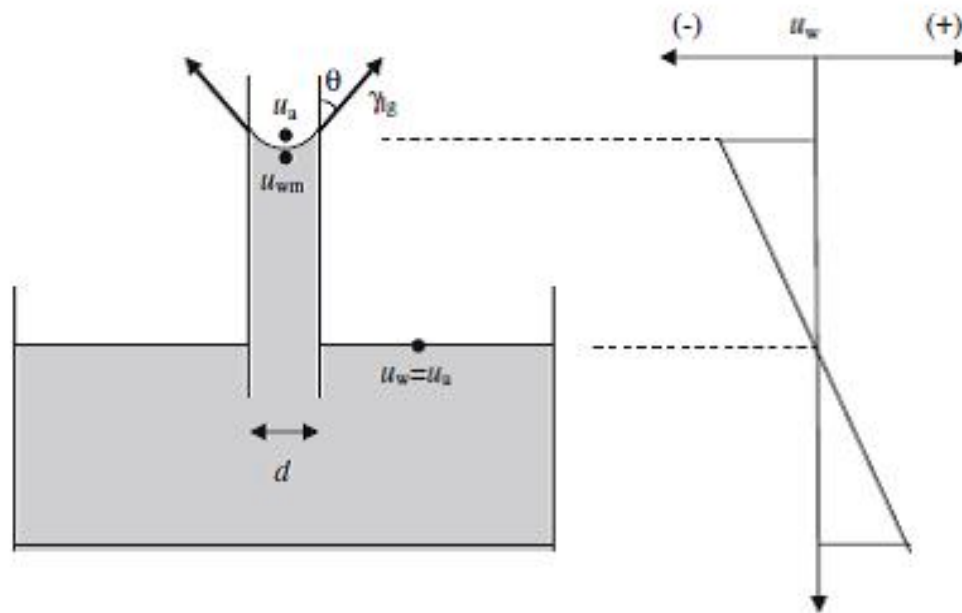


Figure 2.3.2 Idealized capillary tube model of a glass tube inserted into water under atmospheric pressure (Fredlund and Rahardjo, 1993)

The surface tension acting at an angle (contact angle), and its magnitude dependent upon the adhesion between the air-water molecules at the boundary, as well as the material comprising of the tube (i.e., glass); thus, the contact angle between the air-water interface for pure water and clean glass is zero (i.e., $\theta = 0$ or $\cos \theta = 1$). Thus, for a soil system Eqn. [2.3.3] can be simplified, since the radius of curvature, R_S is equal to the radius of a capillary tube:

$$(u_a - u_w) = \frac{2T_s}{r} \quad [2.3.4]$$

where, r is the pore-radius when $\theta = 0$, [m]. Under atmospheric, the pore-air pressure is equal to zero gauge pressure (i.e., $u_a = 0$); therefore, the -PWP is equal to matric suction defined by the capillary head rise:

$$-u_w = \gamma_w h_C \quad [2.3.5]$$

where, γ_w is the unit weight of water (i.e., $\gamma_w = \rho_w g$), [N/m³]; and, h_C is the capillary head rise, [m]. Rearranging equation [2.3.5], and substituting into the Young-Laplace equation (Eqn. [2.3.3]), yields the capillary head rise of pure water (h_C^*) in a vertical glass tube when hydrostatic conditions are established (Marinho et al., 2008):

$$h_C^* = \frac{2T_s}{\gamma_w r} \quad [2.3.6]$$

The height of pure water in a capillary tube made of clean glass is analogous to the pore geometry. The radius of curvature of the menisci concaves towards the lower pressure to balance unequal forces acting on the fluid boundary. When the relative PWP is less than the saturated vapour pressure (i.e. $\bar{u}_v < \bar{u}_{v0}$), a surface tension is produced, thus presenting a RH < 100% in soil-water. Therefore, smaller soil grains will retain more water held under ‘tension’ than that of larger soil grains. Matrix suctions are of also responsible for the changes in volume and strength in finer grained soils that are susceptible to swelling and shrinking (Fredlund, 2006).

Measurement of soil suction is conducted through either direct or indirect methods. Indirect measurement of suction is centered on measuring the moisture equilibrium condition of the soil, whereas, direct measurement involves measuring or controlling matric suction in terms of the negative pore-water pressure in the soil. The following subsections describes more commonly used methods to directly measure matric suction (Sections 2.3.2), and to indirectly measure osmotic suction (Section 2.3.3) and total suction (Section 2.3.3).

2.3.2 DIRECT MEASUREMENT OF MATRIC SUCTION

Matric suction is usually determined through direct measurement techniques. Direct methods are used to measure the negative pore-water pressure (-PWP), where the pore-air pressure (PAP), which is generally measured at atmospheric conditions is equal to zero gauge pressure, minus the negative pore-water pressure yields matric suction. Experimental devices and/or techniques, such as hydraulic tensiometers (also called pressure transducers) and the axis translation technique share a common working principle – the measurement of a pressure differential across a high air-entry porous ceramic (Marinho et al., 2008). The underlying similarities are discussed in the next two subsections.

2.3.2.1 AIR-ENTRY POROUS CERAMICS

A high air entry porous ceramic is made up of small pores of relatively uniform size particles. The porous ceramic acts as a partition between the air and water phase within a soil sample. The pressure differential, that is, the gas pressure minus the liquid pressure

(i.e., $u_a - u_w$) allows for direct measurement of matric suction. The maximum matric suction that can be maintained across the surface of a porous ceramic is called the air-entry value (AEV). The actual AEV of a porous ceramic is typically provided by the manufacturer by measuring the air pressure applied to one side of the ceramic necessary to cause bubbling on the other side, known as the ‘bubbling pressure’ (Marinho et al., 2008).

Porous ceramics are developed from a proprietary mixture of ball kaolinite clay fired to a ceramic body, resulting in a ceramic material, pinkish-tan colour with moderate hardness (SoilMoisture Equipment Corporation, 2008). High air-entry value (HAEV) porous ceramics can withstand maximum pressure differentials ranging from 100 to 1500 kPa. The highest AEV ceramic available is 1500 kPa, while the tensile strength of water is approximately two orders of magnitude greater (Marinho et al., 2008). Specific details regarding commercially available air-entry porous ceramic discs are provided in Table 2.3.1 (SoilMoisture Equipment Corporation, 2008).

Complete liquid-saturation between the porous ceramic (or filter element) and soil specimen provides a continuous liquid phase thereby resisting the flow of air. The ability of the porous filter to withstand the flow of air results from the surface tension developed by the air-water interface, by adjoining the small crevices of the porous filter (Fredlund and Rahardjo, 1993). Under normal conditions, matric suction is equal to the - PWP (i.e. $u_a = atm$). Therefore, direct measurement of matric suction in the laboratory,

is equal to the -PWP. It should be noted hereafter that -PWP or matric suction is synonymous to gauge pressure, relative to atmospheric pressure unless stated otherwise.

The ability of the high AEV porous tips/filters (or disc) to withstand high interstitial fluid pressures makes the porous ceramic suitable for direct measurement of -PWP in an unsaturated soil (Fredlund and Rahardjo, 1993), via the pressure transducer tensiometer and the axis translation technique. The axis translation technique is limited in that it can only be used in laboratory testing, however, this technique is more favorable for long-term measurement, whereas, over the long-term, tensiometers have greater tendencies of forming cavitation.

Table 2.3.1 Properties of commercially available high air entry porous ceramics

Air Entry Value <i>(kPa)</i>	Effective Pore Size <i>(μm)</i>	Hydraulic Conductivity <i>(cm/s)</i>	Approx. Porosity <i>(% volume)</i>
100	2.5	8.60×10^{-6}	45
300	0.7	2.50×10^{-7}	34
500	0.5	1.21×10^{-7}	31
1500	0.16	2.59×10^{-9}	32

* Provided by SoilMoisture Equipment Corp., (2008)

2.3.2.2 PHENOMENON OF CAVITATION NUCLEI

The phenomenon of cavitation occurs when the fluid pressure of a liquid falls below its vapour pressure, forming vapour bubbles in a liquid (Marinho et al., 2008). From a thermodynamic standpoint, water under tension is said to be ‘metastable’ (Gibbs, 1948; cited by Marinho et al., 2008). In other words, ‘unstable’ in the liquid form due to the

presence of tiny gas bubbles, called cavitation nuclei. If any tiny amounts of gas are pre-existing in the liquid phase, water under tension will cause the gas phase to rapidly separate in the liquid (Delage et al., 2008).

Water in its metastable state can experience high -PWPs before cavitation (or nucleation) occurs. According to the van der Waal's isotherms for pure water, liquid water at 20°C can remain in a metastable state when experiencing high tensile pressure slightly greater than 100 MPa (Marinho et al., 2008). Experimentally attained tensile stresses in water ranging from 1.3 – 27 MPa, while (Zheng et al., 1991) was able to measure a tensile stress of 140 MPa in a single crystal of water – value believed to be very close to the maximal tension that water can sustain (Delage et al., 2008; Marinho et al., 2008) before cavitation occurs. (Marinho and Chandler, 1994; 1995) suggested that measurement variations are due to micro-bubbles of entrapped gas (or imperfections) in crevices within a sealed arrangement. These imperfections are caused by the instability and transition of a fluid from one state to another (Take and Bolton, 2003). Imperfections can result in two forms of cavitation nuclei (Delage et al., 2008; Marinho et al., 2008): *heterogeneous nucleation* and *homogenous nucleation*. The latter occurs when thermal motions within the liquid form temporary microscopic voids that constitute cavitation nuclei necessary for rupture and propagate to macroscopic bubbles (Marinho et al., 2008). More often than not, cavitation will occur at the boundary between the liquid and the solid wall of the container or between the liquid and small suspended particles in the liquid (Marinho et al., 2008). Ruptures that occur at these sites are termed heterogeneous nucleation; cavitation of this type is of interest in tensiometer measurement (Marinho et al., 2008).

Consider a conical crevice inside a water reservoir or porous filter of a tensiometer (Figure 2.3.3). In this example (Figure 2.3.3a), the container or porous filter is initially saturated, imperfectly, where there air is entrapped. According to Boyle's law (i.e. $PV = \text{constant}$), if the water pressure in the reservoir drops, the air pressure within the crevice will also decrease, which in turn, causes the volume of gas (or air occupied inside the cavity) to expand (Figure 2.3.3b). As the volume increases, the contact angle increases; the growth of the air cavity becomes instable, and thus separates from the crevice in the form of an air bubble (Figure 2.3.3c) (Marinho et al., 2008).

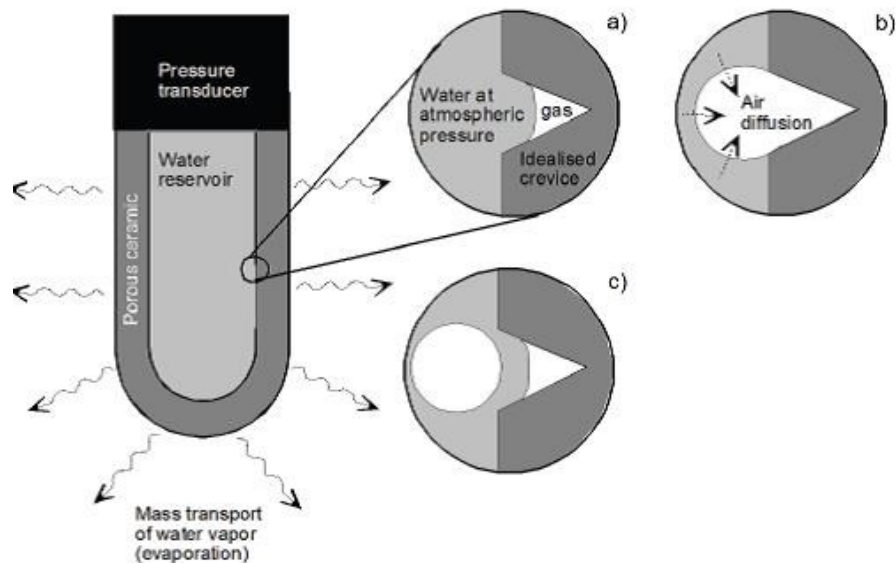


Figure 2.3.3 The crevice model of heterogeneous nucleation (Marinho et al., 2008)

A clear indication of cavitation occurring in a system can be observed when a gas pressure inside a cavity, initially very close to the water vapour pressure, expands, the gauge pressure response drops rapidly from one pressure reading to another (e.g. -200

kPa to -100 kPa) (Marinho et al., 2008). Heterogeneous nucleation can be triggered by gas nuclei entrapped in the water reservoir of a tensiometer, as well as the porous filter (i.e., discussed by (Tarantino and Mongiovi, 2001; Tarantino, 2003)). It is virtually impossible to completely remove nucleation sites from the water reservoir and porous ceramic filter, and thus, nucleation will inevitably occur in tensiometers (Delage et al., 2008).

2.3.2.3 PRESSURE TRANSDUCER / TENSIO METERS

Pressure transducer tensiometers (or tensiometers) take advantage of the available the high AEV porous ceramics in the range of $100 - 500$ kPa (Marinho et al., 2008). Tensiometers are designed to permit the water reservoir of a device (e.g. shown in Figure 2.3.4) to experience true tensile pressures (Ridley, 1993; Ridley and Burland, 1995). Ridley and co-workers (Ridley, 1993; Ridley and Burland, 1995) have measured suctions in the range of 100 to 480 kPa. The maximum sustainable matric suction of a tensiometer is strictly a function of the AEV of the porous filter (Marinho et al., 2008), albeit, Ridley and Burland (1995), Delage et al. (2008), observed experimentally that the CI-Trento tensiometers are capable of measuring beyond its' nominal AEV before nucleation. UMS GmbH (2009) has also claimed that the T5x pressure transducer is capable of measure beyond the AEV. However, particular attention be paid when interpreting suction measurements beyond the AEV. For instances, (Take and Bolton, 2003; Take and Bolton, 2004) conducted further investigations to assess the reliability of such measurements. They found that there was a lag-time during the second stage when suctions were above the AEV, indicating that short-term generation of high capillary

tensions reduced the permeability of the porous filter element. Similar observations have been reported by Ridley and Burland (1995), Marinho et al. (2005), and Delage et al. (2008). Take and Bolton (2004) speculated that this increase in tension caused the menisci to be exposed at the surface of the porous filter, regressing further into the ceramic. The tension will beginning with the largest of the exposed pores and advance via the depth of the porous filter element into the smaller pores. From the latter hypothesis, Take and Bolton (2004) concluded that the degree at which suctions can be recorded beyond a nominal AEV is considered to be directly influenced by the thickness of the porous filter (i.e., a result in delaying the desaturation process). The most important factors in determining the success or failure of tensiometer measurements however, relates to the saturation and pre-condition of the water contained within the porous cup and the reservoir of the device (Marinho et al., 2008).

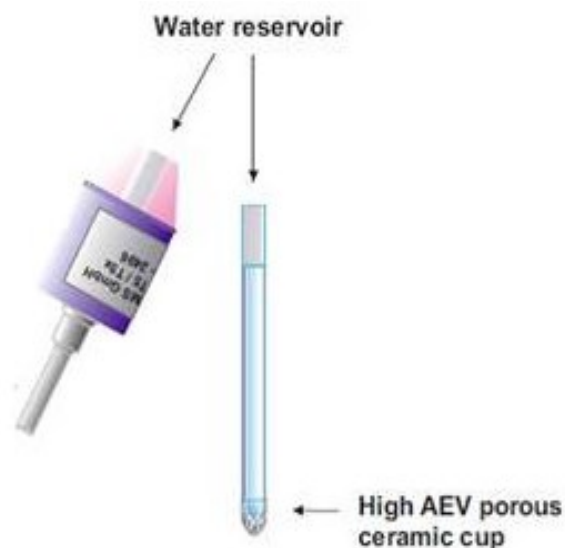


Figure 2.3.4 A schematic of a pressure transducer tensiometer model, T5x from UMS GmbH, Germany (2009)

Nucleation rupture sites within the small crevices or the porous tip and sensing body can be avoided by fully saturating the tensiometer / transducer. The working principle of pre-saturating a high AEV porous tip is based on the assumption that the air-water interface is flat, and that the porous tip of an initial degree of saturation, and an initial absolute pressure, will compress according to Boyle's law (Fredlund and Rahardjo, 1993; Sedano et al., 2007; Marinho et al., 2008). Boyle's law states under isothermal conditions, the product of the pressure and the volume of a fixed amount of gas remains constant. In other words, when a differential pressure is applied, water is allowed to enter the pores of a porous media that was once occupied by air (Marinho et al., 2008). Henry's law dictates however, that the increased pressure will also result in additional air will dissolved into the liquid phase (Take and Bolton, 2003; Tarantino and Mongiovi, 2001; and Marinho et al., 2008). Therefore, the theoretical magnitude of applied pressure is thus a function of both the absolute air pressure within the void spaces, and the initial degree of saturation of the porous material (Marinho et al., 2008). Take and Bolton (2003) and Marinho et al. (2008), also made note of the initial dryness of a porous filter element, in that, it should be as 'dry' as possible so that the pressure required to completely saturate the porous tip can be minimized. Take and Bolton (2003) proposed a two-stage saturation process by introducing a tensiometer to water under high vacuum before applying a high positive water pressure. The change in pressure is considered sufficient to dissolve most of the air in both the porous tip and water reservoir, but not all (Marinho et al., 2008). The reason for this occurrence is due to the presence of air cavities at the air-water interface, retracting into small pores of the ceramic tip as well as the crevices on the reservoir walls, which are no longer flat, but rather a meniscus

concaving towards the water side (Marinho et al., 2008). On the other hand, if high positive water pressures are sustained at the meniscus, the oxygen diffusion coefficient will decrease, thus preventing air from dissolving into the liquid phase. To illustrate this, consider an idealized conical crevice in that once consisted of a flat air-water boundary (Figure 2.3.5a). Whereas, in Figure 2.3.5b, the cavity is subjected to negative water pressure which causes the meniscus to concave towards the water side in correspondence with the larger air pressure (i.e., $u_a > u_w$). One can also consider the depth of the air cavity, which is dependent upon the positive water pressure, gas pressure, the advancing contact angle, and the crevice opening (Mongiovi and Tarantino, 2002). Mongiovi and Tarantino (2002) suggest that the application of positive water pressure will cause the decrease in depth of the air cavity, while negative pressure will increase the amount of air that dissolves in water. Similarly, an increase in surface tension will facilitate the formation of cavitation nuclei at these sites. However, if the water pressure was returned to atmospheric pressure, the dissolved air will preferentially be exsolve from the liquid phase (Ridley and Wray, 1996; cited by Mongiovi and Tarantino, 2002). The amount of gas within the system can therefore, be reduced as the water pressure is decreased or returned to atmospheric pressure.

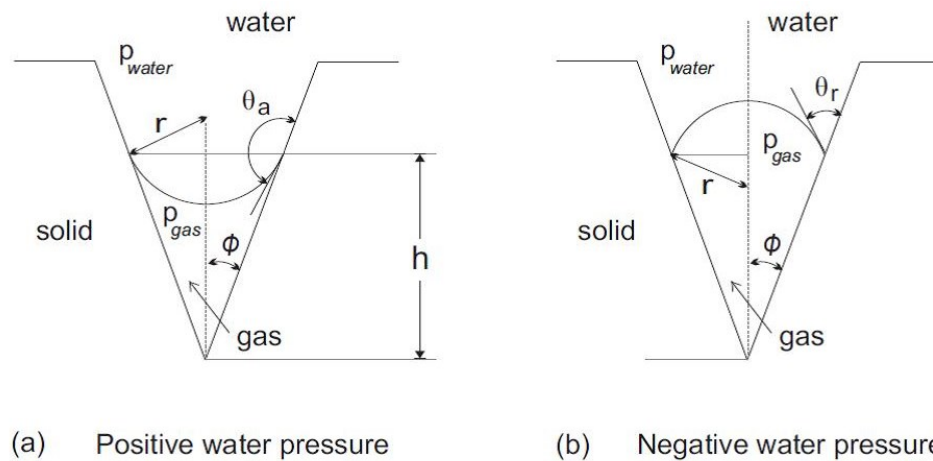


Figure 2.3.5 Idealized conical crevice (Marinho et al., 2008)

According to (Harvey et al., 1944) air cavities that remain entrapped in these crevices are likely to trigger cavitation when the positive water pressure is reduced. This in turn, will cause the curvature of the meniscus to reverse (or concaved towards the water side). It has been suggested that the cavitation nuclei that remains undissolved upon pressurisation can be removed by cycles of vacuum followed by pressurization (Take and Bolton, 2003; Tarantino and Mongiovi, 2001; 2002; and Marinho et al., 2008), where large cavitation nucleation sites rupture first at lower tensile stresses, while higher tensile stresses initiate subsequent nucleation of the smaller sites/cavities. In practice, it is impossible to eliminate nucleation inside the porous tip and/or the water reservoir at high tensile pressures, however, successive stages of vacuum and positive pressures is widely accepted (by Tarantino and Mongiovi, 2001; Tarantino, 2003; and Marinho et al., 2008) that it will significantly improve measurement duration and maximize the sustainable tensile pressures experienced at the air-water interface, rather than pressurisation itself.

Reliability of matric suction measurements when using tensiometers are dependent upon: (1) establishing good contact between the porous ceramic tip and specimen; (2) the presence of dissolved solutes or ions in the pore-water; and, (3) stability of long-term measurement. Contact between the porous filter element and the soil in question is integral in measuring real-time PWP response. The most dramatic example of this is when the tensiometer is not in contact with any material. In this scenario, the tensiometer significantly desaturate as it attempts to come into moisture equilibrium with the air in the gap between the tensiometer tip and the surface of the soil (Marinho et al., 2008). The measured suction in the soil is no longer representative of the actual suction. Marinho and co-workers (i.e., Marinho et al., 2005; 2008; and Delage et al., 2008) recommend that a small amount of slurry be placed at the tip to establish good contact between the soil and the tip. Presence of dissolved solutes (e.g., salts) may also effect matric suction measurement by overestimating the direct measurement of matric suction, and in fact, measure the soil suction somewhere in between matric and total suction. Albeit, Marinho and Chandler (1994) have suggested that the fine porous stone interface could prevent the passage of dissolved ions in soil water if the effective pore-size is small enough. Results from a study conducted by Tarantino (2004) confirmed this hypothesis for dissolved NaCl, indicating that the high air-entry ceramic did have an osmotic effect, at least for this type of solute (Marinho et al., 2008).

The use of tensiometers for long-term measurement is limited. It is impossible to attain perfect saturation. The stabilization afforded by the pre-conditioning process is viewed as temporary, where water held in the tensiometer is metastable, and thus, will inevitably

experience nucleation (Marinho et al. 2005; 2008). No experimental data currently exists to accurately predict the length of time a tensiometer can remain operational at high suctions, such as the variability in the stability of surface tension breakdown (Marinho et al., 2008). Although convenient for field use, tensiometers are limited, in that no long-term measurement of hydraulic testing of an unsaturated porous media can be accomplished. An alternative method, called the axis translation technique is used, preferentially for the long-term measurement of matric suction in laboratory conditions.

2.3.2.4 AXIS TRANSLATION TECHNIQUE

The axis translation technique was developed for laboratory testing to overcome measurement constraints associated with tensiometers (e.g., cavitation). Early developments of this technique by (Richards, 1931; Richards, 1947; Gardner, 1956) started with the pressure plate extractor. This technique is associated with the matric suction component, in which the water potential is controlled by means of liquid phase transfer through a saturated interface of a high AEV porous ceramic disk (Delage et al., 2008).

The working principle of axis translation technique is based on the familiar capillary pore model for a typical case (Figure 2.3.6a), where the pore-water is subjected to atmospheric pressure. Whereas, in the second case (Figure 2.3.6b), the water level will rise to a capillary height proportionate to that of the atmospheric pressure, since the water pressure is less than atmospheric. In a laboratory environment, if the capillary tube was

close-ended at the top and subjected to an elevated air pressure, the system would respond in the same way (Marinho et al., 2008).

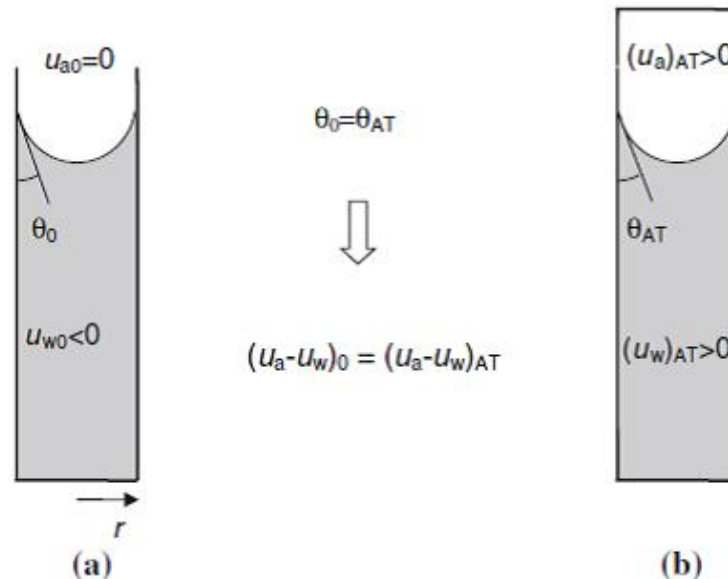


Figure 2.3.6 Capillary pore model: working principle of axis translation technique (Marinho et al., 2008)

The capillary pore model assumes that the water and solid boundaries are sufficiently incompressible, such that the curvature of the air-water interface remains unchanged or is significantly altered (Olson and Langfelder, 1965). Therefore, the Laplace equation predicts that the pressure difference also remains unchanged. In this way, the water pressure within the capillary tube rises to a positive gauge pressure. Similarly, if the air pressure is increased inside the capillary tube, the pressure head will also rise. If the pressure head is fixed or held at constant pressure, both the air and water pressures are known, in which the difference of these two pressures equals to matric suction. The significance of increasing water pressure is related to the translational technique for the

measurement of matric suction, because the water pressure inside a closed chamber is translated upwards with the air pressure origin and away from the metastable states (i.e. negative water pressure regime) (Marinho et al., 2008), via to the more stable state (i.e. liquid phase), as depicted in Figure 2.3.7. In other words, any change in the reference PAP, such as through artificial increase of the atmospheric pressure in which the soil is immersed, is directly translated into an equal increase in matric suction (Hilf, 1956; as cited by Marinho et al., 2008). It is this principle that affords the axis translation technique superior in terms of long term measurement of matric suctions greater than 200 kPa (Mongiovi and Tarantio, 2002).

The translation procedure involves using a pressure plate extractor/chamber, equipped with a saturated high AEV porous disc (Figure 2.3.8). The plate extractor is completely sealed to prevent air advection in and out of the pressure chamber. Matric suction within a soil sample is then measured by increasing the PAP within the axis translation cell, while the PWP is regulated through a saturated interface in contact with the sample.

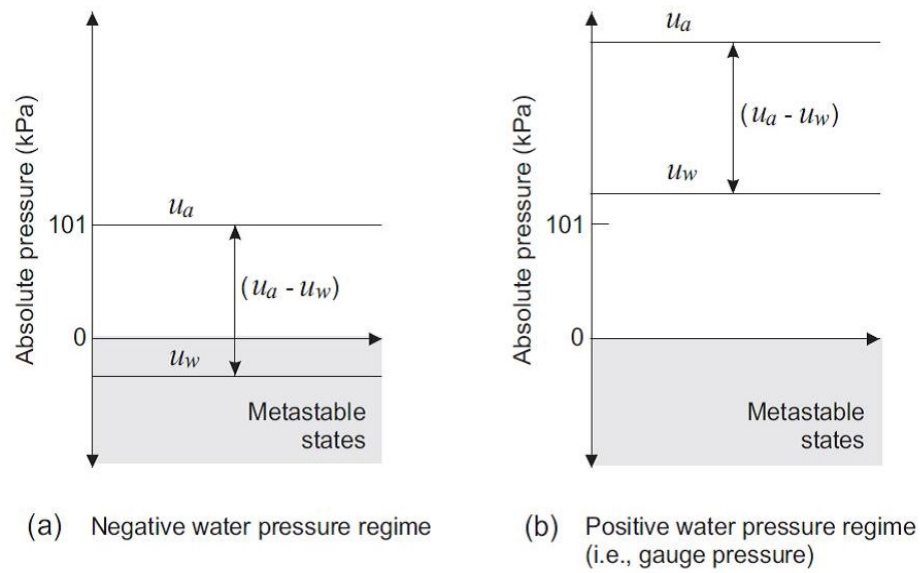


Figure 2.3.7 Axis translation technique to avoid metastable states via to stable states (Marinho et al., 2008)

Unlike tensiometer devices, actual matric suction measurements are usually unaffected by the presence of cavitation nuclei in an imperfectly-saturated high AEV porous disc (Delage et al., 2008; Marinho et al., 2008). The reason for this is that the disc and the water reservoir are never subjected to negative gauge pressure (Marinho et al., 2008). As a result, rigorous pre-saturation procedures such as pre-conditioning of the tensiometers to suppress nucleation sites are not typically followed. Rather an initially dry ceramic porous disc is saturated by submersing under water in a pressure chamber. A measurement of the saturated hydraulic conductivity of the disc is a good indicator of whether saturated conditions are achieved in the system (Marinho et al., 2008). The reliability of actual matric suction measurements using this technique are however, affected by the presence of occluded air bubbles in the system, specifically within the water reservoir, beneath the high AEV porous disc.

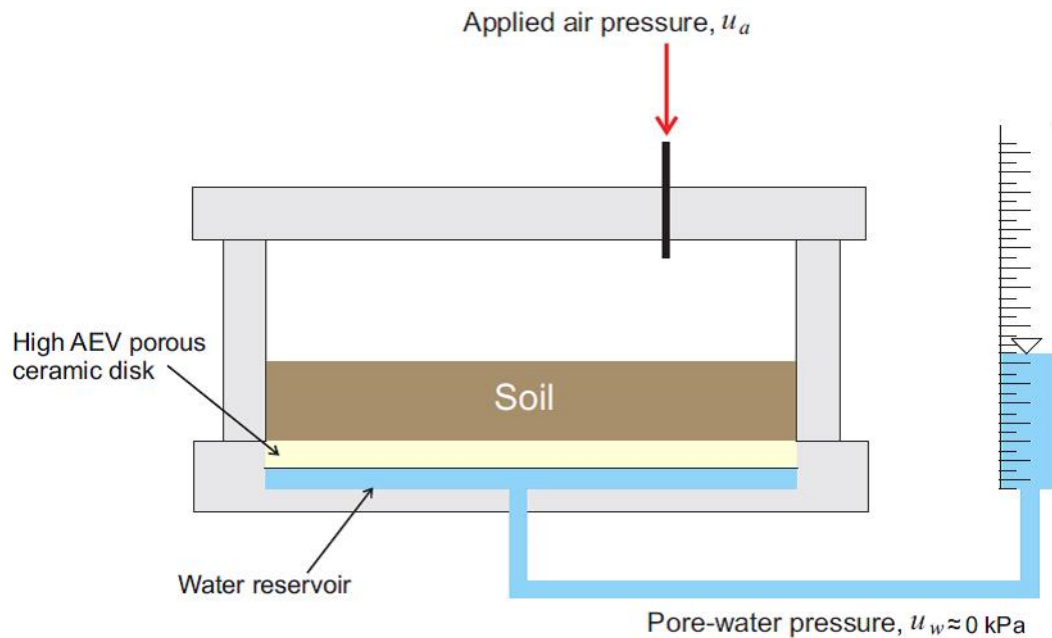


Figure 2.3.8 Schematic of the axis translation test cell

Discontinuities in the water phase are prevented through proper saturation, water recirculation through the line via water reservoir, and establishing good contact between the soil sample and porous disc (Marinho et al., 2005; Marinho et al., 2008; Vanapalli et al., 2008; Delage et al., 2008). It is integral that the porous disc be highly saturated prior to testing and maintained throughout the testing period. A continuous water phase must be maintained at the soil-ceramic boundary and via, the water reservoir to allow water to drain freely as artificial PAP is applied. Any discontinuities in this phase will prevent water from draining, consequently acting as a no flow boundary condition at the liquid-solid contacts (Marinho et al., 2008).

Measurement range of this technique is limited by two factors: (1) the maximum air pressure that can be imposed on the system, and (2) the AEV of the ceramic disk

(Marinho et al., 2008). In practice, the maximum measurable suction using the axis translation technique is strictly a function of the AEV of the porous ceramic disc. The highest AEV of currently available ceramics is nominally a 15 bar or 1500 kPa disc (SoilMoisture Equipment Corporation, 2008). High matric suction measurements can be obtained using the axis translation technique, however careful consideration should be noted when interpreting these results. Suction measurements can also be affected by operational and equipment malfunctions (e.g., imperfect pressure chamber, occluded air bubbles, etc.), yielding erroneous measurement results. Other factors that may affect the reliability of matric suction measurements include: (1) long equilibration times; (2) an initially high degree of saturation of the specimen in question; and, (3) air diffusion through the porous disc (Marinho et al., 2005, 2008; Vanapalli et al., 2008).

Unlike the tensiometer, the axis translation technique does not yield instantaneous results, and so prior to recording any measurement changes, such as the amount of water loss from the soil at an applied air pressure, the system must reach equilibrium. Here, the term equilibrium refers to the time required for a porous media (e.g., soil) to come into equilibrium with a change in air pressure (Marinho et al, 2005). Long equilibrium times may facilitate advection of air flow through the porous disc and produce occluded air bubbles in the water reservoir. This can produce error in the measured volume changes and water loss, because entrapped air is not taken into account. Marinho et al. (2005, 2008) and Vanapalli et al. (2008) have suggested that equilibration times for suction less than 500 kPa will require up to 24 hours; for suctions greater than 500 kPa will require approximately 48 hours; and for suction greater than 1000 kPa will require at least 92

hours. It should however be noted that the equilibration times for these suction measurement ranges are only approximations. The time required for equilibrium to be attained is dependent upon two factors: (1) the initial degree of saturation, and (2) the size of the soil sample being tested. For example, in the absence of soil, equilibrium times (i.e., time required for a porous filter to come into equilibrium with a change in air pressure) is in the order of a few minutes (Marinho et al., 2008). Equilibrium times are longer if the sample is large (Vanapalli et al., 2008).

The initially degree of saturation of a soil sample is also an important variable when determining the reliability of the translational method. If the sample has an initially high degree of saturation then the assumption that the water and solid is sufficiently incompressible is no longer valid (i.e., soil and meniscus deforms). Any free water that is drained during the test will overestimate: the equilibrium time; the volume change; and the AEV of the sample, because air diffusion is greater in free water than in soils (Marinho et al., 2008, and Vanapalli et al., 2008). Any applied pressure for a long period will cause the meniscus to deform (water pressure is no longer constant), nullifying the working principle of the translational technique altogether, because measurement of the pressure differential becomes indeterminate. Long equilibrium times, as well as the presence of air bubbles in the water reservoir will also overestimate the volume changes and water content. More details regarding the successes and failures of this axis translation technique can be found in (Vanapalli et al., 2008).

2.3.3 INDIRECT MEASUREMENT OF OSMOTIC SUCTION

Osmotic suction depends on the concentration of ions dissolved in pore-water. As the soil-water desaturates the concentration of dissolved ions increase, and so does the osmotic component of suction. Osmotic suction can be measured using several indirect methods, such as the saturation extraction method and the pore-fluid squeezer technique. Use of the latter method, involves extracting pore-water from the soil in question. The osmotic suction is determined by measuring the electrical conductivity for the pore-water chemistry for the entire range of osmotic suction (Krahn and Fredlund, 1972). The technique consists of squeezing a soil specimen to extract the macro pore-water and then measuring its electrical conductivity (Pan et al, 2010). The electrical conductivity is related to the total concentration of dissolved ions present in the soil sample. This technique has shown to give the most reasonable measurement of osmotic suction (Krahn and Fredlund, 1972; Zhang et al., 1996). Measurement results of the pore-fluid squeezing technique appears to be affected only by the magnitude of the extraction pressure applied, which in turn, is influenced on the type of soil (Pan et al., 2010).

2.3.4 INDIRECT MEASUREMENT OF TOTAL SUCTION

Total suction measurement techniques are based on measuring the moisture equilibrium condition of the soil rather than measuring or controlling the suction directly. The moisture equilibrium condition of the soil can be determined by primary means as in the vapour pressure, secondary means as through another porous medium or tertiary means as in measuring other physical properties of the porous medium that indicates its moisture equilibrium condition (Bulut and Leong, 2008). Suctions measured through primary

means include an array of psychrometers (e.g., thermocouples, transistors and chilled-mirror types). Suctions measured through secondary and tertiary means include the non-contact filter paper method and thermal and electrical conductivity sensors, respectively. Indirect suction measurements are used for measuring the complete range of soil suction. In this section, three methods of indirect measurement techniques are discussed in more detail: the chilled-mirror dew point technique, and the non-contact filter paper method.

2.3.4.1 CHILLED-MIRROR DEW POINT TECHNIQUE

The working principle of this technique, measures the total suction of a soil by relating the soil-water to the vapour pressure of air in equilibrium with a soil sample (Decagon Devices, 2007). This relationship is defined (previously in Section 2.3.1) by the Kelvin equation (Eqn. 2.3.1]). Put simply, total suction is inferred from measuring the RH of the soil-water. This technique is referred to as the chilled-mirror dew point method, which is used to infer the total suction – that is, the matric and osmotic portion of soil-water energy.

A measuring device, called a chilled-mirror hygrometer / psychrometer utilizes a technique in which the vapour pressure of air is measured using a chilled mirror, and the saturation vapour pressure is obtained from the soil sample temperature (Decagon Devices, 2007). The total suction is measured under isothermal conditions by equilibrating the liquid water phase of the sample with the vapour water phase in the headspace of a closed chamber, and then measuring the vapour pressure of the headspace (Decagon Devices, 2007; Bulut and Leong, 2008). In otherwords, the hygrometer

measures dew point and temperature of the headspace above the soil specimen. The specimen is contained in a special closed chamber to minimize drying of the specimen (Pan et al., 2010). Water vapour of the soil specimen is allowed to condense on the mirror where a photoelectric cell (dew point sensor) is used to detect the exact point at which condensation first appears on the mirror. The dew point sensor measures the dew point temperature of the air, and the infrared thermometer measures the sample temperature. The fan inside the chamber speeds up equilibrium time, as well as controls the boundary layer conductance of the dew point sensor (Decagon Devices Inc., 2005). From these measurements, the vapour pressure of the air in the headspace is computed as the saturation vapour pressure at dew point temperature. The RH of the soil-water is computed when the sample and the air headspace are in equilibrium, the measurement of the headspace vapour pressure and sample temperature (from which saturation vapour pressure is calculated) yields the total suction (Decagon Devices Inc., 2005).

The chilled-mirror technique offers a fundamental characterization of humidity in terms of the temperature at which vapour condenses (Pan et al., 2010). Therefore, temperature control is extremely important, and thus, the measurement difference between dew point and sample temperature must be kept small (Leong et al., 2003), such that the specimen and the device is kept under the same conditions for temperature equilibrium prior to testing. Otherwise, it will result in long equilibration times as well as inaccurate measurement reading. It is also important to avoid contamination of the instrument. Leong et al. (2003) reported that the technique could be used to quantify total suctions as low as approximately 150 kPa, albeit, the value is considered small in the case of total

suction measurement, where much larger error can be expected (Pan et al., 2010). This technique is considered to be the most accurate means for measuring total suction, if the equilibrium between the specimen and the vapour headspace is maintained (Leong et al., 2003; Pan et al., 2010).

2.3.4.2 FILTER PAPER METHOD

An alternative indirect method of measuring total suction works on the principle that the soil-water vapour equilibrates with the surround environment. The filter paper method covers a wide range of suction measurements. For the non-contact technique, a dry filter paper is suspended above the soil specimen in a sealed chamber so that the water vapour between the filter paper and soil specimen reaches equilibrium at a constant temperature (Leong et al., 2002). The vapour space above the specimen acts as a true semi-permeable membrane, which is only permeable to water vapour, and not to its ions from the pore-water (Pan et al., 2010). The separation between the filter paper and the soil by a vapour barrier limits water exchange to the vapour phase only, and prevents solute movement. Therefore, in this technique, total suction is measured. Having achieved equilibrium, the filter paper is removed and water content of the filter paper is determined as quickly as possible to prevent any loss of moisture due to evaporation. Then, by using the appropriate filter paper calibration, the suction of the soil is estimated. Prior to total suction measurements, filter papers are calibrated to determine the relationship between equilibrium water content and RH (Pan et al., 2010). The calibration curve for the non-contact filter paper technique is established using vapour equilibrium technique (e.g. described by Leong et al., 2002).

The filter paper method is a simple and economical technique; it can be reliable if the basic principles of the method are understood, and a strictly practiced laboratory protocol is carefully followed. There are still some concerns however, about the reliability of the filter paper method. For example, the accuracy of the filter paper method is dependent upon the accuracy of the filter paper water content versus suction calibration curve. The calibration technique has been investigated by numerous researchers (e.g. Chandler and Gutierrez, 1986; Bulut et al., 2001; 2002; Leong et al., 2002), in that proper measures be taken into consideration with the calibration equations, where they should be developed specifically for the specific filter paper being used (Pan et al., 2010). Measurement accuracy of the filter paper method should also be considered here as well. Ridley and Wray (1995) found that the measurement accuracy diminishes at the lower range of total suction (Leong et al., 2002). The limitations of the non-contact filter paper method is its long equilibration time and strict protocol needed during the experiment, as compared to the chilled-mirror dew point technique.

2.4 FLOW IN UNSATURATED SOILS

Flow of water through saturated soils is described by Darcy's law (Eqn. [2.4.1]). Darcy's law states that the hydraulic flow rate (or flux) through a soil mass is directly proportional to the pressure gradient and inversely proportional to the length of a soil column (Richards, 1931) called the hydraulic head gradient. Darcy's law may be stated for the vertical direction, y :

$$q = -k_s \frac{\partial h}{\partial y} \quad [2.4.1]$$

where, q is the seepage velocity or Darcy's flux, [m/d]; k_s is the saturated hydraulic conductivity (or coefficient of permeability), [m/d]; and $(\partial h/\partial y)$ is the hydraulic head gradient with respect to the depth y , [m/m].

The saturated hydraulic conductivity can vary more than 10 orders of magnitude (i.e., gravels to clay) (Fredlund et al., 1994), and is relatively constant for any given soil that is completely saturated (when void spaces are completely filled with water). Flow through saturated soils are dominated by the gravitational water alone, where proportionality existing between the hydraulic conductivity and the flux. This relationship does not extend between the two parameters for an unsaturated soil, because the intergranular pore space is shared by a fraction of both air and water.

By making use of the Darcy's Law, Richards (1931) derived an equation that was analogous of Poiseuille's Law (i.e., laminar flow of liquids through capillary tubes) to describe flows through partially saturated media. Applying the mass conservation principle in the vertical direction, such that the mass inflow, minus the mass outflow is equal to the change in storage, yields:

$$-\frac{\partial q}{\partial y} = \frac{\partial \theta}{\partial t} \quad [2.4.2]$$

where, $-(\partial q/\partial y)$ is the change in flux in a downward vertical direction, y , relative to the datum, $y = 0$, and $(\partial\theta/\partial t)$ is the volumetric (or change in) storage.

In an unsaturated soil system, water between the soil particles cannot drain freely by means of a pressure head gradient and gravity alone, but rather through capillary potentials (matric suctions), which are interdependent upon the water content. The hydraulic conductivity thus, becomes non-linear as well, such that:

$$K = K(\theta, \psi) \quad [2.4.3]$$

where, K is the unsaturated hydraulic conductivity as a function (HCF) of the water content, θ or suction ψ , [m/d]. By substituting the HCF into Darcy's flux (Eqn. [2.4.1]), and substituting the expression into the left-hand side of Eqn. [2.4.2], yields a 1-D unsaturated flow equation, also referred to as Richards (1931) equation for an unsaturated porous media. The 1-D unsaturated flow equation may be stated in terms of volumetric storage – referred to as the '*mixed*' form of the Richards equation (Thode, 2008):

$$\frac{\partial\theta}{\partial t} = -\frac{\partial}{\partial y} \left[K(\theta) \frac{\partial h}{\partial y} \right] \quad [2.4.4a]$$

Alternatively, it may be stated in terms of total head – referred to as the '*h-base*' (Thode, 2008):

$$-S_s \frac{\partial h}{\partial t} = \frac{\partial}{\partial y} \left[K(\psi) \frac{\partial h}{\partial y} \right] \quad [2.4.4b]$$

where, S_s is the specific storage, [m^{-1}]; $K(\psi)$ is the unsaturated (HCF) as a function of matric suction, [m/d]; and, h is the total head, which is equal to the pressure head plus the elevation head ($h = h_p + z$), [m]. The compressibility of a soil system due to the change in PWP at saturation, which is defined by:

$$m_v = \frac{S_s}{\gamma_w} \quad [2.4.5]$$

where, γ_w is the bulk unit weight of water, [N/m^3]; and, m_v is the coefficient of compressibility (or volume change), [kPa^{-1}], which is equal to the derivative with respect to matric suction of the water-retention curve (WRC). The above equation is posed using the total head as the primary variable, however, PWP and suction can be used instead to produce identical results (Thode, 2008).

Equation [2.4.4] is a 2nd order partial differential equation (PDE), whose solution is quite complicated due to non-linear dependency of the suction head, water content and unsaturated hydraulic relationships (Lee, 2007). A number of commercial finite element models are routinely used to solve numerically the PDE in the unsaturated zone. This usually requires predetermination and/or measurement of the hydraulic properties of porous material; namely, the water-retention curve (WRC), also referred to as the soil-water characteristic curve (SWCC), and the unsaturated HCF.

Several laboratory tests are used as a direct measurement of the required soil properties. For example, a modified direct shear test can be used to measure the relationship between

matric suction and shear strength (Fredlund et al., 1997). Often times however, direct methods are not possible due to a number of reasons (given by Mualem, 1986, and among others) as being costly and time-consuming, and properties being hysteretic in nature, etc. Therefore, it may be necessary to revert to indirect procedures to estimate the water retention properties. Several empirical and statistical methods pertinent to this study are discussed in subsequent sections.

2.4.1 WATER CONTENT-SUCTION RELATIONSHIP

The WRC is a function that describes the relationship between the water content and soil suction. This relationship is usually expressed in terms of water content, either on a gravimetric basis (i.e. gravimetric water content) or volumetric basis (volumetric water content), where both variables define the amount of water contained in within the pore spaces of a soil. Another commonly used term to indicate the percentage of voids that are filled with water is the degree of saturation. These variables can also be used in a normalized form, where the water contents are referenced to a residual water content (Fredlund and Xing, 1994).

Some primary characteristics of a WRC for any soil under consideration are provided in Figure 2.4.1. A typical WRC is always comprised of an upper bound and/or lower bound. The upper and lower boundaries are referred to as the desorption (or drying) curve, and the adsorption (or wetting) curve, respectively. In between these two boundaries lie infinite scanning curves that are unique as a result of soil hysteresis – a soil's history of having been subjected to cycles of wetting and drying processes (i.e.,

climatic changes). Other key components of a WRC are the saturation suctions or residual air content (saturation zone), the air-entry value (AEV), and matric suction range (desaturation zone), and the residual water content beyond the desaturation zone (in the residual zone). The AEV (also referred to as the bubbling pressure) it is the matric suction where air starts to enter the largest pore spaces. For example, on the drying path, the AEV is the maximum matric suction at 100% saturation, where water is held under tension, which is referred to the ‘tension-saturated’ zone. This is where initial, displacement of the liquid water with air, occurs. Further desaturation along the drying path would require matric suctions greater than the AEV, since water desaturates from larger pores to smaller pore (i.e. Laplace equation) until residual water content is reached. The residual water content (θ_r) is defined as the water content where a large suction change is required to remove additional water from smaller pores. The total suction corresponding to water content approaching zero is approximately 10^6 kPa (Fredlund and Xing, 1994). This appears to be essentially the same for all types of soils (i.e., Richards, 1965; Fredlund and Xing, 1994; Fredlund et al., 1994), such that there is a maximum suction value that corresponds to a zero relative humidity in any given soil. The WRC for any given soil is also a function of pore-geometry (i.e. Laplace equation). Thus, the water content at saturation (θ_s), and the AEV will generally increase with a smaller grain-size soil. Many models have been developed to show the relationship between the WRC and the PSD (i.e. Fredlund et al., 1997; Simms and Yanful, 2002; 2004).

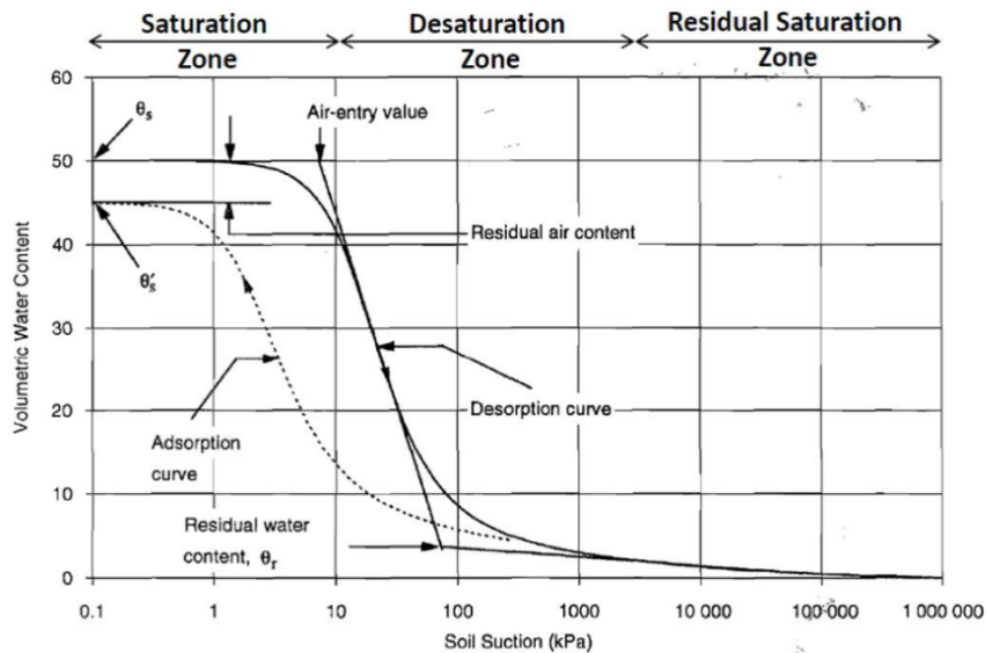


Figure 2.4.1 Typical desorption and adsorption curves for a fine-grain soil at its saturated water content, θ_s (Fredlund and Xing, 1994)

2.4.1.1 EXPERIMENTAL MEASUREMENT OF THE $\theta(\psi)$ RELATIONSHIP

Experimental measurement of the WRC is achieved by measuring the water content at any given suction, by means of direct or indirect methods. The determination of the volumetric water content (VWC) or degree of saturation in a soil requires information on gravimetric water content (GWC), and sometimes the void ratio. Volume change measurements are recommended (Fredlund and Rahardjo, 1993; Fredlund, 1999; 2006) deformable soils, especially when other material parameters are required (e.g., AEV at saturation, the coefficient of volume change, and shrinkage limit).

Water contents are obtained by measuring the change in mass of the soil specimen, and tracking its volume changes of the soil structure after equilibrium is attained at each

suction measurement during incremental stages of testing, such that the WRC can be ascertained for a given soil. A summary of the direct and indirect methods of suction measurements are provided in Table 2.4.1. An entire range of suctions can be measured by combining methods to measure matric suctions and total suctions.

Table 2.4.1 Summary of suction measurement methods (adapted from Pan et al., 2010)

		Technique (Method)	Suction range (kPa)	Equilibrium time
Direct suction measurement	Matric	Axis translation technique Pressure transducer	0 - 1500	hours minutes
Indirect suction measurement	Osmotic	Pore-squeezing technique	0 - 15000	Days
Indirect suction measurement	Total	Chilled-mirror hygrometer Non-contact filter paper	150 - 300000 all	10 minutes 7 - 14 days

The WRC can be easily measured experimentally; the same cannot be regarded for the hydraulic conductivity function (HCF). Mualem (1986) discusses the main reasons why the HCF is not routinely measured directly, but rather estimated through use of either empirical equations or statistical models. The use of these models however, requires pre-determination of the WRC and the saturated hydraulic conductivity. Presented in this next section (Section 2.4.1.2) are some empirical equations are used to fit the experimental WRC of any soil under consideration.

2.4.1.2 EQUATIONS FOR THE WATER-RETENTION CURVE

The empirical approach of estimating the water content-suction relationship consists of using a mathematical formula that fits best with the available WRC data. These equations can be divided into two categories of two-parameter equations and three-parameter equations (Fredlund and Xing, 1994). The first variable bears the relationships to the AEV of the soil, while the second variable describes the shape of the WRC – the rate at which the soil desaturates or saturates. The third variable, if present in the model describes the shape of the WRC at low suction range near the AEV, which is independent of the high suction range near the residual water content (Fredlund, 2006). It is more common to express water contents or the degree of saturation in terms of normalized variables for modelling purposes, which takes on the form of (Fredlund and Xing, 1994):

$$\Theta = \frac{\theta - \theta_r}{\theta_s - \theta_r} = \frac{V_w / V}{V_v / V} = \frac{V_w}{V_v} = \frac{S - S_r}{S_s - S_r} = S_e \quad [2.4.6]$$

where, Θ is the normalized volumetric water content or relative degree of saturation, S_e ; V_w is the volume of water, [cm^3]; V_v is the volume of voids, [cm^3]; θ_s is the saturated volumetric water content; and, θ_r is the residual volumetric water content.

Similarly, if the GWC is referenced to zero water content, the normalized GWC can be written as follows (Fredlund et al., 1994):

$$w' = \frac{w}{w_s} = \frac{M_w / M_p}{M_{ws} / M_p} = \frac{M_w}{M_{ws}} = \frac{V_w \gamma_w}{V_v \gamma_w} = \frac{V_w}{V_v} = S_e \quad [2.4.7]$$

where, w' is the normalized GWC or relative degree of saturation, S_e ; w_s is the saturated GWC; M_w is the weight of water, [g]; M_p is the weight of soil particles, [g]; M_{ws} is the weight of water when the soil is at saturation, [g]; V_w is the volume of water, [cm³]; V_v is the volume of voids, [cm³]; and, γ_w is the bulk unit weight of water, [N/m³].

Several empirical models have been proposed over the years to describe the water-retention behaviour. A number of these models are listed in Table 2.4.2. Among the earliest of such, was proposed by Brooks and Corey (1964), in the form of a power-law relationship:

$$\Theta = \left(\frac{\psi_b}{\psi} \right)^\lambda \quad [2.4.8]$$

where, ψ_b is the bubbling pressure or AEV, [kPa]; ψ is the soil suction, [kPa]; and, λ is the pore-size distribution index. The Brooks and Corey (1964) model has been verified through several studies (as cited by Fredlund and Xing, 1994), however, studies have been limited to data for relatively homogenous and isotropic samples, where the PSD curves were quite narrow, where a rapid change in suction occurred at low suctions (i.e., very steep slope) beyond the AEV (Leji et al., 1996). The Brooks and Corey (1964) implies that the WRC there is a sharp discontinuity in suctions near saturation (Fredlund

and Xing, 1994) – this is particularly characteristic of some coarse-grain sands, however most medium-to-fine soils show a gradual transition in the AEV region near saturation. Therefore, the Brooks and Corey (1964) equation appears only to be valid for suctions beyond the AEV. In contrast, van Genuchten (1980) proposed an equation that described a continuous function in the AEV region near saturation (van Genuchten, 1980):

$$\Theta = \left[1 + (\alpha\psi)^n \right]^{-m} \quad [2.4.9]$$

where, α , m , and n are fitting parameters and are functions of the soil properties. This equation provides a more flexibility than other WRC models. van Genuchten (1980) related parameters m and n through the equation, $m = 1 - 1/n$ to obtain a closed-form expression for the relative coefficient of permeability function. Many authors (as cited by Mualem, 1986) have discussed the validity range of the related parameters, and thus, it has been suggested (Fredlund et al., 1994; and, Fredlund and Xing, 1994) that leaving m and n with no fixed relationship to achieve more accurate results. Fredlund and Xing (1994) suggested that van Genuchten (1980) WRC model has its own limitations, such that the empirical equation is only applicable at suctions less than residual conditions, whereas experimental data has shown that after the residual water content, the plot should decrease linearly to a value of approximately 10^6 (Fredlund and Xing, 1994). Fredlund and Xing (1994) proposed a WRC equation that uses a least-squares algorithm to determine the best-fit parameters for experimental data. The Fredlund and Xing (1994) model that defines the entire range of the WRC (i.e., 0 – 10^6 kPa) is given by follows (Fredlund et al., 2011):

$$w(\psi) = \theta(\psi) = C(\psi) \frac{w_s}{\left\{ \ln \left[e + (\psi/a)^n \right] \right\}^m} \quad [2.4.10]$$

where, $w(\psi)$ is the water content at any soil suction; w_s is the saturated water content; and a , n , and m are fitting parameters associated with the WRC. The variable e is the base of the natural logarithm. The correction factor, $C(\psi)$ is written as follows (Fredlund et al., 2011):

$$C(\psi) = 1 - \frac{\ln(1 + \psi/\psi_r)}{\left\{ \ln \left[1 + (10^6/\psi_r) \right] \right\}} \quad [2.4.11]$$

where, ψ is the soil suction, and ψ_r , is soil suction at residual conditions; both have a unit of [kPa]. Fredlund and Xing (1994) equation is based on the assumption that the shape of the WRC is dependent upon the pore-size distribution (PSD) of the soil – in other words, the desaturation is a function of the PSD, which takes on the form of an integrated frequency distribution curve (Fredlund et al., 1994). The correction factor that takes into account the interconnecting pores of a soil, which are randomly distributed (Fredlund and Xing, 1994). The main advantages of the van Genuchten (1980) and the Fredlund and Xing (1994) equations are that both can be used to obtain the hydraulic conductivity function.

Table 2.4.2 Water-retention curve models (Sillers and Fredlund, 2001)

Model	Equation	
Brooks and Corey (1964)	$\Theta_d = 1$	$\psi < AEV$
	$\Theta_d = (\psi/a_c)^{-n_c}$	$\psi > AEV$
Brutsaert (1966)	$\Theta_d = 1/(1 + (\psi/a_r))^{-n_r}$	
McKeey and Bumb (Boltzman exponential form)	$\Theta_d = 1$	$\psi < AEV$
	$\Theta_d = \exp((a_z - \psi)/n_z)$	$\psi > AEV$
Fredlund and Xing (1994)	$\Theta_d = \left(1/\ln(e + (\psi/a_f)^{n_f})\right)^{m_f}$	
Gardner (1956)	$\Theta_d = 1/(1 + a_g \psi^{n_g})$	
van Genuchten (1980)	$\Theta_d = \left(1/(1 + (a_v \psi)^{n_v})\right)^{m_v}$	
van Genuchten (1980) – Burdine (1953)	$\Theta_d = \left(1/(1 + (a_b \psi)^{n_b})\right)^{(1-2/n_b)}$	
van Genuchten (1980) – Mualem (1976)	$\Theta_d = \left(1/(1 + (a_m \psi)^{n_m})\right)^{(1-1/n_m)}$	

Definition of variables: Θ_d is the dimensionless water content; a is the first soil fitting parameter; n is the second soil fitting parameter; and, m is the third soil fitting parameter

2.4.2 UNSATURATED HYDRAULIC CONDUCTIVITY

The permeability of an unsaturated soil is not a constant, but rather a function of the VWC, which in turn, is dependent upon suction. Soil suction is one of the two stress state variables that control the behaviour of soils (Fredlund et al., 1994); therefore, it seems only appropriate within this context that the term, permeability or hydraulic conductivity function (HCF) be to represented in terms of suction, $K(\psi)$. It is more common to represent the HCF in terms of its relative permeability:

$$k_r(\psi) = \frac{K(\psi)}{k_s} \quad [2.4.12]$$

where, $k_r(\psi)$ is the relative permeability; $K(\psi)$ is the permeability at a given suction, [m/d]; and k_s is the saturated permeability, [m/d].

2.4.2.1 EQUATIONS FOR THE HYDRAULIC CONDUCTIVITY FUNCTION

There are a number of mathematical equations that have been proposed to estimate the unsaturated HCF, also commonly referred to as the water permeability function. These models are categorized as empirical equations and theoretical / statistical equations (Fredlund, 2006). Empirical equations can be used to estimate the HCF by fitting a mathematical equation to the available hydraulic conductivity data or using an “indirect” approach by measuring water content distribution profiles, infiltration rate, or cumulative infiltration under prescribed boundary conditions (Mualem, 1986). Several empirical equations to estimate the HCF are listed in Table 2.4.3. One major restriction of such

models is that there is no single formula valid for all types of soils. Statistical models do however; provide more flexibility than the empirical models.

Table 2.4.3 Empirical equations for the unsaturated coefficient of permeability $k(\psi)$ (Fredlund et al., 1994)

Function	Reference
$k = k_s$, for $\psi \leq \psi_{aev}$	Brooks and Corey (1964)
$k_r = (\psi / \psi_{aev})^{-n}$ for $\psi \geq \psi_{aev}$	
$k_r = \exp(-\alpha\psi)$	Gardner (1958)
$k = k_s / (a\psi^n + 1)$	
$k = a\psi + b$	Richards (1931)
$k = k_s$ for $\psi \leq \psi_{aev}$	Rijtema (1965)
$k_r = \exp[-\alpha(\psi - \psi_{aev})]$ for $\psi_{aev} \leq \psi \leq \psi_1$	
$k = k_1 \left(\frac{\psi}{\psi_1} \right)^{-n}$ for $\psi > \psi_1$	
$k = \alpha\psi^{-n}$	Wind (1955)

Notes: ψ_1 is the residual soil suction (i.e., ψ_r), and k_1 is the coefficient of permeability at $\psi = \psi_1$.

Theoretical models are derived as macroscopic and microscopic statistical models, which are based on assumptions regarding the PSD and interpretation of the WRC, such as the AEV (Fredlund, 2006; Mualem, 1986). Statistical models make use of both the WRC and the saturated hydraulic conductivity, which are primarily determined by the PSD of a given soil. The difference between the macro- and microscopic models are the assumptions made about the PSD. For example, micro- models are based on a random variation of pore-size, whereas macro- models are based on uniformly distributed pore-size. A more comprehensive review of these assumptions can be found in (Mualem, 1978).

The macroscopic models provide an analytical, closed-form equation for the unsaturated hydraulic conductivity. These models take on a more general form (Fredlund, 2006):

$$k_r(S_e) = S_e^\eta \quad [2.4.13]$$

where, k_r is the relative hydraulic conductivity (or relative permeability), which is equal to any coefficient of permeability divided by the saturated coefficient of permeability; S_e is the effective degree of saturation, or normalized volumetric water content (i.e., Eqn. [2.4.6]); and, η is a fitting parameter. The value of the fitting parameter, η , depends on the assumptions made in deriving the hydraulic conductivity equations. For example, the Brooks and Corey (1964) model showed that for a soil with a uniform PSD index, the exponent is equal to $\eta = (2 + 3\lambda/\lambda)$, while Mualem (1976) suggests using $\eta = 3 - 2m$ (Fredlund, 2006).

The saturated hydraulic conductivity and the WRC(s) are used to solve the integral form of the statistical models, such as proposed by Burdine (1953), Childs and Collis-George (1950), and Mualem (1976a), and thereby compute a HCF. Models that are more commonly used are the closed-form analytical models proposed by van Genuchten (1980), which makes use of the statistical models proposed by Burdine (1953):

$$k_r(\psi) = \frac{1 - (\alpha\psi)^{n-2} [1 + (\alpha\psi)^n]^{-m}}{[1 + (\alpha\psi)^n]^{2n}}, \quad m = 1 - \frac{2}{n} \quad [2.4.14]$$

And, Mualem (1976b):

$$k_r(\psi) = \frac{\{1 - (\alpha\psi)^{n-1}[1 + (\alpha\psi)^n]\}^2}{[1 + (\alpha\psi)^n]^{1/2}}, \quad m = 1 - \frac{1}{n} \quad [2.4.15]$$

where, both models utilize different fitting parameters, m (van Genuchten, 1980).

Fredlund et al. (1994) makes use of the Fredlund and Xing (1994) and solved the Childs and Collis-George (1950) microscopic model with the Fredlund and Xing (1994) WRC model (Eqn. [2.4.10]) (Fredlund et al., 1994):

$$k_r = \frac{\int_{\psi}^{\psi_r} \frac{\theta(y) - \theta(\psi)}{y^2} \theta'(y) dy}{\int_{\psi_{AEV}}^{\psi_r} \frac{\theta(y) - \theta_s}{y^2} \theta'(y) dy} \quad [2.4.16]$$

where, ψ_r is the suction corresponding to the residual water content, [kPa]; ψ_{AEV} is the air-entry value, [kPa]; y is a dummy variable of integration, representing suction; and θ' is the derivative of Eqn. [2.4.10].

The closed-form HCF(s) proposed by van Genuchten (1980), Fredlund et al. (1994), Brooks and Corey (1964), and Campbell (1974) are presented in Table 2.4.4. A more comprehensive review of some of the aforementioned statistical models is discussed by Mualem (1986).

Table 2.4.4 Some statistical hydraulic conductivity functions based on the water-retention curves and saturated hydraulic conductivity (Ebrahimi et al., 2004; as cited by Fredlund, 2006).

Models	References for the water-retention curve			
	van Genuchten (1980)	Fredlund & Xing (1994)	Brooks & Corey (1964)	Campbell (1974)
Childs & Collis-George (1950)	---	$k_r = \frac{\int_{\psi}^{\psi_r} \frac{\theta(y) - \theta(\psi)}{y^2} \theta'(y) dy}{\int_{\psi_{AEV}}^{\psi_r} \frac{\theta(y) - \theta_s}{y^2} \theta'(y) dy}$	---	$k_r = \left(\frac{\psi}{\psi_{AEV}} \right)^{-2\left(\frac{2}{b}\right)}$
Burdine (1953)	$k_r(\psi) = \frac{1 - (\alpha\psi)^{n-2} [1 + (\alpha\psi)^n]^{-m}}{[1 + (\alpha\psi)^n]^{2n}}$ $m = 1 - \frac{2}{n}$	---	$k_r(\psi) = (\alpha\psi)^{-2-3\lambda}$	---
Mualem (1976b)	$k_r(\psi) = \frac{\{1 - (\alpha\psi)^{n-1} [1 + (\alpha\psi)^n]\}^2}{[1 + (\alpha\psi)^n]^{1/2}}$ $m = 1 - \frac{1}{n}$	---	---	---

Definition of variables: k is the unsaturated coefficient of permeability; k_s is the saturated permeability coefficient; k_r is the relative permeability; α and λ are fitting parameters; and, y is a dummy variable.

2.5 MODELS FROM SOIL MECHANICS

Characteristics of CPB have been considered to interact and behave, similar to cemented soils. In the past, cemented soil models assumed that the material behaved perfectly plastic, because of the brittle and rigid inter-particle binding (Vatsala et al., 2001; Fourie et al., 2007). Elastoplastic models have also been used to define the stress-strain behaviour of cemented materials; however, Fourie et al. (2007) conferred that cemented soils demonstrate anything but rigid or plastic, despite the addition of a binder. Just because porous material contains a binder does not mean that fundamental soil mechanics principles are not available to understand such materials (Fourie et al., 2007). In the scope of this research, the aforementioned models are not discussed further.

One of the most important principles in soils mechanics is the effective stress, which originated from Terzaghi's (1923) principle for saturated soils. The effective stress principle may be stated as:

$$\sigma' = \sigma - u_w \quad [2.5.1]$$

where, σ' is the effective stress, which represents the average stress carried by the solid matrix (or skeleton), equal to the total pressure, σ , minus the PWP, $[u_w = \rho_w g h_p = \rho_w g (H_T - z)]$.

It is not uncommon that mining operations employ CPB mixtures containing fine-grained tailings with rates that often result in more than 10m vertical rise per day (le Roux, 2004). The combination of PSD and fill rates has important ramifications on the rate of

consolidation and strength gain in CPB. The consolidation behaviour may be studied using two consolidation models: the traditional 1-D small-strain consolidation theory, and the 1-D large-strain consolidation theory, which have been described in Section 2.5.1 and 2.5.2, respectively.

2.5.1 SMALL-STRAIN CONSOLIDATION MODEL

The generalized form of the small-strain consolidation model is derived from Terzaghi's (1923, 1936) 1-D consolidation theory. This theory assumes that during the consolidation process (Priestley et al., 2011): all voids are completely filled with water; water and soil are incompressible (i.e., densities are constant); Darcy's law is valid; the permeability and compressibility are both constant; the relationship between the void ratio / change in volume and effective stress is linear; strains are infinitesimal; and self-weight loading of a soil is neglected. Terzaghi's (1923, 1936) 1-D consolidation equation in the vertical direction, y , may be stated as:

$$\frac{\partial u_w}{\partial t} = c_v \frac{\partial^2 u_w}{\partial y^2} \quad [2.5.2]$$

where, c_v is the coefficient of consolidation, and u_w , is the PWP. This fundamental equation is used to predict the settlement or the dissipation of the PWP.

In above equation, the PWP or total head is the dependent variable, whose boundary conditions are generally no flow and/or constant pressure (Bangoyina, 2008). The

primary disadvantage of using pressure, as a dominant variable seems to be that in a large deformation formulation becomes highly non-linear (Bangoyina, 2008).

2.5.1.1 DAVIS AND RAYMOND MODEL

Based on the Terzaghi (1923, 1936) 1-D consolidation theory, Davis and Raymond (1965) derived a fully coupled, non-linear consolidation equation, which takes into account the variations of permeability and compressibility of the soil during the consolidation process by using the effective stress as the independent variable (Bangoyina, 2008). During the consolidation process, the model assumes that the decrease in permeability is proportional to the decrease in compressibility:

$$c_v = \frac{k}{m_v \gamma_w} \rightarrow k = c_v m_v \gamma_w \quad [2.5.3]$$

where, c_v is the coefficient of consolidation; m_v is the coefficient of compressibility (or volume change); k is the permeability; and γ_w is the bulk unit weight of water.

The Davis and Raymond (1965) 1-D small-strain consolidation model in the vertical direction, y , may be stated as (Bangoyina, 2008):

$$\frac{\partial \sigma'}{\partial t} = -c_v \sigma' \left[\frac{1}{\sigma'} \frac{\partial^2 u_w}{\partial y^2} - \left(\frac{1}{\sigma'} \right)^2 \frac{\partial u_w}{\partial y} \frac{\partial \sigma'}{\partial y} \right] \quad [2.5.4]$$

Findings were reported that when deformation of the soil was taken into account, PWP dissipation occurred at a slower rate than the Terzaghi equation (Eqn. [2.5.2])

(Bangoyina, 2008). The result of this is a relatively constant coefficient of consolidation while including the nonlinear properties of permeability and compressibility, this formulation still assumes infinitesimal strains (Bangoyina, 2008; Priestley et al., 2011).

It has been shown (e.g., Gibson et al., 1967; Schiffman et al, 1985; as cited by Feldkamp, 1989) that the compressibility of a saturated soil is a non-linear function of effective stress. When large strains take place, the soil skeleton significantly deforms, resulting in a decrease in the void ratio, which non-linearly relates to an increase in effective stress (Bangoyina, 2008). Conversely, a smaller void ratio would result in a decrease in permeability due to water. To that end, these constitutive relationships need to be considered if large deformations are to be expected.

2.5.2 LARGE-STRAIN CONSOLIDATION MODEL

In contrast, the Gibson et al., (1967, 1981) large-strain theory is based on the large deformations, compared to the thickness of the compressible layer, which occurs due to the consolidation process (Lei et al., 1996). Gibson's equation assumes that the compressibility, α ; the permeability, k ; and the effective stress, σ' , to behave non-linearly, because it is a function of the void ratio, e , (Helinski et al., 2007b; Uchaipichat, 2011):

$$\alpha = \alpha(e) \quad [2.5.5]$$

$$k = k(e) \quad [2.5.6]$$

$$\sigma' = \sigma'(e) \quad [2.5.7]$$

This theory assumes that during the consolidation process (Priestley et al., 2011): all voids are completely filled with water; water and soil are incompressible; Darcy's law is valid; the permeability, compressibility, and effective stress are non-linear with respect to the change in volume; and deformations are large due to self-weight loading. The form of the Gibson 1-D consolidation equation may be stated as (Helinski et al., 2007c):

$$\underbrace{\frac{\delta u_w}{\delta t}}_{(A)} + \underbrace{\left[(1+e_o) \frac{\delta \sigma'}{\delta e} \right]}_{(D)} \left\{ \underbrace{\frac{\delta}{\delta a} \left[\frac{k}{\gamma_w} \left(\frac{1+e_o}{1+e} \right) \frac{\delta u_w}{\delta a} \right]}_{(C)} + \underbrace{\frac{\delta k}{\delta a}}_{(B)} \right\} = \frac{\delta \sigma}{\delta t} \quad [2.5.8]$$

where, a is a Lagrangian coordinate; u_w is the PWP; k is the hydraulic conductivity; e is the void ratio; σ' is the vertical effective stress; and σ is the total stress. In this equation, the term A is the rate of change in PWP as a result of a rate of application of the total stress (term B), term C is the volumetric strain, which is controlled by the permeability of the material, k , and the hydraulic gradient ($\delta u_w / \delta a$), and term D describes the current stiffness of the material (Helinski et al., 2007c).

The constitutive non-linear relationships connecting the compressibility, the permeability, and effective stress with void ratio are presumed to exist and take on the following form (Feldkamp, 1989; Helinski et al., 2007c):

$$\alpha(e) = \frac{\alpha e^{a_c}}{(1+e)} \quad [2.5.9]$$

$$k(e) = \frac{c_k (e)^{d_k}}{(1+e)} \quad [2.5.10]$$

$$e = a_c (\sigma')^{b_c} \quad [2.5.11]$$

where, a_c and b_c are soil compression constants with values depending on the units of σ' ; and, c_k and d_k are permeability constants (Helinski et al., 2007c).

It has been reported (e.g., by Feldkamp, 1989; Lei et al., 1996; Priestley et al., 2011) that the use of the Gibson equation properly accounts for the solid-phase and liquid-phase transport as well as for arbitrary material properties to be used in the model (Feldkamp, 1988). For example, larger Poisson ratio will result in greater consolidation (Priestley et al., 2011).

2.5.2.1 LARGE-STRAIN, FULLY COUPLED WITH SELF-DESICCATION

Helinski and co-workers developed a fully coupled, large-strain consolidation-hydration model (Helinski et al., 2007a, b, c; 2010; 2011) that takes into account self-desiccation (Helinski et al., 2011):

- Degree of consolidation is strictly due to the change in void ratio; however, Yilmaz et al. (2008) have reported that consolidation occurs less for pastes with higher binder content.
- Increased stiffness of the solid matrix due to paste hydration and compression of the solid skeleton

- Decreased in permeability of the paste material due to the growth of cement gel in the pore spaces and reduction in void ratio due to the compression of the solid matrix.
- Net volume loss that occurs due to the result of hydration ('chemical shrinkage'), leading to the effect of self-desiccation. Hydration acts as an internal 'sink' for water, which has been investigated by Powers and Brownyard (1947) (Brouwers, 2004; 2005), and Acker (2005).

Helinski and co-workers' model is based upon the assumption that CPB stopes are fully saturated. They suggested that combination of rapid filling rate and the fine grain of material means that the self-weight loading conditions may often be closer to undrained scenario (Helinski et al., 2006). Therefore, Helinski et al. (2007a) developed an analytical model to account for self-desiccation under an undrained analysis. A fully-coupled 2D numerical model, under the name of CeMinTaCo (Helinski et al., 2007c) was later developed, demonstrated and compared them against experimental results as well with in-situ measurements (Helinski et al, 2007b; 2011). The numerical results were shown to be in very good agreement, especially with regards to PWP estimates (Helinski et al., 2007a). Helinski et al. (2007b) showed that in some cases, incorporating self-desiccation produced results that were counter-intuitive; specifically with regards to consolidation. The investigators found that the greatest degree of consolidation in reducing PWPs occurred with backfill whose permeabilities were lower. This finding essentially implied that the rate of consolidation or how quickly PWPs dissipated were dependent upon how and to what degree self-desiccation occurred.

2.5.3 CONSOLIDATION MODELS AND UNSATURATED FLOW MODEL

A brief summary, outlining important differences between the small- and large- strain consolidation models have been compared, superficially in Table 2.5.1.

Table 2.5.1 Key differences between the small- and large- strain consolidation models and the unsaturated flow model

1-D Model	Flow Regime	Coordinate Systems	Independent Variable	Permeability	Stiffness
Davis & Raymond (1965)	Darcy's law	Eulerian	Effective stress (σ')	$k = c_v m_v \gamma_w$	$m_v \propto k$
Gibson et al. (1967, 1981)	Darcy's law	Lagrangian	Void ratio (e)	$k(e) = c_k (e)^{d_k} / (1+e)$	$\uparrow m_v; \downarrow e$
Richards (1931)	Unsaturated	Eulerian	PWP or ψ	$K = K(\psi)$	$m_v \propto \Delta V_v / V_T$

It has been demonstrated on a limited study (Bangoyina, 2008) that simulates the PWP's in hardening grout and a cohesive soil using the small-strain consolidation model tend to underestimate its distribution compared to the large-strain consolidation model, when comparing the numerical results with experimental measurements. Bangoyina (2008) reported these discrepancies between the models due to the assumption wherever the coefficient of permeability was considered constant. Further, large deformity found in cohesive soils was due to the permeability, which varied during the consolidation process. This was also confirmed by Priestley et al. (2011). As the effect of this change, permeability will diminish progressively and consequently the rate of consolidation (bleeding) will also decrease and tends for some time to become equal or less than that

assumed in the small-train theory (Bangoyina, 2008). Therefore, the discrepancy between consolidation (displacement or excess PWP dissipation) predict by both models will decrease or at most remain unchanged after some time (Bangoyina, 2008).

CHAPTER 3

3 AN UNSATURATED FLOW THEORY FRAMEWORK

Distribution of pore-pressures in CPB material may be delineated by a modified 1-D unsaturated flow model. Current models, such as the fully coupled large-strain consolidation model, evaluated stress distributions throughout CPB stopes in undrained cases, where hydrating paste fill material was fully saturated. Evidence, such as the evolving saturated hydraulic conductivity, pore-pressure dissipation and matric suction generation in laboratory and field environments, may suggest that hydrating CPB material may become unsaturated, because of self-weight consolidation, coupled with the self-desiccation phenomenon. To that end, a modified one-dimensional unsaturated flow model to estimate the distribution of PWPs has been proposed.

3.1 A MODIFIED 1-D UNSATURATED FLOW EQUATION

Dissipation of PWPs and/or generation of matric suction in hydrating CPB stopes may be estimated by a modified 1-D unsaturated flow equation (Eqn. [2.4.4]), which may be stated as:

$$-\gamma_w m_v \frac{\partial h}{\partial t} = \frac{\partial}{\partial z} \left[K(\psi) \frac{\partial h}{\partial z} \right] - S_k \quad [3.1.1]$$

where, γ_w is the bulk unit weight of water at standard ambient temperature and pressure (SATP); m_v is the coefficient of volume compressibility or slope of the WRC in the

+PWP range (or fully saturated regime) of the WRC curve. The product of the unit weight of water and coefficient of compressibility is equal the specific storage (S_S) at saturation. $K(\psi)$ is the unsaturated hydraulic conductivity as a function of matric suction, h is the total hydraulic head, and S_K is the sink term to account for the removal of water, caused by an inequality between the loss of water volume and the acquired volume of hydration products.

The use of the unsaturated flow equation required measurement of CPB's material properties. However the used of Eqn. [3.1.1] is complicated by the evolution in the material properties due to binder hydration (i.e. formation of hydrate precipitates). There are presently no published techniques to measure the complete evolving water-retention characteristics of hydrating materials. This is in part, because most techniques have relied upon achieving a steady-state condition, which is not possible when the material's properties are constantly evolving. It is however, possible to measure properties of paste tailings without and with binder once hydration has almost ceased after 28 days, using existing laboratory techniques to measure the lower and upper boundaries of these properties during the pre- and post-hydration stages, respectively.

3.2 APPLICATION TO CEMENTED PASTE FILL

The laboratory experiments presented in this study have been designed to generate the following properties, namely, the WRC and the unsaturated hydraulic conductivity function during the post-hydration period (i.e., after 28 days). The necessary information need to formulate an internal sink term (i.e., the reduction of pore-water volume) has also

been considered. These properties are used to calibrate the 1-D unsaturated flow model, with the addition of a sink term. Some underlying assumptions have been made for this undertaking.

The assumptions are as followed:

1. CPB material posed properties similar to a deformable soil (e.g., clays) and may thus experience significant pore-structural changes during desaturation.
2. Design of CPB is based on its early-age curing strength after 28 days of hydration, therefore, the material is fully hydrated, and changes in pore-pressures are considered negligible.
3. Temperature effects on the water-retention curves were assumed to be small during the 28 days of curing.
4. Rate of cement hydration in laboratory conditions was assumed to proceed identically as it did in the field, where the total stress was assumed not to affect the rate of hydration.

The axis translation technique (Hilf, 1956) is used to measure the water-retention curves (WRCs) of paste tailings without binder and cemented paste once significant hydration has ceased after 28 days of curing. The lower and upper coefficients of compressibility prior to the AEV of the material are determined as well. Self-desiccation tests, similar to those conducted by Simms and Grabinsky (2009) are used to measure the generation rate of matric suction, as well as the internal water removal rate amount 'consumed' during

binder hydration, for different binder(s) and wt.% binder dose. Microstructural changes during binder hydration are assessed, using mercury intrusion porosimetry (MIP). It should be noted here that these analyses, under drained conditions were assumed to have occurred in the field, thus, residual bleed water is removed after paste settlement.

A column test experiment is conducted to simulate the distribution of the pore-water behaviour observed in the field (Williams Mine). Water content and matric suctions are monitored during paste deposition and subsequent binder hydration.

The material properties obtained from the laboratory experiments are used to serve as ‘inputs’ for an unsaturated flow modelling software package – SVFlux (Soil Vision, 2009). PWP profiles in multi-layered column are simulated by alternating between the pre- and post-hydration properties.

CHAPTER 4

4 MATERIALS AND EXPERIMENTAL PROCEDURES

The purpose of this study was to demonstrate the use of an unsaturated flow framework to be able to describe the behaviour of PWPs in CPB stope. In order to accomplish this, a series of experiments were performed with the aim of determining the relevant material properties of hydrated paste fill.

The materials and experimental procedures needed to accomplish this study are further described in this chapter. The experimental design of this study was comprised of the pre-laboratory methods: the characterization of the materials (Section 4.1), and the cemented paste preparations (Section 4.2). Following this, are the phase-specific procedures described in Sections 4.3 to 4.6 into four main phases:

- *Physical Characterization of Paste Tailings*, aimed to characterize the grain-size distribution, Atterberg limits and the specific gravity of tailings used in this study (Section 4.1).
- *Preparations: Sample Specimens*, provided recipes for controlled sample specimens versus site-specific recipes of paste backfill from two different paste streams used in this study (Section 4.2).
- *Phase I: Calibrations and Treatment Protocols*, calibration of the displacement sensor to track volume changes (Section 4.3.1) and the ECH2O electrical

capacitance (EC) probes to infer water contents (Section 4.3.2). Saturation treatments of high air-entry value (HAEV) porous ceramics to measure matric suctions (Sections 4.3.3 and 4.3.4, respectively).

- *Phase II: Pre- and Post- Hydration Experiments* water-retention properties and compressibility (or material stiffness) for paste without binder prior to hydration, and paste with binder after 28 days of curing (Section 4.4).
- *Phase III: Hydration-Time Dependent Experiments*, aimed to capture the effects of binder hydration, via through self-desiccation (or matric suction generation), removal of ‘consumable’ pore-water and changes in pore-volume compressibility (Sections 4.5.1 and 4.5.2, respectively).
- *Phase IV: Paste Filled Column Experiment*, aimed to simulate in-situ PWP profiles; specifically, the dissipation of +PWPs upon consolidation and induced suctions during cement curing. Further, this experiment was aimed at the application of the modified 1-D unsaturated flow model to gain a better understanding of CPB systems (Section 4.6).

It should be noted, for all experiments, distilled water was used. And, in some cases, specifically where any porous ceramics discs were used, distilled water was de-aired by using a vacuum chamber (as described in Section 4.3.3). Any experimental protocols common to other experimental procedures have been described once and made reference to thereafter.

4.1 PHYSICAL CHARACTERIZATION OF PASTE TAILINGS

The particle-size distribution (PSD) test, Atterberg limit test and specific gravity (SG) tests are the physical properties tested in this study. The following subsections briefly describe the test methods used, as per the ASTM Standard Test Methods.

These tests were conducted on Williams and Kidd tailings. Four (4) specimens were prepared for each test. Details such as, samples sizes are provided in Appendix A – Williams and Kidd Tailings [Raw Data], page 263.

4.1.1 PARTICLE-SIZE / GRAIN-SIZE DISTRIBUTION

Two methods were used to generate the PSD curves: the sieve analysis, and the hydrometer analysis. Both test procedures utilized air-dried tailings (as per the applicable ASTM D421-85, Standard Test Method). The percentage of sand, silt and clay in the inorganic fraction of a soil was measured.

4.1.2 ATTERBERG LIMIT

The applicable ASTM Standard Test Method used to determine the liquid and plastic limit is the ASTM D4310-10 (2010) Standard Test Methods for Liquid Limit, Plastic Limit and Plasticity Index of Soils was performed for the Williams and Kidd tailings. And, for the shrinkage limit test: ASTM D4943-08 (2008) Standard Test Method of Fine-Grained Soils by Wax Method was used rather than the ASTM Standard Method, ASTM-D427.

4.1.3 SPECIFIC GRAVITY

The applicable ASTM Standard Test Method for measuring the specific gravity (SG) of paste tailings were performed as prescribed in the ASTM D854 (2010) Standard Test Method for Specific Gravity of Soils, Method A. An average of the three measurements was used to report the SG.

4.2 PREPARATIONS: SAMPLE SPECIMENS

Before any set of experiments were performed, paste tailings (Section 4.2.1) and the binder mix designs (Section 4.2.2) were prepared. Binder requirements (% dry wt.), were based upon the dry mass of solids of paste tailings.

4.2.1 'PUMPING' WATER CONTENTS

Williams and Kidd Creek tailings were prepared as 'paste' tailings. Processed mine water and tailings were shipped in separate 20 gallon buckets. Tailings were labeled as 'filter cakes' – densely packed tailings, comprised of only $\frac{1}{4}$ of processed water. Paste tailings were prepared at a pumping GWC (or mining GWC) that were used the respective mines. Process water was added to the filter cake to achieve the desired GWC. %wt. of the tailings' compositions used in this study is shown in Table 4.2.1.

The initial water contents were pre-determined, and then adjusted by either removing or adding water to the required water content. For example, the initial water content was determined by thoroughly mixing the filter cake, such that a homogenous mixture was attained. Next, three (3) aluminum (oven-safe) cups were numbered and weighed. A

tablespoon size of tailings were transferred into the cups and weighed, and then placed into an oven, set at 110°C for 24 hours.

Table 4.2.1 Pumping water contents for Williams, Kidd Creek and Çayeli mine tailings (Simon, 2010)

Paste Streams	% Tailings	% Silica	% Solids	% Water	% GWC ^a	% GWC ^b
<i>(Based on % dry wt. of solids)</i>						
Williams Mine	100.0	--	72.0	28.0	38.9	28.0
Kidd Creek	45.0	55.0	78.0	22.0	28.2	22.0
Çayeli Mine	100.0	--	73.5	26.5	36.1	26.5

^a Geotechnical gravimetric water content ($GWC = M_w/M_s$)

^b Mining process gravimetric water content ($GWC = M_w/M_t$)

4.2.2 CEMENTED PASTE FILL RECIPES

Each paste stream was prepared as a cemented paste material, as specified in Table 4.2.2, which were the CPB recipes used at each mine. The binding agents and admixtures used for the CPB mixtures are Type 10 Portland Cement (PC), blast furnace slag (BFS) and fly ash (FA). The amount of admixture (if any) and binding agent were weighed and used, based on the dry mass of tailings (i.e. percent wt. of solids). The dry mass was determined when preparing the tailings into paste material.

The cemented paste samples were prepared by transferring well-mixed (e.g., homogeneous) paste tailings into a large mixing bowl. The mass of the bowl and paste tailings were weighed and recorded. The amount of binder to be added to the paste was determined by back calculating the mass of dry tailings contained in the bowl of paste.

The amount of binder was weighed out to an accuracy of 0.01 grams, and carefully transferred into the bowl, and mixed with an electrical hand beater for 2 minutes. Three (3) oven-dried samples were made to confirm the initial GWC of the cemented paste samples, prior to each of the tests that were performed.

Table 4.2.2 CPB recipes used at Williams, Kidd Creek and Çayeli Mine (Simon, 2010).

CPB Recipes	Admixtures	Binder
	<i>(% dry wt. of solids)</i>	
Williams Mine		
3% binder	50 % FA	50% PC
5% binder	50 % FA	50% PC
7% binder	50 % FA	50% PC
Kidd Creek Mine		
2.2% binder	90% BFS	10% PC
4.5% binder	90% BFS	10% PC
Çayeli Mine		
4.5% binder	--	4.5% PC
8.5% binder	--	8.5% PC

4.3 PHASE I: CALIBRATIONS AND TREATMENT PROTOCOLS

4.3.1 NON-CONTACT VERTICAL DISPLACEMENT / PROXIMITY SENSOR

The Ultrasonic proximity sensor E4B with an analogue output (Omron, 2010) was used to measure the non-contacting distance between the transducer and the proximity sensor's target (e.g., surface of a specimen). The working principle of the ultrasonic proximity sensor uses a piezoelectric transducer to send and detect sound waves, by generating a high frequency of sound waves and evaluates the echo by the detector to which is

received back after, reflecting off the measurement target. The sensor then calculates the time interval between sending the signal and receiving the echo to determine the distance to the target. When the target enters the operating range, the output switches. The ultrasonic proximity switches are equipped with temperature sensors and a compensation circuit, in order to be able to compensate for changes in operating distance caused by temperature fluctuations. Detection of the target can be in the solid, liquid, granular or powder state, and thus, unaffected by the properties of said target (Omron, 2010).

This sensor was used to determine the displacement of the sample(s) and/or test chambers in question. The non-contact displacement measurements were used to track volume changes of sample specimens (in Phase II). The sensor output was given in units of current (milliamps - mA), and therefore required calibrating so that a unit of length (in millimeters) could be related to the sensors' output data in mA. The set-up of the sensor (i.e., connected to the power source and digital-analogue converter) is as shown, in Figure 4.3.1.

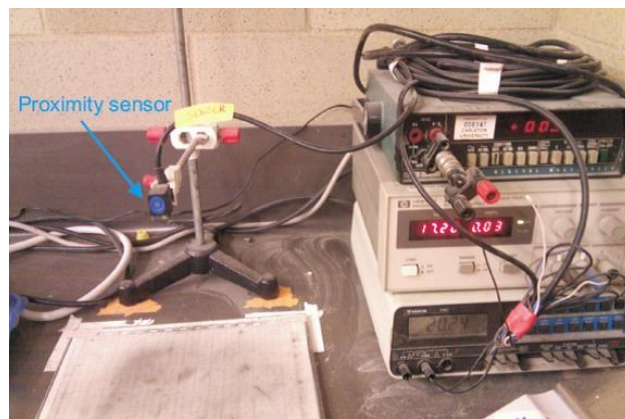


Figure 4.3.1 Set-up of the non-contact vertical displacement sensor

The sensor's upper and lower limit currents were 20.24 mA and 4.04 mA, respectively, and calibrated within this range by placing an empty 500 mL beaker beneath the sensor (transducer) with an initial reading of 20.04 mA. Water was slowly added into the beaker until the output / measurement reading changed from its initial reading. Once it was observed that there was no disturbance at the water surface and/or current fluctuations, the water level was marked off on the surface of the beaker with a non-permanent marker. The corresponding current was also recorded. More water was added again, slowly increasing the water level – each time, marking the level of water and recording the current until the lower limit was reached. The recorded readings were then converted into measurements of length in millimeters, by taking a ruler and measuring the distance between each marking, using the sensor's transducer as the reference point. A scatter plot was generated from each displacement measurement recorded in millimeters (mm) with its corresponding current (mA) output.

4.3.2 ELECTRICAL CAPACITANCE SENSORS

The soil-moisture sensors used in this study were electrical capacitance (EC) probes, specifically the 10HS and ECH₂O EC-5 sensors from Decagon Devices Inc., WA, USA (Figure 4.3.2). Specifications of Decagon's EC sensors are provided in Table 4.3.1. Data for each sensor was recorded using the ECH₂O EM50G Digital/Analogue Data Logger from Decagon Devices Inc., WA, USA.



Figure 4.3.2 Decagon’s soil-moisture sensors: (a) ECH₂O EC-5 sensor, and (b) 10HS sensor

Table 4.3.1 Specifications for Decagon’s EC volumetric sensors (Campbell, 2002; Cobos, 2007; 2009)

EC Sensor	Measurement Range (cm^3/cm^3)	Output Range (mV)	Operating Temperature (°C)	Dimensions (cm x cm x cm)	Volume Sensitivity* (cm^3)
EC-5	0 - 100 %	250 – 1000	-40 to 50	8.9 x 1.8 x 0.7	181 ^a
10HS	0 - 57 %	300 – 1250	0 – 50	14.5 x 3.3 x 0.7	1160 ^b

* Total volume of influence of EC sensors as recommended by Cobos (2007).

^{a, b} Decagon recommends that sensors should not be installed within 5 to 10 cm of the soil surface or any foreign objects, respectively.

The data logger reported data in two forms: (1) unprocessed data, or raw data as voltage output in millivolts, and (2) processed data as VWCs, to which were based upon Decagon’s standard calibration equations. Processed data reported as VWC(s) for both EC sensors (as indicated by subscripts EC-5 and 10HS) were given by Decagon’s standard calibration equations for mineral soil

$$VWC_{EC-5} = 8.5 \times 10^{-4}(mV) - 0.48 \quad [4.3.1]$$

and,

$$VWC_{10HS} = 1.17 \times 10^{-9}(mV)^3 - 3.95 \times 10^{-6}(mV)^2 + 4.9 \times 10^{-3}(mV) - 1.92 \quad [4.3.2]$$

where, mV is the voltage output or raw data.

4.3.2.1 WILLIAMS PASTE TAILINGS

The calibration of both EC sensors were performed to measure the volumetric water content (VWC) of Williams paste tailings, prepared at the ‘pumping’ GWC. One sample specimen was used to calibrate the EC-5 and the 10HS sensor, following the systematic instructions on soil-specific calibrations described in Decagon’s Application Note by Campbell (2002). A known mass of air-dried sample of tailings were used, and on each measurement day, a known mass of water was added and recorded. It should be note here that a constant volume of paste was aimed by adding dried tailings to the sample container to 670 cm³. Raw output data was collected for 5 hours, and averaged over a frequency of 30 minutes.

4.3.2.2 WILLIAMS 3% AND 7% BINDER MATERIAL

As per Campbell’s (2002) calibration procedure, both EC sensors were calibrated for Williams 3% and 7% binder containing material, albeit, modified to take into account the changes in the bulk density (or mass of solids to volume of paste ratio) as a result of binder hydration and desiccation (or ‘drying out’).

Two tests were conducted in order to calibrate the EC-5 and the 10HS sensors for specimens containing 3% binder and 7% binder material. The first test was conducted from March 10 to April 10, 2010. The EC-5 sensor was calibrated with 3% binder material, and the 10HS sensor was calibrated with 7% binder material. The second test was conducted from April 10 to April 26, 2010. The EC-5 sensor was calibrated with 7% binder material, and the 10HS sensor was calibrated with 3% binder material.

One batch containing 3% binder and the other containing 7% binder were prepared. Each batch was divided into 2 containers: (1) a PVC container*, where volumetric samplers were used to determine the total volume of paste; and thus, VWC(s) as well; and, (2) a Tupperware container, to which an EC sensor was submerged into the prepared paste so that the voltage data could be recorded. Samples were also retrieved for oven-drying (gravimetric water contents). Both sample containers were left uncovered to dry out. Water content samples and volume samples were retrieved and recorded. Raw data from both EC sensors during the calibration procedures were recorded in real-time at a frequency of 60 Hz. A calibration curve was generated for each test (e.g., paste tailings and cemented paste) by plotting laboratory measured water contents as a function of voltage output (mA).

* PVC Container: Volumetric sampling

Volumetric samples were obtained by driving the sampler[†] to the bottom of the container with force. The length of the sample retrieved was marked off on the outside of the pipe

[†] *Sampler: a stainless steel pipe, whose inner diameter and length of the sample retrieved was measured using Vernier calipers to the nearest 0.01 mm.*

with a marker, and carefully removed from sampler, and transferred into a weighing dish for oven drying to determine the GWC so that the VWC could be calculated.

The VWC for the retrieved sample is calculated by

$$\theta_V = GWC \frac{\rho_b}{\rho_w} \quad [4.3.3]$$

where, θ_V is the VWC, [cm^3/cm^3]; ρ_w is the density of water at 25°C, [$1.00 \text{ g}/\text{cm}^3$]; GWC is the water content, which was determined through means of oven-drying the retrieved sample; and, ρ_b is the bulk density, [g/cm^3], which is calculated by

$$\rho_b = \frac{m_s}{V_t} = \frac{[m_t / (GWC + 1)]}{\pi r^2 h} \quad [4.3.4]$$

where, m_s is derived using the GWC definition ($GWC = m_w / m_s$, where $m_w = m_t - m_s$); and V_t is the volume of the retrieved sample, [cm^3].

4.3.3 PRE-TREATMENT OF CERAMIC DISCS

Pre-treatment of the high AEV porous discs (5 bar and 15 bar discs) from GCTS Testing Systems, AZ, USA, required conditioning prior to use, through means of water saturation. The applicable Test Methods were the ASTM D5084 (measuring the saturated hydraulic conductivity of porous disc), and the ASTM D6836-02(2008), Method C – Determination of the Soil Water Characteristic Curve for Desorption Using Hanging Column, Pressure Extractor, Chilled Mirror Hygrometer, or Centrifuge.

4.3.3.1 SATURATION PROCESS

Product specifications for the 5 bar and 15 bar porous discs are provided in Table 4.3.2. These discs were pre-saturated by submerging them in a desiccator vacuum chamber for a period of 24 hours, until no visible gas bubbles were present (as per ASTM D6836-02, Section 8.2.2).

Table 4.3.2 Technical specifications of the 5 bar and 15 bar ceramic porous discs (SoilMoisture Equipment Corp., 2008)

AEV Disc	Bubbling Pressure	Approximate Porosity	Maximum Pore Size	Hydraulic Conductivity	Flux
<i>(bar)</i>	<i>(kPa)</i>	<i>(% vol.)</i>	<i>(μm)</i>	<i>(m/s)</i>	<i>($\text{m}^3/\text{s}\cdot\text{m}^2$)</i>
5	552	31%	0.5	1.21×10^{-9}	1.97×10^{-6}
15	1517	32%	0.16	2.59×10^{-11}	1.36×10^{-8}

A pump with a capacity of 700 mm Hg (94 kPa gage pressure) was connected to a rubber tube and valve to a desiccator chamber (as shown in Figure 4.3.3). Distilled water was transferred to the desiccator, filling it with water, just below the valve. Vacuum grease was smeared sparingly onto the contact surfaces of the O-ring between the chamber and the cover/lid. Distilled water was de-aired by applying negative pressure for 15 minutes.

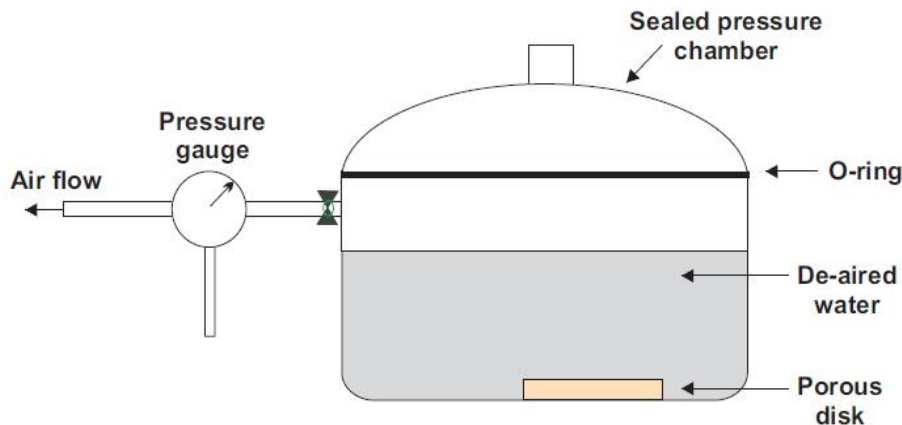


Figure 4.3.3 Saturation chamber for saturating porous discs and tensiometers

Prior to saturating the discs, initially dry porous discs were weighed, using an electronic scale with a precision of 0.1 grams. The dry mass of the discs were recorded. The ceramic discs were then soaked for an hour in the desiccator chamber in de-aired water. For the saturation process, a vacuum of at least 94 kPa was applied to the chamber for 15 minutes, intermittently cycling between vacuum and no vacuum. This procedure was repeated until no visible air bubbles were observed for at least three (3) consecutive applications of vacuum. Once there were no air bubbles or nucleation sites on the surface of the porous disc, the saturation weight of the ceramic discs were determined, by placing a container with de-aired water onto the scale, and tared to zero; transferring the disc into the container. The mass of the container, plus water and disc was weighed and recorded. The saturation mass of each porous disc was calculated by subtracting the mass of the empty container from the mass of the container with water. The porous discs were then placed back into the desiccator chamber under vacuum for an additional 15 minutes. After 20 hours, the discs were weighed and recorded again, in the same manner described

earlier. It was assumed that the discs were completely saturated once the ‘wet’ mass remained unchanged.

4.3.3.2 SATURATED HYDRAULIC CONDUCTIVITY

After the saturation process, the saturated hydraulic conductivity of the 5 bar and 15 bar porous discs were determined. The determination of the hydraulic conductivity of a porous disc prior to any test is considered a standard test method of ensuring complete saturation (Marinho et al., 2008; ASTM D6836-02(2008)).

The saturated hydraulic conductivity of the porous disc was determined, using Darcy’s law when the initial pressure head and outflow water flux is measured. Recalling Darcy’s law, the saturated hydraulic conductivity is stated by

$$q = -k \frac{dh}{dL} \rightarrow k = -\frac{q}{dh/dL} \quad [4.3.5]$$

where, q is Darcy’s flux, [m/s]; k is the saturated hydraulic conductivity, [m/s]; and, dh/dL is the hydraulic gradient, [m/m].

The hydraulic gradient is defined as the rate of change of pressure head per unit length of flow at a given direction. In this case, it was the height of water (or head) over the thickness of the ceramic disc, flowing in downwards direction. The hydraulic gradient is defined by

$$\frac{dh}{dL} = \frac{\psi}{\rho_w g L} \quad [4.3.6]$$

where, ψ is the applied air pressure, [kPa]; γ_w is the unit weight of water, [N/m³]; and, L is the thickness of the porous disc, [m]. If the volumetric flow rate (\dot{Q}), and dimensions of the porous disc is known, then Darcy's flux can be rewritten in terms of the amount of water that permeates through the porous disc, over a time interval by

$$q = -\frac{\dot{Q}}{A} = -\frac{m_w}{\rho_w t} \times \frac{4}{\pi d^2} \quad [4.3.7]$$

where, A is the surface area of the porous disc, [mm²]; \dot{Q} is the volumetric flow rate, [m³/s]; m_w is the mass of water, [kg]; ρ_w is the density of water at 20°C, [1000 kg/m³]; t is the time interval during drainage, [s]; and, d is the diameter of the porous disc, [m]. Equations [4.3.5] and [4.3.6] are substituted into Eqn. [4.3.7], such that, the saturated hydraulic conductivity (k) of a porous ceramic disc may be given by

$$k = \left[\frac{4m_w}{\pi d^2 t} \right] \times \left[\frac{gL}{\psi} \right] \quad [4.3.8]$$

The dimensions (i.e., thickness and diameter) of the porous disc were measured using Vernier calipers. The saturated disc was then set in-placed, above the water reservoir on the base of the test cell (pressure chamber). The internal and external chamber walls were placed on the base of the cell. The mass of the empty cell containing the emplaced disc was weighed and recorded. Vernier calipers were then used to measure the inside

diameter of the cell, and recorded. The depth of the cell was measured using the non-contact displacement sensor, by taking a number of readings for displacement (in mA) along ‘ N ’ points on the surface of the extractor disc, and then taking the average current. This was recorded as the distance between the sensor and the surface of the porous disc, h_i in terms of current. A reference measurement, h_o at the top of the cell was determined, also by using the proximity sensor. The difference between these two measurements (as depicted in Figure 4.3.4) was calculated as the depth of the cell (i.e., $\Delta h = h_i - h_o$), by applying the calibration to convert the current output readings (mA) into units of length (mm). The empty volume of the cell was calculated from the length and inner diameter. The test cell (or pressure plate extractor) was then weighed and recorded as the empty mass (m_c). Approximately 20 mL of distilled water was then poured into the cell, weighed and recorded as (m_{cw}). The amount of water transferred into pressure chamber, prior to an applied air pressure was calculated as the difference of the two measurements (i.e. $m_{wo} = m_{cw} - m_c$).

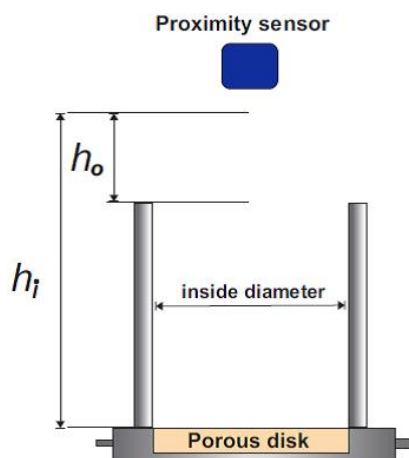


Figure 4.3.4 Reference measurements to calculate the volume of the test cell

The pressure plate extractor was set-up, as illustrated in Figure 4.3.5. Components of the pressure chamber system (i.e., burette, glass tubing and air trapper) were connected, as well as the gas pressure lines to and from the pressure cell and compressed air, respectively. All valves were ‘closed.’ In order to fill the water reservoir, distilled water was added from the top of the burette. Placing a finger on the opening of the water outflow tube, and opening the valve of the burette to allow water to flow and circulate through the air-trapper and into the recirculation tubes to fill the inside reservoir of the test cell. Occluded air within the reservoir and the recirculation system was removed by rolling out the bubbles with a tube roller, until no visible air bubbles passed through the air trapper. The top plate of the pressure cell was then placed and sealed with vacuum grease to prevent air leaking from the enclosed system. The compressed air (nitrogen gas) supply was then attached to the gas line and pressure manifold of the test chamber.

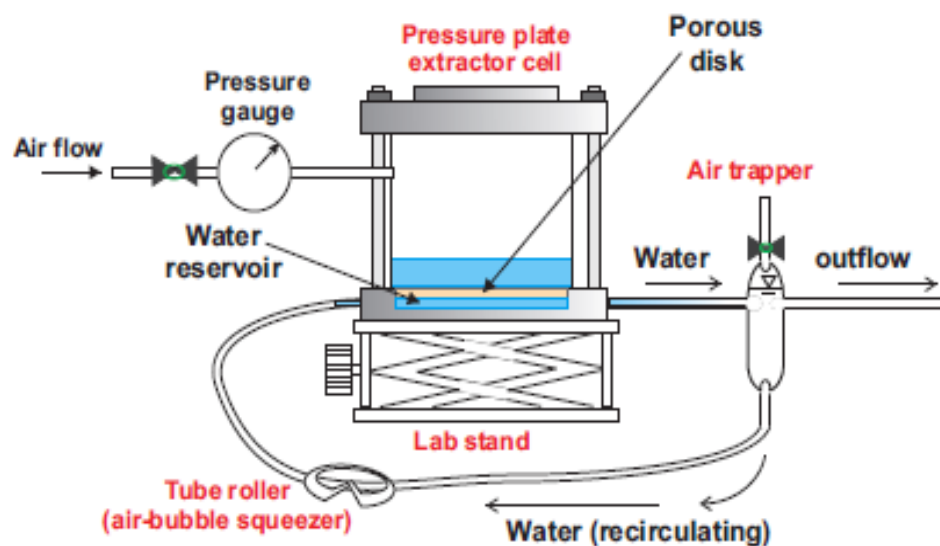


Figure 4.3.5 Equipment set-up: volumetric pressure plate extractor system and gas line

An air pressure of 250 kPa was applied for a period of 20 hours, which was recorded with a stopwatch. The pressure was then turned off, and the final mass of the pressure cell was measured and recorded (m_{wf}). This difference from the initial mass of the cell with water to the final mass with the remaining water was calculated as the mass of water that was extracted (m_{we}) over the length of time, while air pressure was being applied (i.e., $m_{we} = m_{wo} - m_{wf}$).

The initial and final head, h , was calculated from the initial and final mass of water remaining in the test cell, by the following equation:

$$h = \frac{m_w}{\rho_w \pi r^2} \quad [4.3.9]$$

Measured water permeabilities of the porous discs were obtained using the dimensions and mass flux of water (i.e. Δm_w over time, t) passing through a 10.55 ± 0.005 mm thick disc at an applied air pressure by following the calculations via Eqn.(s)[4.3.5] through [4.2.9]. Supplementary data is provided in Appendix A.3 (page 273).

4.3.4 SATURATION METHOD: PRESSURE TRANSDUCERS

High-grade pressure transducers / tensiometers called the T5x (as shown in Figure 4.3.6a), from USM GmbH, Germany were pretreated, prior to use for measuring matric suctions for *Phase III* and *IV* (Sections 4.5.1 and 4.6). Similar to the treatment used to saturate the porous disc, dry tensiometer tips and sensor bodies were subjected to cycles of vacuum. The components of a T5x are illustrated in Figure 4.3.6.

The water reservoir of a T5x's sensing body and shaft were filled with de-aired water, by submerged under water inside the desiccator chamber using a syringe. The vacuum chamber was then sealed, and the vacuum pump was turned on, applying negative pressure of 94 kPa_(g) for 10 to 15 minutes. The pump was then turned off, and set aside for 30 minutes. Entrapped air along the inside walls of the water reservoir and porous cup were removed by tapping the exterior wall of the shaft. This was done by placing an index finger on the opening of the shaft, and carefully removing the tensiometer tip out of the water, while using the other hand to tap out air bubbles. The shaft was then placed under water to allow the air bubbles to escape, and be replaced by water. Air bubbles from the sensor's body were also removed by gently 'tapping' the body, while keeping it submerged in water. Again, the chamber was sealed and vacuum was applied for the duration of 10 – 15 minutes. This process of applying negative pressure back to zero gage pressure was repeated three (3) times, after which the tensiometer shafts' were carefully screwed into the sensor body while still submerged under water. Once the tips were tightly secured, they underwent another 2 cycles of vacuum, before checking the response time (pressure readings as described in the User Manual by USM GmbH, 2009). Pretreated tensiometers were then placed in a container of de-aired water, and set aside until they were used for the self-desiccation tests (Phase III) and the column outflow test (Phase IV).

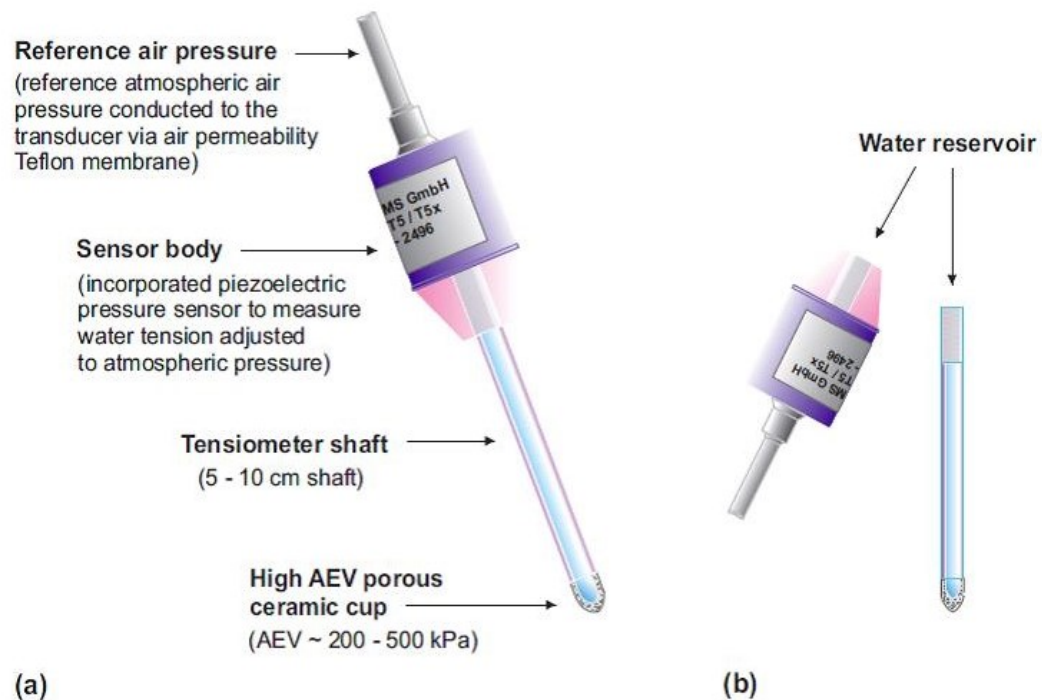


Figure 4.3.6 (a) A schematic of the T5x / T5 Tensiometer; and (b) water reservoir, where the T5 body and tips are filled with de-aired water (UMS GmbH, 2009)

4.4 PHASE II: PRE- AND POST- HYDRATION EXPERIMENTS

In this Phase, the pre- and post-hydration experiments were aimed to quantify the material properties (e.g., water-retention curve and compressibility) of paste tailings containing no binder (pre-hydration period), and properties of paste with binder once hydration has ceased (post-hydration period).

4.4.1 DETERMINATION OF THE WATER-RETENTION CURVES

The entire range of the water-retention curve (WRC) was measured using two methods outlined in the ASTM Standards, ASTM D6836-02(2008) Standard Test Method for the

Determination of the Soil-Water Characteristic Curve for Desorption using Hanging Column, Pressure Extractor, Chilled Mirror Hygrometer, or Centrifuge. Measurement of the matric suction portion (i.e., matric suctions below the AEV of porous disc) of the WRCs were carried out using the axis translation technique (Method C), while the total suction portion (i.e., suctions beyond the AEV) was determined using the chilled mirror dew point technique (Method D).

4.4.1.1 MEASUREMENT OF MATRIC SUCTIONS

Matric suctions were directly measured using the axis translation technique, Method C – Pressure Chamber with Gravimetric Water Content Measurements. Matric suctions were measured by imposing an applied air pressure within the pressure chamber, while controlling the pore-water pressure such that it is equal to zero gauge pressure (or atmospheric pressure); and hence, translating the applied air pressure into matric suctions. The range of suctions that were measured in paste tailings were dependent upon the 500 kPa (AEV) porous ceramic disc that was used.

A volumetric pressure plate extractor (Figure 4.4.1) – the SWC-150, Fredlund SWCC Device, from GCTS Testing Systems, Arizona, USA was used to determine the matric suction component of the WRC. The axis translation equipment set-up, as shown in Figure 4.4.2, was modified by removing the pressure manifold, so that only the test cell and porous ceramic disc were used, while the remaining components, such as the air-trapper, burette, and recirculation system (from SoilMoisture Equipment Corporation, CA, USA) were retro-fitted to operate in a similar fashion as the Fredlund SWCC device

with the exception that volume change measurements were estimated (i.e. non-contact displacement sensor).



Figure 4.4.1 SWC-150 Fredlund SWCC Device (GCTS Testing Devices, 2009)

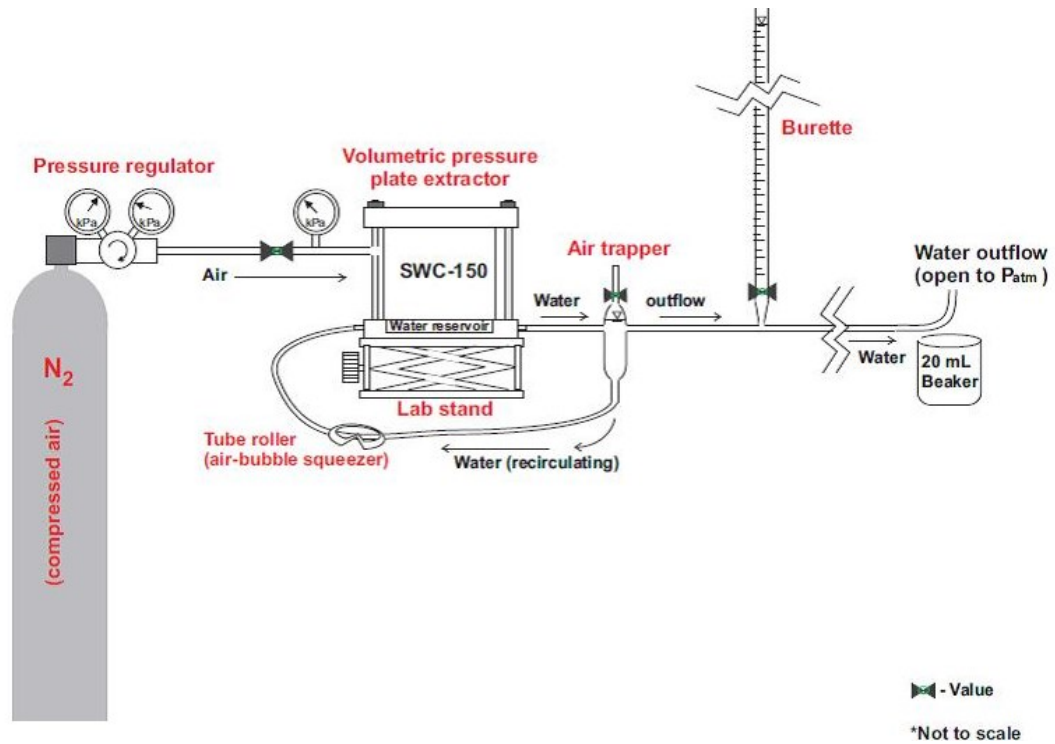


Figure 4.4.2 Axis translation equipment test set-up

Prior to commencing the experiments, porous disc(s) were pretreated, weighed and recorded as the empty mass of the test cell. The specimen was prepared at a pumping GWC and transferred into the test cell. The mass of the cell with paste was measured and recorded. The paste specimen was then covered with plastic wrap to prevent water loss through evaporation. De-aired water was transferred into the burette to recirculate water through the reservoir and air trapper. Air bubbles were removed by rolling the squeezer along the length of the recirculation tubes, which was done whenever the test cell was re-assembled to the pressure manifold. The specimen settled and consolidated over a period of 12 hours, after which, the cell was disconnected from the recirculation tubes. Visible bleed water on the surface of the specimen was removed by carefully pouring out the water into a weighing dish. The water was weighed and recorded. The test cell and paste specimen was also weighed and recorded as the initial GWC at zero suction (0 kPa). The initial volume was measured and calculated by removing the cover of the test cell and, taking vertical displacement measurements using the non-contact proximity sensor and subtracting it from the volume of the empty test cell. The burette was filled with water, and served only as a source to flush the system with water (Figure 4.4.2). The beaker (shown in the diagram) collected any water that had drained; the water that was collected was not used for measurement purposes, but merely, to maintain a tidy workspace.

The test cell was connected to a pressurized air supply, in which nitrogen gas was used. An air-pressure of 40 kPa was applied for 48 hours until it was observed that there was no water draining out from the system (e.g., described by Hilf, 1956). After which, the pressure was turned off, and disconnected from tubes. The weight of the test cell and

paste specimen was measured and recorded to the nearest 0.01 g. Volume change was also estimated by taking displacement measurements, and taking the average to calculate its volume. The GWC(s) were converted into VWC(s), as discussed in Section 4.4.2. Applied air pressures were then increased thereafter in increments of 30 kPa and/or 40 kPa. GWC and volume changes were measured and recorded at each increment once equilibration of the system was observed (after approximately 48 hours).

The axis translation technique was used to determine the WRCs of the pre-hydration period for Williams and Kidd's paste stream for matric suctions below 500 kPa. After which, Method D (described in Section 4.3.2.2.), was employed to determine the total suctions.

4.4.1.2 MEASUREMENT OF TOTAL SUCTIONS

Once direct measurements of matric suctions were no longer possible; specifically, when suctions were beyond the AEV of the porous disc and/or when sample specimens have reached the residual water contents of approximately 9%GWC or less were reached, total suctions were measured indirectly, using the chilled mirror dew point technique, Method D – Chilled Mirror Hydrometer (Method D of the ASTM D6836-02 Standard Test Methods), using the WP4 – DewPoint PotentialMeter from Decagon Devices, WA, USA. This device is reported to measure suctions from 0 to 300 MPa with an accuracy of ± 0.1 MPa from 0 to 10 MPa, and $\pm 1\%$ from 10 to 300 MPa.

With the WP4 – DewPoint psychrometer, three (3) small samples (approximately < 50 g) were removed from the test cell and transferred into the WP4 sample cups. Each sample cup was placed into the loading chamber until the sample equilibrated with the headspace of the sealed chamber containing a mirror that detects the condensation on the mirror. Once this occurred for each sample, the total suctions were recorded. The samples were then transferred into three (3) separate weighing dishes; weighed and recorded, and placed in the oven to determine the gravimetric water content. Three (3) samples were measured and recorded once a day to obtain an average suction and residual water content. Volume change measurements were not performed.

4.4.2 PRE-HYDRATED WATER-RETENTION CURVES

This test was conducted on Williams and Kidd tailings. Williams tailings containing no binder settled over a period of 24 hours, after which 31.5 grams of bleed water was removed, whereas, Kidd tailings (amended) settled within the first 20 hours, after which 21.7 grams of bleed water was removed. Sample sizes and initial water contents after settling (or prior to testing) have been provided in Table 4.4.1.

Table 4.4.1 Sizes and initial water contents of the test specimens used in the pre-curing phase axis translation experiments

Test Specimens	Initial Sample Size		Initial Water Content	
	Mass	Volume	GWC	VWC
	(RE ± 0.05 g)	(RE ± 0.005 cm ³)	(± 0.01 %)	
Williams tailings	653.0	369.77	38.09	48.71
Kidd (amended) tailings	366.3	156.07	21.92	38.74

Water contents and volume change measurements recorded for Williams paste containing no binder were obtained for matric suctions ranging from 0 to 320 kPa, and total suctions ranging from 1.2 MPa to 150 MPa.

4.4.3 POST-HYDRATED TESTING

An additional Standard Method applicable to this test including the two test procedures described in this section, is the ASTM C1699-09 Standard Method for moisture retention curves for porous building materials using pressure plates.

This test was conducted on Williams and Kidd paste fill material. The preparation of Williams containing 3% binder and Kidd containing 2.2% binder paste specimens have been provided in Tables 4.4.2 and 4.4.3, respectively.

Table 4.4.2 Williams paste prepared with 3% binder, cured in the volumetric pressure plate extractor for 28 days prior to the axis translation test

<i>Mass</i> (<i>RE</i> ±0.005 g)	<i>Williams 3% Binder</i> ^b (1.5% FA : 1.5% PC) ^a	
M_{paste}	622.6	
M_{solids}	447.36	
M_{water}	175.24	
<i>Initial Water Content</i> (± 0.05 %)	39.2%	28.1% *
M_{PC}	6.71	
M_{FA}	6.71	
$M_{water\ removed}$	0.00	
M'_{paste}	636.02	
M'_{solids}	460.78	
M'_{water}	175.24	
% <i>solids</i> (by wt.)	72.45%	
% <i>water</i> (by wt.)	27.55%	
<i>Final Water Content</i> * (± 0.05 %)	38.0%	27.6% *

^a FA - Fly ash; PC - Portland cement

^b Note: only 299.50 grams of paste containing 3% binder was transferred and cured in the test cell

* GWC based on geotechnical (M_w/M_s), and mining process (M_w/M_{paste}) calculations, respectively

Table 4.4.3 Kidd paste prepared with 2.2% binder, cured in the volumetric pressure plate extractor for 28 days prior to the axis translation test

Mass (<i>RE</i> ±0.005 g)	Kidd 2.2% Binder^b (2.2% BFSM) ^a	
M_{paste}	466.03	
$M_{45\% \text{ Tailings}}$	163.2	
$M_{55\% \text{ Sand}}$	199.47	
M_{water}	103.36	
Initial Water Content (± 0.05 %)	28.5%	22.2% *
M_{BFSM}	7.98	
$M_{water \text{ removed}}$	0.00	
M'_{paste}	474.01	
M'_{solids}	370.65	
M'_{water}	103.36	
% solids (by wt.)	78.19%	
% water (by wt.)	21.81%	
Final Water Content* (± 0.05 %)	27.9%	21.81% *

^a BFSM - Blast furnace slag mixture (pre-mixed with 10% PC and 90% slag)

^b Note: only 389.6 g of 2.2% binder CPB was cured in the test cell

* GWC based on geotechnical (M_w/M_s), and mining process (M_w/M_{paste}) calculations, respectively

The initial sample sizes and initial water contents for each paste specimen, prior to the axis translation tests have been provided in Table 4.4.4.

Table 4.4.4 Sizes and initial water contents of the test specimens used in the post-curing phase

Test Specimens	Initial Sample Size		Initial Water Content	
	Mass (<i>RE</i> ± 0.05 g)	Volume (<i>RE</i> ± 0.005 cm ³)	GWC (± 0.01 %)	VWC
Williams with 3% binder (Trial #1)	373.4	201.06	36.31	49.47
Williams with 3% binder (Trial #2)	299.5	159.48	36.49	50.21
Kidd with 2.2% binder	372.2	179.34	19.83	34.34

The WRCs for Williams 3% binder and Kidd 2.2% binder containing paste specimens were tested post-hydration (after 28 days of cement curing), using the axis translation for suctions between 60 – 540 kPa with a porous disc having an AEV of 1500 kPa. Suctions beyond 600 kPa were measured using the chilled mirror dew point technique.

Good contact between the cemented paste specimen(s) and ceramic disc (i.e., continuity between the water phase) was necessary for these tests. Therefore, freshly prepared paste was poured and allowed to settle inside the test cell. The cell was sealed with plastic wrap, and curing at SATP for 28 days. On the 29th day, the post-hydrated specimen was re-saturated to 100% degree of saturation. This was conducted as prescribed by the ASTM C1699-09 test method, steps 7.3 to 7.5 and 7.8, by fully immersing the specimen in full contact with the base of the cell in de-aired water for a minimum of 8 hours, until a constant weight was attained (ASTM C1699-09, 2011).

A confirmatory GWC was obtained for the post-hydrated specimen prior to the axis translation test, by scrapping the surface of the specimen with a straight-edge (e.g. chisel), and transferring the retrieved sample into a weighing dish, where it was weighed and recorded, and placed in an oven for 15 hours to dry. After oven-drying the sample, it was weighed and recorded to determine the initial GWC at zero suction (or zero applied air pressure). The axis-translation test was then performed as previously described. Changes in GWC, volume and matric suctions were measured and recorded from 0 – 540 kPa, after which total suctions and GWC were measured.

4.4.4 ANALYSIS AND CALCULATIONS

The following equations were used to generate the WRCs as well as Shrinkage curves, where water content and the degree of saturation is a function of matric suction.

The mass of water remaining in test specimen, m_w at incremental matric suctions, ψ , is given by

$$m_w(\psi_i) = m_{(cell+paste)}(0) - m_{(cell+paste)}(\psi_i) \quad [4.4.1]$$

where, $m_w(\psi_i)$ is the mass of water remaining in the test specimen, [g]; $m_{(cell+paste)}(0)$ is the mass of the cell and specimen at 0 kPa, [g]; $m_{(cell+paste)}(\psi_i)$ is the mass of the cell, and specimen 'i' after each increment of matric suction; where $i = 40, 80, 120, \dots, 500$ kPa.

Volume changes of the test specimen were estimated, such that the VWC (θ_v) at suction 'i' could be computed by

$$\theta_v(\psi) = \frac{m_w(\psi_i)}{\rho_w V_{paste}} = \frac{V_w}{V_{paste}} \quad [4.4.2]$$

where, V_w is the volume of water remaining in the test specimen, [cm³]; ρ_w is the density of water, [1.0 g/cm³]; and, V_{paste} is the total volume of the paste, [cm³].

The volume of paste throughout the duration of the axis translation test was estimated by using the non-contact displacement sensor. The vertical displacement that was measured

is the distance between the surfaces of the paste specimen to the top of the pressure chamber. Therefore, the volume of paste is determined by

$$V_{paste}(\psi) = \pi r^2 (h_{cell} - \Delta h) \quad [4.4.3]$$

where, h_{cell} is the length of the pressure chamber, [cm]; and, Δh is the distance between the paste and the top of the pressure chamber, [cm]. Displacement measurements are given in current (mV), which were then converted into a unit length (mm) by using the calibration curve obtained from Phase I (Section 4.3.1).

Volume change measurements were required to determine the volumetric water content (as per Eqn. [4.4.2]), as well as the degree of saturation. The degree of saturation (S) is computed by

$$S(\psi) = \frac{V_w}{V_v} \quad [4.4.4]$$

where, V_v is the volume of voids (i.e., $V_v = V_{paste} - V_w$) within the specimen, [cm³]. The shrinkage curve was also generated from the axis translation test, where the void ratio is a function of the GWC. The void ratio is given by

$$e = \frac{V_w}{V_s} \quad [4.4.5]$$

where, V_s is the volume of solids (i.e., $V_s = V_p - V_v$) within the specimen, [cm³]. In addition to obtaining the WRCs and shrinkage curves, the material's compressibility in

the +PWP region (i.e., in the saturation zone of the WRC) is determined by (Fredlund and Rahardjo, 1993):

$$m_v = \frac{\partial \varepsilon_v}{\partial (u_a - u_w)} \quad [4.4.6]$$

where, m_v is the coefficient of volume change (or compressibility), [kPa^{-1}]; $\partial(u_a - u_w)$ is the change in matric suction at complete saturation, [kPa], and $\partial \varepsilon_v$ is the incremental changes in volumetric strain as a function of matric suction, [cm^3/cm^3], such that

$$\varepsilon_v = \frac{\Delta V_v}{V_T} \quad [4.4.7]$$

where V_T is the total volume of the solid matrix and water, [cm^3], and ΔV_v is the actual change in void volume due to compression, which is identical to the change in bulk volume, ΔV_T , [cm^3]. Calculations using Eqn.(s) [4.4.1] through [4.4.7]) were performed for all test methods using the axis translation technique conducted in this study, including the post-hydrated cemented paste tests.

4.5 PHASE III: HYDRATION-TIME DEPENDENT EXPERIMENTS

In this Phase, cement hydration experiments were aimed at capturing the rate of paste hydration in terms of matric suctions and pore-water consumption by conducting a number of self-desiccation tests. A test to track the changes in pore-structure of

hydrating paste material was also employed by use of the mercury intrusion porosimetry (MIP) method.

4.5.1 SELF-DESICCATION TESTS

The T5x pressure transducers / tensiometers from Umwelt-Monitoring-Systeme (UMS GmbH), Germany were used to directly measure the matric suction during cement hydration. The T5x is capable of measuring pore-water pressures up to 100 kPa and suctions up to 250 kPa and in some instances, up to 400 kPa (UMS, 2009). Prior the use of these sensors, the T5xs were pretreated as described previously (Section 4.3.4).

4.5.1.1 WILLIAMS PASTE FILL MATERIAL

Cemented paste specimens from Williams paste containing 0, 3, 5 and 7% binder were prepared (as per Table 4.5.1), and poured into small PVC concrete curing containers (inner diameter of 10 cm and height of 25 cm). The T5xs were inserted in the paste material and covered with plastic wrap to prevent water loss from evaporation. The release of bleed water during the first 4 hours of setting for all three (3) binder specimens were observed, and carefully removed with a syringe. The control(s) containing no binder were allowed to settle for 24 hours, before removing the bleed water from the surface with a syringe. Matric suction measurements were recorded every 5 minutes for the first 48 hours and every 10 minutes thereafter for 28 days. Replicate samples were prepared and oven-dried once a day to track the changes in the solids-to-water ratio for a period of 28 days.

Matric suctions were recorded every 5 minutes for the first 48 hours and at every 10 minutes thereafter for 28 days (Williams CPB specimens) and 24 days (Kidd CPB specimens). Some release of bleed water typically occurred within the first couple of hours of setting for all three binder specimens, while the control (with no binder) settled for over 24 hours. Water that had pooled on the surface from settling was removed with a syringe. Water contents before and after the release of bleed water are presented in these Tables as well.

Table 4.5.1 (Trial #1) Williams CPB recipes for 3, 5 and 7% binder containing specimens

Mass (RE of +/- 0.005g)	3 % Binder (1.5% FA: 1.5%PC)	5 % Binder (2.5% FA:2.5%-PC)	7 % Binder (3.5% FA:3.5%PC)
M _{paste}	1068.16	1025.19	1034.76
M _{solids}	766.64	735.80	742.67
M _{water}	301.52	289.39	292.09
M _{evaporable water (removed)}	23.25	13.59	9.12
<i>Initial Water Content* (%)</i>		<i>39% / 28%</i>	
M _{PC}	11.50	18.39	25.99
M _{FA}	11.50	18.39	25.99
M' _{paste} ⁺	1091.16	1061.98	1086.75
M' _{solids} ⁺	789.64	772.59	794.66
M' _{water}	278.27	275.80	282.97
% _{solids}	72.37	72.75	73.12
% _{water}	25.50	25.97	26.04
<i>Final Water Content* (%)</i>	<i>35% / 25.5%</i>	<i>36% / 26%</i>	<i>35.6% / 26%</i>

* Gravimetric water contents of CPB based on geotechnical (M_w/M_s), and mining process (M_w/M_{paste}) calculations, respectively.

⁺ Includes the amount of binder, comprised of 50% PC and 50% FA.

This test was conducted a second time for repeatability. The sample specimens were prepared as indicated in Table 4.5.2.

Table 4.5.2 (Trial #2) Williams CPB recipes for 3, 5 and 7% binder containing specimens

Mass (RE of +/- 0.005g)	3 % Binder Specimen	5 % Binder Specimen	7 % Binder Specimen
m_{bowl} (+/-0.05 g)	1004.9	1012.5	1007.6
$m_{\text{bowl+ paste}}$ (+/-0.05 g)	2258.3	2058.5	2131.4
m_{paste}	1253.4	1046.0	1123.8
m_{solids}	902.5	753.2	809.2
m_{water}	350.9	292.8	314.6
<i>Initial gWC (%)</i>	<i>38.88</i>	<i>38.88</i>	<i>38.88</i>
m_{PC}	13.5	18.8	28.3
m_{FA}	13.5	18.8	28.3
m'_{paste}	1280.5	1083.7	1180.4
m'_{solids}	929.6	790.8	865.8
% _{solids} (by wt.)	72.60	72.98	73.35
% _{water} (by wt.)	27.40	27.02	26.65
<i>Final gWC (%)</i>	<i>37.75</i>	<i>37.03</i>	<i>36.34</i>

4.5.1.2 KIDD'S BINDER PASTE MATERIAL

This same test was carried out twice for the Kidd Mine cemented paste material containing 0, 2.2 and 4.4% binder (as per Table 4.5.3). The first trial was performed in the same manner as described for the Williams cemented paste, followed by replicated samples to track water contents. However, for the second trial, a larger sample specimen of the 2.2% was prepared and poured into two large PVC containers. From this, suction and water contents were measured, via through intrusive sampling, followed by oven-drying.

Table 4.5.3 Kidd's CPB recipes for 2.2 and 4.5% binder containing specimens

Mass ($RE \pm 0.005$ g)	2.2% Binder (2.2% BFSM) ^a		4.5% Binder (4.5% BFSM) ^a	
M_{paste}	1175.8		1705.6	
$M_{45\% \text{ Tailings}}$	432.5		624.7	
$M_{55\% \text{ Sand}}$	527.4		761.8	
M_{water}	215.9		319.1	
<i>Initial Water Content* (%)</i>	<i>22.49%</i>	<i>18.36%</i>	<i>23.01%</i>	<i>18.71%</i>
M_{BFSM}	21.6		63.8	
$M_{\text{water removed}}$	1.6		1.0	
M'_{paste}	1195.8		1768.4	
M'_{solids}	981.5		1450.3	
M'_{water}	214.3		318.1	
<i>% solids (by wt.)</i>	<i>82.08%</i>		<i>82.01%</i>	
<i>% water (by wt.)</i>	<i>17.92%</i>		<i>21.81%</i>	
<i>Final Water Content* (%)</i>	<i>21.83%</i>	<i>17.92%</i>	<i>21.93%</i>	<i>17.99%</i>

^a BFSM - Blast furnace slag mixture (pre-mixed with 10% PC and 90% slag)

* GWC based on geotechnical (M_w/M_s), and mining process (M_w/M_{paste}) calculations, respectively

4.5.2 MERCURY INTRUSION POROSIMETRY

The associated ASTM Standard, (ASTM D4404-10, 2010) Standard Test Method for Determination of Pore Volume and Pore Volume Distribution of Soil and Rock, more commonly referred to as the Mercury Intrusion Porosimetry (MIP).

4.5.2.1 THEORY OF MERCURY INTRUSION POROSIMETRY

MIP has been used to characterize a variety of porous media, including oil/gas reservoir rocks and construction materials. Measurement of the relative PSD of a porous medium

by mercury intrusion is based on the fact that mercury is a ‘non-wetting’ fluid that has to be pressurized in order to penetrate a porous medium (Diamond, 1970). The resistance to mercury penetration is caused by capillarity, which is characterized by the surface tension of mercury–solid interface, T_s , and by the mercury–solid contact angle, θ (Delage et al., 2006). The relationship between the mercury pressure and the corresponding pore-size radius is defined by the Washburn (1921) equation (Delage et al., 2006):

$$P_{Hg} = \frac{2T_s \cos \theta}{r_p} \quad [4.5.1]$$

where, P_{Hg} is the pressure of the intruded mercury, [MPa], with $T_s = 0.484$ N/m and $\theta = 141.3^\circ$, and r_p is the pore-size diameter, [μm]. Mercury intrusion tests are performed by running a progressive mercury pressure increase from atmospheric pressure up to 200 MPa (Delage et al., 2006). Based on Eqn. [4.5.1], these pressures respectively correspond to a maximum entrance pore-radius of $7.5\mu\text{m}$, and to a minimum entrance radius of 3.7nm (37\AA) (Delage et al., 2006), which are commonly referred to as the critical pore-diameter and threshold diameter, respectively.

The MIP test was performed by first preparing dry-freeze samples using liquid nitrogen (as prescribed by (Delage et al., 1982; Delage et al., 2006)). Dry-freezing technique is used to create a phase change from solid to vapour (sublimation). The sublimation technique is improved upon by using liquid pentane and immersing the specimen in a cooled liquid of low melting point itself cooled by the liquid nitrogen (Simms, 2003). The boiling point of liquid nitrogen is -196°C . Liquid pentane was introduced to the

nitrogen bath to allow the pentane to reach its approximate melting point ($-129.8\text{ }^{\circ}\text{C}$). This was observed to occur when there were no visible signs of vapour (or on the cusp of a phase change, via solid). Pentane was used to accelerate ‘flash’ freezing of the samples, thereby minimizing volume expansion (or the formation of water crystals).

4.5.2.2 SAMPLE PREPARATIONS

Specimens were prepared from Williams paste tailings containing no binder (Control), and Williams paste containing 3% and 7% binder. The sample prepared from the control, was set aside to consolidate for at least 48 hours to remove as much bleed water as possible (re: dry-freezing technique). Once the sample batches were prepared, samples were cut into small 1 by 1 cm squares specimens. Pentane was carefully poured into a metal cup ladle, approximately $\frac{1}{4}$ full, and dipped in and out of the nitrogen bath until there was no visible vapour observed from the pentane. Each specimen was freeze-dried separately. A 1 cm square sample was placed into a tea strainer over sub-cooled pentane, while intermittently dipping the pentane into the nitrogen bath for approximately 5 minutes until the specimen appeared ‘freezer-burned’ by turning white in colour. Each specimen was then labeled and placed into a dish, and into a desiccator. Specimens were prepared for each day during hydration (i.e., Day 1 through Day 28). Dehydrated specimens were shipped via FedEx to the University of Toronto where they were tested using a Mercury Porosimetry. The MIP analyses were conducted by Dragana Simone in 2010 and 2011 at the University of Toronto.

4.6 PHASE IV: PASTE FILLED COLUMN EXPERIMENT

In this Phase, the CPB column experiment was designed to simulate a backfilled CPB stope to examine the hydraulic behaviour from deposition to subsequent drainage and hydration.

4.6.1 COLUMN SET-UP

The column test was conducted in a 0.30 by 0.30 m square Plexiglas column with a height of 1.20 m. The column comprised of a draining port at the bottom with a 5 cm drainage layer, comprised of a geotextile underlying a gravel layer. Water flowing out of the drainage port was collected in a beaker, which rested on a digital scale (with a measurement accuracy of 0.1 g). The column had a number of ports for 5 tensiometers (UMS GmbH), 5 10HS and EC-5 ECH₂O probes (Decagon Devices) and 5 pore-water sampling ports, as illustrated in Figure 4.6.1.

The T5xs and soil-moisture sensors were pretreated and calibrated, respectively, prior to use. The beaker was weighed and zeroed. All measurements were recorded using a data acquisition system (DAS) and NI LabView from National Instruments, TX, USA.

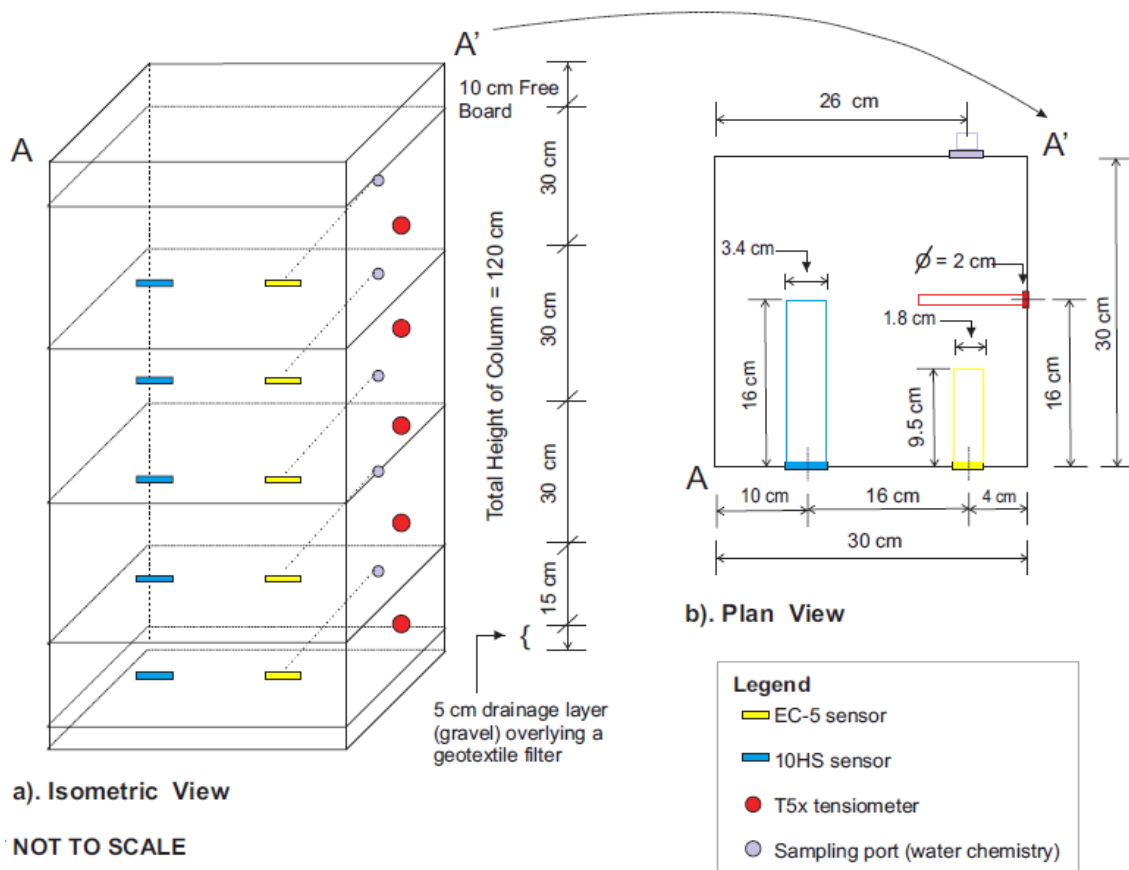


Figure 4.6.1 Design specifications of the column test

4.6.2 BACKFILLING

Williams 3% binder containing paste material was prepared and weighed prior to emplacement. The CPB material was placed in 4 subsequent layers, or ‘lifts’ and left to cure with a cover placed on top of the column to minimize evaporation.

The first layer, the ‘paste plug,’ 0.15 m thick was placed and left to cure for 20 days, while the other three (3) subsequent layers were 0.30 m thick, and allowed to cure for 30 to 34 days. A summary of each ‘lift’ and curing period is provided in Table 4.6.1.

Table 4.6.1 Summary of each 'lift' placement in the test column

Date of 'Lift' Placed <i>(dd/mm/yy)</i>	Layer <i>(pour)</i>	Thickness of Lift <i>(m)</i>	Curing Period <i>(days)</i>
1/10/10	Paste plug	0.15	20
22/10/10	1st Main pour	0.30	30
18/11/10	2nd Main pour	0.30	32
20/12/10	3rd Main pour	0.30	35

The outflow of (drained) water was collected from the bottom of the column after the placement of each paste layer. The amount of water collected from each pour was weighed and recorded in real-time, where a digital scale with an accuracy of 0.1 grams was connected to the DAS. The initial and final conditions (after consolidation and loss of drainage water) has been provided in Table 4.6.2. This data was used to calculate the bottom boundary conditions, given by equation [4.3.5]. Once vertical drainage had ceased, the water was collected and sent to Accutest Laboratories for analyses.

Table 4.6.2 Amount of paste deposited and final conditions after settlement and drainage

<i>Lift</i> <i>(pour)</i>	Initial Deposition				After Consolidation			
	$h_{initial}$ <i>(cm)</i>	$V_{initial}$ <i>(cm³)</i>	$M_{initial}$ <i>(± 0.05g)</i>	$GWC_{initial}$ <i>(%)</i>	h_{final} <i>(cm)</i>	V_{final} <i>(cm³)</i>	M_{final} <i>(± 0.05g)</i>	GWC_{final} <i>(%)</i>
Plug	15	13500	24808	37	14.2	12780	24007.5	32.6
Main 1	30	27000	49200	36.6	29.9	26910	48047.8	33.4
Main 2	30	27000	49950	36.8	29.6	26640	49388.2	35.3
Main 3	30	27000	49700	36.5	30.1	27090	49205.3	35.1

During subsequent 'lifts,' cavitation occurred with the tensiometers in the plug layer, 1st and 2nd main pour. These tensiometers were replaced with newly prepared tensiometers, by first coating the ceramic tips with saturated paste tailings, and then inserting them into the T5x ports of the column. At the end of the column test, a final water content sample was retrieved from the 3rd main layer, weighed, recorded, and placed in the oven to dry for 24 hours. Additionally, 2 samples were retrieved for total suction measurements using the WP4 DewPoint Potentiometer.

CHAPTER 5

5 EXPERIMENTAL RESULTS AND DISCUSSION

The purpose of this study was to capture the unsaturated properties of cemented paste fill material as a function of paste hydration, and use them to test the validity of a model to describe the behaviour of PWPs in CPB stopes, using an unsaturated soils framework. The following chapter presents the results from each of the experimental phase of this study with the aim of determining, as well as tracking changes in the unsaturated material properties of hydrating cemented paste tailings before and after 28 days of hydration.

The experimental work was completed in four phases, plus the physical characterization of the tailings used in this study. The results of the experimental portion of this study are presented in the order of:

- *Physical Properties of Paste Tailings* (Section 5.1);
- *Phase I: Calibrations and Treatment Protocols* (Section 5.2);
- *Phase II: Pre- and Post- Hydration Experiments* (Section 5.3);
- *Phase III: Hydration-Time Dependent Experiments* (Section 5.4);
- And, lastly, *Phase IV: Paste Filled Column Test* (Section 5.5)

5.1 PHYSICAL PROPERTIES OF PASTE TAILINGS

Geotechnical tests on two backfills are presented. One backfill material was from the Williams Gold Mine in Northern Ontario. The water content (mass of liquid/mass of solids) was 38.9%, with a slump of 8 inches. The tailings themselves were predominantly silt size, and non-plastic (approximately PL 23%, PI 2%). The other backfill, also from northern Ontario, was from the Kidd Copper-Gold Mine. The gold tailings were similar to Williams, however the backfill comprised of 55% sand and 45% tailings, differed in their physical properties, due to the addition of alluvial sand, and lower water content – 21.9% GWC. The Atterberg Limits and particle size-distribution (PSD) curves, respectively for both tailings and sand are presented in Table 5.1.1 and Figure 5.1.1.

Based on the PSD and Atterberg Limit test results, both tailings are comprised mainly of silty-clays, or CL-ML of the Unified Soil Classification System (USCS). However, because the PI was between 4 and 7, and the LL between 12 and 25, both tailings may also be classified as SC-ML, or silty clayed-sand. Williams tailings comprised of approximately 3% fines, while Kidd tailings comprised of approximately 10% fines. The alluvial sand used in the Kidd paste fill material was provided by Kidd Mine, initially as well-graded sand with gravel, or SW. It should be noted here that the PSD of sand used for Kidd paste represents only three quarters of the amount of bulk sand that passed sieve No. 4 (particles smaller than 4.75 mm).

Table 5.1.1 Atterberg Limits and bulk densities of the materials used in the experimental phase

Tailing Stream	LL	PL	PI	SL	Specific Gravity (g/cm^3)
		(%)			
Williams Tailings	23.9	22.7	2.2	14.6	2.73
Kidd Tailings	24.1	22.9	2.3	12.1	2.81
Alluvial Sand	--	--	--	--	2.74*

* Specific gravities reported by Kidd Creek' Porcupine Gold Mine Material Safety Data Sheets (MSDS, 2009)

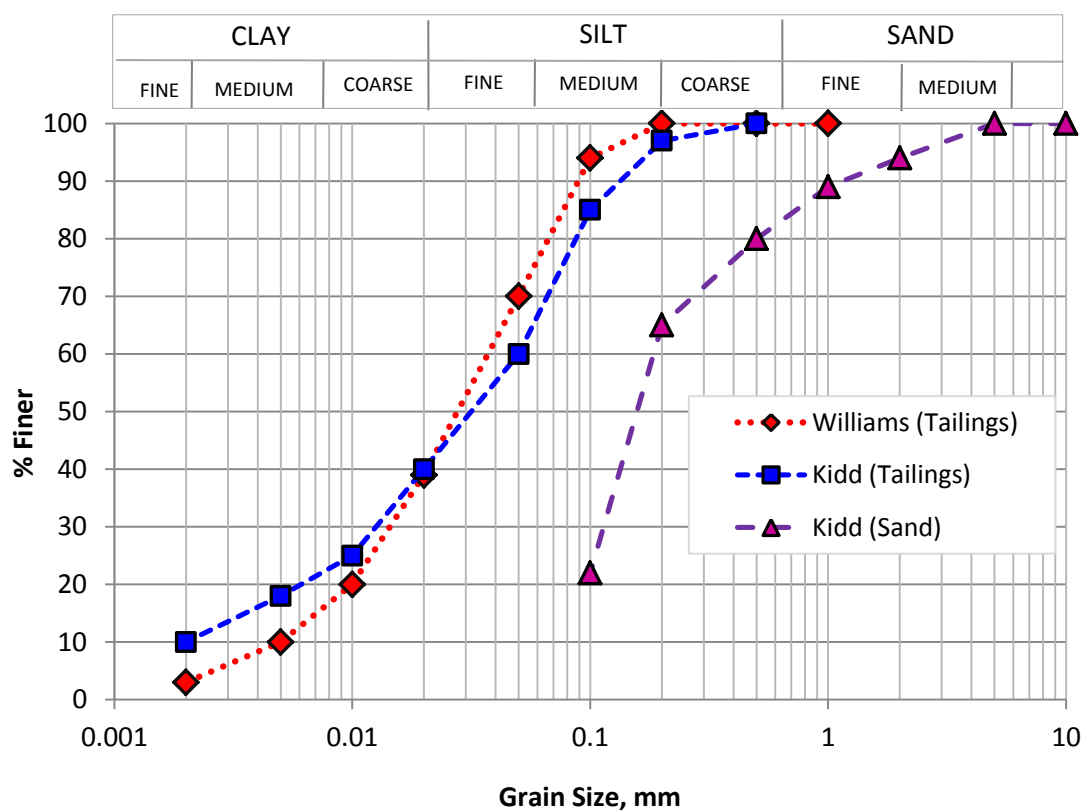


Figure 5.1.1 Grain-size distributions for tailings and aggregates in Williams and Kidd CPB mixtures

5.2 PHASE I: CALIBRATION CURVES AND TREATMENT RESULTS

Phase I: Calibration Curves and Treatment Results, examines the limits and characteristics of the non-contact vertical displacement / proximity sensor in Section 5.2.1, as well as the EC soil-moisture sensors in Sections 5.2.2. The saturated hydraulic conductivity of the ceramic porous disc(s) used in the WRC testing is examined in Section 5.2.3.).

5.2.1 VERTICAL DISPLACEMENT SENSOR

The calibration of the non-contact vertical displacement sensor was tested at various voltages (Figure 5.2.1). A linear regression was observed when displacement was plotted as a function of the output current, yielding

$$y = 7.6978(mV) - 11.876 \quad [5.2.1]$$

where, y is the estimated vertical displacement, and mA is the output current. The calibration equation (Eqn. [5.2.1]) was used to estimate the vertical volume changes during the axis translations tests.

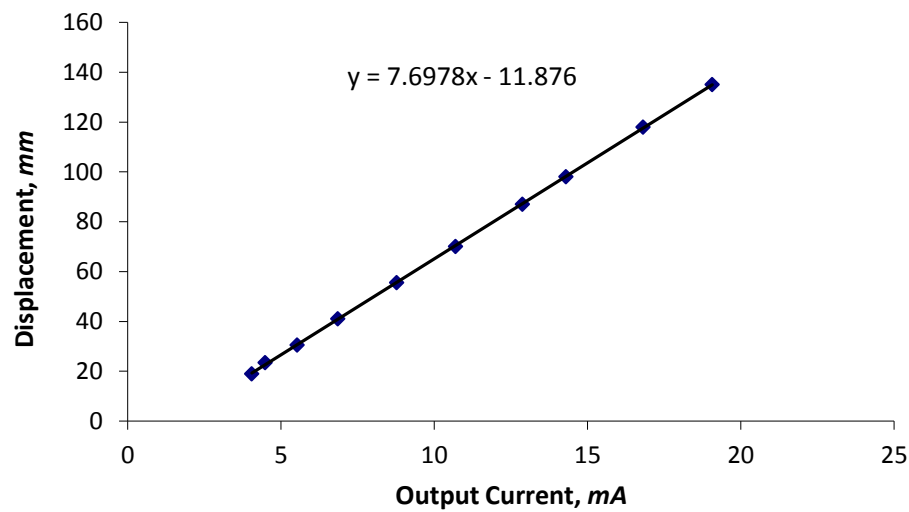


Figure 5.2.1 Calibration curve: non-contact displacement / proximity sensor

5.2.2 ECH2O SOIL-MOISTURE SENSORS

The EC-5 and 10HS sensors measure the dielectric constant (permittivity) of the soil in order to find its VWC. The permittivity of a soil is related to the capacitance of soil-water, and thus, voltage. Mineral content and pore-water may affect measurements of soil permittivity, thus, EC-5 and 10HS sensors were calibrated with Williams tailings containing (i) no binder, and paste containing (ii) 3% and (iii) 7% binder.

These soil-moisture sensors provide output data in two formats. One, in terms of VWC (m^3/m^3), which is a standard calibration (i.e. manufactory calibrated) provided by Decagon Devices Inc. for a generic mineral soil (Campbell, 2002). The second set of data is in the form of *raw data* or voltage, in units of millivolts (mV). The output data and experimentally measured water contents were used to generate soil-specific calibration curves.

5.2.2.1 WILLIAMS PASTE TAILINGS

Voltage output (raw data) was collected and recorded at a 60 second frequency. For practical purposes, an average value was calculated over a 20 point moving average. The data was compared with the computed (Decagon's) VWCs (Decagon's factory calibration), with the experimentally measured VWCs (Section 4.3.2, pg. 110) as a function of the raw data. Table 5.2.1 provides a summary of these results for Williams' tailings. Decagon's standard calibration for mineral soil and material specific calibration curves for the EC-5 and 10HS sensors are presented in Figure 5.2.2 and Figure 5.2.3, respectively.

Table 5.2.1 Williams Tailings: Measured volumes, water contents and averaged raw data (voltage output from Decagon's data logger)

Sample No.	10HS	EC-5	V_{paste}	V_{water}	VWC	GWC
	<i>Raw Data (mV)</i>					
1	665.83	522.50	670	3	0.45	0.43
2	683.75	544.33	670	8	1.19	1.35
3	694.55	551.64	670	20	2.99	3.18
4	760.25	614.00	670	56	8.36	7.76
5	886.45	709.09	670	124	18.51	12.34
6	1107.00	849.57	670	188	28.06	17.83
7	1366.60	957.45	670	249	37.16	23.33
8	1377.54	992.23	670	258	38.51	24.24

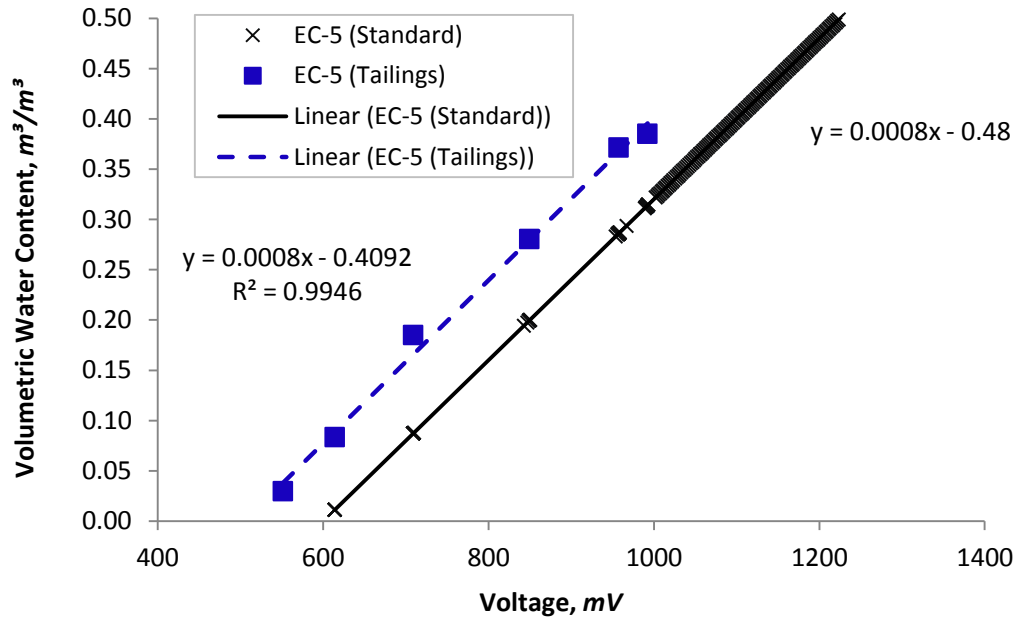


Figure 5.2.2 Calibration of the EC-5 sensor: (1) VWC estimate based upon measured values obtained experimentally, calibrated for Williams' tailings, and (2) Decagon's calibration for mineral soil.

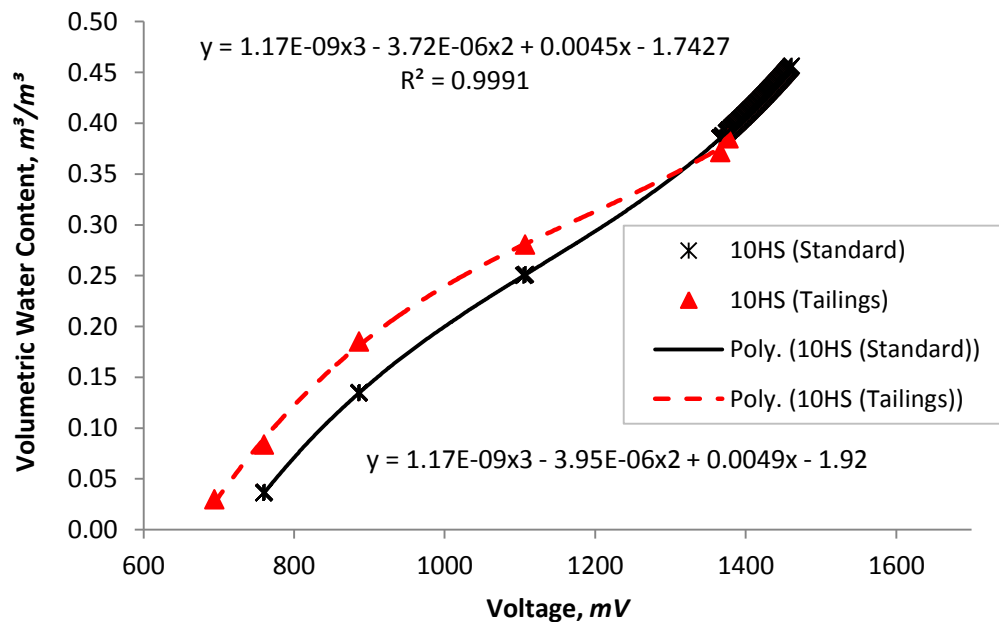


Figure 5.2.3 Calibration of the 10HS sensor: (1) VWC estimate based upon measured values obtained experimentally, 'soil-specific' calibration, and (2) Decagon's calibration for mineral soil

It appears that for both sensors, there is an off-set between the standard and material specific calibration curves. A linear equation was used to fit the calibration data of the EC-5 (Figure 5.2.2), which off-sets the VWCs of the standard calibration by an approximately 5% VWC increase. For the 10HS sensor, the off-set is significant, especially because the relationship between the voltage output and water content appears to be non-linear. A third order polynomial was used to fit the experimental data, as suggested by Decagon Devices' User Manual for Soil-specific Calibrations (Campbell, 2002). The polynomial appears to fit well with the experimental data. Each sensor operates between set excitation voltages.

5.2.2.2 CEMENTED PASTE: 3% AND 7% BINDER MATERIAL

Williams paste containing 3% and 7% binder were prepared respectively, at approximately 37% and 36% GWC. The samples were then allowed to dry, completely exposed to the air in the laboratory. Figure 5.2.4 presents the measured volumetric and gravimetric water contents for the 3% and 7% binder paste as function of time for Test #1 (March, 2010). Figure 5.2.5 presents the measured volumetric water contents for the 3% and 7% binder paste during Test #2 (April, 2010). It should be noted here, that the measured VWCs were obtained from grab samples.

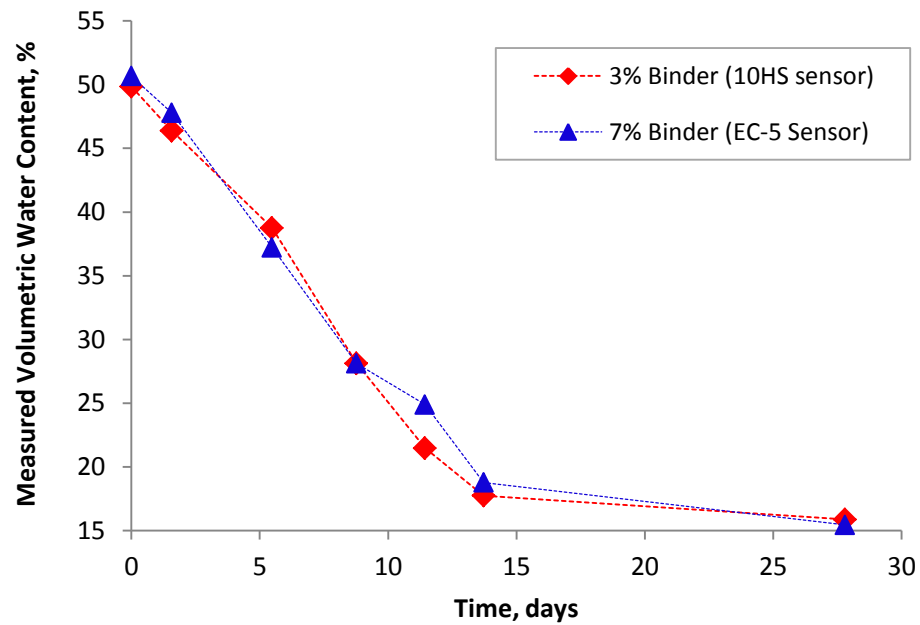


Figure 5.2.4 Test #1: Volumetric water contents from grab samples prepared with 3% and 7% binder (Williams paste)

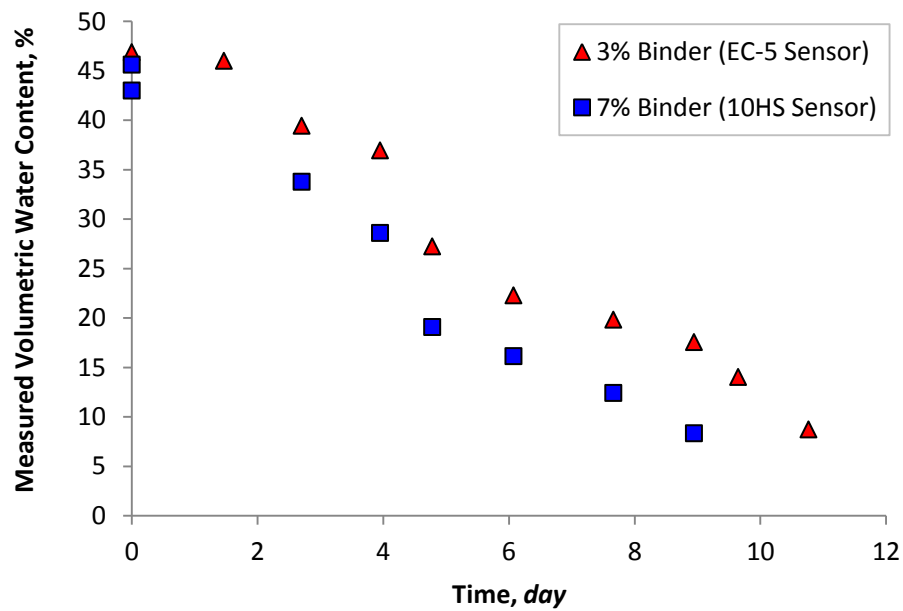


Figure 5.2.5 Test #2: Volumetric water contents from grab samples prepared with 3% and 7% binder (Williams paste)

For Test #1, the 10HS sensor was calibrated for the 3% binder material, while the EC-5 sensor was calibrated for the 7% binder material. The output data (voltage) was recorded at 20 minute intervals for approximately 28 days. The data recorded for the 10HS (3% binder) and the EC-5 (7% binder) were plotted against time (Figure 5.2.6 and Figure 5.2.7, respectively). Variations observed within these data sets are related to noise (i.e., sample disturbances while retrieving samples for oven-drying). Two linear equations were fitted to both data sets in order to extrapolate the voltage output at the time of each sampling measurements. In other words, the experimental data in Figure 5.2.4 was transformed using the linear equations to convert time into voltage output. Voltages were correlated with the measured VWCs to generate the calibration curves. The results of Test #1 have been summarized and presented in Table 5.2.2.

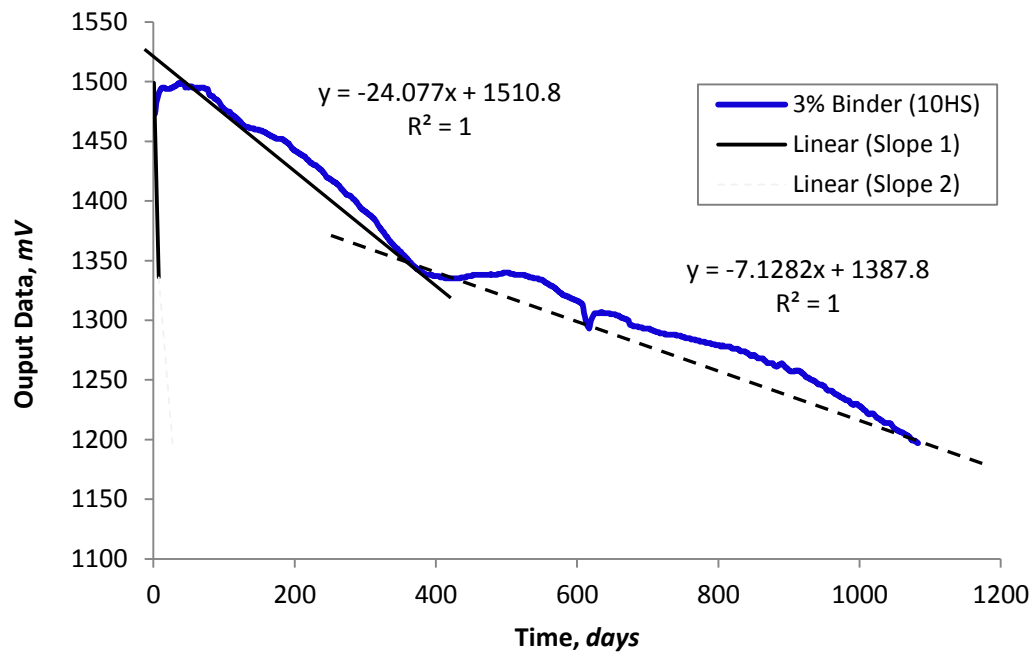


Figure 5.2.6 10HS Sensor calibrated for 3% binder material (Test #1): Output data as a function of Time

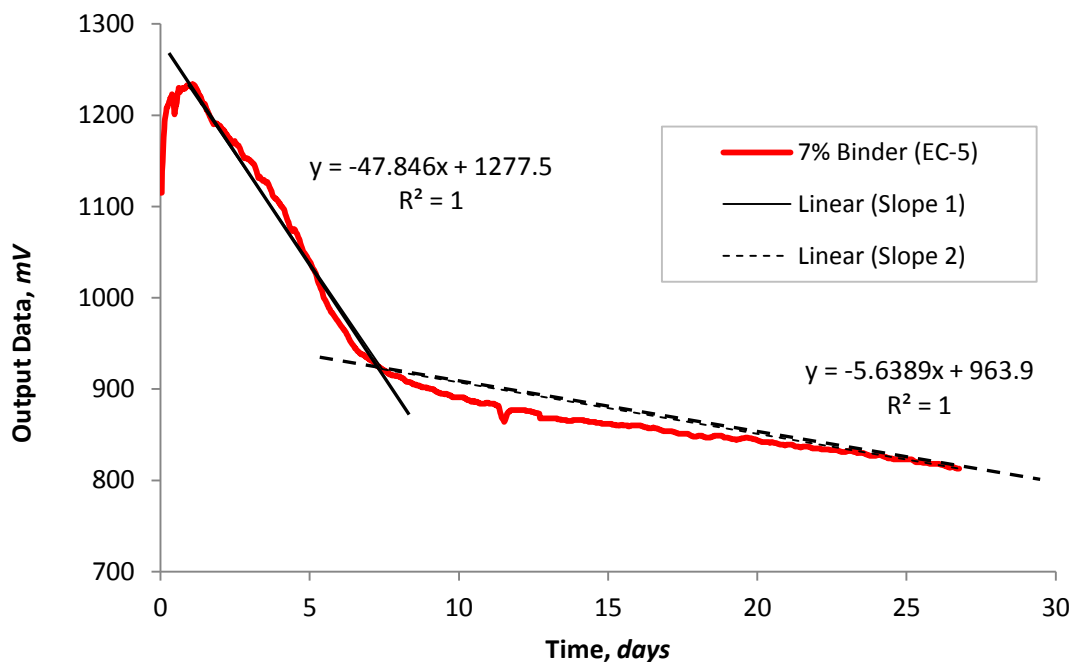


Figure 5.2.7 EC-5 Sensor calibrated for 7% binder material (Test #1): Output data as a function of Time

Table 5.2.2 Calibration data for Williams' 3% and 7% binder material (Test #1): water contents, and raw data from the 10HS and EC-5 sensors

Day	<i>7% Binder</i>		<i>3% Binder</i>	
	VWC (%)	EC-5 (mV)	VWC (%)	10 HS (mV)
0	50.7	1278	49.9	1511
2	47.8	1202	46.4	1473
5	37.2	1015	38.8	1379
9	28.1	914	28.1	1325
11	24.9	899	21.5	1306
14	18.8	887	17.8	1290
28	15.5	807	15.9	1190

For Test #2, the EC-5 sensor was calibrated with 3% binder material, while the 10HS sensor was calibrated with 7% binder material. Data obtained for Test #2 was processed in the same way as previously described. The results of Test #2 are summarized in Table 5.2.3. Due to higher binder content of the 7% paste material day, volume samples were not retrieved after the 9th (due to hardening).

Table 5.2.3 Calibration data for Williams' 3% and 7% binder material (Test #2): water contents, and raw data from the EC-5 and 10HS sensors

Day	3% Binder		7% Binder	
	VWC (%)	EC-5 (mV)	VWC (%)	10 HS (mV)
0	46.9	1067	45.6	1578
1	46.0	999	43.0	1464
3	39.4	943	33.8	1369
4	36.9	886	28.6	1273
5	27.2	848	19.1	1209
6	22.3	789	16.2	1109
8	19.8	716	12.4	987
9	17.6	658	8.4	888
10	14.0	626	--	--
11	8.7	575	--	--

The calibrations curves for the 10HS and the EC-5 sensors calibrated with Williams 3% and 7% binder materials are presented in Figure 5.2.8 and Figure 5.2.9., respectively. A linear equation was used to fit the data for the EC-5 sensor, and a 3rd order polynomial was used to fit the data for the 10HS sensor.

VWCs for the tailings containing 3% can be determined by using the following calibration equations, where x is the voltage output (or raw data) in mV.

For the EC-5 sensor

$$VWC_{EC-5} = 0.0806x - 37.459 \quad [5.2.2]$$

And, for the 10HS

$$VWC_{10HS} = 3.289 \times 10^{-6} x^3 - 0.0144x^2 + 21.107x - 10313 \quad [5.2.3]$$

Similarly, VWCs for the tailings containing 7% can be determined using the following calibration equations:

$$VWC_{EC-5} = 0.0764x - 44.632 \quad [5.2.4]$$

And, for the 10HS

$$VWC_{10HS} = -1.81 \times 10^{-7} x^3 + 0.000697x^2 - 0.8215x + 316.28 \quad [5.2.5]$$

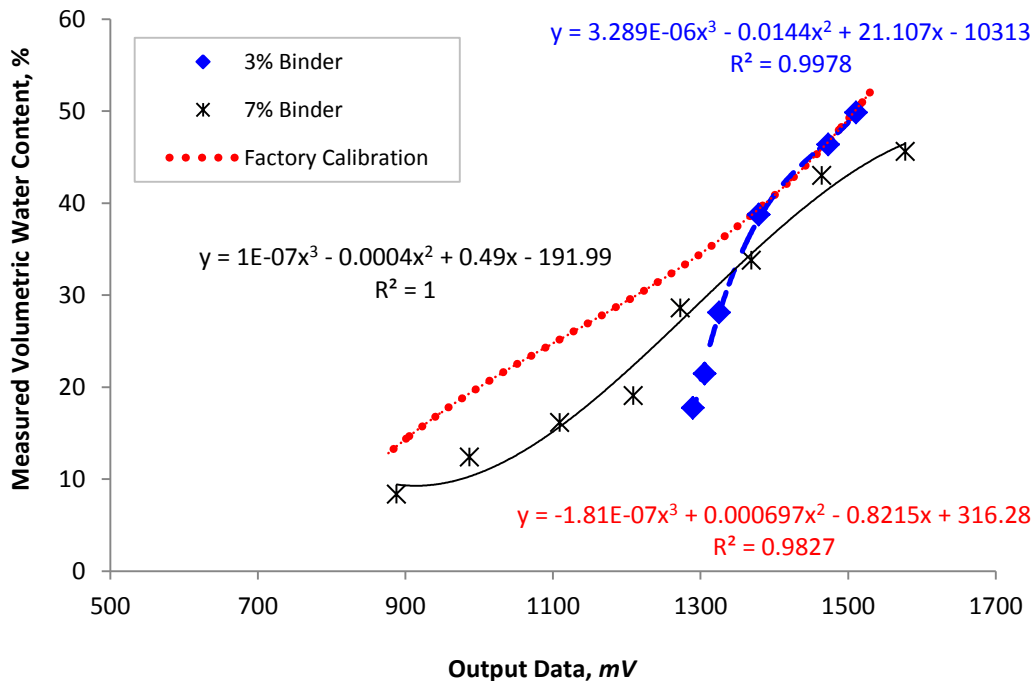


Figure 5.2.8 10HS calibration curves that were calibrated for Williams' paste containing 3% and 7% binder

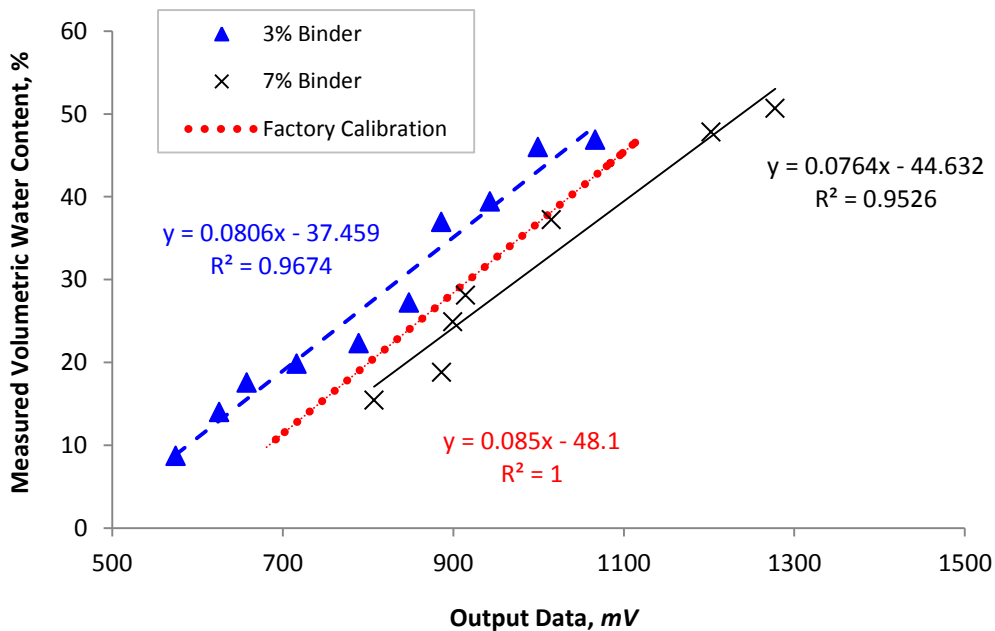


Figure 5.2.9 EC-5 calibration curves that were calibrated for Williams' paste containing 3% and 7% binder

5.2.3 SATURATION METHOD: HIGH AIR-ENTRY VALUE POROUS DISCS

The saturation mass of the 5 bar and 15 bar ceramic porous discs were weighted at 171.6 and 174.1 \pm 0.05g, respectively. It is assumed that the complete saturation condition is met when the pre-treated ceramic porous discs weighed the respective saturation mass. This assumption is based on a protocol discussed by Marinho et al. (2008) once the saturation hydraulic conductivity of the disc has been measured, compared and verified with the manufacturer's value (Table 5.2.4).

The experimentally determined hydraulic conductivities of the 5 bar and 15 bar ceramic discs were 1.16×10^{-9} m/s and 2.45×10^{-11} m/s, respectively. Reported permeabilities (provided by SoilMoisture Equipment Corp., 2008 catalogue) for the 5 bar and 15 bar are 1.21×10^{-9} m/s and 2.59×10^{-11} m/s, respectively. The percent error (% Error = |Estimated – Actual|/Actual) for the 5 bar is 4.1%, and for the 15 bar is 5.4%. A summary of these values are provided in Table 5.2.4.

Based on the relatively low % error, it was assumed that the condition of complete saturation was attained when the wet mass of the porous discs after pre-treatment were equal to the saturation mass of 171.6 g for the 5 bar and 174.1 g for the 15 bar porous disc. The saturation mass of each disc was to serve as a quality control measure to ensure that complete saturation of each disc was obtained prior to each use in the axis translation technique.

Table 5.2.4 Measured versus actual saturated hydraulic conductivity of the 5 bar and 15 bar ceramic porous discs

AEV Disc (bar)	ψ (m·H ₂ O)	Time (h)	dh/dL (m·H ₂ O/m)	Flux (m ³ /s·m ²)	K _s Estimate (m/s)	K _s Actual*	ERR (%)
5	2.21	21.1	211.1	2.45 x 10 ⁻⁷	1.16 x 10 ⁻⁹	1.21 x 10 ⁻⁹	4.1
15	4.97	36.6	471.0	1.15 x 10 ⁻⁸	2.45 x 10 ⁻¹¹	2.59 x 10 ⁻¹¹	5.4

* Published values provided in by SoilMoisture Equipment Corporations, Ceramics Catalogue (2008)

5.3 PHASE II: PRE- AND POST-HYDRATION RESULTS

Phase II: Pre- and Post-Hydration Results, examined the lower and upper bound material properties of paste with no binder (pre-hydration conditions) and paste with binder (post-hydration conditions). The materials' properties of the pre- and post-hydration periods for Williams and Kidd tailings without binder and with binder are presented in Section 5.3.1. The differences between the two tailings stream are compared and discussed in Section 5.3.2.

5.3.1 DIRECT AND INDIRECT SUCTION MEASUREMENTS

Direct and indirect measurement results of the pre- and post-curing period of the material, allowed for the entire range of the WRC to be determined, the shrinkage curves and the volumetric (or shrinkage) strain curves in the +PWP regime to be obtained. The results of the pre- and post-hydration tests for Williams (Section 5.3.1.1) and Kidd (Section 5.3.1.2) are presented and discussed in these next two subsections.

5.3.1.1 WILLIAMS PASTE: PRE- AND POST-HYDRATION

Water contents and volume change measurements recorded for Williams paste containing no binder were obtained for matric suctions ranging from 0 to 320 kPa, and total suctions ranging from 1.2 MPa to 150 MPa. The results of direct and indirect methods are provided in Table 5.3.1. The entire range of the lower bounded WRC of Williams containing no binder is provided in Figure 5.3.1.

Table 5.3.1 Pre-water retention data for Williams paste tailings containing no binder

Suction (kPa)	VWC	GWC (%)	Degree of Saturation	Void Ratio (m ³ /m ³)
1	44.53	31.42	100.00	0.93
30	39.04	22.06	100.00	0.58
50	40.02	22.18	100.00	0.57
90	27.57	14.85	74.80	0.54
130	19.65	10.47	54.30	0.53
190	13.61	7.25	43.40	0.46
250	10.44	5.56	33.30	0.46
320	8.34	4.44	26.60	0.46
1150	5.13	3.06	18.00	0.46
1220	4.67	2.97	17.40	0.46
1670	4.35	2.50	14.70	0.46
1670	4.35	2.50	14.70	0.46
2140	4.48	1.81	10.60	0.46
4160	3.20	1.25	7.30	0.46
7905	1.55	0.60	3.50	0.46
90540	0.46	0.15	0.90	0.46
133830	0.59	0.21	1.20	0.46
141190	0.36	0.12	0.70	0.46
149560	0.29	0.12	0.70	0.46

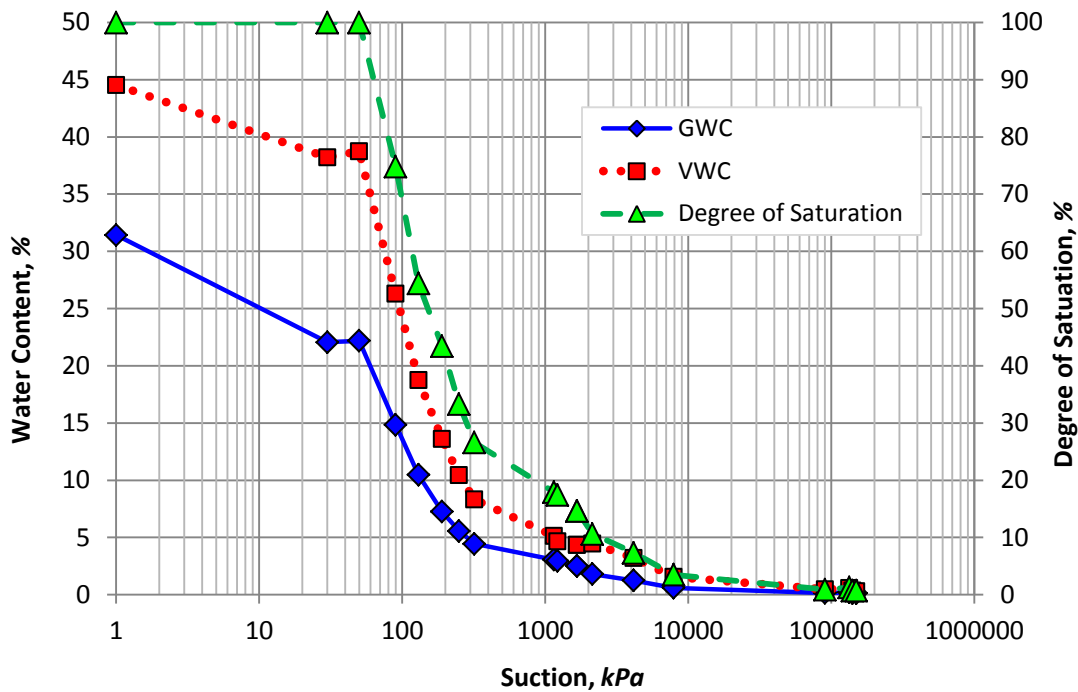


Figure 5.3.1 Williams' pre-hydrated water-retention curve data

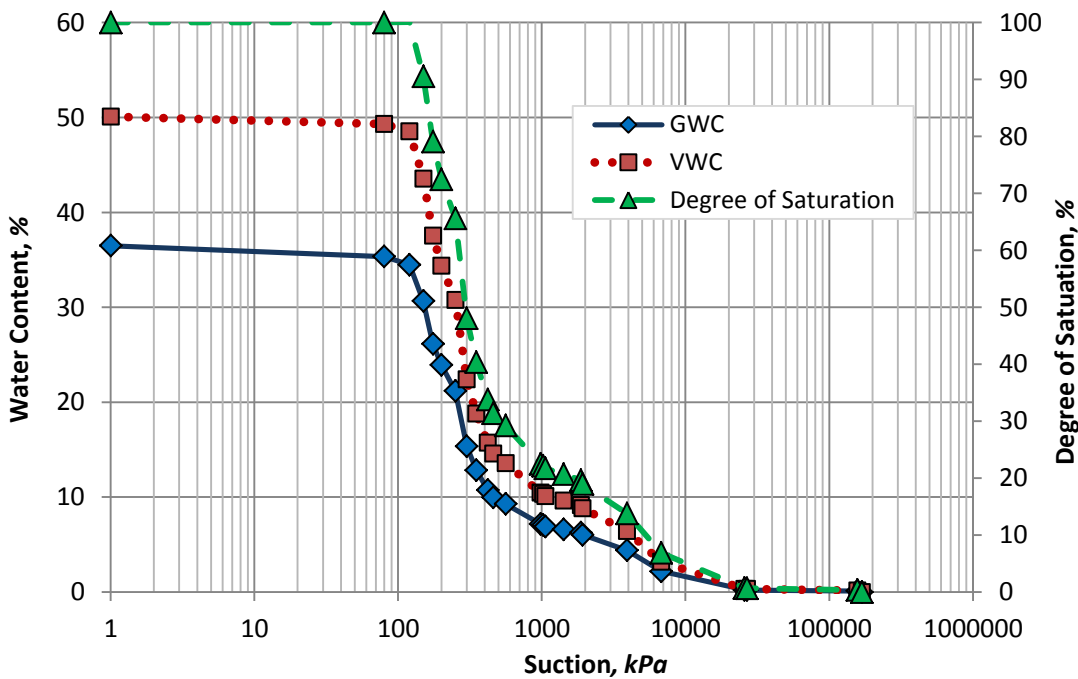


Figure 5.3.2 Williams' Trial #2, post-hydrated water-retention curve data in terms of water content and degree of saturation

Table 5.3.2 Williams' post-hydrated water-retention curve data (Trial #2) for specimen containing 3% binder

Suction (kPa)	GWC	VWC (%)	Degree of Saturation	Void Ratio (m ³ /m ³)
1	36.49	50.08	100.00	0.99
80	35.35	49.31	100.00	0.96
120	34.48	48.55	100.00	0.94
150	30.66	43.53	90.57	0.93
175	26.14	37.55	79.09	0.90
200	23.91	34.37	72.47	0.90
250	21.18	30.76	65.61	0.88
300	15.34	22.40	48.06	0.87
350	12.84	18.78	40.40	0.87
420	10.74	15.72	33.82	0.87
460	9.97	14.58	31.38	0.87
560	9.28	13.58	29.23	0.87
980	7.17	10.48	22.53	0.87
1020	7.06	10.32	22.19	0.87
1060	6.91	10.10	21.71	0.87
1420	6.59	9.63	20.71	0.87
1870	6.25	9.14	19.65	0.87
1920	6.03	8.82	18.96	0.87
3920	4.39	6.42	13.79	0.87
6781	2.19	3.20	6.88	0.87
25723	0.23	0.34	0.72	0.87
26820	0.21	0.31	0.66	0.87
157230	0.11	0.16	0.35	0.87
168260	0.00	0.00	0.00	0.87

The prominent differences between the pre- and post-hydrated WRCs are the slope before the AEV, and the AEV itself. The AEV of each specimen was observed at the +PWP or at 100% degree of saturation. This region, suctions, prior to the AEV is often times referred to as the tension-saturated region, where water is held due to capillary forces. For the pre-hydrated Williams containing no binder, the AEV was observed at 50 kPa,

and for the post-hydrated cemented paste material, the AEV was observed at 120 kPa, which is expected due to cement hydration. In Figure 5.3.3 the decrease in water content, greater than 23% GWC is almost concurrent with shrinkage. In other words, the change in volume of water is roughly equal to the change in volume of voids for water contents greater than 23% GWC. The paste specimen is initially saturated (i.e., ~ 31% GWC), and follows the saturation line until air begins to enter the intergranular spaces (voids). This point is an indication of the AEV (~50 kPa). As the specimen begins to desaturate, it reaches the minimum void ratio of 0.46, at which no further volume changes occur; hence reaching the shrinkage limit. The shrinkage limit for the fully hydrated 3% containing specimen (Figure 5.3.4) is approximately 31% GWC. As one would expect the shrinkage limit is significantly higher than that of the specimen containing no binder, due to the formation of the cemented gel grains of the post-hydrated paste. One would also suspect that the permeability also decreased, such that water flow was restricted; and hence, impeding any significant reduction in volume changes. As expected in Williams with no binder (Figure 5.3.1), the material drying from the water content above its shrinkage limit (~ 31% GWC) produces a larger slope. Whereas, the slope of the fully hydrated WRC, prior to the AEV (or tension saturated region) was quite flat. As discussed in Simms and Grabinsky (2009), the flatness of the curve allows significant matric suctions to develop when relatively small quantities of water are consumed during hydration. The slope of the WRC before the AEV is correlated to stiffness of the solid matrix, such that the stiffer the material, the more resistant it is to dewatering by squeezing from matric suction.

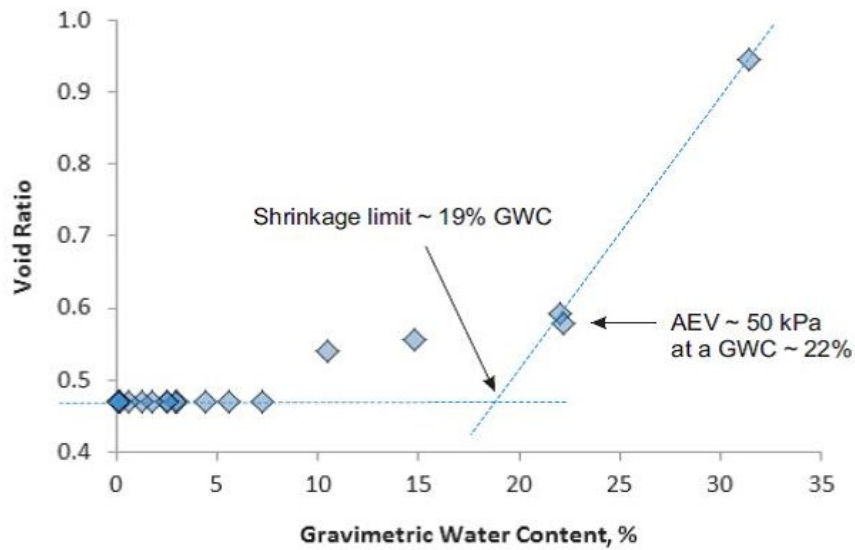


Figure 5.3.3 Pre- shrinkage curve for Williams tailings containing no binder

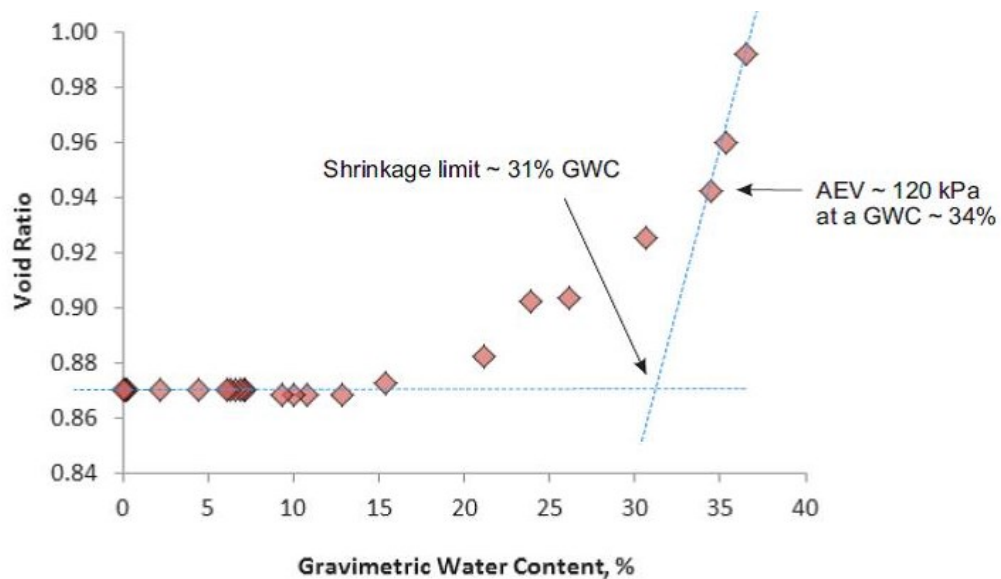


Figure 5.3.4 Post- shrinkage curve for Williams containing 3% binder

An increase in stiffness is indicated by the volumetric strain versus matric suctions curves in the +PWP regime, prior to the AEV (Figure 5.3.5). The compressibility or stiffness of the solid matrix, commonly referred to as the coefficient of volume change

(compressibility), m_v , (at 100% degree of saturation) is an index of the material's compressibility (of the solid matrix). The smaller the coefficient, the less compressible or more resistant the material is to undergo further compression that may be facilitated at higher suctions (i.e. during desaturation). Provided in Figure 5.3.5 and Figure 5.3.6, are the volumetric strain measurements made prior to reaching the AEV(s) for the uncemented tailings specimen and the cemented paste 3% binder specimen, respectively. The coefficient of volume change for Williams tailings containing no binder determined in the range of 0 – 50 kPa was 0.0038 1/kPa. Whereas, the compressibility of the post-hydrated 3% binder specimen in the range of 0 – 80 kPa was 0.00021 1/kPa. The coefficient of compressibility of the post-hydrated CPB material is as expected, smaller than the paste tailings containing no binder. The effect of cement hydration increases the water-retention properties (i.e., WRC and AEV) and stiffness.

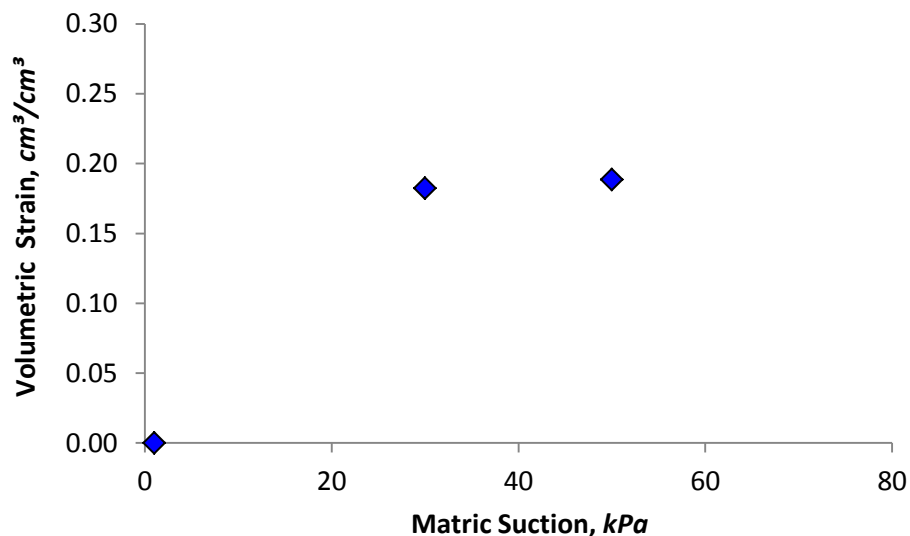


Figure 5.3.5 Williams' specimen containing no binder: pre- volumetric strain curve in the positive pore-water pressure region

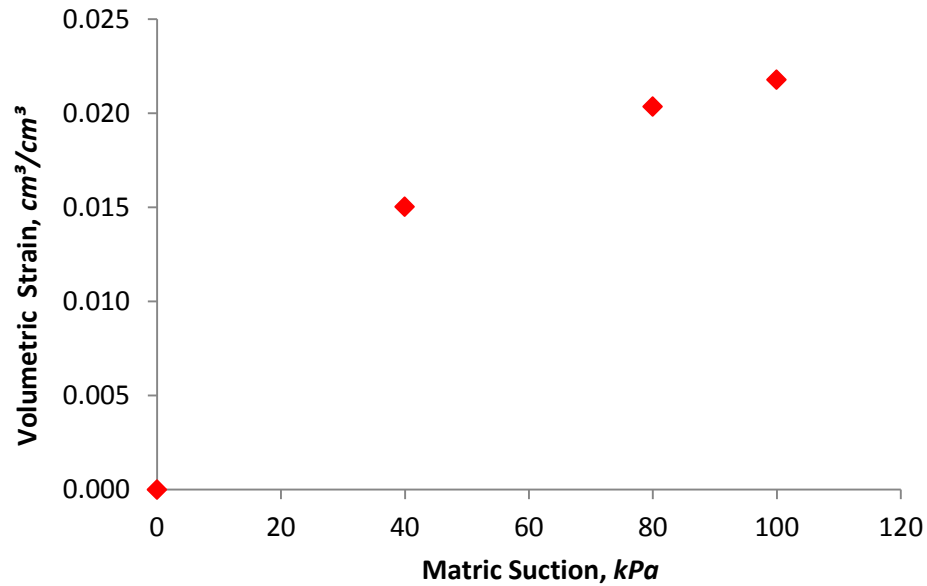


Figure 5.3.6 Williams 3% binder containing specimen: post- volumetric strain curve in the positive pore-water pressure region

5.3.1.2 KIDD PASTE: PRE- AND POST-HYDRATION

Results for Kidd paste were found (i.e., AEV(s), volume change and material compressibility) with the Kidd tailings with and without binder. The axis translation technique was employed for Kidd paste tailings (with no binder) and Kidd CPB material containing 2.2% binder, post-hydration after 28 days.

The uncemented Kidd tailings specimen was allowed to settle for 24 hours prior to testing. Bleed water pooled on the surface, and 21.7 grams of water was removed with a syringe. The pre-WRC of Kidd paste is presented in Figure 5.3.7. The WRC data for Kidd tailings obtained via the axis translation technique and the chilled mirror dew point psychrometer. The axis translation technique was used to measure matric suctions in the range of 0 to 230 kPa. Once it was found that there was very little change in mass,

indirect measurement of total suction was employed, measuring suctions from approximately 850 kPa to 162 MPa. Matric suctions for the fully hydrated Kidd paste that contained 2.2% binder were measured between the ranges of 0 to 540 kPa. The post-WRC for Kidd 2.2% paste is presented in Figure 5.3.8. While the residual water content, total suction measured in the range of approximately 830 kPa to 107 MPa.

The lower and upper bounded WRCs, for Kidd tailings, respectively, without binder and with 2.2% binder, underwent significant changes. The AEV of the pre-hydrated Kidd tailings at 100% saturation was observed to be approximately 40 kPa (Table 5.3.3), and for the post-hydrated cemented Kidd tailings, the AEV was observed at 140 kPa (Table 5.3.4).

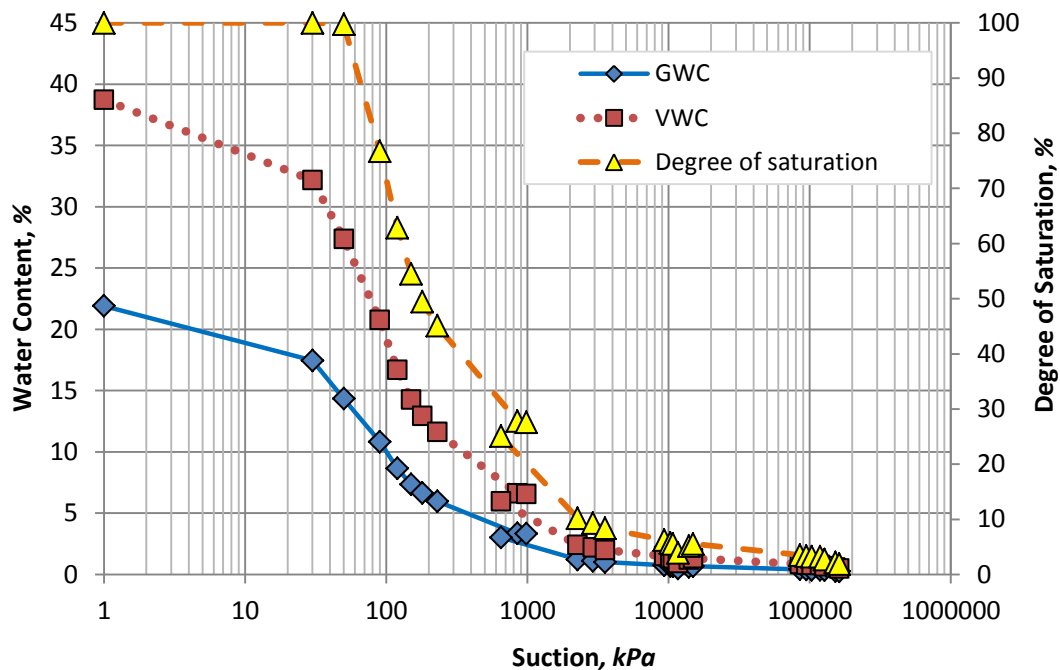


Figure 5.3.7 Pre- water-retention curve data in terms of water content and degree of saturation (S) for Kidd material containing no binder

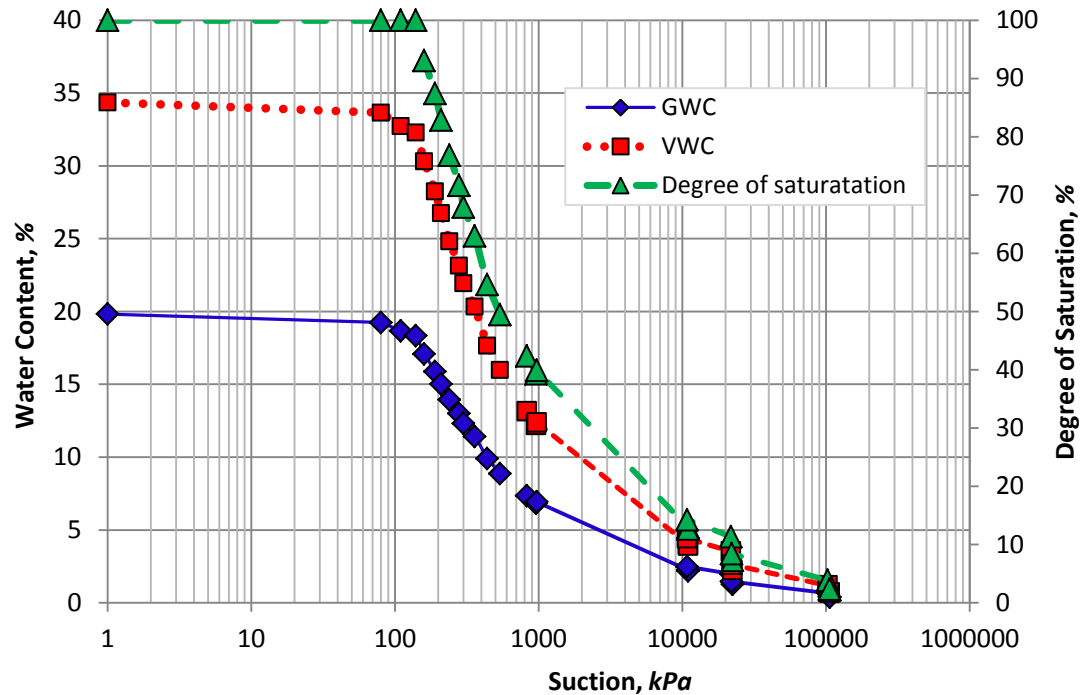


Figure 5.3.8 Post- water-retention curve data in terms of water content and degree of saturation (S) for Kidd material containing 2.2% binder

Similar to Williams pre- and post-hydrated WRC(s), the decrease in water content for the uncemented Kidd tailings is also concurrent with shrinkage. The shrinkage limit for Kidd tailings is observed at approximately 12% GWC (Figure 5.3.9), whereas the shrinkage limit of the fully hydrated CPB material is observed at approximately 15% GWC (Figure 5.3.10). This difference is prominently due to the small changes in volume / shrinkage strain when the material is fully hydrated), versus no binder and no hydration.

Table 5.3.3 Water-retention data for Kidd paste tailings containing no binder

Matric Suction <i>(kPa)</i>	GWC	VWC <i>(%)</i>	Deg. Sat	Void Ratio <i>(cm³/cm³)</i>
0	21.92	38.74	100	0.47
30	17.46	32.19	100	0.41
50	14.34	27.36	99.35	0.36
90	10.82	20.76	76.75	0.35
120	8.65	16.7	62.89	0.34
150	7.34	14.26	54.51	0.33
180	6.66	12.93	49.49	0.33
230	5.97	11.64	45.08	0.33
850	3.35	6.63	27.85	0.33
980	3.32	6.57	27.57	0.33
650	3.02	5.97	25.08	0.33
2270	1.23	2.43	10.19	0.33
2910	1.12	2.22	9.31	0.33
3540	1.01	1.99	8.37	0.33
9340	0.75	1.49	6.25	0.33
10270	0.69	1.37	5.73	0.33
10720	0.67	1.32	5.54	0.33
11640	0.48	0.94	3.94	0.33
13920	0.62	1.22	5.13	0.33
14870	0.67	1.33	5.57	0.33
85250	0.42	0.84	3.51	0.33
94670	0.40	0.8	3.36	0.33
103350	0.39	0.77	3.25	0.33
127610	0.34	0.67	2.67	0.33
152150	0.28	0.55	2.20	0.33
161780	0.24	0.47	1.88	0.33

Table 5.3.4 Water-retention data for post-hydrated Kidd paste containing 2.2% binder

Matric Suction <i>(kPa)</i>	GWC	VWC <i>(%)</i>	Deg. of Saturation	Void Ratio <i>(cm³/cm³)</i>
0	19.83	34.34	103.65	0.5
80	19.25	33.66	103.62	0.48
110	18.67	32.74	101.34	0.48
140	18.35	32.3	100.79	0.47
160	17.09	30.31	96.14	0.46
190	15.87	28.25	90.34	0.46
210	15.03	26.76	85.6	0.45
240	13.94	24.81	79.37	0.45
280	13.00	23.15	74.05	0.45
300	12.33	21.95	70.20	0.45
360	11.43	20.34	65.07	0.45
440	9.91	17.65	56.45	0.45
540	8.86	15.99	51.13	0.45
830	7.36	13.15	42.39	0.45
960	6.94	12.39	39.92	0.45
970	6.83	12.2	39.33	0.45
10820	2.48	4.43	14.28	0.45
10990	2.24	4.01	12.92	0.45
11020	2.2	3.93	12.67	0.45
21910	1.97	3.52	11.35	0.45
22100	1.46	2.61	8.43	0.45
22400	1.27	2.27	7.31	0.45
102700	0.67	1.2	3.86	0.45
106200	0.4	0.72	2.33	0.45
106500	0.39	0.7	2.25	0.45

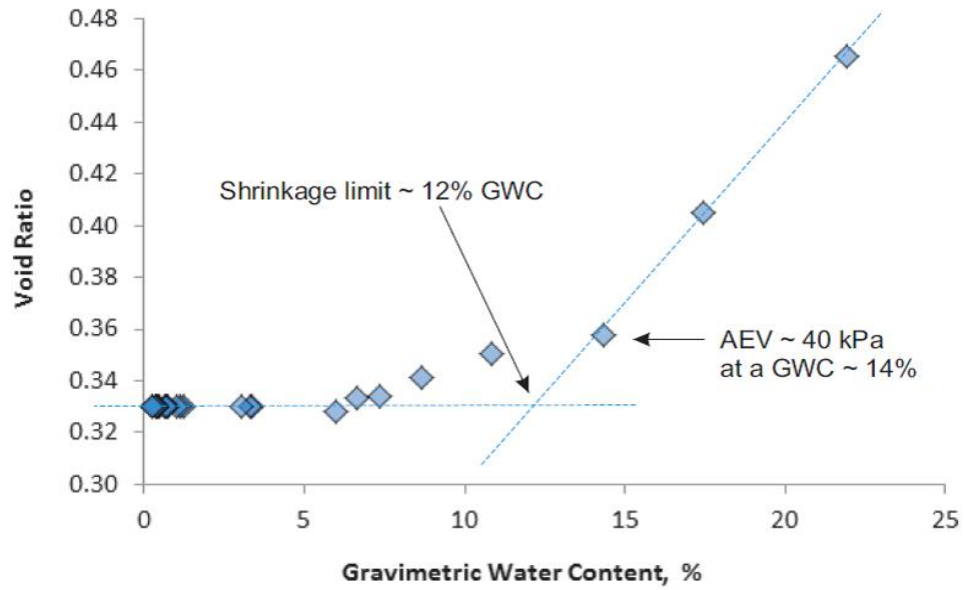


Figure 5.3.9 Pre- shrinkage curve for Kidd paste material with no binder

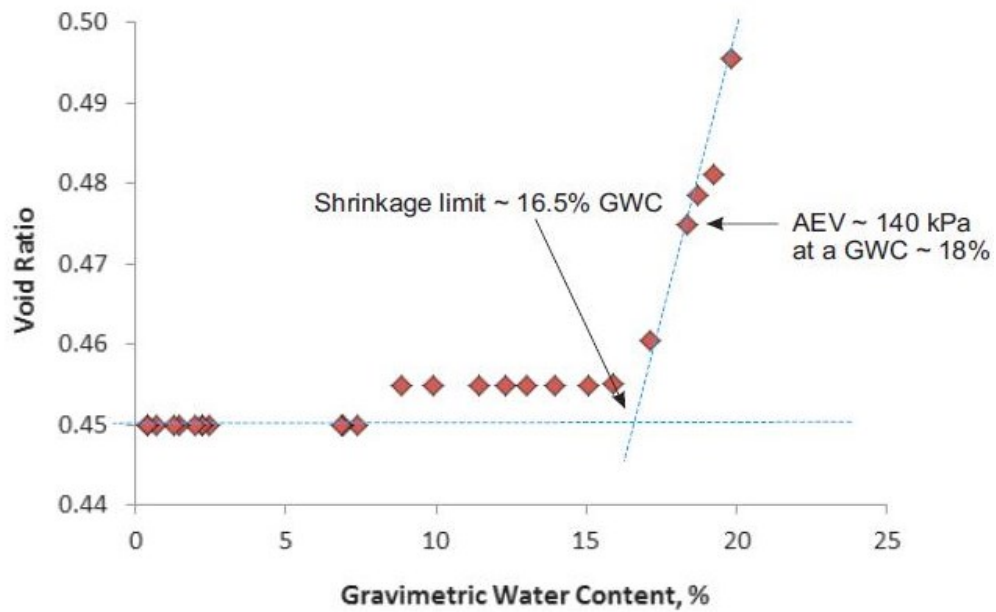


Figure 5.3.10 Post- shrinkage curve for Kidd paste with 2.2% binder

Figure 5.3.11 and Figure 5.3.12 represents the volumetric strain measurements made before the AEV(s) of the uncemented specimen and the 2.2% binder specimen, respectively. The material compressibility of the uncemented Kidd tailings was determined to be 0.0014 kPa^{-1} in the range of 0 – 30 kPa. For the fully hydrated CPB specimen, the material compressibility was determined to be 0.00012 kPa^{-1} in the range of 0 – 80 kPa. The smaller coefficient of volume change is expected, since the fully hydrated material is significantly stiffer than the tailings alone.

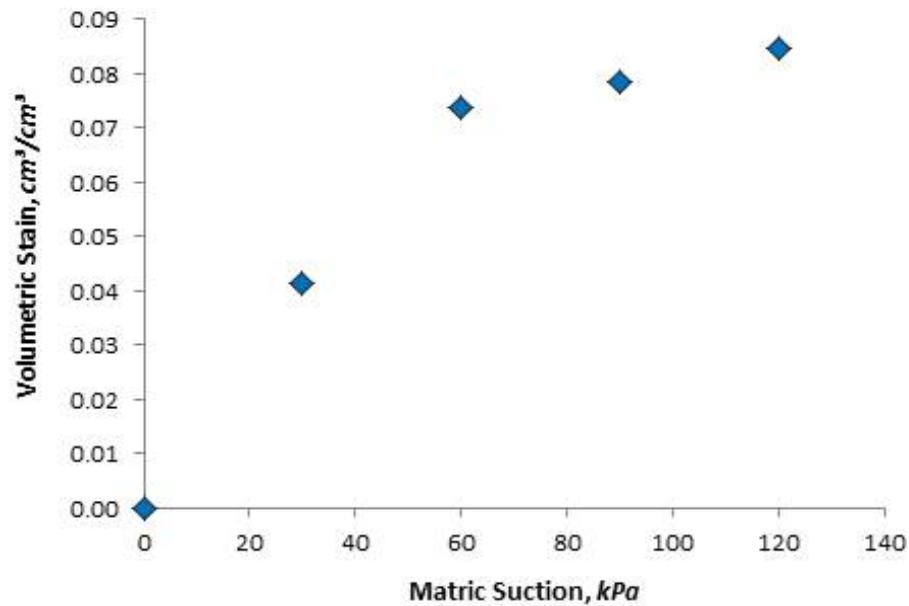


Figure 5.3.11 Kidd paste specimen containing no binder: pre- volumetric strain curve in the positive pore-water pressure region

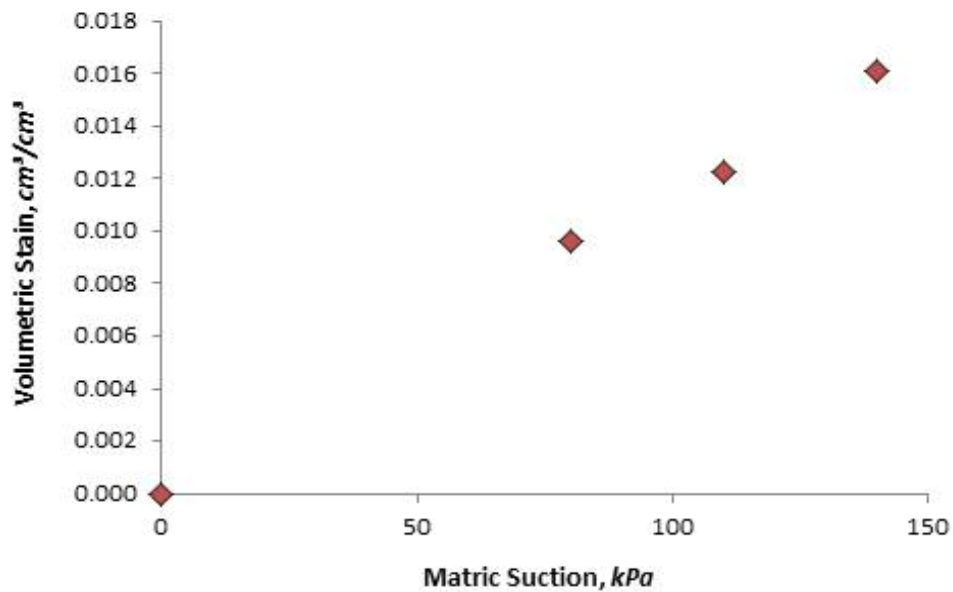


Figure 5.3.12 Kidd paste containing 2.2% binder: post- volumetric strain curve in the positive pore-water pressure region

5.3.2 SUMMARY: PRE- AND POST-HYDRATION PROPERTIES

The pre- and post-hydration properties; namely, the initial GWCs, the AEVs, the lower and upper limit void ratios, and the coefficients of volume change for Williams and Kidd paste streams have been summarized in Table 5.3.5.

Table 5.3.5 Summary of the pre- and post- hydration properties of Williams and Kidd paste

Paste Material	Initial GWC (%)	AEV (kPa)	Shrinkage Limit (GWC - %)	Minimum void ratio cm^3/cm^3	Compressibility (1/kPa)
Williams tailings	31.4	50	19%	0.46	0.0038
Kidd paste tailings	21.9	40	12%	0.33	0.0014
Williams 3% CPB	36.5	120	31%	0.87	0.0002
Kidd 2.2% CPB	19.8	140	16.50%	0.45	0.00012

* Approximate values obtained from shrinkage curves via axis translation technique

The degree of saturation for the post-curing samples have more or less the same shape as the GWC curves, as very little volume changes occurred during the post-hydration tests. The WRCs looked quite different for the un-amended tailings (i.e. Figure 5.3.1, page 162 and Figure 5.3.7, page 168), as significant amount of volume change occurred at low suctions. The AEV of unamend Williams tailings was observed at 50 kPa, whereas for amended Kidd paste tailings, the AEV was observed to be approximately 40 kPa, which was slightly less than that of Williams. The smaller AEV is expected, since the grain-size distribution (Figure 5.1.1, page 147) of the paste material is comprised of a coarser fraction of particles (i.e. 55% by dry wt. of alluvial sand). The addition of the alluvial sand would indeed cause the material to become less susceptible to undergo significant volume changes. Kidd tailings without binder (amended tailings) was less prone to such changes; and hence, a smaller coefficient of compressibility (i.e. 0.0014 1/kPa), compared to Williams tailings (i.e., 0.0038 1/kPa), which was comprised of a higher clay fraction.

The type of binder (slag-Portland cement mix) used for Kidd paste is also a contributing factor relating to the rate of hydration. Godbout et al. (2007) and Fall et al. (2009) reported that slag-Portland cement mixes improves the pore-structure (producing greater solid volume) compared to fly ash-cement mixes. Slag-cement mixes tend to produce a cement matrix that is more densely packed. The authors found that the threshold diameters from MIP results for samples containing slag-based mixes exhibited slightly smaller pore-sizes than those comprised of fly ash-based mixes (findings from Fall et al., 2009). It was speculated that slag-based binders produced a greater degree of fines in the

solid matrix. For Williams tailings (Figure 5.3.3, page 165), the overall change in volume was greater than the Kidd tailings (Figure 5.3.9, page 172), where the initial GWC was greater than Kidd tailings by approximately 9%. This was largely in part, due to the alluvial sand, which is evident when examining its pre- and post- shrinkage curves. The latter can be observed for Kidd 2.2% CPB compared to Williams 3% CPB, in that the 2.2% material was impervious to experiencing any significant deformation. The primary factors controlling the shrinkage behaviour was the PSD. Therefore, deviations in the change in volume of Williams paste were more significant than that compared with Kidd paste.

The AEV for the fully hydrated Williams containing 3% binder is 120 kPa, whereas for the fully hydrated Kidd 2.2% binder paste is 140 kPa. The difference in the pre- and post- AEV of Kidd paste can be explained by the initial water content and the type of binder used, which was formerly discussed. As for the former (i.e., when comparing the pre- and post- initial GWC ~ 22% in Table 5.3.5, page 169, and ~20% in Table 5.3.2, page 163), it was observed that when a diminutive amount of bleed water is removed (< 4% GWC), the Kidd paste (characteristically) becomes stiffer and hence, more rigid, even with no binder. The rigidity and stiffness that Kidd paste acquired is also owed to the addition of alluvial sand, which is extensively discussed in Abdelaal (2011). This would also provide an explanation for the (smaller) compressibility values of 0.00012 kPa^{-1} and 0.0014 kPa^{-1} , respectively, for Kidd tailings with and without binder, as compared to 0.0002 kPa^{-1} and 0.0038 kPa^{-1} for Williams tailings with and without binder, respectively.

The experimental results from this phase (Phase II) have demonstrated with both materials/tailings, the compressibility decreased by an order in magnitude, because of binder hydration. The lower water-to-solids ratio, coupled with subsequent cement hydration and hydration products, transforms the cemented paste tailings by increasing the particle-to-particle contact, increasing material stiffness and hence pore-structure, and increasing its water-retention properties.

5.4 PHASE III: BINDER HYDRATION

In this phase, Williams tailings containing 3, 5, and 7% binder, and Kidd paste containing 2.2 and 4.5% binder during binder hydration, aimed to examine the degree of hydration via: (1) induced matric suction (Section 5.4.1); (2) water consumption / 'sink' (Section 5.4.2); and, (3) pore-volume changes (Section 5.4.3), all as functions of hydration time.

The effects of temperature on self-desiccation for Çayeli paste containing 4.5% and 8.5% binder was studied by Jayasinghe (2010). Experimental results gathered by the investigator are presented and discussed in this section (Section 5.4.4) as well.

5.4.1 GENERATION OF MATRIC SUCTIONS

Results of the self-desiccation tests for Williams 0, 3, 5 and 7 % binder specimens and for Kidd 0, 2.2 and 4.5% binder specimens are respectively, presented in Figure 5.4.1 and Figure 5.4.3. A strong correlation between the generation of matric suction and the amount of binder, which follows in proportion to the binder content for each tailings specimen, which was observed in both paste streams. Simms and Grabinsky (2009)

observed similar trends in matric suction generation (Figure 2.2.2, page 29) in laboratory prepared Williams' CPB specimens containing 1.5, 3, 5 and 7% binder (comprising of

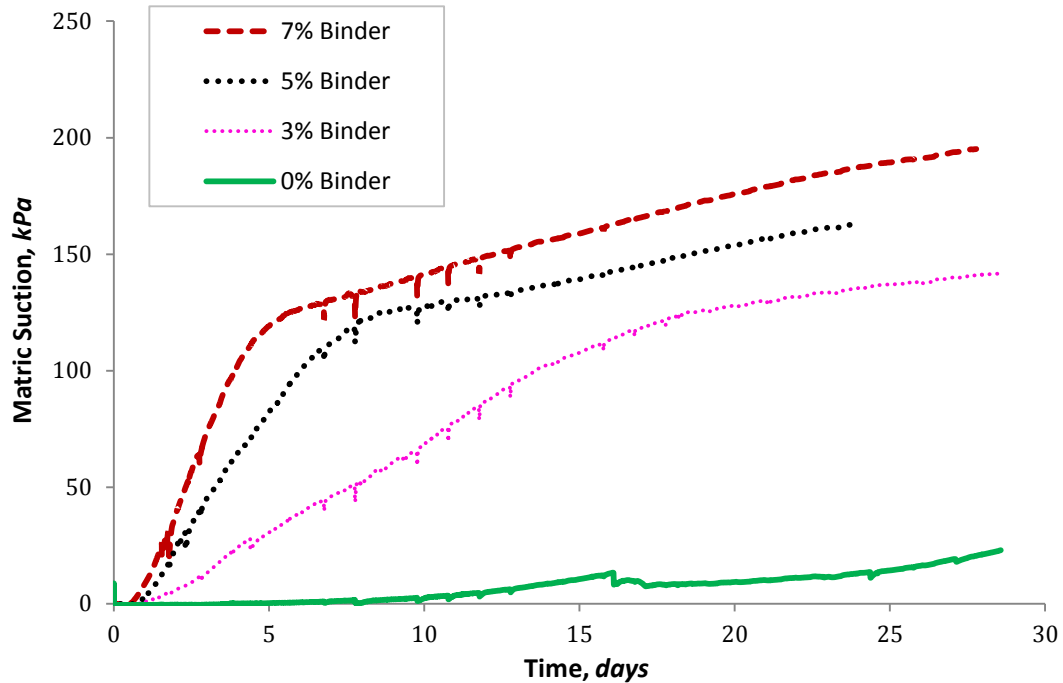


Figure 5.4.1 (Trial #1) Williams CPB specimens in sealed samples: induced matric suctions during 28 days of paste hydration

For Williams' non-cemented sample (control), matric suctions were observed after day 9. This indicated that some evaporation did occur within the sealed samples. For Williams CPB specimens, all of the data exhibited a change (or rather decrease) in the rate of suction generation after 100 kPa. Repeatability of these results has been provided in Figure 5.4.2 (Trial #2).

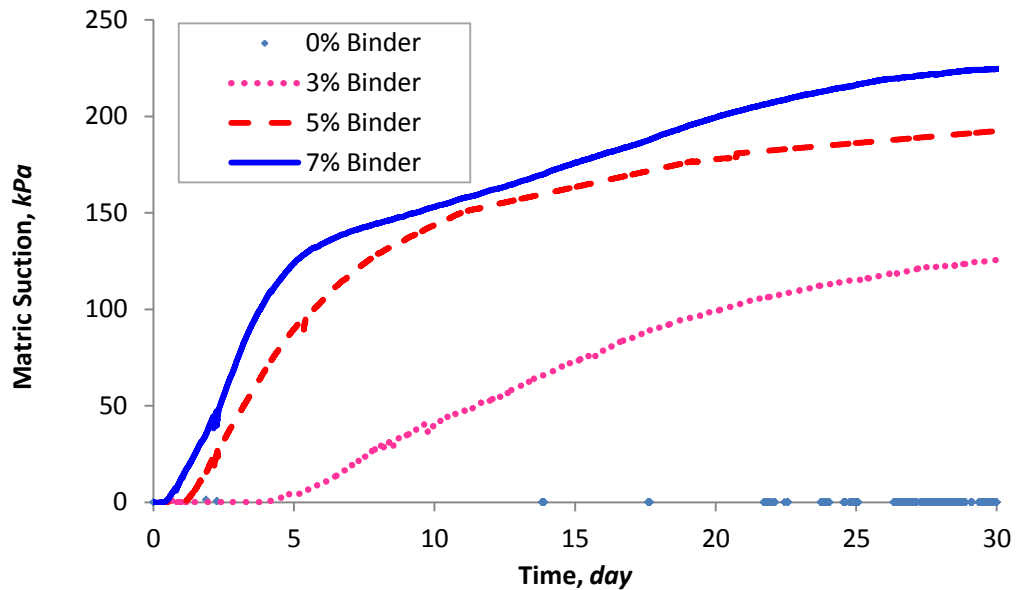


Figure 5.4.2 (Trial #2) Williams CPB specimens in sealed samples: induced matrix suctions during 28 days of paste hydration

A similar transformation of rate of matrix suction generated after 50 kPa was also observed in Kidd's 2.2% binder specimen. These transformations may be the result of the AEV being exceeded as hydration progressed, and so the rate of matrix suction, to which water was being removed, changed; or possibly the pace of hydration slowed down due to limited pore-water. One might suspect however, cavitation in the tensiometers as the cause, but the T5xs generally show a very sharp drop in suction, subsequent to cavitation (as demonstrated in Figure 5.4.3, for Kidd's 4.5% binder specimen after day 9 of hydration). A very rapid decrease in matrix suction was observed towards the end of these tests, which were caused by cavitation in the water reservoirs of the pressure transducers (e.g., discussed by Marinho et al, 2008). Rapid increases in matrix suction generation observed in Kidd's CPB specimens compared to Williams' were largely due

to the initial solids concentration, where the initial GWC(s) were approximately 18% in the former.

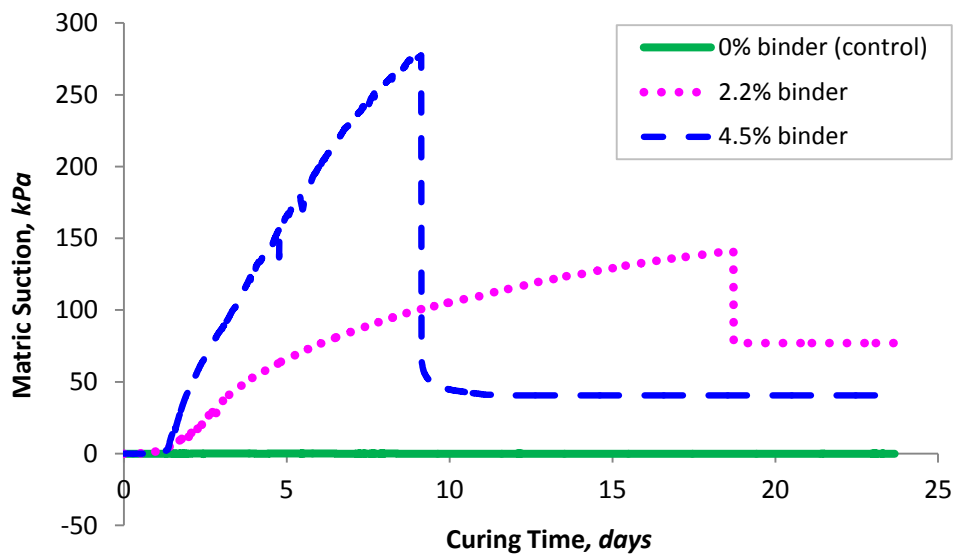


Figure 5.4.3 (Trial #1) Kidd CPB specimens in sealed samples: induced matrix suctions during 20 days of paste hydration

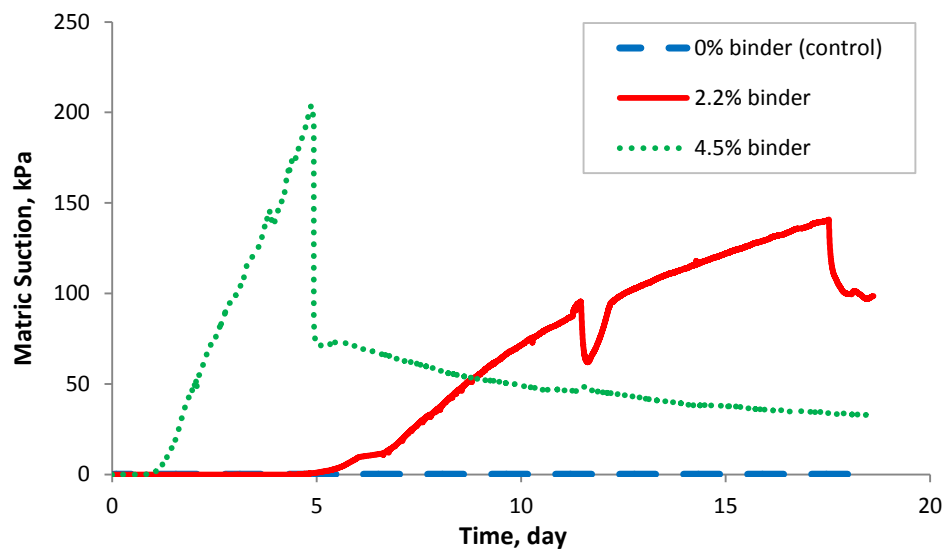


Figure 5.4.4 (Trial #2) Kidd CPB specimens in sealed samples: induced matrix suctions during 20 days of paste hydration

With both trials (in Figures 5.4.3 and 5.4.4), it was observed that cavitation in the tensiometers occurred with both sample specimens (containing 2.2% and 4.5% binder). The specimens containing 4.5% binder cavitated once suctions reached approximately 200 kPa, whereas, specimens containing 2.2% binder, cavitated once the AEV (~ 150 kPa) of the material was reached, which is close to the post-AEV of the fully hydrated paste material (~ 140 kPa).



Figure 5.4.5 Kidd cemented paste specimens containing 2.2% binder (a), and 4.5% binder (b), post- self-desiccation tests (on the 22nd day of hydration)

Photographs (Figure 5.4.5) were taken after the self-desiccation to illustrate the presence of large voids, as well as rigidity (or less chalky characteristics) of Kidd paste containing 2.2% and 4.5% binder on the 22nd day of hydration. A chisel was used to fracture the material so that pressure transducers could be retrieved from each specimen. It was also observed here, that Kidd had acquired significant stiffness (and presumably, strength as well) during early-age curing, compared to Williams. A study conducted by (Abdelaal,

2011) found that cemented paste tailings comprised of sand increased both strength and the stiffness acquired during early-age curing.

5.4.2 RATE OF WATER REMOVAL

The rate of water content depletion as a function of the hydration time for Williams 3% paste and Kidd 2.2% and 4.5% paste are presented and discussed in this section. In Figure 5.4.6, the change in water contents represented the rate of water consumed by hydration alone. This data was obtained from replicated sealed samples, where the overall change in mass was negligible; whereby, the water content represented the change in proportion of the mass of water to the mass of solids.

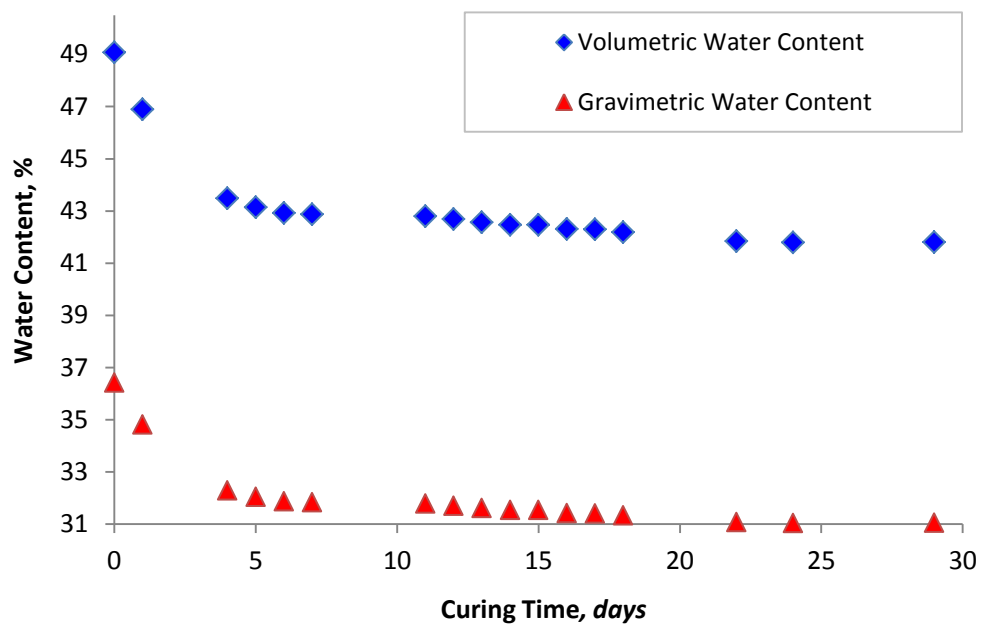


Figure 5.4.6 Water contents of replicate samples for Williams with 3% binder, showing decrease in water content due to binder hydration

The self-desiccation tests were conducted in attempt to describe hydration in terms of both water consumption and induced suctions. In Figure 5.4.7, the loss of water volume or water-to-total volume ratio and the rate of suction development exhibited a non-linear trend. Initially, the rate of water ‘uptake’ was higher during the first 4 days, after which the VWC decreases by 7%. This was somewhat expected in the beginning, as the binder ‘sets’ and began to form cement bonds between the particles in replacement of the pore-water. After the first 24 hours, matrix suctions were observed to develop, and steadily increased thereafter – up to 140 kPa. While there was an obvious trend with these rates, it was observed however, that these rates differed in an unexpected way. In the beginning, the removal rate occurred quicker than the suctions being produced. After the fifth day, the rate of water removal began to plateau as the availability of free water became limited. The rate at which suctions developed remained unchanged, until suctions stabilized around 140 kPa. It is interesting to point out here, that this was very close to the AEV (i.e., 120 kPa) of the post-hydrated paste material.

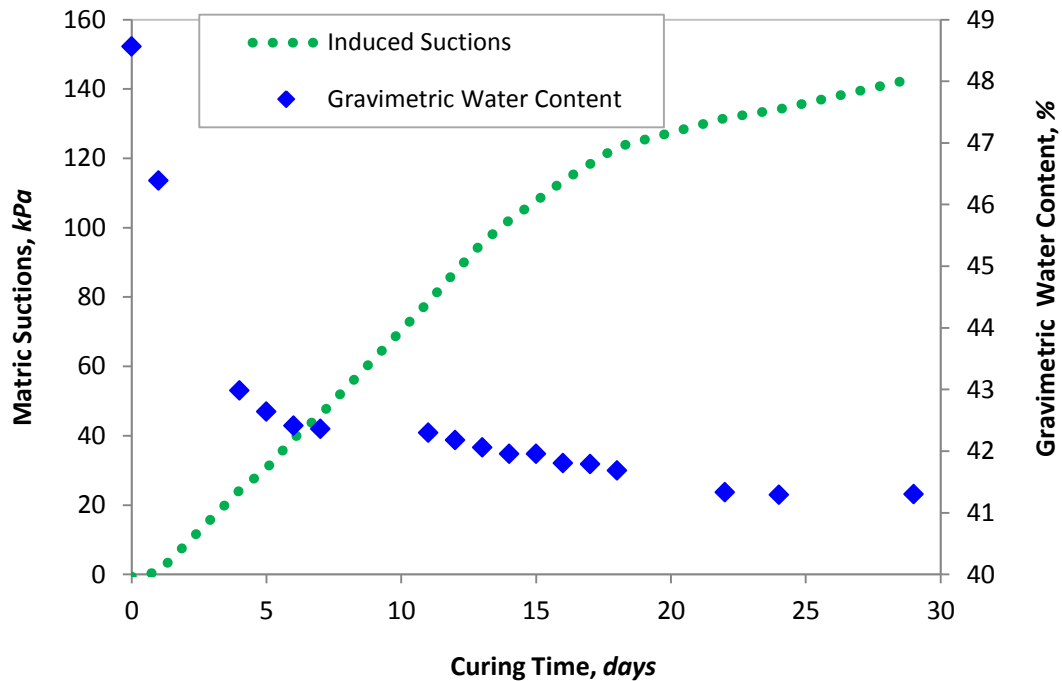


Figure 5.4.7 Rate of hydration for Williams' 3%: induced matric suctions and water consumption as a function of the hydration time

At some point during hydration period, the material went under a transformation, where the material properties transitioned from the pre- to post-hydration, where it acquired strength and stiffness. An attempt was made to illustrate when the material may have transformed close to the post-hydrated stiffness, by using the experimental results to back calculate the material compressibility, assuming that there was no flow, and hence no drainage. To that end, Eqn. [3.1.1] was thus, simplified in order to describe the changes of the coefficient of compressibility based upon the relationship between the rate of water removal and the generation of matric suction:

$$m_v = \frac{-S_K}{\left(\frac{\partial\psi}{\partial t}\right)} \quad [5.4.1]$$

where, $(\partial\psi/\partial t)$ is the change in matric suction as a function of hydration time, [kPa/day], which has been determined, via experimentally; and, $-S_K$ is the rate of water removal, [1/day].

The analytical solution for hydrating paste has been summarized in Table 5.4.1. As anticipated by hydration, the coefficient of compressibility decreased with hydration time, and in turn, suctions increased as well as the evaporable pore water.

Table 5.4.1 Material compressibility as a function of hydration time

Average Curing Time <i>(day)</i>	Average Suction <i>(kPa)</i>	Sink <i>(1/d)</i>	Mv Evolution <i>(1/kPa)</i>
0.5	0	0.0217	0.0316
2.5	12	0.0116	0.0023
4.4	27	0.0038	0.0006
5.4	35	0.0022	0.0003
6.3	46	0.0006	0.0001
11.5	83	0.0014	0.0002
12.3	91	0.0014	0.0002
13.3	74	0.0010	0.0002
15.4	87	0.0017	0.0003
17.3	121	0.0011	0.0002
19.8	127	0.0009	0.0001
23.0	137	0.0002	0.0000
26.5	143	0.0000	0.0000

In Figure 5.4.8, the average coefficient of compressibility prior to the pre-hydrated AEV (~50 kPa) was approximately 0.0009 1/kPa, which is slightly larger than the compressibility as compared with the pre-WRC (0.0038 kPa⁻¹), which did not take into account the effects of paste hydration. For the post-hydrated AEV (~120 kPa), the coefficient of compressibility was estimated to be approximately 0.0002 1/kPa, which was the same, when compared with the post-WRC (0.0002 kPa⁻¹).

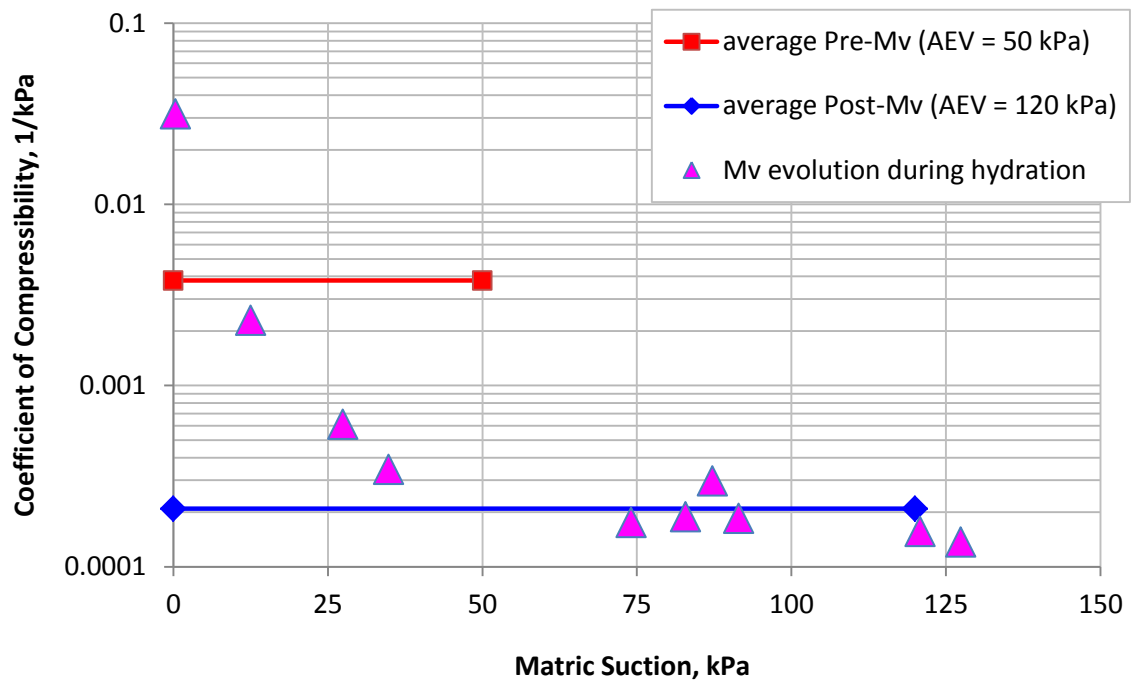


Figure 5.4.8 Estimated coefficient of compressibility(s) during paste hydration, compared with the pre- and post- values at respective air-entry values

As suggested by Fall et al. (2009) and Abjelaal (2011), stiffness is gained during binder hydration, which is controlled by the bonding hydration reactions between the clinker and water. It is interesting to point out here that the coefficient decreased with hydration

time, which resembled closely to what was expected to have occurred – the coefficient decreasing an order of magnitude during early-age curing. The results of these estimations, prior to the AEV(s) of the pre- and post- properties have demonstrated that stiffness was acquired through paste hydration and uptake in pore water, which in turn, induced the generation of matric suctions.

Matric suction and water consumption as a function of paste hydration for Kidd paste containing 2.2% binder has been presented in Figure 5.4.9. It is interesting to note here, that the generation rate of suction was found to have correlated strongly with the rate of water consumption through binder hydration. These results were comparable to Williams hydrating 3% paste. The removal rates and suction development had however, occurred slightly quicker during the first 5 days, after which it had slowed down. The removal of water was observed to plateau at approximately 15% GWC, while suctions increased to approximately 140 kPa, followed by a sudden drop in suction. This was where cavitation in the T5x was observed to have occurred. Peak matric suction in hydrating 2.2% Kidd paste was also close to the AEV (~140 kPa) of the post-hydrated Kidd paste at approximately 15% GWC.

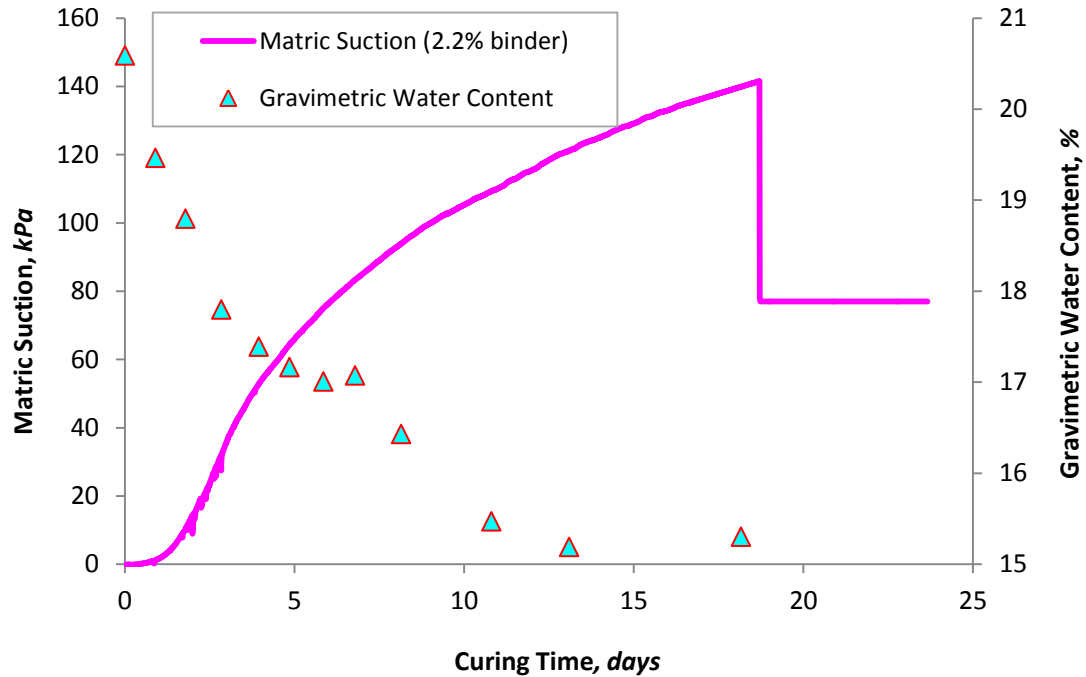


Figure 5.4.9 Rate of hydration for Kidd 2.2% binder paste

With both hydrating specimens, GWC(s) observed to plateaued at different water contents, albeit, closer to the respective AEV(s). An explanation for the observed water content(s) plateauing at different values of suction may be explained by the fact that pore-water reduction eventually became more and more difficult as matric suctions approached the AEV as surface tensions increase. Self-desiccation therefore, may have significant implications on the micro-structure as well.

5.4.3 MICRO-STRUCTURAL CHANGES DURING PASTE HYDRATION

Mercury intrusion porosimetry (MIP) test specimens (Williams cemented paste material) contained 3% and 7% binder. MIP results for Williams specimens containing 3% binder are presented, respectively, as: (i) Figure 5.4.10 and Figure 5.4.13, the

differential pore-size distribution; (ii) Figure 5.4.11 and Figure A.5.1. (Appendix A.5, page 285), total MIP porosity and incremental porosity; and (iii) Figure 5.4.12 and Figure 5.4.14, threshold diameter and critical pore diameter, as a function of hydration time.

In Figure 5.4.10, the differential PSD(s) for Williams containing 3% binder, for different days of curing is presented. The controlled sample (S2_tailings) exhibited a smaller pore-radius ($\sim 0.11\mu\text{m}$) than the 3% binder specimens cured for 2 and 3 days ($\sim 0.15\mu\text{m}$). Upon this comparison, the mean pore-radius was almost the same as that to hydrating sample at day 7 (Specimen Day 7). The smaller pore-radius of the control sample can be understood by the fact that the rate of hydration of the 3% binder material may be proportionate to the % binder content (e.g. presented in Figure 5.4.1, page 178). In other words, the 3% binder initially ‘sets’ before hydration commences, whereas for the control sample, consolidated, initially by squeezing out pore-water, and hence reducing void-space as the solid matrix underwent a compression [e.g. comparing the lower and upper limit void ratio(s) of Williams with (~ 0.87) and without binder (~ 0.46) in Table 5.3.5, page 174]. Simply put, settlement was observed to be less pronounced when binder was added to the paste tailings. Deschamps et al. (2008) also reported similar findings, where the addition of binder decreased settlement and thus, the total MIP porosity was greater in specimens containing binder. The total MIP porosity also increased with higher %wt. binder dose.

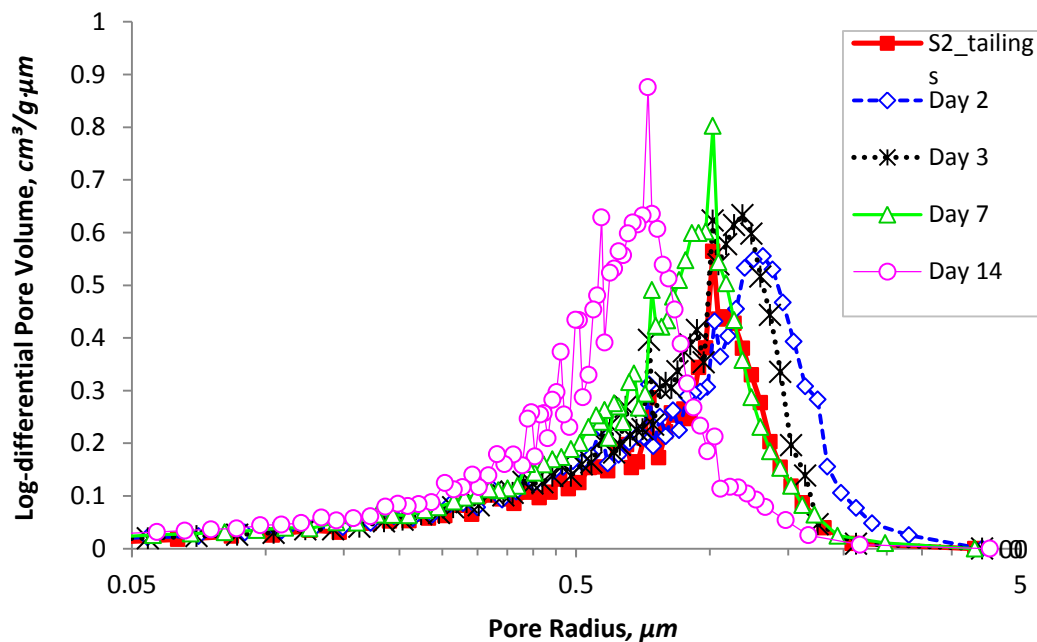


Figure 5.4.10 Differential pore-size distribution for 3% binder paste during binder hydration

Similarly, total MIP porosity increased as hydration time increased (Figure 5.4.11a). The total MIP porosity increased overall from approximately 40% to 41%. The incremental porosity exhibited a similar trend, albeit, inversely proportional to the total MIP porosity, where it decreased with hydration time (Figure 5.4.11b). There were very little changes in the total porosity and in the differential PSD of the 3% specimens during earlier stages of curing; specifically, from day 2 to day 7. It was not until afterwards, that there was somewhat, a more noticeable transformation (i.e. day 12 and day 14). The critical pore-diameter (CPD) and threshold diameter (THD) was also found to have decreased with hydration time. The CPD represented the maximum continuous pore radius, corresponding to the largest fraction of interconnecting pores. It may also be defined as the smallest pore at which significant intruded mercury volume is to be detected

(Halamickova and Detwiler, 1995). The CPD was determined as the point of inflection (POI) value of the total MIP porosity curve (Figure 5.4.11*a*), or the maximum value on the differential porosity curve (Figure 5.4.11*b*). The THD may be defined as the minimum fraction of interconnecting pores, representing the pore-size above, which there was comparatively little mercury intrusion, and below where the main intrusion occurred (Deschamps et al., 2008). It may also be defined as the largest pore diameter at which significant intruded mercury volume is to be detected (Halamickova and Detwiler, 1995). The THD was determined as the minimum pore diameter on Figure 5.4.11*b*. The THD(s) and CPD(s) as a function of curing days have been summarized in Figure 5.4.12. Both THD(s) and CPD(s) decreased as curing time increased. It was observed that the THD(s) decreased from approximately 4.3 to 2.5 μm , and the CPD(s) decreased from approximately 2.8 to 1.5 μm , respectively from 2 to 12 days of curing. The reduction in both pore-diameters concurred with Deschamps et al. (2008) and Fall et al. (2009) observations.

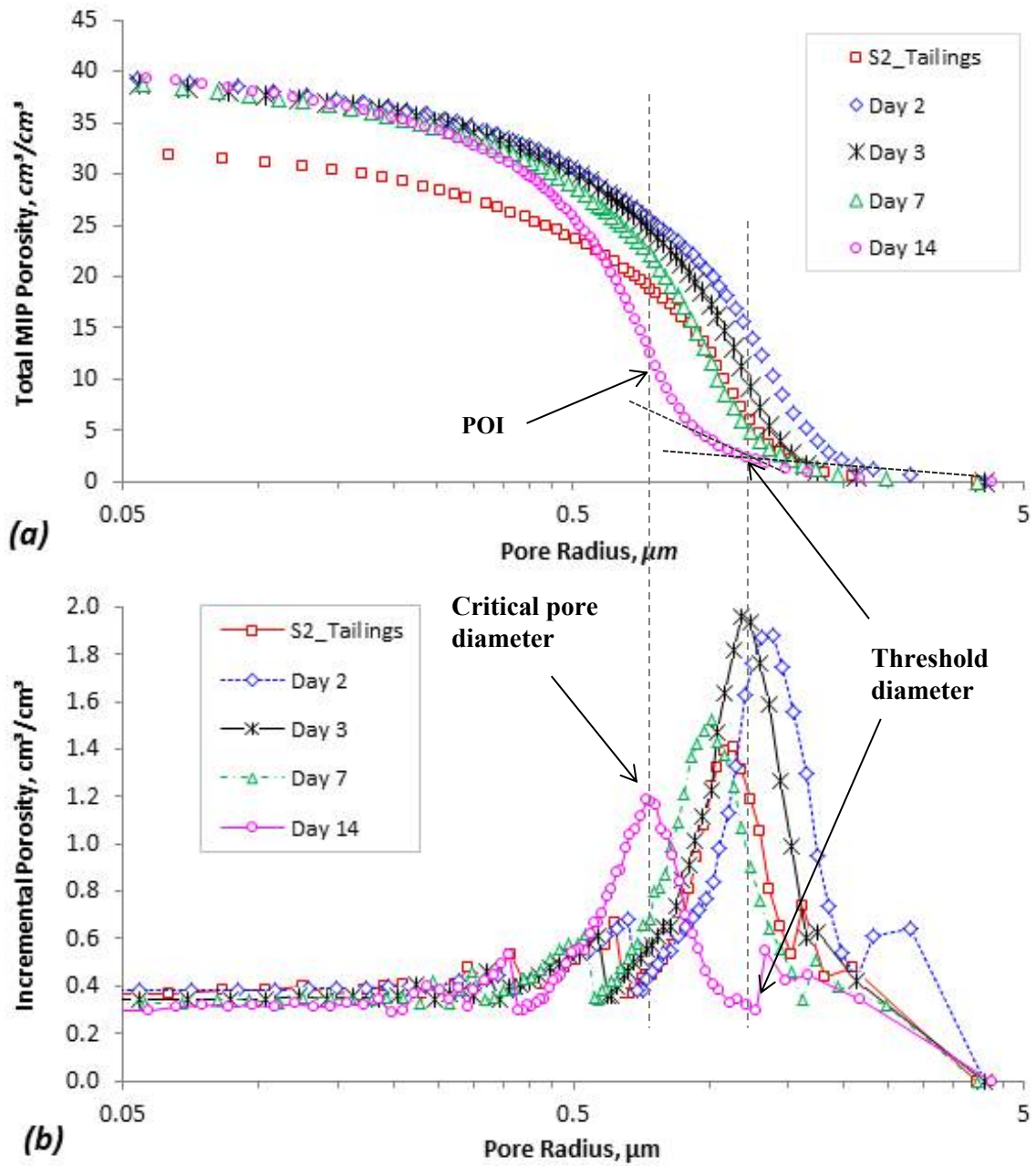


Figure 5.4.11 3% binder: (a) total MIP porosity; and (b) incremental porosity as a function of pore radius

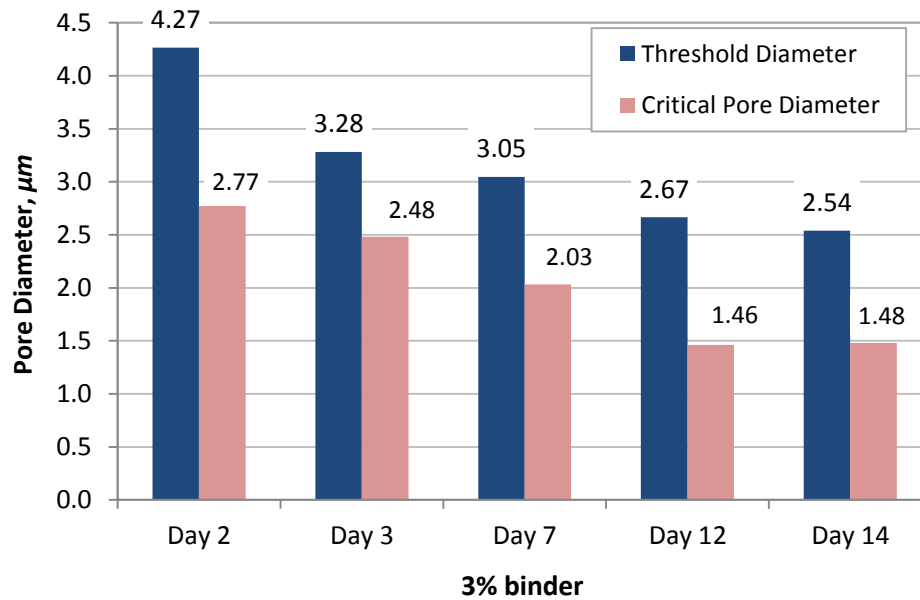


Figure 5.4.12 Threshold diameter and critical pore diameter for Williams 3% binder specimens cured for 2, 3, 7, 12, and 14 days

For the 7% binder specimens, more noticeable transformations were observed in the PSD curves (in Figure 5.4.13) with curing time. It was not surprising that the differential PSD(s) decreased as hydration proceeded as well as with higher binder contents. The total MIP porosity(s) appeared to have increased from approximately 41% to 44% during the first 12 days of curing, after which it decreased to approximately 41%. The THD(s) and CPD(s) both decreased with curing time, as illustrated in Figure 5.4.14. The CPD decreased from first day of curing to the 16th day of curing, respectively from 1.76 μm to 0.91 μm. The THD(s) also decreased from 3.05 μm to 1.20 μm. The progression of smaller THDs correlated as stiffness increased for paste material containing more binder (e.g., smaller THD exhibited in the 7% binder specimens, versus the 3% binder specimens).

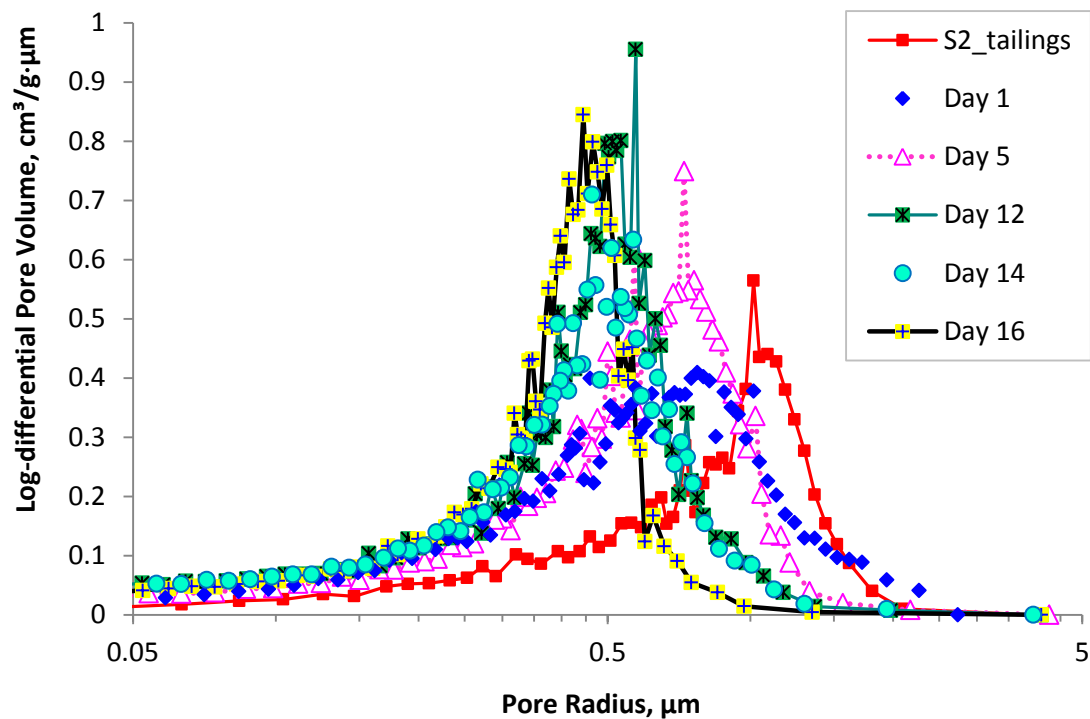


Figure 5.4.13 Differential pore-size distribution for 7% binder paste during binder hydration

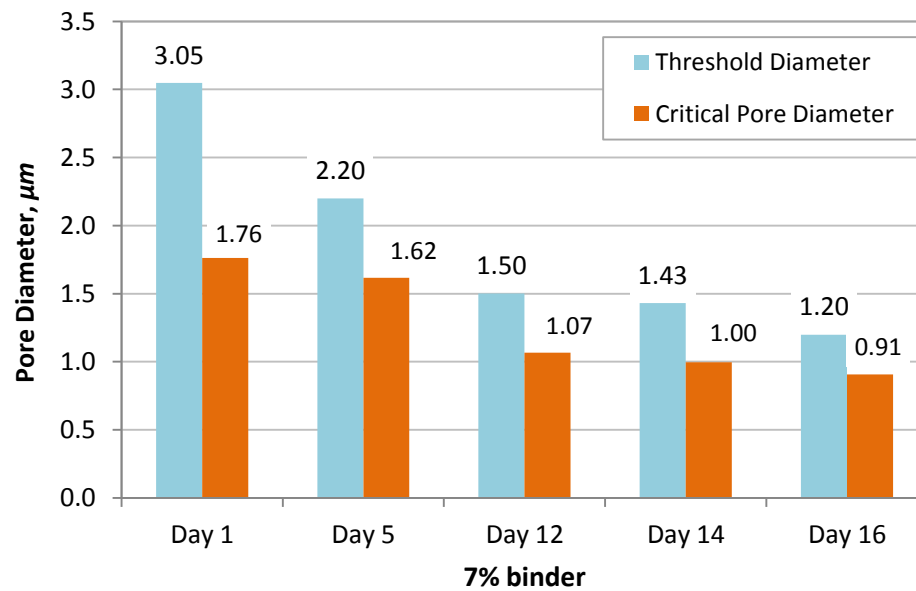


Figure 5.4.14 Threshold diameter and critical pore diameter for Williams 7% binder specimens cured for 1, 5, 12, 14, and 16 days

With both the 3% and the 7% binder material specimens, appeared visible trends with binder content and curing time. These results have been summarized in Table 5.4.2. While there were visible trends with reduced THD(s) with higher binder content and longer curing time, the total MIP porosity appeared to have an overall trend as well, where it increased with binder content as well as curing time. However, it appeared that there was a slight discrepancy between the total porosity for the 7% binder specimens on day 14 and 16. Similar observations were noted as well with the void ratios increasing in specimens containing 3% binder, and a reduction in specimens containing 7% binder.

Visible transformations of the specific surface area were observed to have increased with %wt. binder as well as with increased curing time. This can be explained by the process of hydration and self-desiccation. The former had an effect of increasing the total porosity due to a less pronounced settling, which occurred when binder was added. As suggested by Deschamps et al. (2008), when the amount of binder was increased, the reactivity of binder hydration is thought to have been enhanced, which also increased the total MIP porosity. Similar findings were observed by Benzaazoua (2000) and Deschamps et al. (2008). An increase in specific surface area is due to the formation of new hydration products, but also the effect of self-desiccation. Persson (2005) found that the increase in material fineness (or specific surface area) was owed to the rate of self-desiccation, which would explain an increase in specific surface area, especially for the 7% binder specimens, compared to the 3% binder specimens. Therefore, higher %wt. binder dose may be correlated to increased stiffness, and hence strength, where higher

UCS values for materials acquiring higher specific surface areas (Deschamps et al., 2008).

The CPDs also decrease with % binder content. This is not surprising that this would occur, because the CPD represents the largest fraction of interconnecting pores, which essentially influences fluid transport properties (Halamickova and Detwiler, 1995), such as permeability. The effect of self-desiccation also reduces the IRH, which in turn, results in smaller pore-size reductions.

Table 5.4.2 Results of the MIP tests (threshold diameter, critical pore diameter, specific surface, total porosity, and void ratio as functions of curing time

Paste Material	Curing Time	Threshold Diameter	Critical Pore Diameter	Specific Surface	MIP Total Porosity	Void Ratio
		μm		m^2/g	%	cm^3/cm^3
<i>S2_Tailings</i>	0	3.05	2.18	0.814	32.25	0.476
3% binder (Williams)	2	4.27	2.77	1.989	40.75	0.688
	3	3.28	2.48	2.238	40.47	0.680
	7	3.05	2.03	2.483	40.68	0.686
	12	2.67	1.46	2.952	42.38	0.736
	14	2.54	1.48	2.432	41.42	0.707
7% binder (Williams)	1	3.05	1.76	3.110	41.26	0.702
	5	2.20	1.62	3.475	42.41	0.736
	12	1.50	1.07	5.397	44.06	0.788
	14	1.43	1.00	5.143	40.60	0.684
	16	1.20	0.91	4.932	41.03	0.696

It is rather intuitive that smaller pore-size reductions would increase the water-retention properties (i.e., AEV of 50 kPa to 120 kPa). Fall et al. (2009) have discussed the effects of early-age curing, such that pores and void spaces are densely packed, resulting in a fluid permeability reduction. Similar trends, such as a reduction in pore diameters and capillary porosity caused by the hydration process were observed in studies conducted by Belem et al. (2001), and Benzaazoua et al. (2004), confers with these same results presented in this section.

5.4.4 EFFECTS OF TEMPERATURE ON SELF-DESICCATION

Temperature rises during binder hydration was observed at Çayeli Mine during the first 5 days of curing (Figure 2.2.9, page 42). The rate of self-desiccation as a function of the temperature for Çayeli paste containing 4.5 and 8.5% binder was investigated by Jayasinghe (2010). The binder-mix was comprised of 100% cement (from Ünye, Turkey).

A number of self-desiccation – heat tests were carried out at ambient temperature (24°C), 40°C and 50°C. Selected results of the self-desiccation – heat tests for specimens containing 4.5% binder and 8.5% binder are presented in Figures 5.4.13 and 5.4.14, respectively. At ambient temperatures, the generation rate of matric suctions were observed to increase, steadily during the first 18 / 20 days of hydration. The rate at which suctions developed reflected the amount of binder, meaning that higher binder contents increased the rate of suction development as well as produced higher suctions. For specimen(s) containing 4.5% and 8.5% binder, the maximum suction(s) induced by self-

desiccation were approximately 22 kPa and 90 kPa, respectively. Maximum suctions were observed at room temperature, and reduced as curing temperatures increased. Additional results from the investigator can be found in Appendix B.1 (page 287).

Similar to both Kidd and Williams self-desiccation results, the rate of self-desiccation (or generation of matric suctions) for Çayeli's hydrating paste were generally dependent upon the binder dose, meaning that an increase in binder improved the overall degree of hydration (or reactivity of binder and pore water). Temperature increases during the self-desiccation process, produced surprising results that seemed counter-intuitive. The greatest degree of suction generation was observed to be produced at ambient temperatures, whereas, at higher temperatures, self-desiccation was observed to be delayed (in the 8.5% sample) and/or effectively suppressed (in the 4.5% sample). This occurrence was observed with both sample specimens at 40 and 50°C, however, to a greater degree at 50 °C. In Figure 5.4.14, matric suctions, were reduced (hypothetically speaking) by approximately 20 kPa at 40 °C, and approximately 40 kPa at 50°C. Whereas in Figure 5.4.13, it was observed that matric suctions were suppressed, essentially altogether. Contrary to numerous studies conducted by Fall and co-workers (Fall and Samb, 2008; 2009; Fall et al., 2009; Fall and Pokharel, 2010), found that higher curing temperatures (i.e. < 50°C) produced early-age curing pastes to acquire greater strengths, refinement of the pore-structure, and hence an overall reduction in water permeability. At higher temperatures, the opposite affected was observed (i.e., deterioration of the cement skeleton). Contrary to this however, self-desiccation was observed to have been effectively suppressed at higher temperatures, which in turn, may hinder pore-pressure

dissipation, significantly; and hence, suppress the generation of matric suction. Increased curing temperatures may causes the IRH (or reduce surface tensions) to increase (i.e., as per Laplace equation). Persson (2005) observed that self-desiccation in paste cements increased in material fineness as a result of self-desiccation – or in other words, when cured at ambient temperatures. Temperature effects on pore-structure of cemented paste fill during self-desiccation should therefore, be studied further for more affinitive results, specifically with regards to more MIP testing with binder mixes that contain more than just slag and/or Portland cement.

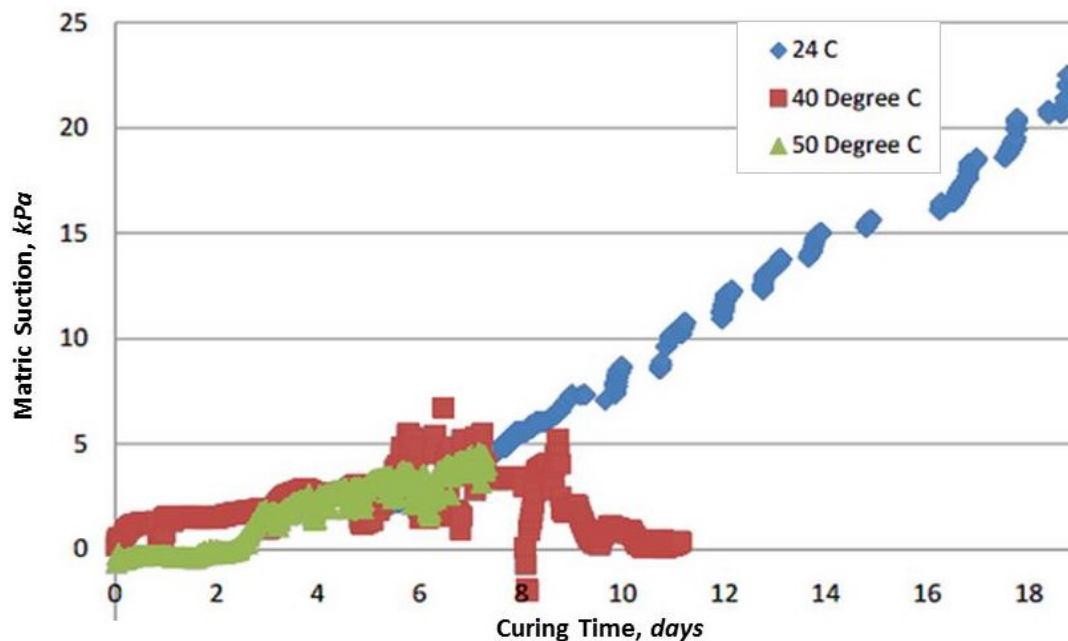


Figure 5.4.15 Çayeli paste containing 4.5% binder: rate of self-desiccation as a function of temperature(s) at 24, 40 and 50 °C

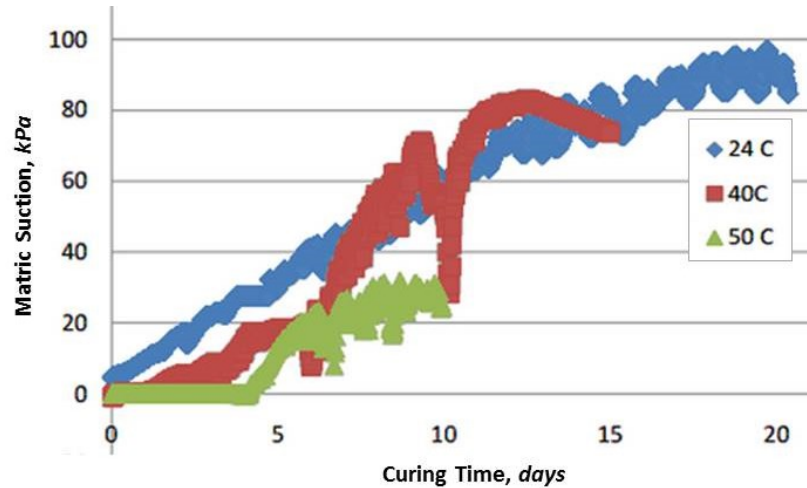


Figure 5.4.16 Çayeli paste containing 8.5% binder: rate of self-desiccation as a function of temperature(s) at 24, 40 and 50 °C

The results of these laboratory experiments presented in this section have therefore, demonstrated that the: (1) initial rate of self-desiccation / matric suction generation can be delayed for samples containing high initial water contents or slow dissipation of +PWPs; (2) rate of matric suctions produced during hydration was dependent upon the amount of binder, where high binder contents increased the rate of self-desiccation, due to the reactivity of the paste; (3) pore water (or water content) stabilized at suctions approaching the AEV of the material due to pore-structural reductions, which in turn, inhibited the permeability, which further reduction in pore-water (or water content) was subdued; and (4) PSD(s), threshold and critical pore diameters decreased as total MIP porosity and specific surface area increased, to which indicated that new hydration products has formed – this lead to increased fineness of the material, such that strength and stiffness developed during self-desiccation.

5.5 PHASE IV: PASTE FILLED COLUMN TEST

This Phase aimed to understand the PWP behaviour of 3% Williams CPB during deposition of fresh cemented paste and subsequent paste hydration. The following section presents the initial pore-water behaviour of freshly deposited cemented paste tailings, via through drainage (Section 5.5.1), and self-desiccation (Section 5.5.2) to estimate the distribution of PWPs in a multi-layered CPB column test.

5.5.1 DRAINAGE

The 30 by 30 cm column was backfilled in 4 stages, or ‘lifts’ with Williams CPB material containing 3% binder. The first pour, ‘paste’ plug was filled to a height of 15 cm, which subsequently consolidated for approximately 48 hours, during which pore-water drainage occurred. Similar behaviours were also observed for the remaining 3 layers.

The cumulative volume of water drained from the column after placement of paste layer is presented in Figure 5.5.1. Real-time data for the 1st Main layer (Main 1) was not recorded, due to a weak cable connection between the scale and the data acquisition system. A stop watch and video camera footage was used to determine the final amount of water collected over an approximate time interval of 7 hours.

The initial and final conditions, such as the change in volume and mass of each bulk pour, and water contents are presented in Table 5.5.1 and Table 5.5.2, respectively.

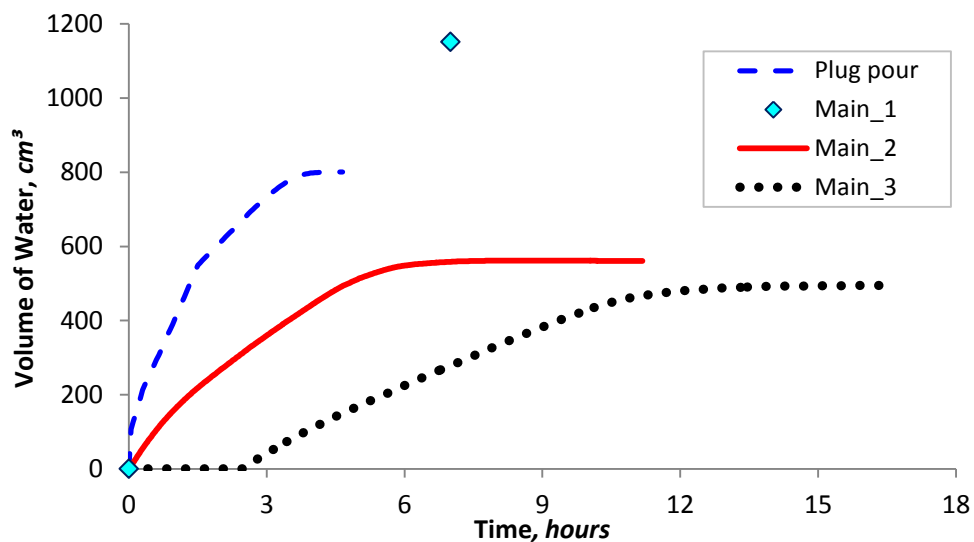


Figure 5.5.1 Cumulative volume of leachates collected after placement of each paste layer

Table 5.5.1 Summary of the initial conditions of each lift (prior to drainage and consolidation)

Lift (pour)	h_{initial} (cm)	V_{initial} (cm^3)	M_{initial}	M_{water} ($RE \pm 0.05g$)	M_{solids}	GWC_{initial} (%)	VWC_{initial} (%)
Plug	15	13500	24808	6704.4	18103.6	37.0	49.66
Main 1	30	27000	49200	13182.4	36017.6	36.6	48.82
Main 2	30	27000	49950	13436.8	36513.2	36.8	49.77
Main 3	30	27000	49700	13289.7	36410.3	36.5	49.22

Table 5.5.2 Summary of the final conditions of each lift after drainage and consolidation

Lift (pour)	h_{final} (cm)	Δh	V_{final} (cm^3)	$M_{\text{water loss}}$	ΔM_{water} ($RE \pm 0.05g$)	M_{final}	GWC_{final} (%)	VWC_{final}
Plug	14.2	0.8	12780	800.5	5903.9	24007.5	32.6	46.20
Main 1	29.9	0.9	26910	1152.2	12030.2	48047.8	33.4	44.71
Main 2	29.6	1.3	26640	561.8	12875.0	49388.2	35.3	48.33
Main 3	30.1	1.2	27090	494.7	12795.0	49205.3	35.1	47.23

Recorded measurements during the experiment allowed for the volumetric flow rates and drainage rates to be determined. It should be noted here that the permeabilities (in Table 5.5.3) obtained from the column test are more or less ballpark estimates, because of the dependency of the overall volumetric flow rates (Q) through the entire column layers. Put simply, the saturated hydraulic conductivities do not take into account of the underlying hydrated paste pours (i.e., where the $S < 100$ %). As one would expect, the saturated hydraulic conductivities decrease with hydration time (Figure 5.5.2) – measured by Veenstra (2010), via through compressive tests with a normal stress of 250 kPa. The final settlement of each lift is illustrated in Figure 5.5.3.

Table 5.5.3 Volumetric flowrate (Q), and drainage rate (v_s), and hydraulic conductivity (k_{sat}) of each lift

Lift	$V_{\text{water loss}}$	t_{drainage}	Q	$v_s = Q/A$	L_c	H_c	$k_{sat} = v_s(L_c/H_c)$
(pour)	(cm^3)	(h)	(m^3/d)	(m/d)	(cm)	(cm)	(m/s)
Plug	800.5	4.67	4.11×10^{-3}	4.57×10^{-2}	14.2	20.0	3.76×10^{-7}
Main 1	1152.2	7.00	3.95×10^{-3}	4.39×10^{-2}	43.3	49.2	4.47×10^{-7}
Main 2	561.8	11.18	1.21×10^{-3}	1.34×10^{-2}	72.0	78.3	1.43×10^{-7}
Main 3	494.7	16.37	7.25×10^{-4}	8.06×10^{-3}	100.8	107.0	8.79×10^{-8}

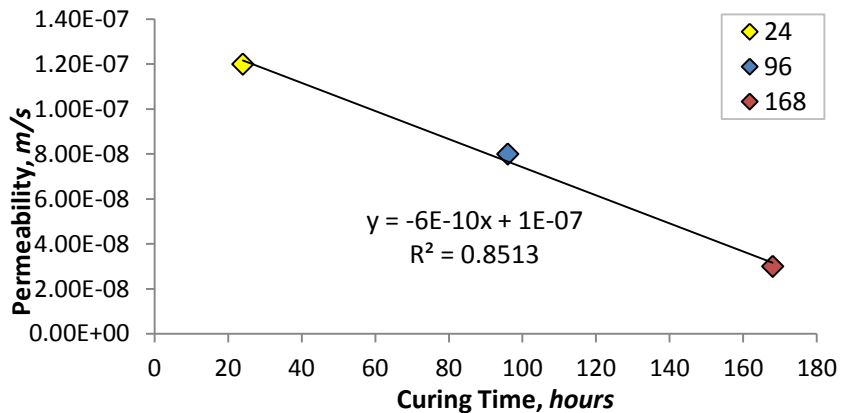


Figure 5.5.2 Permeabilities of 3% Williams CPB as a function of curing age, obtained from a compressive test with a normal stress of 250 kPa (Veenstra, 2010)

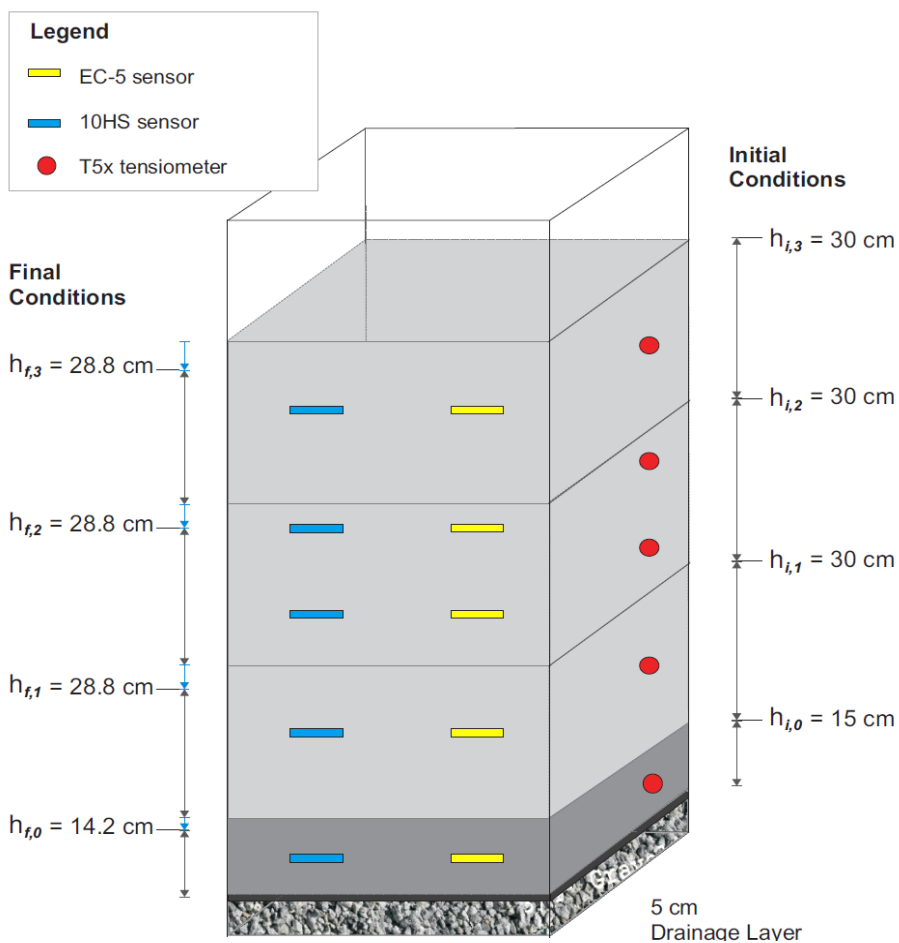


Figure 5.5.3 Initial and final height of each CPB layer after settlement and drainage

5.5.2 MATRIC SUCTION AND WATER CONTENT PROFILES

Matric suction profiles from the column test are presented in Figure 5.5.4. Within the first 2 – 3 days, PWP begin to dissipate rather quickly due to pore-water drawdown (or drainage), and suctions begin to develop, rather slowly. With the addition of a new layer, the response of the underlying layer is as expected, where suctions drop to zero. The PWP behaviour was observed for the remaining layers after emplacing a new paste layer. Matric suctions observed during this experiment do not rise above ~ 70 kPa. This is well below the AEV of the hydrated tailings. The differences in matric suctions between layers were relatively small with the exception of the newly placed lift / layer of fresh CPB material. With the addition of each layer, the rate at which suctions were generated decreased. This was also not surprising given that the demand of water by hydration in the fresh layer can be satisfied by water from the entire column, not just the fresh layer.

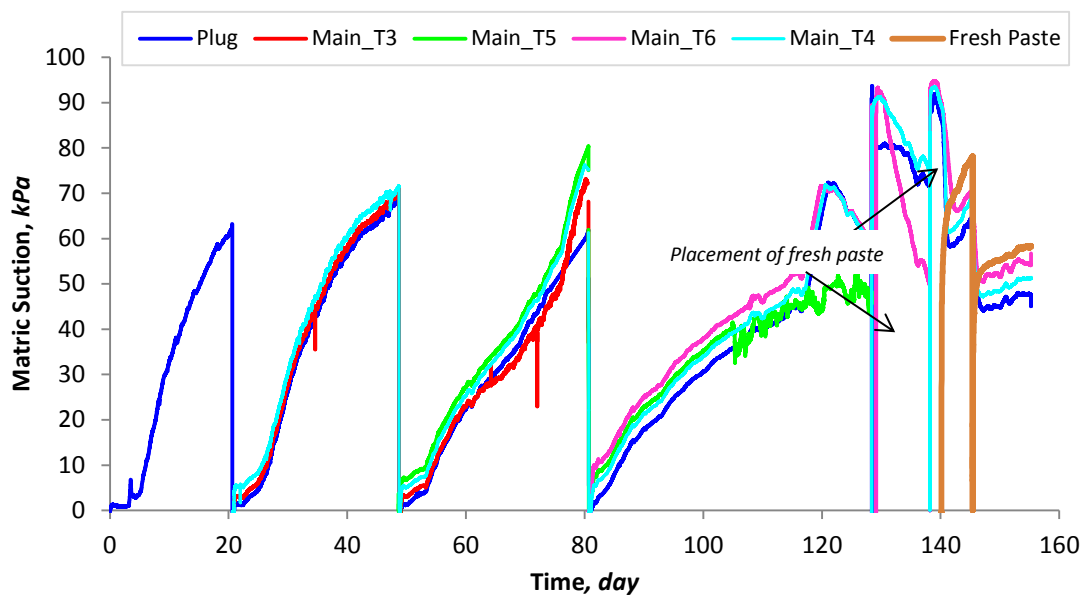


Figure 5.5.4 Measured matric suction values for a multi-layered deposition of Williams 3% CPB material in a 30 by 30 cm square column

The initial VWCs were estimated for each layer (Table 5.5.5), and is compared with the measured VWCs obtained from the EC sensors.

Table 5.5.4 Estimated volumetric water contents of each lift compared to the measured values obtained from the calibrated EC sensors

Lift <i>pour</i>	VWC_{Estimated}	10HS Data	EC-5 Data	VWC_{10HS}	VWC_{EC-5}	% Relative Error	
	%	<i>mV</i>		%	%	10HS	EC-5
Plug	49.10	1477	1088	45.57	50.23	7.19	2.31
Main 1a	46.41	1418	1175	39.92	57.25	13.99	23.34
Main 1b	46.41	1453	1182	43.35	57.81	6.59	24.56
Main 2	49.67	1440	1270	42.14	61.05	15.16	22.91
Main 3	49.36	1431	1195	41.27	54.35	16.40	10.09

VWC profiles from the 10HS and EC-5 sensors are respectively, presented in Figure 5.5.5 and Figure 5.5.6. VWC measurements from each of the EC sensors differed, significantly. VWCs determined by the EC sensors are initially high due to the effect that hydration has on the ionic conductivity of the pore-water. However, water content measurements obtained from the EC-5 sensors were found to be much higher than those measured with the 10HS sensors. Water content as a function of both time and depth, produced from the 10HS sensors (with the exception of the sensor placed at a 20 cm depth) decreased, which also appeared to be more reasonable than those produced from the EC-5 sensors. This also seemed to be the case when comparing the estimated VWCs. Measurements obtained from the 10HS sensors appeared to be more reasonable (with the exception of the Main_1a), as there were noticeable fluctuations in water content when the cover of the column was removed, and increased when a fresh layer of paste tailings was placed, afterwards. Very little changes in VWC measurements obtained from the

EC-5 sensor were observed from the EC-5 measurements. This may be due to the operating voltages of the EC-5 sensor, as it is highly dependent upon a specific excitation voltage of 2500 mV to operate within its lower and upper range of 250 – 1000 mV. As shown in Table 5.5.5, the output voltages were outside this excitation range.

While there were visible trends of decreasing water content, the magnitudes of these changes were relatively small when the 10HS sensor was used (Figure 5.5.5). This is not surprising, due to the high AEV (i.e. 120 kPa) of the fully hydrated paste tailings (Figure 5.3.2, page 162).

For confirmatory purposes, a final water content and total suction reading for the 3rd Main layer (prior to depositing fresh paste) was measured respectively, at 33.6% GWC and 78 kPa. Evaporation rates were monitored for each layer, ranging between 0.158 – 0.29 grams of water per day.

Photographs (Figure 5.5.7) were taken during the column experiment to illustrate the build-up of moisture between desiccated layers. A prospective explanation for this trend was simply that the underlain layer acquires stiffness because of cement hydration, coupled with the overburden stress of the overlain paste pour.

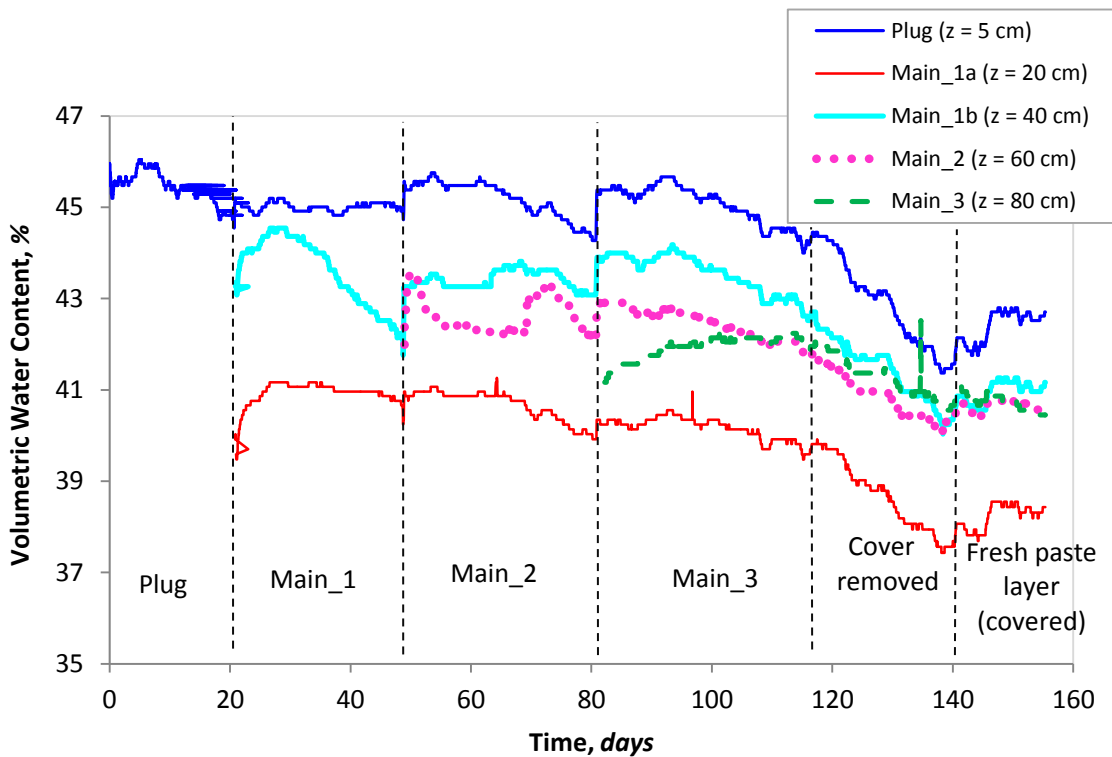


Figure 5.5.5 Water content data from the 10HS soil-moisture sensors

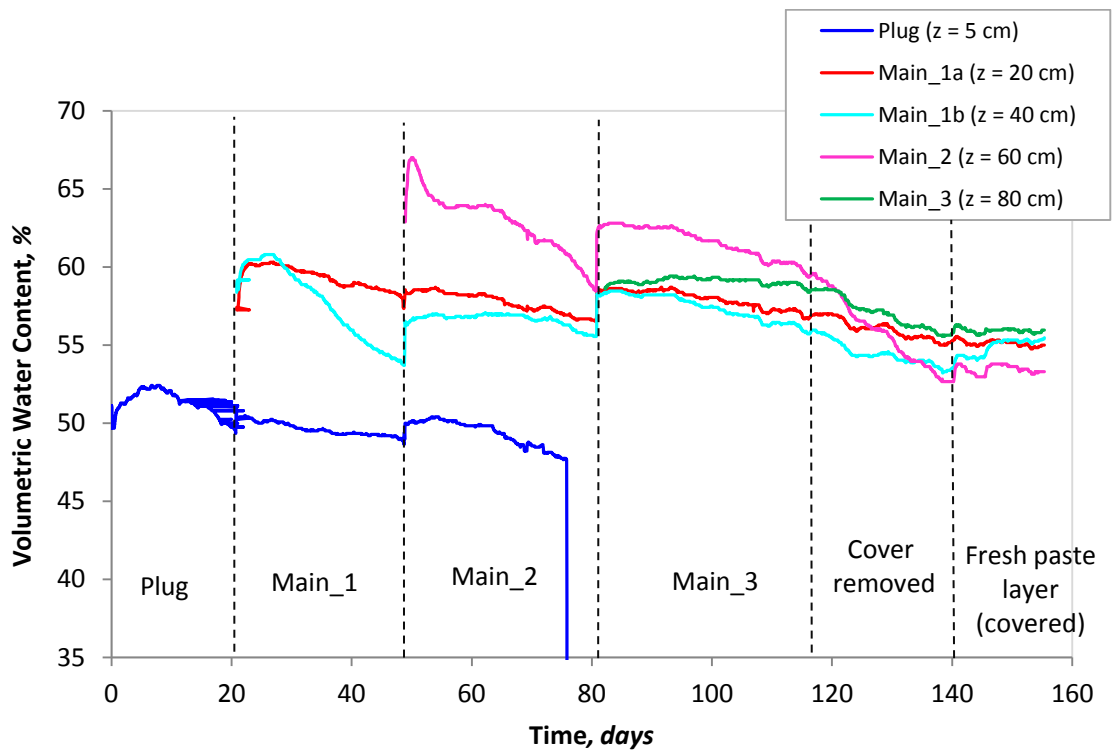


Figure 5.5.6 Water content data from the EC-5 soil-moisture sensors

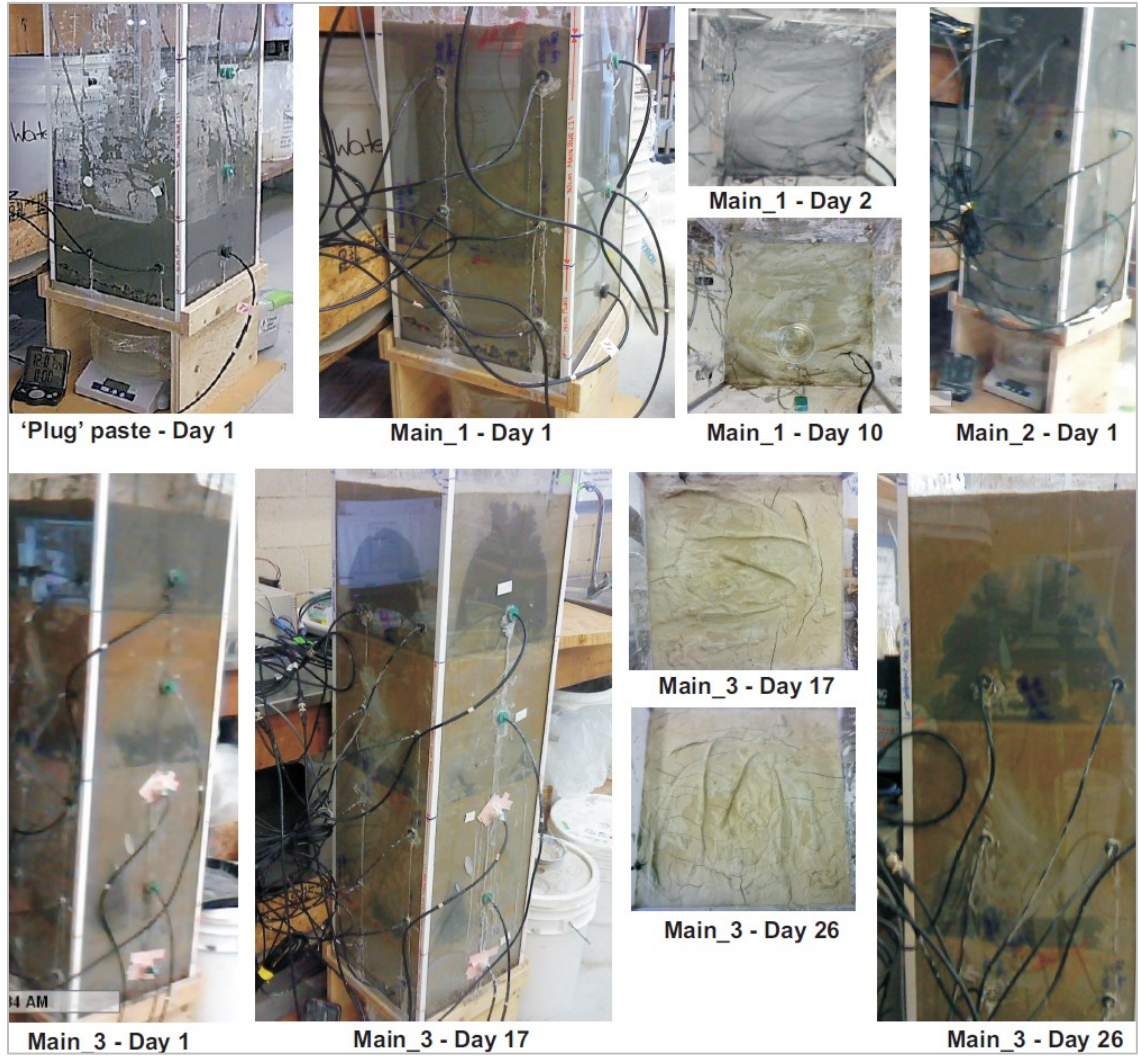


Figure 5.5.7 Column test filled in 4 'lifts': 15 cm 'Plug' paste and 3 main pours, each with 30 cm thick layer

CHAPTER 6

6 UNSATURATED FLOW MODELLING

This Chapter aims to demonstrate the application of the modified 1-D unsaturated flow equation to hydrating cemented paste fill material to estimate the distribution of PWP's in a CPB stope by using the lower and upper boundaries of CPB's material properties.

Two numerical models were performed to estimate the: (1) PWP drawdown down by alternating between the pre- and post- properties to assess the sensitivity of the input parameters; and (2) PWP distribution in a multi-layer cemented paste filled column, similar to the column test experiment. The following sections briefly described the: unsaturated flow model (Section 6.1); methodology adopted to simulate a 5 m thick paste plug layer (Section 6.2); a 1-D distribution of PWP's of a multi-layered paste column (Section 6.3); and, presents and discusses the numerical results (Section 6.5).

6.1 FORMULATION AND GENERAL ASSUMPTIONS

The governing partial differential equations (PDEs) that are used to solve transient-state flow problems assumes water conservation and flow is continuously distributed over space; thus These equations may be written in several forms; the most common forms are identified as the “*h*-based” form, the “*q*-based” form, and the “*mixed* form” (Thode, 2008). Each formulation has advantages over the other. The most commonly implemented form is the “*h*-based,” however, it can suffer from poor mass-balance in

transient problems (Thode, 2008). To overcome the “*h*-based” limitation, (Celia and Bouloutas, 1990) proposed a ‘*mixed*’ form of Richards (1931) equation to improve the mass-balance of the “*h*-based” formulation. The “*h*-based” formulation of the PDE for a transient, one-dimensional problem, incorporating a source or sink term, may be stated as:

$$-\gamma_w m_v \frac{\partial h}{\partial t} = \frac{\partial}{\partial y} \left[K(\psi) \frac{\partial h}{\partial y} \right] \pm S_K \quad [6.1.1a]$$

And, the ‘*mixed*’ formulations for a transient, one-dimensional problem, incorporating a source or sink term, may be stated as:

$$\frac{\partial \theta}{\partial t} = -\frac{\partial}{\partial y} \left[K(\theta) \frac{\partial h}{\partial y} \right] \pm S_K \quad [6.1.1b]$$

The PDEs presented above, states that the difference between the flow entering and leaving a unit volume is equal to the change in water storage and/or VWC (Thode, 2008). This equation assumes that there is no loading or unloading of the soil mass, and pore-air pressures remain constant at atmospheric pressure. Thus, changes in water content are only dependent on changes in matric suction (Thode, 2008).

A finite element software package developed by Soil Vision Systems, called SVFlux (SoilVision Office, 2009) is used to solve the 1-D unsaturated flow equation. This software automatically optimizes time-stepping and mesh geometry. SVFlux can implement either mixed or h-based form into the analyses, depending on what variables are to be solved.

6.2 METHODOLOGY

In CPB, the use of Equation [6.1.1] has been complicated by the fact that the paste properties evolved during hydration as pore-water is consumed to form hydration products. The pre- and post-WRC(s) determined experimentally served as a lower and upper bounds of the water-retention behaviour of hydrating CPB material. Model parameters were defined as user inputs to calibrate the unsaturated flow model are presented in subsequent sections. A sink term was also incorporated into the models to account for the inequalities of water-to-solids caused by self-desiccation.

6.2.1 MODEL ‘INPUTS’: SINK AND WATER-RETENTION PROPERTIES

Experimental data was incorporated into the model(s) as per user inputs. These inputs include the pre- and post- water-retention properties, and the sink data for paste containing 3% binder.

6.2.1.1 3% BINDER SINK

The loss of water volume as a function of hydration time was used to define the sink term, by correlating it with the total volume of paste material, which was expressed as the change in VWC per time ($\text{m}^3/\text{m}^3/\text{day}$). The sink data expressed in equation [6.1.1] has been provided in Figure 6.2.1. The negative sign indicates the loss of water volume per day. This data was then used in SVFlux, which was incorporated into the model in units of cubic meters per day per unit area (m/day), as provided in Figure 6.2.2, for the plug layer and Main layer(s)..

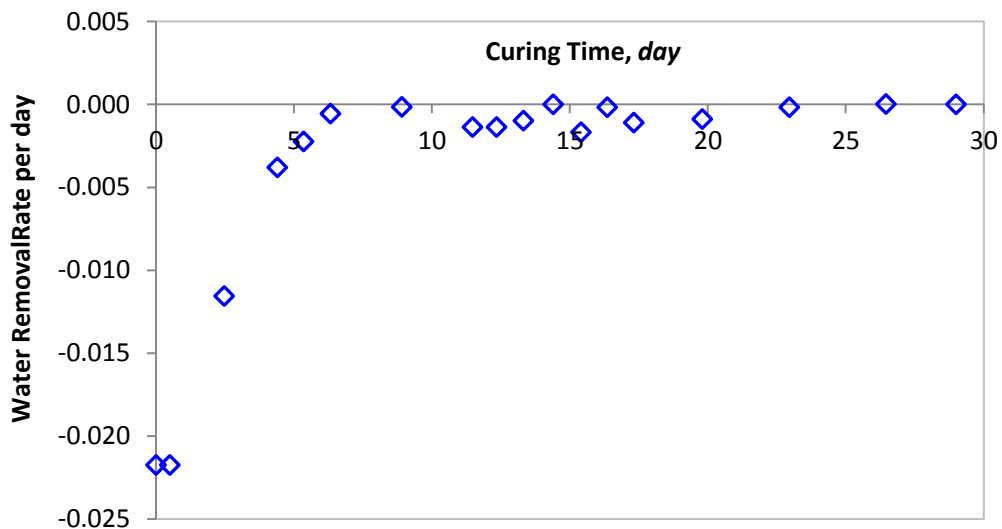


Figure 6.2.1 Rate of water removal from the experimental data (generic rate for a 1.0 m thick layer)

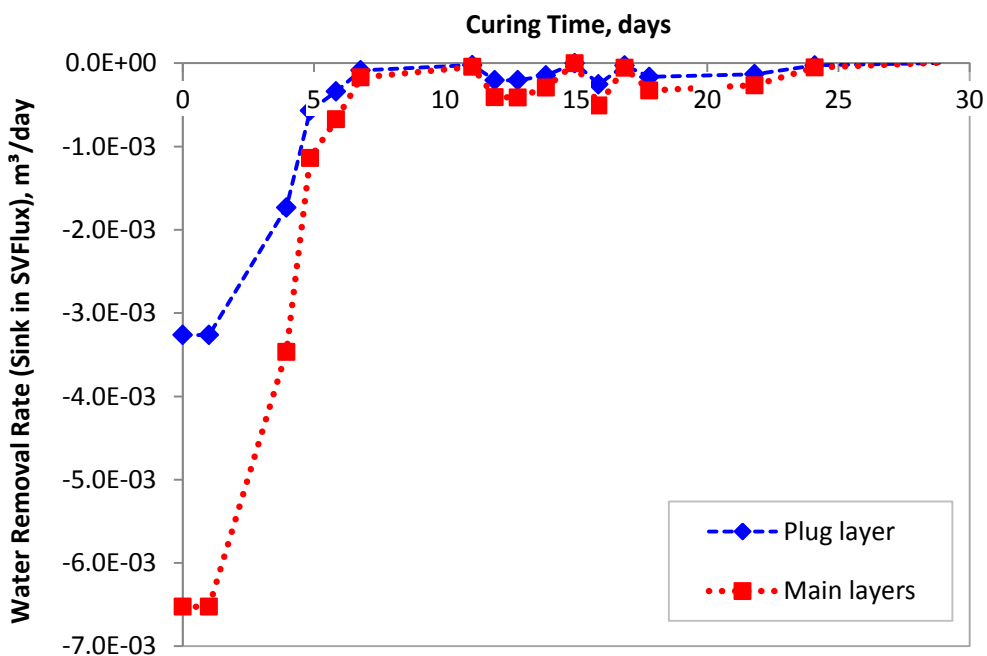


Figure 6.2.2 Water removal rate incorporated into SVFlux for the modelling regions – plug and main layers, expressed in cubic meters per day per unit area (m/day)

6.2.1.2 PRE- AND POST- MATERIAL PROPERTIES

The experimental pre- and post- WRCs, material compressibility, and the saturated hydraulic conductivity of tailings without and with binder are presented in Table 6.2.1. WRC data was inserted into the model, to which were then fitted to the Fredlund and Xing (1994) WRC equation (Eqn. [2.4.10]) to obtain the Fredlund et al. (1994) pre- and post- HCF.

Table 6.2.1 Pre- and post-hydrated input parameters

Material Properties	Experimental Properties			
	AEV (kPa)	K_s (m/d)	Saturated VWC (m^3/m^3)	m_v (1/kPa)
No Binder	40	8.64×10^{-3}	0.45	0.0038
3% Binder	80 - 120	3.46×10^{-4}	0.50	0.0002

The corrected material properties from the Fredlund and Xing (Fredlund and Xing, 1994) fit are presented in Table 6.2.2. The lower and upper bound of the fitted WRC(s) are presented in Figures 6.2.3 and 6.2.4, respectively. As reported by Thode (2008), these values are typically less than the using input / experimental values. The corrected values (in Table 6.2.2) are used to calibrate the Fredlund et al. (1994) permeability model to estimate the pre- and post- HCF (Figure 6.2.5 and Figure 6.2.6). The hydraulic conductivities at saturation (upper bounds) are within the same order of magnitude as the reported values in Chapter 5 (i.e. 10^{-3} m/d and 10^{-4} m/d) for the pre- and post- properties, respectively. The lower bound conductivities of the pre- and post- hydration are in the order of magnitude of 10^{-6} m/s to 10^{-10} m/s, respectively. In Figure 6.2.5, the hydraulic

conductivity of the pre-HCF significantly decreased over a wider range of matric suctions from 20 to 100 kPa, whereas in Figure 6.2.5, the post-HCF decreased over a range of matric suction from 100 to 300 kPa. It is not surprising that the change from saturation to unsaturation post-conductivity occurred more rapidly than the pre-conductivity. As expected, the conductivities decreased significantly, once suctions exceeded the AEV(s).

Table 6.2.2 Fredlund and Xing (1994) estimated material properties for Williams' paste tailings containing no binder and 3% binder

<i>Fredlund and Xing (1994) Estimates</i>					
Material Properties	AEV (kPa)	k_s (m/d)	Saturated VWC (m^3/m^3)	m_w (1/kPa)	R^2
No Binder	40.6	8.560×10^{-3}	0.45	0.000245	0.999
3% Binder	170.8	3.385×10^{-4}	0.44	0.000131	0.996

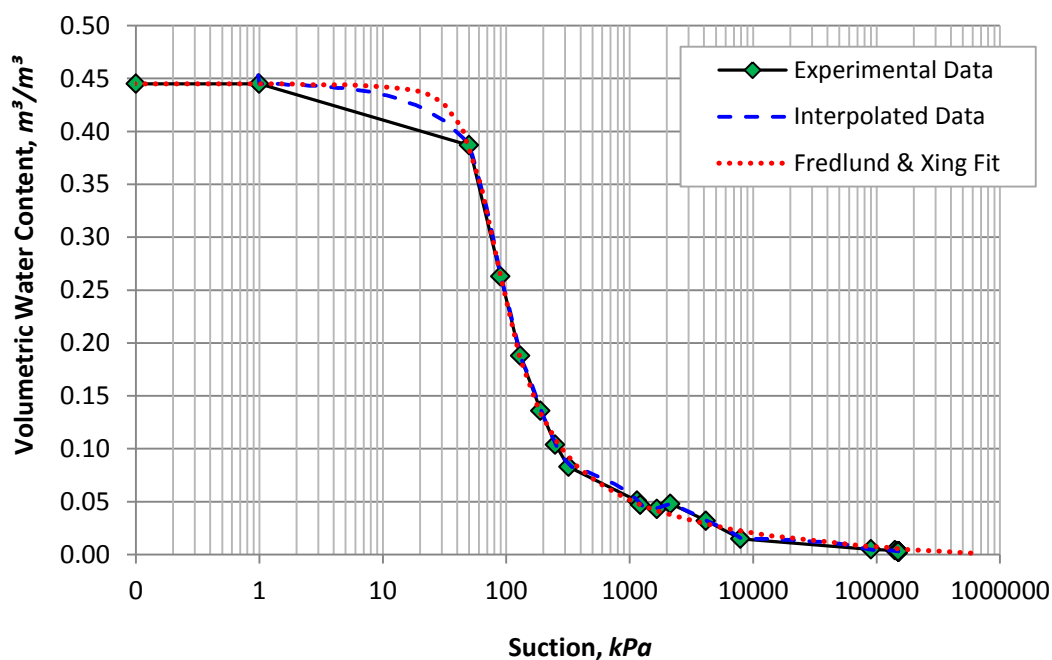


Figure 6.2.3 Water-retention curve of Williams' pre-hydrated tailings containing no binder

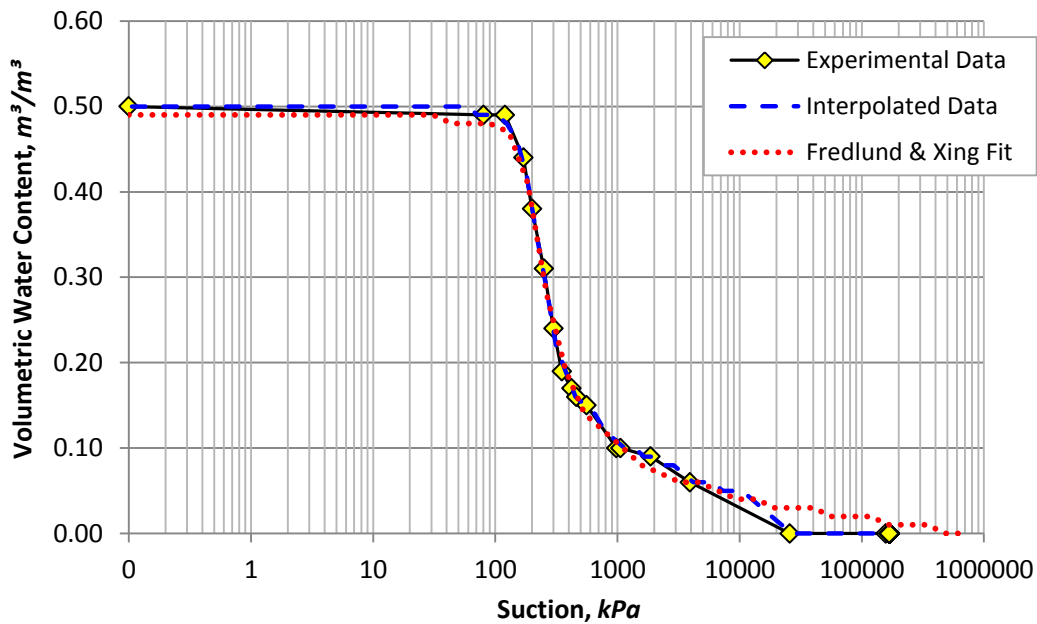


Figure 6.2.4 Water-retention curve of Williams' post-hydrated cemented paste containing 3% binder

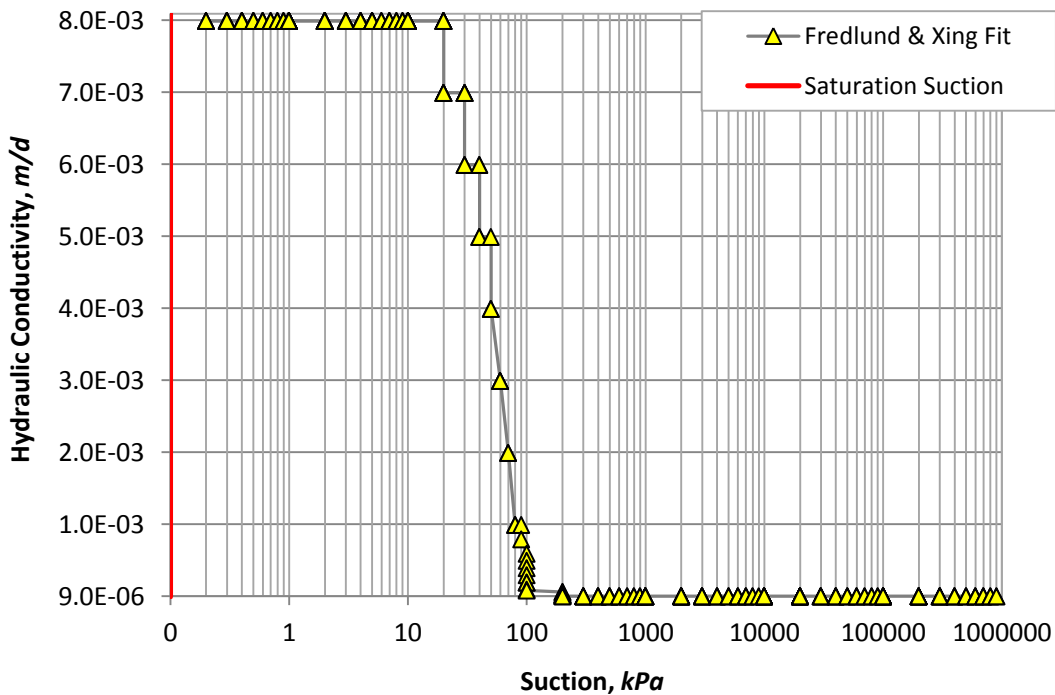


Figure 6.2.5 Unsaturated hydraulic conductivity function of Williams' pre-hydrated paste tailings containing no binder

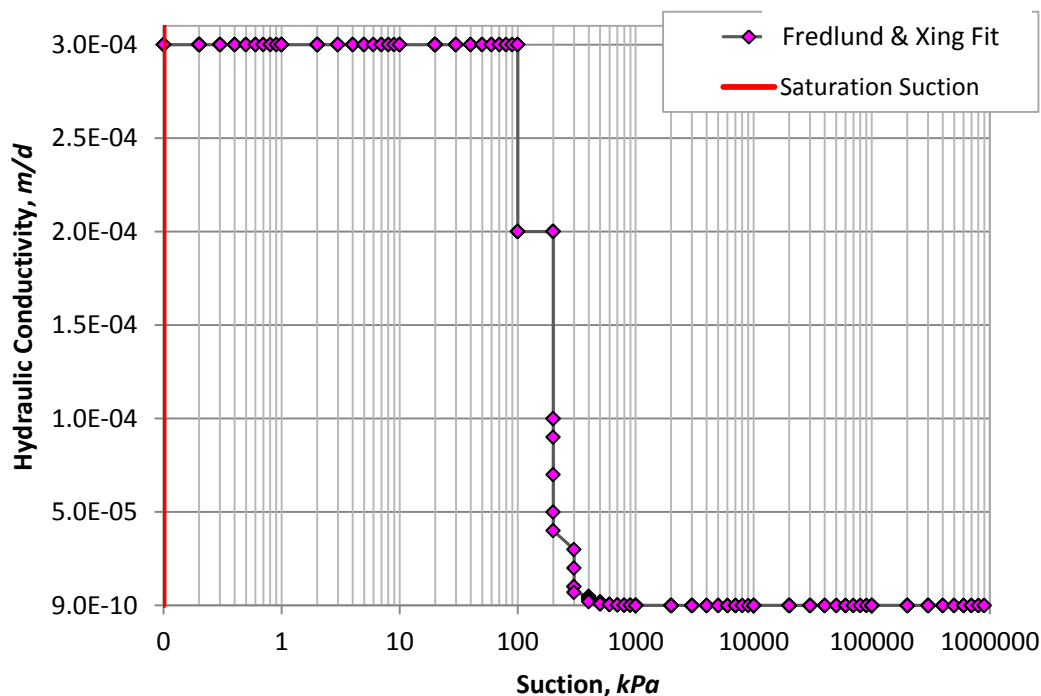


Figure 6.2.6 Unsaturated hydraulic conductivity function of Williams' post-hydrated cemented paste containing 3% binder

6.2.2 GENERIC MODEL OF A PASTE 'PLUG'

The '*h-based*' formulation was used to simulate the distribution of PWPs in a 5m thick column for qualitative purposes, primarily the effects of self-desiccation.

6.2.2.1 MODEL PARAMETERS, INITIAL AND BOUNDARY CONDITIONS

Since it is not known how the relevant properties evolve with time, several analyses have been performed to gain insight on how the input parameters affect PWP dissipation. The pre- or post- WRC, compressibility (0.0038 kPa^{-1} or 0.0002 kPa^{-1}) and hydraulic conductivity ($3.6 \times 10^{-4} \text{ m/h}$ or $3.6 \times 10^{-5} \text{ m/h}$) of the tailings without binder or tailings with 3% binder were alternated for qualitative purposes. Five scenarios were simulated

for an instantaneously placed 5 m thick layer (paste ‘plug) using Williams paste for the duration of 24 hours, while varying model parameters. A summary of each scenario and its modelling parameters have been provided in Table 6.2.3.

An initial hydrostatic PWP distribution was assumed, while the bottom boundary condition was set to a constant head of 0 m, which was conservative, as it underestimated drainage. A sink term was applied to Cases 4 and 5 to simulate the effects of self-desiccation during period.

Table 6.2.3 Modelling scenarios: alternating between the pre- and post-properties (i.e. WRC, compressibility and permeability), and effect of self-desiccation (i.e. sink term)

Modelling Scenarios	WRC	Mv (1/kPa)	Ksat (m/hr)	Sink Term
Case 1	No Binder	0.004	3.6×10^{-4}	No
Case 2	No Binder	0.004	3.6×10^{-4}	No
Case 3	Binder	0.0002	3.6×10^{-5}	No
Case 4	No Binder	0.0002	3.6×10^{-5}	Yes
Case 5	Binder	0.004	3.6×10^{-5}	Yes

6.2.2.2 EFFECTS OF PRE- AND POST- PROPERTIES, AND SINK TERM

Results of the generic model are presented in Figures 6.2.7 and 6.2.8. Figure 6.2.7 illustrated an important point with respect to the material compressibility, as it can be related to the consolidation and hence, drainage. For instance, upon comparing Cases 1 and 2, the coefficient of material compressibility was reduced by approximately an order in magnitude (Case 2), which exhibited a rapid drawdown, to which suctions (or –PWPs)

were induced. For the coefficient of compressibility, the post-hydrated paste was significantly smaller, which was indicative of small changes in volume (settlement) due to self-weight consolidation. In other words, very little to no build-up of pore-pressures had occurred, but rather a rapid drawdown immediately after the deposition of a 5 m thick layer of the paste material. The dissipation of PWP due to self-desiccation has been illustrated in Figure 6.2.8. In Case 5, when using the post-WRC with a sink generated the most negative PWP (or suction), while Case 1, (using the pre-WRC with no sink) generated the least. It was not surprising that Case 4 (using the pre-WRC, plus sink) produced suctions, while Case 3 (using the post-WRC, no sink) did not. Self-desiccation has been known to increase the rate of consolidation; hence, increase rate of PWP dissipation. This was demonstrated by Case 4 when comparing it to Case 3. An increase in water-retention properties (i.e., AEV , k_{sat}) and stiffness resulted in further PWP reductions (Case 5). This confers with findings reported by Helinski et al. (2007).

From these results, it would appear that the pre-WRC properties were more favorable to use in the model, specifically, where consolidation and drainage effects are of concern. The post-WRC properties appeared more reasonable for the post-hydration periods without incorporating the sink term. Incorporating the sink term with the post-hydration properties will most likely over-estimate pore-pressure dissipation during hydration. The post- properties had tendencies of under predicting consolidation and drainage rates, which is not unexpected, since the coefficient of volume change and permeability are both smaller than the pre- properties by an order of magnitude. This translated to less pore-water being ‘squeezed’ and drained through consolidation. Therefore, based on

these results, the pre-hydration properties are used to model the first 28 18 days of cement hydration while incorporating the sink term to account for both drainage and self-desiccation, while the post-hydration properties are utilized as the fully hydrated paste material once hydration has completely ceased.

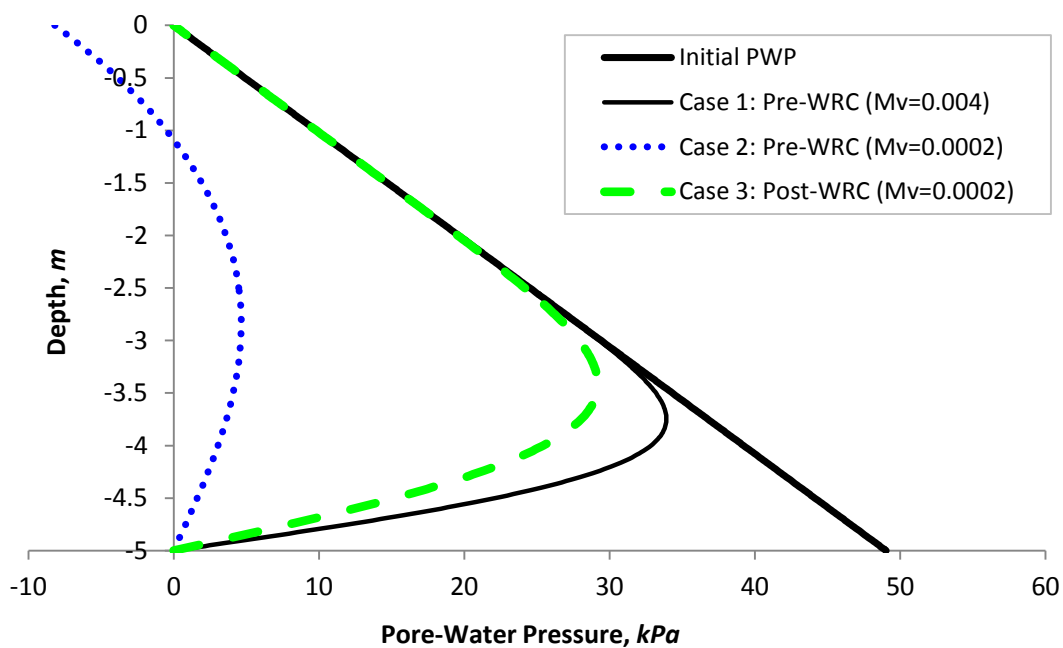


Figure 6.2.7 Simulation of pore-water pressure drawdown after 24 hours varying the coefficient of volume compressibility

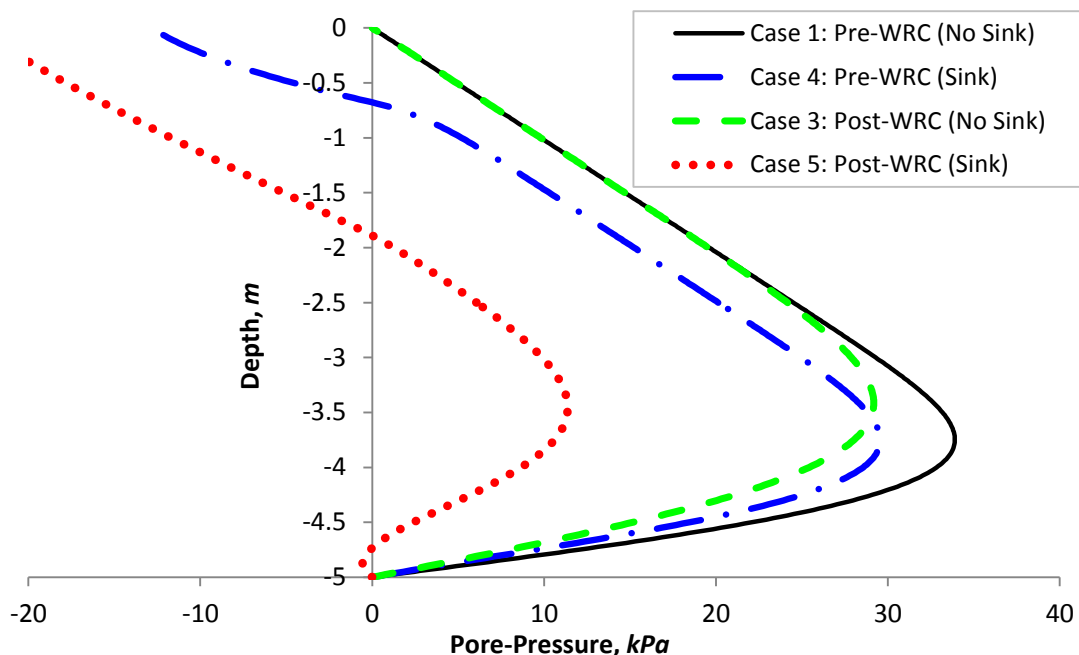


Figure 6.2.8 Simulation of pore-water pressure drawdown after 24 hours, showing relative contributions of drainage and self-desiccation

6.2.3 COLUMN TEST SIMULATION

Simulation of a 1-D column of Williams' 3% paste fill material was conducted to model the PWP profiles of the column experiment. To that end, the column test experiment was simulated to demonstrate the 1-D unsaturated flow application to hydrating CPB. These simulations utilize the 'mixed' formulation (Eqn. [6.1.1.b]).

6.2.3.1 MODEL DESCRIPTION

Numerical modelling of the PWP profile in a 1.05 m column was conducted by simulating 4 models to mimic the 4 stages of paste deposition carried out in the experimental phase. A description of the modelling depth, region and duration of each simulation has been provided in Table 6.2.4. The final condition after each simulation

was assigned as the ‘new’ initial condition for the previously modelled layer (Model Region – R2) in subsequent simulations, while the freshly deposited paste layer (Model Region – R1) was assigned an initial condition of constant head.

Table 6.2.4 Description of model(s) and settings to simulate a 1-D distribution pore-water pressures in a 1.01m length column

Paste Layer	Layer Depth (m)	Cumulative Depth (m)	Model Region*	Model Duration (days)
Plug	0.142	0.142	0.15	21
Main 1	0.288	0.430	0.45	29
Main 2	0.288	0.718	0.75	32
Main 3	0.288	1.006	1.05	37
Final	1.006	1.006	Datum at z = 0 m	119

**Consolidation was accounted for in the simulations by imposing an initial condition of the arithmetic differences between the cumulative depth and model region.*

6.2.3.2 ASSUMPTIONS AND INITIAL CONDITIONS

In order to simulate the 1-D distribution of PWP's in a vertical column, the following assumptions were made.

- Bulk density was considered constant, such that very little insurmountable changes in void ratio were to have occurred when alternating from the pre- to post-hydrated material properties.
- Each lift was simulated as an instantaneous pour, loading hydrostatically after consolidation and subsequent paste settling, with an initial condition of excess pore-pressure.

- Changes in underground backfilling conditions were considered negligible, thus, no evaporative fluxes.
- Cement hydration period of a freshly deposited layer takes place during the first 28 days at a constant RH, after which hydration ceased to occur, such that temperatures effects on the WRC(s) are assumed to be small during 28 days of curing.
- During the curing period, hydrating paste may pose similar properties of tailings with no binder. Therefore, the pre-hydrated material properties were assigned to the fresh paste layer that incorporated an internal sink to account for the removal of water due to the inequality between the loss of water volume and the volume of the hydration products.
- Paste was considered to have posed the same properties to that of the fully hydrated paste fill after 28 days. Thus, the loss of water no longer applied thereafter.
- Distributions of PWP's were a 1-D in the vertical direction on a per unit square meter basis. The datum was assigned at the top of the modelling region / column layer with sign conventions for entering and leaving the regions were positive and negative, respectively.

The initial conditions were based on the differences in VWC(s) before and after consolidation. For example, using the left hand term in the unsaturated flow equation

defines the amount of water stored in the saturated region of the WRC at an initial PWP (i.e. $PWP_{initial} m_v$) is equal to the change in VWC, before and after consolidation (i.e. $PWP_{initial} = \Delta VWC / m_v$). From the experimental data (Table 5.5.3, page 203), the VWC(s) before and after drainage are known, as well as the coefficient of compressibility, therefore, the initial PWP(s), or also referred to here as the initial conditions for each simulated paste layer was calculated and incorporated into the SVFlux program in terms of head. The initial conditions for each simulated layer (or freshly deposited paste layer, [Region 1, R1], was assigned this initial condition. While, the underlying layer or previously simulated layer, [Region 2, R2], was assigned the ‘final’ condition of a previous simulation as the ‘new’ initial condition. A summary of these initial and/or final conditions have been provided in Table 6.2.5.

Table 6.2.5 Initial conditions for each model layer

Simulation	Initial VWC	VWC (after settlement) %	Initial PWP [R1] kPa	Initial Condition [R1]	Final Condition [R1] m	Initial Condition [R2]
Plug	0.4966	0.462	9.11	0.911	-6.63434	-6.63434
Main_1	0.4882	0.447	10.84	1.084	-6.26649	-6.26649
Main_2	0.4977	0.483	3.87	0.387	-6.23397	-6.23397
Main_3	0.4922	0.472	5.32	0.532	-5.97114	-5.97114

6.2.3.3 BOUNDARY CONDITIONS

Top boundary conditions were assigned a ‘zero flux’ condition (as per assumptions). Boundary conditions between layers (R1 and R2), were assigned a ‘no boundary’ condition. The bottom conditions were of Type II, to which an instantaneous ‘flux

condition' (in units of $\text{m}^3/\text{day}/\text{m}^2$) was imposed, by using the experimental outflow data. The bottom boundary condition data for each model layer was imported into SVFlux. Since the outflow volume of water for Main_1 was not recorded as a function of time, an assumption was made that the cumulative volume of drained water followed a similar pattern as the outflow rate of the underlying 15 cm plug layer, which has been illustrated in Figure 6.2.9. Cumulative water volumes of each layer, collected over time were then plotted and fitted to either a 4th or 5th order polynomial. These equations were used to estimate the total volume of water and compared with the experimental values to ensure a level of accuracy (Table 6.2.6).

The 4th order polynomial for Main_1 was used to estimate the cumulative volume of water as a function of time for approximately 7 hours (or 0.3 days). Cumulative volumes were used to calculate the instantaneous fluxes as a function of time. Both variables were imported into the SVFlux solver. The bottom boundary condition of the 14.2 cm plug layer is presented in Figure 6.2.10. Bottom boundary conditions for Main_1, Main_2 and Main_3 are respectively, presented in Figures 6.2.11, 6.2.12 and 6.2.13.

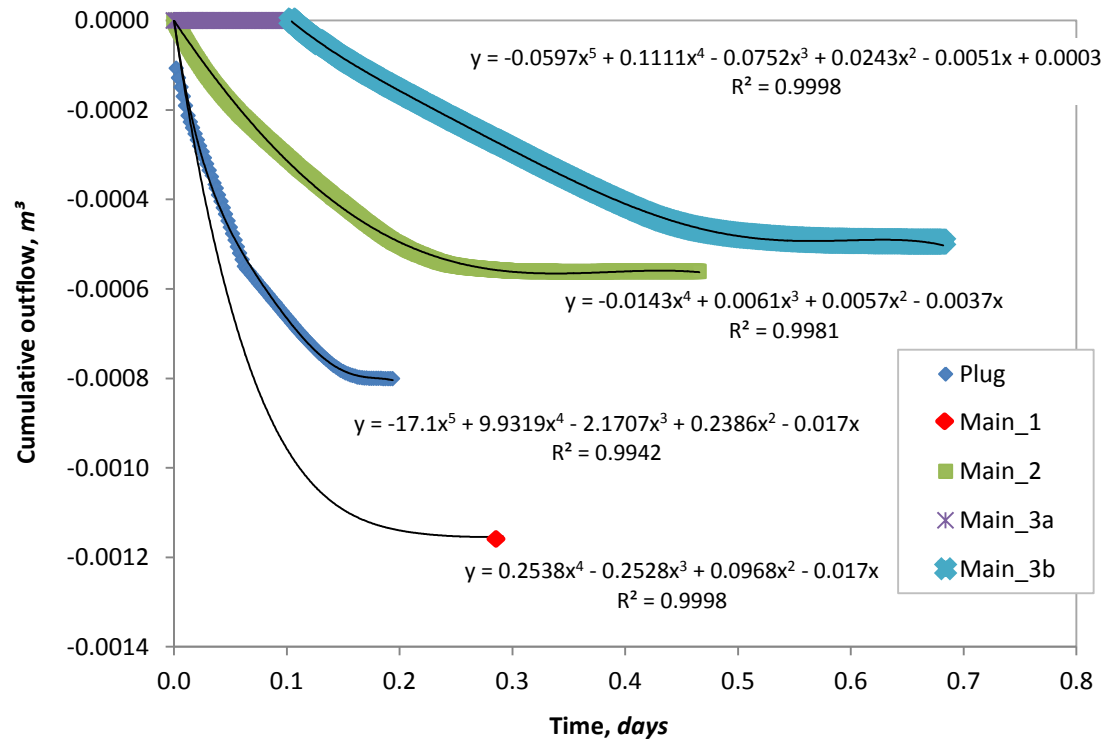


Figure 6.2.9 Cumulative water volumes collected after each paste pour

Table 6.2.6 Estimated outflow volumes compared to experimental volumes

Layer	Time <i>days</i>	Outflow (Experimental) <i>cm</i> ³	Outflow (Estimated)	Rel. ERR %
Plug	0.195	800.5	-798.3	0.28
Main 1	0.292	1152.2	-1159.4	0.62
Main 2	0.466	561.8	-543.4	3.27
Main 3	0.682	494.7	-503.2	1.73

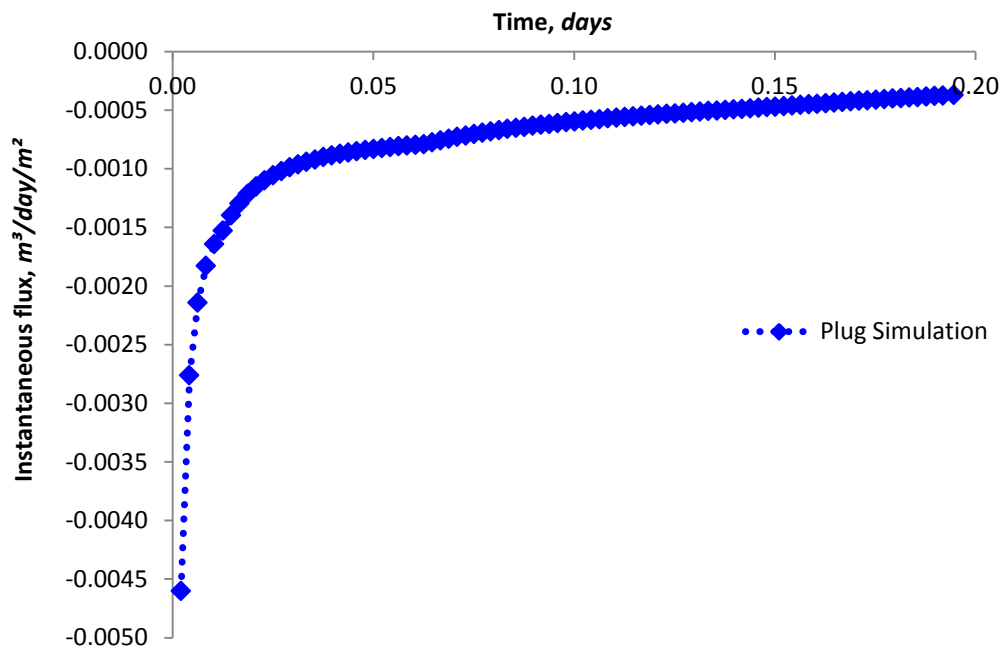


Figure 6.2.10 Simulation #1: bottom boundary condition assigned to the plug layer

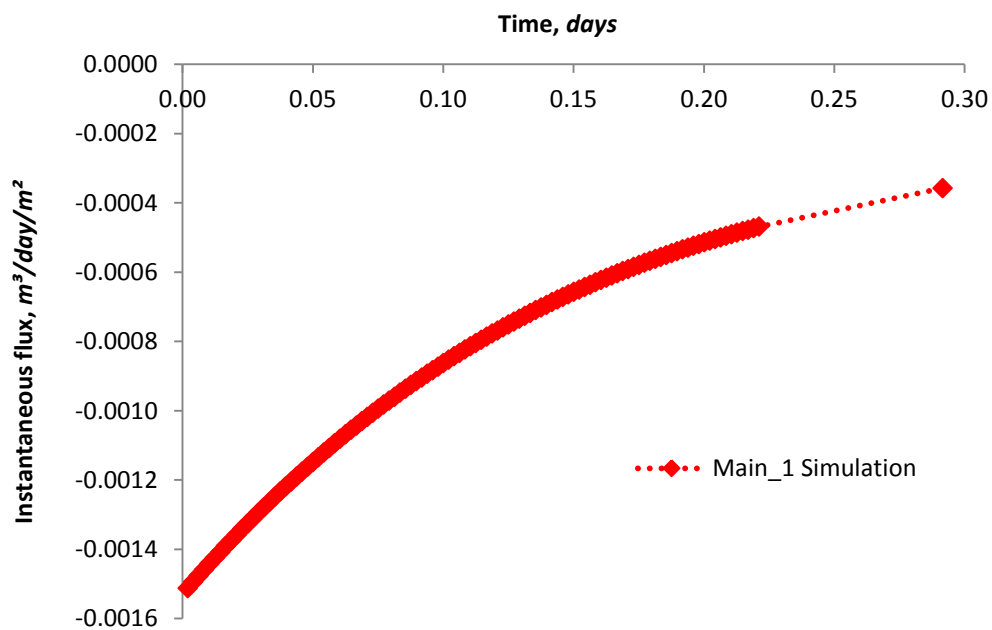


Figure 6.2.11 Simulation #2: bottom boundary condition assigned to the Main_1 layer

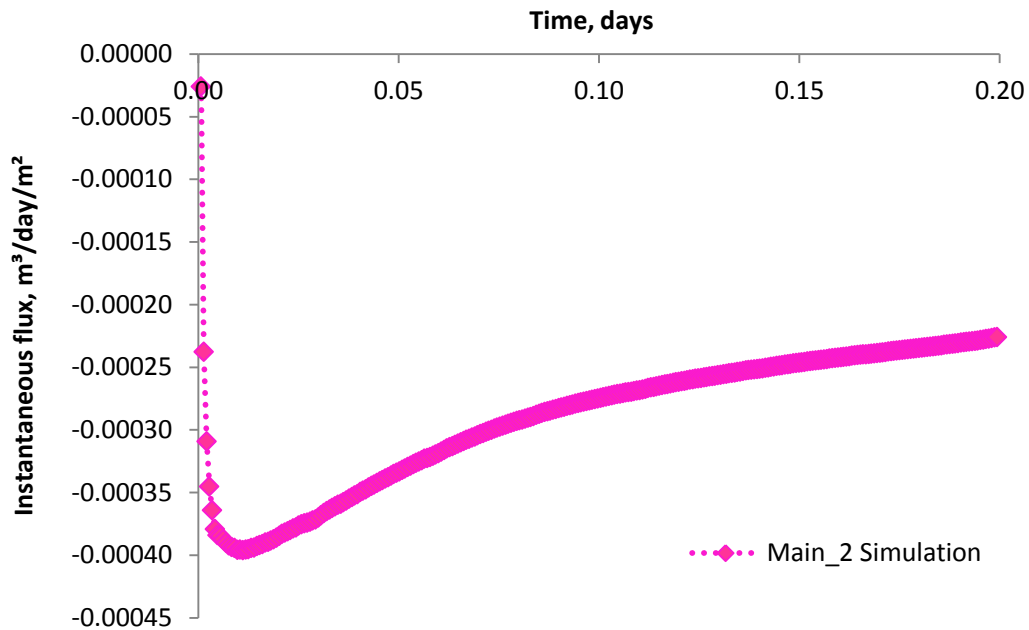


Figure 6.2.12 Simulation #3: bottom boundary condition assigned to the Main_2 layer

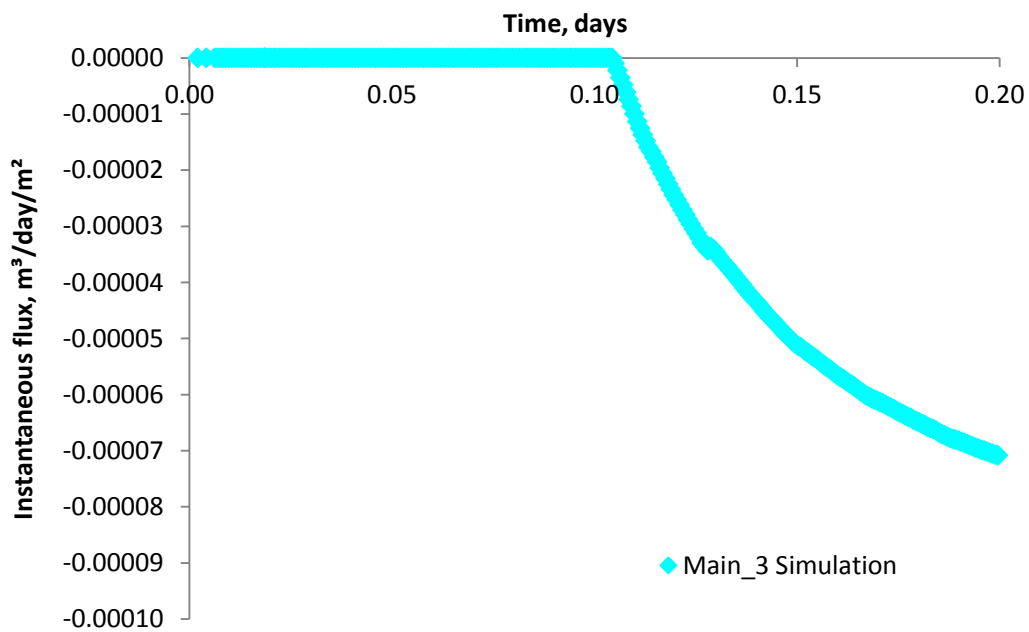


Figure 6.2.13 Simulation #4: bottom boundary condition assigned to the Main_3 layer

6.3 MODELLING RESULTS AND DISCUSSION

Numerical estimations of the distribution of PWP in a column produced reasonable profiles. The results of the finite element solver and a method of verifying such results are presented and discussed in Section 6.3.1. PWP profiles from the column test simulations are also presented and discussed as well in Section 6.3.2.

6.3.1 SOLVER RESULTS AND MODEL VERIFICATION

A method of checking the modelling results against the original material properties were implemented into SVFlux to test the ability of the finite element solver to follow correctly, the non-linear water retention properties associated with model simulations (Thode, 2008). Suction and VWC values were extrapolated from the finite element mesh for each point in the modelling region to solve for nodal points, to which were then plotted on the original WRC(s) and HCF(s). The analyses were solved correctly, which can be illustrated when the finite element nodal points are plotted along the line representing the unsaturated soil properties (Thode, 2008). The results of the finite element solver have been provided in Figure 6.3.1 – Figure 6.3.4. These results demonstrated the correctness of the solver.

Additional measures were taken to ensure the validity of the model, by conducting a water balance. A summary of the modelling results have been provided in Table 6.3.1. Numerical results were found to be in reasonable agreement with the experimental values, as shown in Table 6.3.2. It was observed that the volume estimations of the SVFlux solver were over-estimated, as exhibited by the high % relative error as

subsequent simulations were conducted. The possible causes of this has been discussed in more detail in following subsections.

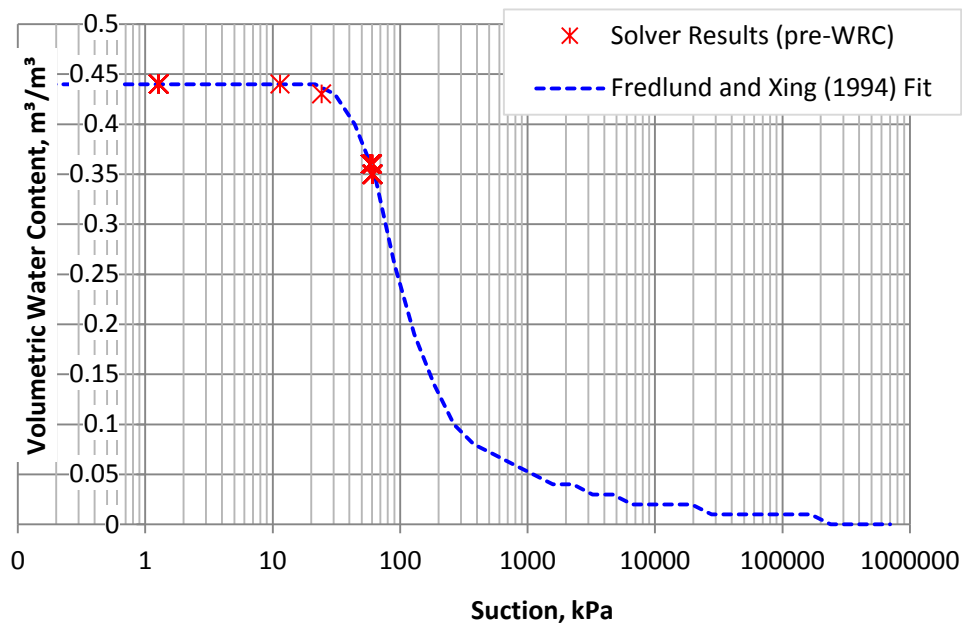


Figure 6.3.1 Finite element solver results using the pre-WRC

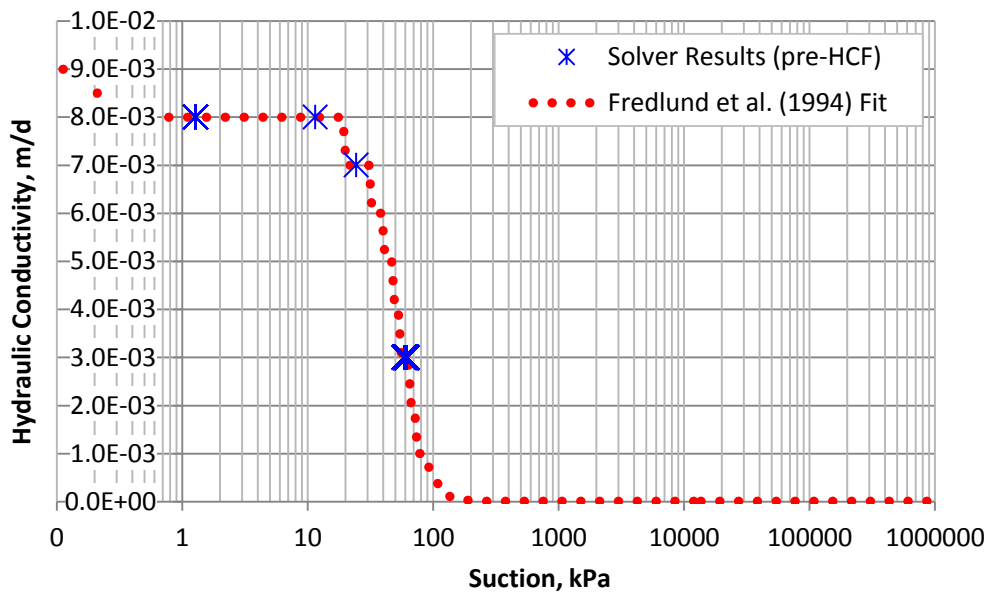


Figure 6.3.2 Finite element solver results using the pre-HCF

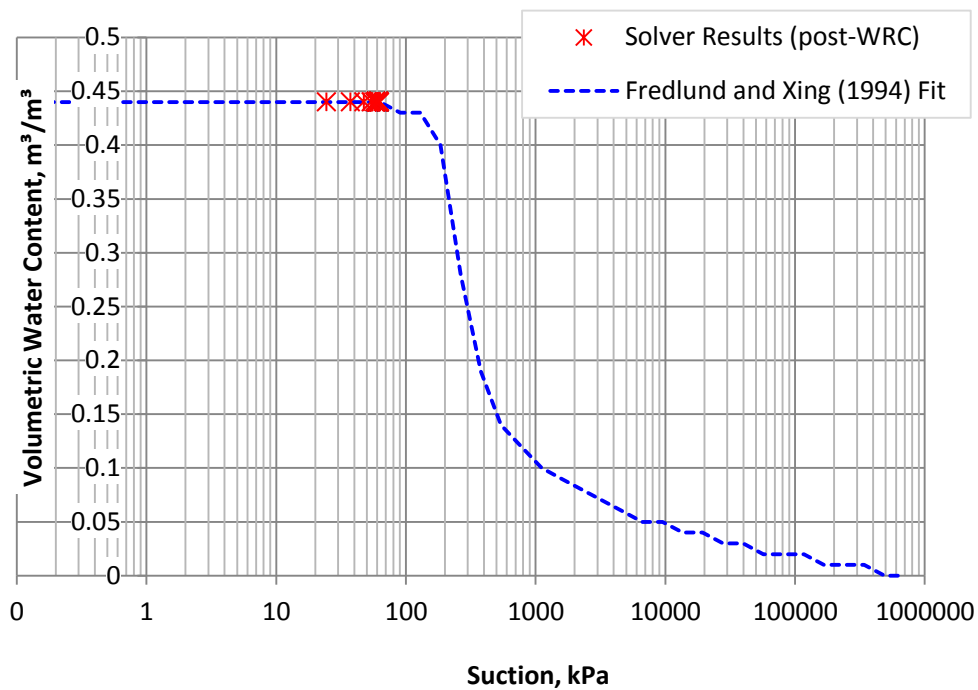


Figure 6.3.3 Finite element solver results using the post-WRC

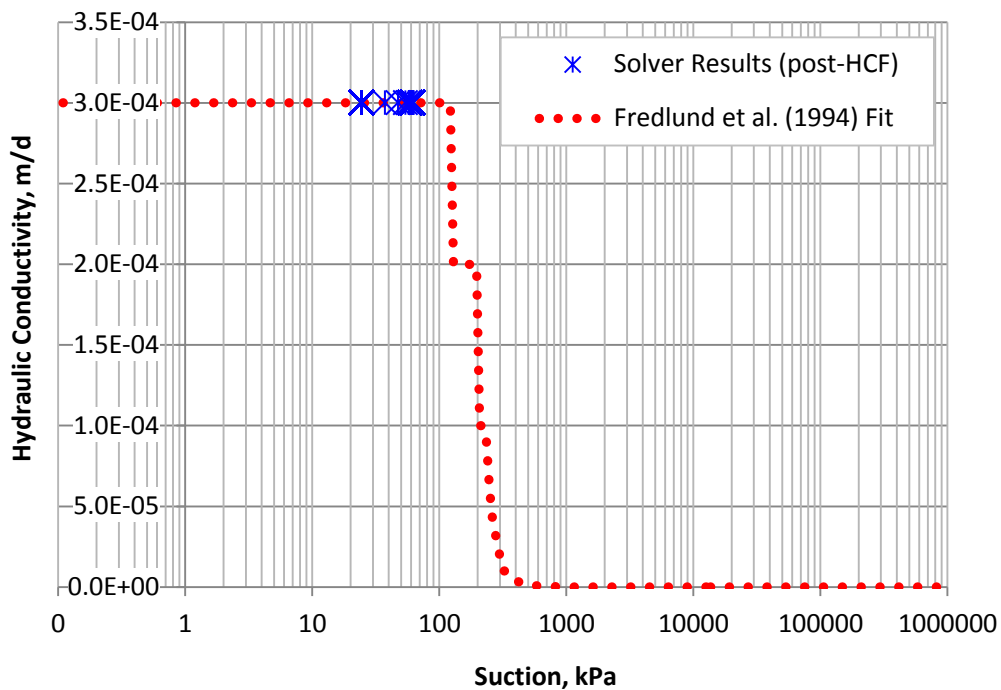


Figure 6.3.4 Finite element solver results using the post-HCF

Table 6.3.1 Numerical results: water balance checks

Model (.svm)	M_w (in)	M_w (out)	M_w (Sink)	$\Delta M_w = M_w$ (out) + M_w (Sink) (kg)	$M_{\text{storage}} = M_w$ (in) - ΔM_w	Cumulativ e storage	V_w (out) (cm^3)
Plug	6.225	0.6734	0.0389	0.7123	5.5130	5.513	673.4
Main_1	12.731	0.9827	2.4850	3.4677	9.2634	14.776	982.7
Main_2	12.066	0.3213	2.4873	2.8086	9.2576	24.034	321.3
Main_3	11.709	0.2328	2.4912	2.7240	8.9846	33.019	232.8

Table 6.3.2 Model verification: numerical versus experimental water balances

Model (.svm)	Numerical Results		Experimental Results		Relative Error	
	M_w^N (in) (kg)	V_w^N (out) (cm^3)	M_w^E (in) (kg)	V_w^E (out) (cm^3)	M_w (in) (%RE)	V_w (out)
Plug	6.225	706.6	6.704	800.5	7.14	11.73
Main_1	12.731	950.3	13.182	1152.2	3.42	17.52
Main_2	12.066	311.4	13.437	561.8	10.20	44.57
Main_3	11.709	232.8	13.290	494.9	11.90	52.96

6.3.2 DISTRIBUTIONS OF PORE-WATER PRESSURES IN A CPB COLUMN

Distributions of the PWP's estimated from these simulations are presented in Figure 6.3.5. It is interesting to note here that the rate of suctions that had developed in each layer immediately after deposition were overestimated compared to the experimental results. From 0 to 50 kPa, the estimated rate of suction generation was rather high initially, after which suctions begin to slow down – this is more apparent in the main layers. With the placement of each layer, suctions begin to taper off, slowly. The differences in the estimated matric suctions between layers were relatively small with the exception of the newly simulated layer. This was also observed with the experimental measurements (Figure 6.3.6).

Both the relatively small differences in matric suctions between layers, and decreased rate in matric suction generation with the addition of each layer, were simulated by the modelling approach by using numerical predictions in the first layer as a new initial condition. This correlated reasonably well with the experimental results, with the exception of the profiles generated once Main_2 and Main_3 were simulated. For instances, not all suctions dissipated to zero when hydrostatic loading was assumed. The decreased rate of matric suction dissipation was less apparent in the last two layers.

Peak suctions (~ 68 to 60 kPa) were underestimated, compared to the experimental results. With the addition of a newly simulated layer, especially in the last layer (Main_3 for T6), peak suctions decreased by approximately 8 kPa from the initial plug layer (T1). The decrease in profiles (suctions) as the remaining layers are simulated may be a result of the increased water-retention properties, when the solver extrapolates from the pre- to post-hydrated properties. For example, each simulation that utilized the pre-hydration properties (i.e. Figure 6.3.1 and Figure 6.3.2) illustrated that the flow regime was unsaturated (i.e. suctions exceeding the AEV). When subsequent simulations were performed, the post- properties were then used, illustrating that an unsaturated flow regime was not attained (i.e. Figure 6.3.3 and Figure 6.3.4).

More on this will be discussed in Section 6.4. In whole, however, the column test simulations produced relatively reasonable estimations. The assumptions made were also somewhat reasonable, given that only the lower boundary condition of the second

simulation was estimated. Pore-pressure dissipation initially after placement of a lift was ever over-estimated as well as the overall generation of matric suctions.

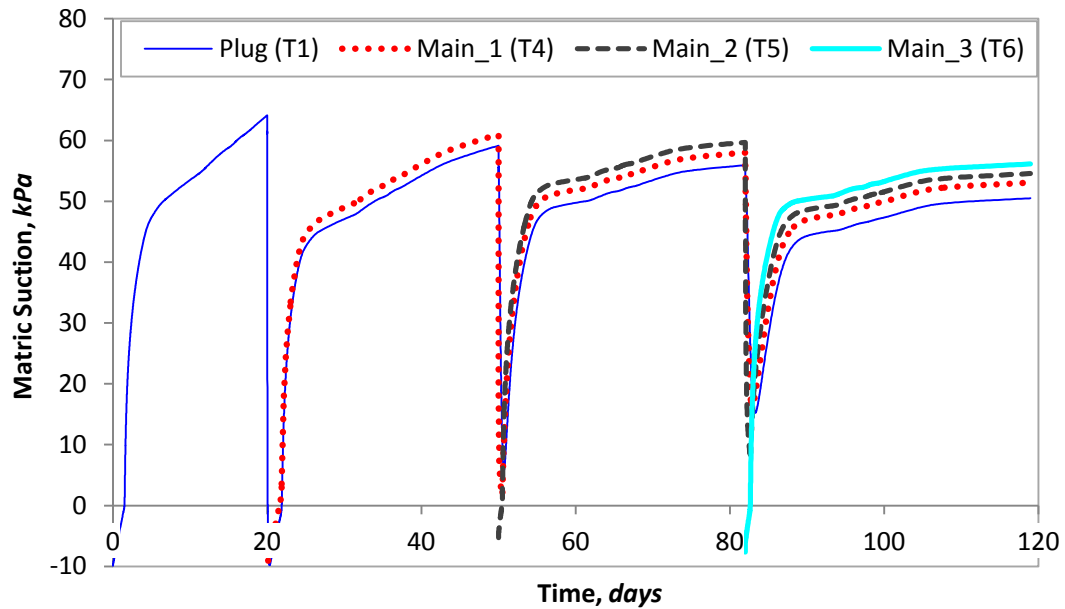


Figure 6.3.5 Simulated distribution of pore-water pressures in a cemented paste filled column

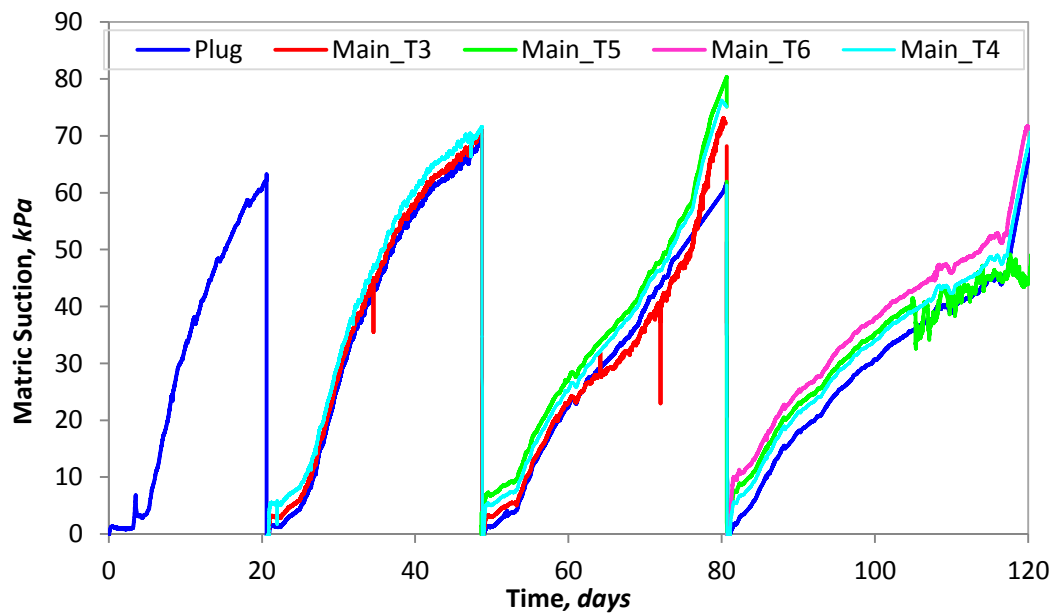


Figure 6.3.6 Experimentally measured pore-water pressure distribution in a cemented paste filled column

6.4 LIMITATIONS

The application of the unsaturated flow model has its own limitations, especially when alternating between the pre- and post-hydration properties. These numerical simulations however, described only a preliminary version of modelling the effects of drainage and self-desiccation in hydrating cemented paste fill – preliminary in the sense that these effects were not coupled, but rather inferred (i.e. consolidation). Consolidation is a critical factor in defining the bottom boundary condition, as well as the initial loading. Thus, it would be more appropriate to model self-desiccation with a consolidation model.

Estimated pore-pressures were also one-dimensional, and thus any contributions made through arching effects were neglected, thereby, underestimating the rate of PWP dissipation. In the field, arching affects will actually influence the total stresses and pore-pressures experience within hydrating CPB filled stopes. Other constraints include, the laboratory conditions, in which the material properties were measured are not representative of actual field conditions. Changes in relative humidity are most likely to occur due to thermally induced stresses as well as variation in seepage rates (e.g., rate of consolidation and rate-of-rise).

SVFlux as a numerical tool to simulate PWP profiles can be a very useful tool for modelling flows through unsaturated porous media. However it was observed that alternating between the pre- and post-WRC properties (Column test simulation) actually caused the model to add more water into a layer than it previously had as the final condition (as illustrated in Figure 6.4.1). The amount of water added into the model was

not considered significant in the first two layers, albeit, significant in the last two layers (or simulations – Table 6.3.2, page 232). This was due to using the pre-WRC properties for the first 28 days, after which the final suction was used to extrapolate the initial VWC from the post-WRC for the subsequent simulations. This was not surprising, since a WRC described the interrelated relationship between suctions and water content. Simulations which relied on the pre-WRC produced suctions beyond the AEV (~ 40 kPa), where it was considered as an unsaturated media, however once hydration had ceased, the post-WRC was applied. Suctions that had developed in the post- material layers were less than the AEV (~ 120 kPa) of the post-hydrated material. In other words, that the once ‘unsaturated’ paste (Figure 6.3.1) was now ‘saturated,’ according to the post-WRC (Figure 6.3.3). This was due to the assumption surrounding the 1-D unsaturated flow equation, such that, water flow is conserved.

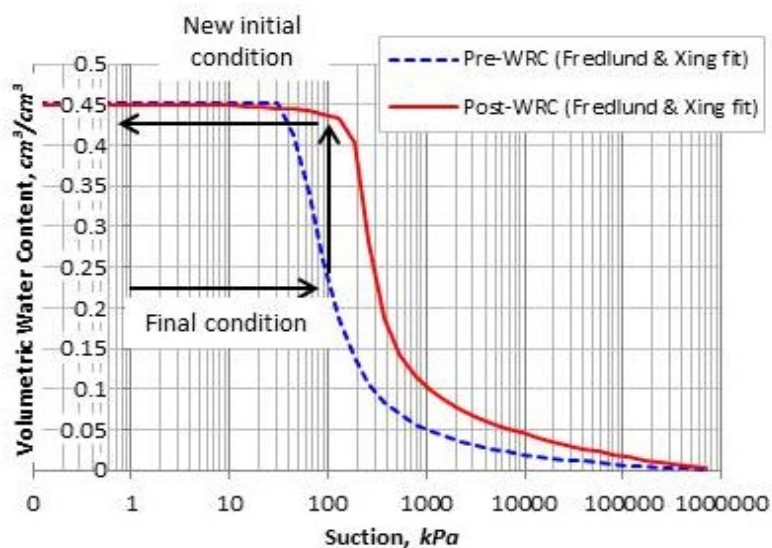


Figure 6.4.1 Alternating between pre- and post-WRC properties when defining a ‘new initial condition’ based on the results of a previous ‘final condition’

CHAPTER 7

7 SUMMARY AND CONCLUSIONS

7.1 RESTATEMENT OF THE PROBLEM

The aim of this research was to improve understanding of the pore-water pressures (PWP) behaviour in cemented paste backfilled (CPB), by using an unsaturated flow framework. PWPs are a necessary component of defining the internal stresses of backfill, and stresses acting on containment barricades. Being able to understand how PWPs dissipate upon fill placement can help improve current designs practices of underground support systems and minimize operational requirements.

Current design methodologies rely heavily on compressive strength indices on laboratory cured specimens. These indices provide useful information on the evolving strength properties, providing however, limited information on consolidation and self-desiccation on stress and strength distributions throughout a CPB stope. Being able to capture the unsaturated properties of CPB as a function of paste hydration may provide a better understanding of how PWPs dissipate under drained analyses, coupled with the self-desiccation phenomenon. The 1-D unsaturated flow equation was proposed to model the PWPs in a CPB stope. An additional term, *sink*, is incorporated into the equation to account for early-age curing of CPB material. The modified 1-D unsaturated flow equation is stated as:

$$-\gamma_w m_v \frac{\partial \psi}{\partial t} = \frac{\partial}{\partial y} \left[K(\psi) \frac{\partial \psi}{\partial y} \right] - S_K$$

where, $K(\psi)$ is the unsaturated HCF as a function of matric suction, [m/d]; m_v is the compressibility of a soil system due to the change in PWP at saturation, [1/kPa]; γ_w is the bulk unit weight of water, [N/m³]; and, S_K is the sink term to account for removal of water due to inequality between the loss of water volume and the volume of generated hydration products.

The objectives of this study was to therefore, (1) determine the water-retention properties to describe the PWP behaviour of CPB as a function of paste hydration (Section 7.2); and (2) demonstrate the application of a 1-D unsaturated flow equation to estimate PWP distributions in cemented paste filled column test (Section 7.3).

This research is part of a collaborative research project on CPB, involving three universities, headed by the University of Toronto. The overall goal of this project was geared towards addressing the ambiguities that exist with current methodologies in the geomechanical mine design of CPB systems. This work presented in this thesis was intended to support the goals of the CPB project, by imparting the results described in Milestone 8 – unsaturated property testing of paste backfill.

7.2 EVOLUTION OF CEMENTED PASTE FILL PROPERTIES

Paste hydration alters the water-retention properties. Self-desiccation induced suctions represent individual WRC(s) and AEV(s) for every suction that were produced during binder hydration, however tracking these properties are rather difficult, because existing techniques require steady-state conditions, which is not possible, due to hydration. Therefore, direct and indirect techniques were used to study the lower and upper bounds of the water-retention behaviour of paste tailings, respectively, without binder and with binder after 28 days of early-age curing. These tests also allowed for the coefficient of compressibility of tailings during the pre- and post- hydration period to be determined.

7.2.1 PRE- AND POST-HYDRATED WATER-RETENTION PROPERTIES

The results of the lower and upper bound WRCs measured for Williams and Kidd paste produced similar findings. For both paste streams, the water-retention properties increased due to the hydration bonds and newly formed products. The results of the pre- and post-hydrating tests have been summarized as follows.

- 1) For Kidd paste, the pre- and post- AEV evolved from an initial value of 40 kPa to 140 kPa. The coefficient of compressibility evolved from 0.0014 1/kPa to 0.00012 1/kPa.
- 2) For Williams' tailings, the pre- and post- AEV evolved from an initial value of 50 kPa to 120 kPa. The coefficient of compressibility also evolved from 0.0038 1/kPa to 0.0002 kPa.

- 3) Kidd tailings underwent a more significant transformation compared to Williams, because of the addition of alluvial sand, and the slag-based binder. In both instances, it increased the water-retention properties as well the material's stiffness.

Binder hydration thus, had an overall effect of increasing the water-retention properties and stiffness of the material.

7.2.2 SELF-DESICCATION AND PORE-STRUCTURE

To understand how these properties changed from the lower to upper water-retention properties, the generation of matric suction and rate of water removal was studied, by conducting numerous self-desiccation tests on Kidd 0%, 2.2% and 4.5% binder, and Williams 0%, 3%, 5% and 7% binder. MIP tests were also conducted, however for a limited number of Williams' 3% and 7% binder specimens. From the results of these tests, the follow conclusions were drawn.

- 1) Initial rate of self-desiccation was delayed when the initial water content was high. Dissipation of excess PWP's through drainage facilitated self-desiccation.
- 2) Rate of self-desiccation was dependent upon the %wt. binder dose. Higher binder contents generally, increased the generation rate of suctions and rate of water removal, due to enhanced reactivity of hydration.
- 3) Rate of matric suctions produced, and rate of water removal during binder hydration was dependent upon the %wt. binder dose for both paste streams, where

higher binder contents and lower initial water contents increased the rate of self-desiccation.

- 4) Pore-water desaturation (by self-desiccation) stabilized when suctions approached the AEV of the material as water volume became limited.
- 5) Relative PSD(s), threshold and critical pore diameter decreased with curing time, and %wt. binder content. The total MIP porosity and specific surface was increased with curing time and %wt. binder dose, which conferred that the hydrating material acquired stiffness and strength.
- 6) Degree of self-desiccation was largely affected by curing temperature. An increase in temperature by 10°C significantly increased the interstitial fluid surface tension, which suppressed and/or delayed the generation of matric suctions.

An attempt was made to estimate changes in the stiffness that hydrating paste acquires. It was found that the estimated coefficient of compressibility at 50 kPa was less than the pre-hydrated tailings, and slightly greater than the post-hydrated paste at 120 kPa, confirming that the material does indeed, become more rigid as paste hydration proceeds. Hydrating 3% Williams and 2.2% Kidd specimens during self-desiccation reached a respective post-AEV(s) by the 20th day of hydration, however, the rate of self-desiccation for Kidd paste was significantly higher than Williams were. This was due to the initially lower water content of Kidd's' (~22% GWC, versus Williams' ~35% GWC), as well as with the addition of the alluvial sand. Slag-mixed binder has also been reported to yield more desirable properties (i.e., strength, stiffness), versus fly-ash based

binders. Self-desiccation was facilitated once minimal amount bleed water is removed, such as through drainage, after which only a few days of hydration, paste material was capable of producing suctions closer to the AEV(s) of the post-hydrated material.

Contributions of paste hydration are important, because it relates to how quickly +PWP dissipation in CPB material. To that end, the self-desiccation phenomenon has significant ramifications in terms of strength distributions in CPB stopes, as it is of particular importance when the rate of consolidation is of concern.

7.3 AN UNSATURATED FLOW IN A PASTE FILLED COLUMN

Use of the modified 1-D unsaturated flow equation to estimate PWP distributions in a CPB column, showed some promise when simulating the column test experiment. It was found that matric suctions and volumetric water contents profiles from the column test showed visible trends of decreasing water content and increasing matric suctions. The changes in water content however, were relatively small. This was not surprising, due to the relatively low suctions produced. Matric suctions did not reach beyond 70 kPa, which was well below the post-AEV. The differences in matric suction between layers were also small. The rate of matric suction generation decreased with the addition of a new paste layer, due to the demand of water through paste hydration in the fresh layer, and satisfied by water from the entire column. Both the relatively small difference in matric suctions between layers, and the decrease in matric suction generation with the addition of each layer, was well simulated by the modelling approach, by using the numerical predictions of the previous layer to model subsequent layers. The numerical

predictions for the different layers report matric suction values less than the measured, in-situ PWP's in the column. The only significant differences between the experimental and numerical results were the initial generation of matric suctions. The numerical results appeared to have overestimated this rate, which would suggest that one or more of the following had an effect: (1) the bottom boundary condition overestimated drainage; (2) the sink term overestimated the rate of hydration during the first few days; and/or (3) the saturated hydraulic conductivity used for the underlying layers in the model were too high. On the other hand, the measurements involved in defining the sink term may have produced inaccurate removal rates, because the samples that were retrieved were in the order of a tenth of a gram per day for samples that should have been measured with more accuracy due to the small gram samples that were obtained. The use of a better system for measuring volumetric water content is recommended for future work.

Other issues that were found during this evaluation were the actual SVFlux solver results, themselves. It was observed that alternating between the pre- and post-WRC properties caused some issues regarding the use of the 'final condition' from previous simulation as the 'new initial condition' for succeeding simulation(s). The 'final condition' was generated from the solvers results, using the pre-WRC properties. This was then used the 'new initial condition' in conjunction with the post-WRC properties. Since the post-WRC properties were shown to have increased the water-retention properties, the SVFlux code, instantaneously adds more water to satisfy the new initial condition. This having occurred with these simulations was more or less due to the assumptions surrounding the 1-D unsaturated flow equation (i.e. conservation of mass flow).

Despite these issues mentioned above, the modified 1-D unsaturated flow equation has been demonstrated in a column test simulation to estimate the distribution of PWPs in hydrating CPB material. As suggested by the suctions generated in the multi-layer column experiment, as well as the numerical simulations, it may be in fact, possible that the hydrating paste fill never actually reaches the unsaturated regime (or $-PWP$ region). However, more studies are required to confirm this. The application of the 1-D unsaturated flow model was only tested with Williams paste in a laboratory setting, where properties and flow regime may differ in field conditions. Some suggestions to improve and build upon this study have been discussed in this next chapter, Chapter 8.

CHAPTER 8

8 RECOMMENDATIONS FOR FUTURE WORK

Initially, this work, specifically the column test experiment was conducted with the intention of solving the Richards (1931) equation, experimentally, so that an inverse solution of the unsaturated hydraulic conductivity function could be obtained. This method is formerly known as the instantaneous profile methods (IPM), developed by Watson (1996). The IPM involves capturing the matric suction profile as a function of depth and time [i.e., $\psi(z, t)$], and the moisture profile, also as a function of depth and time [i.e., $\Theta_v(z, t)$]. While the suctions were obtained successfully, the same is cannot be said definitively for the moisture profiles that were obtained. Being able to obtain more accurate moisture profiles, would allow for the unsaturated hydraulic conductivity to be ascertained.

Simon and Grabinsky (2007) have reported problems that arise with customized EC calibrations for CPB material, because the capacitance probe's VWC readings were dependent upon the electrical conductivity of the hydrating material, which varies as cement hydration progresses. The most practical approach in calibrating the EC sensors were adopted, however the results are questionable. One way of addressing this issue, so that more accurate VWCs could be obtained is the use of non-destructive NMR sensors, developed by a research group at the University of New Brunswick (Cano-Barrita et al., 2009). There are numerous applications, in which NMR can be used for, such as

measuring the WRC of various porous media, as well as tracking moisture diffusion, and multi-phase flows. Additionally, NMR techniques could also be applied to situations where uncertainties exist, such as regarding the rate of water removal. In this study, intrusive sampling techniques were used. It is possible that the oven-dried samples obtained for water content measurements were not representative of the actual water content. Meaning that, it was observed that the measured water contents for different days of hydration seemed to have been inaccurately measured due to the small size of the sample(s), and level of accuracy of the digit scale (i.e. +/- 0.05 g).

The numerical estimates that were obtained in this study could be improved by coupling the unsaturated flow framework with a consolidation modeling tool, such as SVSolid (SV Office Suite, 2009). Similar studies by Helinski and co-workers have had great success in obtaining numerical estimates that conferred with their experimental results, by using a large-strain consolidation model.

Further MIP testing is recommended so that the evolution of the micro-pore structure may be analyzed, especially when higher curing temperatures are imposed during early-age curing. It has been reported for conventional cement pastes that the self-desiccation phenomenon will actually increase the fineness (or specific surface area) of the material, compared to paste hydrating at higher curing temperatures. Contrary to this, hydrating CPB material at higher curing temperatures has also been reported to produce a finer pore-structure. With either hypothesis, further studies are recommended for future work to obtain more finite results.

As for Kidd mine tailings, the experimental results along with preliminary field results provide somewhat different observations, compared to Williams paste stream, especially with regards to the PWP behaviour during self-desiccation, as well as the materials' compressibility, as it appeared to be much stiffer / rigid than the post-hydrated Williams. It would be advantageous to conduct further studies using this framework, and coupling the effects of curing temperatures during self-desiccation, specifically by measuring the RH and conducting MIP testing. This framework would be well suited for paste tailings that are comprised with silica sand, because it was observed that the transformation of Kidd's properties occurred very early during paste hydration (i.e. water-retention properties), however this may also be the result of the type of binder used. MIP testing to track porosity and pore structural changes would also provide insight on how slag-based binders combined with silica aggregates, may facilitate the reduction in capillary porosity. The effects of temperature, particularly with Kidd paste should also be considered for future analyses to consolidate other research findings (Abdelaal, 2011) and field measurements (Thompson and co-workers).

REFERENCES

- Abdelaal, A.M.G.M.I. (2011). Early Age Mechanical Behavior and Stiffness Development of Cemented Paste Backfill with Sand. Ph.D. Dissertation, Department of Civil Engineering, Univeristy of Toronto.
- Acker, P. (2004). Swelling, shrinking and creep: a mechanical approach to cement hydration. *Materials and Strucures / Concret Science and Engineering*, Issue 37: 237-243.
- ASTM C1699-09. (2011). ASTM C1699-09 Standard Method For Moisture Retention Curves for Porous Building Materials using Pressure Plates. ASTM Standards Association International, Geotechnical Engineering Standards, West Conshohocken, PA, 2011.
- ASTM D1140-00. (2010). Standard Test Method for Amount of Material in Soils Finer than the No. 200 (75-um) Sieve. ASTM International, West Conshohocken, PA, 2010.
- ASTM D2216-10. (2010). Standard Test Method for Laboratory Determination of Water (moisture) Content of Soil and Rock by Mass. ASTM Standards Association International, Geotechnical Engineering Standards, West Conshohocken, PA, 2010.
- ASTM D421-85. (2007). Standard Practice for Dry Preparation of Soil Samples for Particle-Size Analysis and Determination of Soil Constants. ASTM Standards Association International, Geotechnical Engineering Standards, West Conshohocken, PA, 2007.
- ASTM D422-63. (2007). Standard Test Method for Particle-Size Analysis of Soils. ASTM Standards Association International, Geotechnical Engineering Standards, West Conshohocken, PA, 2010.
- ASTM D4318-10. (2010). Standard Test Methods for Liquid Limit, Plastic Limit and Plasticity Index of Soils. ASTM Standards Association International, Geotechnical Engineering Standards, West Conshohocken, PA, 2010.
- ASTM D4404-10. (2010). ASTM D4404-10 Standard test method for determination of pore volume and pore volume distribution of soil and rock by mercury intrusion porosimetry. ASTM Standards Association International, Geotechnical Engineering Standards, West Conshohocken, PA, 2007.
- ASTM D4943-08. (2008). Standard Test Method for Shrinkage Factors of Soils by the Wax Method. ASTM Standards Association International, Geotechnical Engineering Standards, West Conshohocken, PA, 2008.

- ASTM D6836-02. (2008). Standard Test Methods for Determination of the Soil Water Characteristic Curve for Desorption using Hanging Column, Pressure Extractor, Chilled Mirror Hygrometer, or Centrifuge, In: B-1. ASTM Standards Association International, Geotechnical Engineering Standards, West Conshohocken, PA, 2008.
- ASTM D854-10. (2010). Standard Test Method for Specific Gravity of Soils. ASTM Standards Association International, Geotechnical Engineering Standards, West Conshohocken, PA, 2010.
- ASTM D6913-04. (2009) Standard Test Methods for Particle-Size Distribution (gradation) of Soils using Sieve Analysis. ASTM Standards Association International, Geotechnical Engineering Standards, West Conshohocken, PA, 2009.
- Bachmann, J., and van der Ploeg, R.R. (2002). A review on recent developments in soil water retention theory: interfacial tension and temperature effects. *J. Plant Nutr. Soil Sci.* 165(2002): 468-478.
- Baker, S. J. (1986). Assessment of hydraulic backfilling in metal mines within the the state of Idaho. Idaho Department of Water Resources. State of Idaho, October 1986.
- Bangoyina, P., (2008). Aging and large-consolidation of cemented based grouts. M.A.Sc Thesis. Dept. of Civil Engineering & Management, University of Twente, Enschede, Netherlands.
- Barret, J.R., Coulthard, M.A., and Dight, P.M. (1998). Determination of fill stability, mining with backfill. In *Proceedings of the 12th Canadian Rock Mechanics Symposium*. Special vol. 19, pp. 85-91. Quebec: Canadian Institute of Mining and Metallurgy.
- Barrick Gold Corporation. (2004). Teck Corona Operating Corporation. TeckCominco and Barrick Gold Corp. www.mining.ca.
- Barrsotti, C. (1978). The evolution of fill mining at the Ontario Division of Inco Metals. In *Proceedings of the 12th Canadian Rock Mechanics symposium, Mining with Backfill*. CIM special volume, 19: 37-42..
- Belem, M., Benzaazoua, B., Bussiere, B., and Dagenais, A. M. (2002). Effects of settlement and drainage on strength development within mine paste backfill. In P. b. Balkema, *Tailings and Mine Waste '02* (pp. pp. 139-147). Fort Collins, Colorado, USA: 2002 Swets & Zeitlinger B.V., Lisse, The Netherlands.
- Belem, T., and Benzaazoua, M. (2008). Design and application of underground mine paste backfill technology. *Geotech Geol Engineering*, 26: 147-174.
- Belem, T., Benzaazoua, M., and Bussiere, B. (2000). Mechanical behaviour of cemented paste backfill. In *Proceedings of the Canadian Geotechnical Conference*,

- "Geotechnical Engineering at the dawn of the third millennium," 15-18 October 2000, Montreal, Quebec. Canadian Geotechnical Society, pp. 373-374.
- Belem, T., Bussiere, B., and Benzaazoua, M. (2001). The effect of microstructural evolution on the physical properties of paste backfill. (R.A. A.A. Balkema, Ed.), In Proceedings of Tailing and Mine Waste '01, Fort Collins, Colorado USA, 16-19 January 2001, pp. 365-374.
- Belem, T., Fourie, A., and Fahey, M. (2010). Time-dependent failure criterion for cemented paste backfills. In Proceedings of the 13th International Seminar on Paste and Thickened Tailings, PASTE 2010 - R. Jewell, and A. Fourie (Eds.), 3-6 May 2010, Toronto, ON., Canada. Australian Centre for Geomechanics, Perth, pp. 147-162.
- Belem, T., Harvey, A., Simon, R., and Aubertin, M. (2004). Measurement and prediction of internal stresses in an underground opening during its filling with cemented fill. In Proceedings of the 5th International Symposium on Ground Support in Mining and Underground Construction, Australian Centre of Geomechanics, Perth, pp. 619-630.
- Belem, T., Fourie, A.B., and Fahey, M. (2010). Time-dependent failure criterion for cemented paste backfills. In Proceedings of the 13th International Seminar on Paste and Thickened Tailings, PASTE 2010 - R. Jewell, and A. Fourie (Eds.), 3-6 May 2010, Toronto, ON. Canada. 2010 Australian Centre for Geomechanics, Perth. pp. 147-162
- Benzaazoua, M., and Belem, T. (2000a). Optimization of sulfurous paste backfill mixtures for increasing long-term strength and durability. M. Sanchez (Ed.), Waste treatment and environmental impact in the mining industry, Clean Mine Technology, Vol. 1(2000): 343-352.
- Benzaazoua, M., Belem, T., and Bussiere, B. (2002c). Chemical aspects of sulfurous paste backfill mixtures. Cement and Concrete Research, 32(7): 1133-1144.
- Benzaazoua, M., Bois, D., Belem, T., Gauthier, P., Ouellet, S., Fall, M., and St-Onge, J. (2002b). Chemical factors that influence on the performance of mine sulphidic paste backfill. Cement and Concrete Research, Vol. 3(7): 1113-1114.
- Benzaazoua, M., Fall, M., and Belem, T. (2004). A contribution to understanding the hardening process of cemented pastefill. Minerals Engineering, Vol. 17(2004): 141-152.
- Benzaazoua, M., Marion, O., Picquet, I., and Bussiere, B. (2004a). The use of pastefill as a solidification and stabilization process for the control of acid mine drainage. Minerals Engineering, Vol. 17: 233-243.

- Benzaazoua, M., Ouellet, J., Servant, S., Newman, P., and Verburg, R. (1999). Cementitious backfill with high sulfur content: Physical, chemical and mineralogical characterization. *Cement and Concrete Research*, 29: 719-725.
- Bernier, R.L., Li, M.G., and Moerman, A. (1999). Effects of tailings and binder geochemistry on the physical strength of paste backfill. In *Proceedings of Mining and the Environment II, Sudbury '99*. Edited by N. Goldsack, P. Belzile, Yearwood and G. Hall. Issue 3.
- Bicalho, K.V., Znidarcic, D., and Ko, H-Y. (2003). Influence of air entrapment on the unsaturated hydraulic conductivity functions. (P. E. Culligan, Ed.) In: *12th Panamerican Conf. on Soil Mech. Geotech. Eng.*, vol. 2(2003): 1597-1602.
- Bodi, L., Hunt, G., and Lahnalampi, T. (1996). Development and shear strength parameters of paste backfill. In *Proceedings of the 3rd International Conference on Tailings and Mine Waste '96, Fort Collins, Colorado, 16-19 January*, pp. 169-178.
- Brouwers, H.J.H. (2004). The work of Powers and Brownyard revisited: Part 1. *Cement and Concrete Research*, 34(2004): 1697-1716.
- Brouwers, H.J.H. (2005). The work of Powers and Brownyard revisited: Part 2. *Cement and Concrete Research*, 35(2005): 1922-1936.
- Bulut, R., and Leong, E.C. (2008). Indirect measurement of suction. *Journal of Geotechnical and Geological Engineering*, Vol. 26(6): 633-644.
- Campbell, C.S. (2002). *Calibrating ECH2O soil moisture probes*. Decagon Devices Inc. Pullman WA 99163 USA.
- Cano-Barrita, P.F. de J., Marbel, A.E., Balcom, B.J., Garcia, J.C., Masthikin, I.V., Thomas, M.D.A., Bremnew, T.W. (2009). Embedded NMR sensors to monitor evaporable water loss caused by hydration and drying in Portland cement mortar. *Cement and Concrete Research*, Vol. 39(2009): 324-328.
- Celia, M.A., and Bouloutas, E. (1990). A general mass-conservation numerical solution for the unsaturated flow equation. *Water Resource Research*, July 1990, Vol. 26 (4): 1483-1496.
- Childs, E. (1972). Concepts of soil water phenomena. (J. C. Tedrow, Ed.) *Soil Science*, Vol. 113(4): 246-253.
- Cobos, D.R. (2007). *10HS Volume of sensitivity*. Decagon Devices Inc. Pullman WA 99163 USA.
- Cobos, D.R. (2009). *EC-5 Volume of sensitive*. Decagon Devices Inc. Pullman WA 99163 USA.

- Croney, D., and Coleman, J.D. (1961). Pore pressure and suction in soils. In: Proceedings on Pore Pressure and Suction in Soils, Butterworths, London. pp. 31-37.
- de la Vergne, J. (2003). Hard rock miner's handbook, Edition 3. North Bay, ON., McIntosh Engineering Limited.
- Decagon Devices Inc. (2005). WP4 - DewPoint PotentiaMeter: Operator's Manual Version 2.1. Retrieved 2009, from:
<http://soils.cals.uidaho.edu/soils415/Laboratory/WP4man21.pdf>
- Decagon Devices, Inc. (2008). EC-20, EC-10, EC-5 Soil Moisture Sensors: User Manual, v.8. Pullman WA 99163 USA.
- Decagon Devices, Inc. (2009). 10 HS Soil Moisture Sensor: User Manual, v.3. Pullman WA 99163, USA.
- Delage, P., Marcial, D., Cui, Y.J. and Ruiz, X. (2006). Ageing effects in a compacted bentonite: a microstructure approach. *Geotechnique*, Vol. 56(5): 291-304.
- Delage, P., Romero, E., and Tarantino, A. (2008). Recent developments in the techniques of controlling and measuring suction in unsaturated soils. Key Lecture, In Proceedings of the 1st European Conference on Unsaturated Soils, pp. 33-52.
- Delage, P., Tessier, D., and Marcel-Audiguier, M. (1982). Use of the Cryoscan apparatus for observation of freeze-fractured planes of a sensitive Quebec clay in scanning electron microscopy. *Canadian Geotechnical Journal*, Vol. 19(1): 111-114.
- Deschamps, T., Benzaazoua, M., Bussiere, B., Aubertin, M., and Belem, T. (2008). Microstructural and geochemical evolution of paste tailings in surface disposal conditions. *Minerals Engineering*, Vol. 21 (2008): 341-353.
- Diamond, S. (1970). Pore size distributions in clay. *Clays and Clay Minerals*, Vol. 18: 7-23.
- Ducic, V., Miletic, S. (1987). Sulphate corrosion resistance of blended cement mortars. *Durability Build Mater*, Issue 4: 343-356.
- Ebrahimi, B.N., Gitirana, G.F.N., Jr., Fredlund, D.G., Fredlund, M.D., and Samarasekera, L. (2004). A lower limit for the water permeability coefficient. In: Proc., 57th Canadian Geotechnical Conf., Quebec City, Que., Canada, pp. 12-19.
- Eching, S.O., Hopmans, J.W., Wendroth, O. (1994). Unsaturated hydraulic conductivity from transient multistep outflow. *Soil Science Society American Journal*, 58(1994):687-695.
- Edlefsen, N.E., and Anderson, A.C. (1943). Thermodynamics of soil moisture. *Higardia*, Vol. 15: 31-288.

- Fahey, M., Helinski, M., and Fourie, A. (2009). Some aspects of the mechanics of arching in backfilled stopes. *Canadian Geotechnical Journal*, 46(2009): 1322-1336.
- Fall, M., and Benzaazoua, M. (2003). Advances in predicting performance properties and cost of paste backfill. In: *Proceedings on Tailings and Mine Waste '03*, October 12-15, Vail, USA, Balkema, Rotterdam, pp. 73-85.
- Fall M., Benzaazoua, M. Oullet, S. (2004). Effect of tailings properties on paste backfill performance. In: *8th International Symposium on Mining with Backfill, MINEFILL '04*, 19-21 September, Beijing. Available online: [http://www.enviro-geremi.polymtl.ca/pdf/articles/Falletal.Papier1MineFill2004_\(MB\).pdf](http://www.enviro-geremi.polymtl.ca/pdf/articles/Falletal.Papier1MineFill2004_(MB).pdf)
- Fall, M., and Samb, S.S. (2008). Pore structure of cemented tailings materials under natural or accidental thermal loads. *Material Characterization*, 59 (2008): 598-605.
- Fall, M., and Samb, S.S. (2009). Effect of high temperature on strength and microstructural properties of cemented paste backfill. *Fire Safety Journal*, 44(2009): 647-651.
- Fall, M., Adrien, D., Celestin, J.C., Pokharel, M., Toure, M. (2009). Saturated hydraulic conductivity of cemented paste backfill. *Minerals Engineering*, 22(2009): 1307-1317.
- Fall, M., and Pokharel, M. (2010). Coupling effects of sulphate and temperature on the strength development of cemented tailings backfill: Portland cement-paste backfill. *Cement and Concrete Composites*, 32(2010): 819-828.
- Feldkamp, J.R. (1989). Numerical analysis of one-dimensional nonlinear large-strain consolidation by finite element method. *Transport in Porous Media*, 4 (1989): 239-257.
- Fourie, A.B., Helinski, M., and Fahey, M. (2007). Using effective stress theory to characterize the behaviour of backfill. In: *Proceedings of the 9th International Symposium in Mining with Backfill, MINEFILL 2007*, 29 April - 2 May, 2007, Montreal, Quebec. Canadian Institute of Mining, Metallurgy and Petroleum (CIM). Paper No. 2480 [CD-ROM].
- Fredlund, D.G. (2006). Unsaturated soil mechanics in engineering practice. *Journal of Geotechnical and Geoenvironmental Engineering*, Copy right ASCE (2006), 132(3): 286-318.
- Fredlund, D.G, and Xing, A. (1994). Equations for the soil-water characteristic curve. *Canadian Geotechnical Journal*, 31(3):521-532.
- Fredlund, D.G., Rahardjo, H. (1993). *Soil mechanics for unsaturated soils*. Department of civil engineering, Univeristy of Saskatchewan, and School of civil and structural engineering, Nanyang Technological University, Wiley-Interscience.

- Fredlund, D.G., Sheng, D., Zhao, J. (2011). Estimation of soil suction from the soil-water characteristic curve. *Canadian Geotechnical Journal*. Issue 48: 186-198.
- Fredlund, D.G., Xing, A., and Huang, S. (1994). Predicting the permeability function for unsaturated soils using the soil-water characteristic curve. *Canadian Geotechnical Journal*, Issue 31: 533-546.
- Fredlund, M.D. (1999). Ph.D. Dissertation: The Role of Unsaturated Soil Property Functions in the Practice of unsaturated soil mechanics. University of Saskatchewan, Department of Civil Engineering. Saskatwn, Saskatchewan, Canada.
- Fredlund, M.D., Wilson, G.W., and Fredlund, D.G. (1997). Prediction of the soil-water characteristic curve form grain-size distribution and volume-mass properties. In *Proceedings of the 3rd Brazilian Symposium on Unsaturated Soils*. 1, 22 – 25 April 1997, Rio do Janeiro, Brazil. A.A. Balkema, Rotterdam. pp. 202-207.
- Gardner, W. (1956). Mathematics of isothermal water conduction in unsaturated soils. Highway Research Board Special Report 40, International symposium on physicochemical phenomenon in soils, pp. 78-87.
- GCTS. (2009). SWC-150 Fredlund SWCC Device. Retrieved 2009, from GCTS.com: <http://www.gcts.com/pdf/SWC-150.pdf>
- Godbout, J., Bussiere, B., Aubertin, M., and Belem, T. (2007). Evolution of cemented paste backfill saturated hydraulic conductivity at early curing time. *Canadian Geotechnical Conference (2006)*, pp. 2230-2236.
- Grabinsky, M. (2007). NSERC CRD Proposal - 103546. University of Toronto, Dept. Mining Engineering, Toronto.
- Grabinsky, M. (2010). In situ monitoring for underground truthing paste backfill design. In *Proceedings of the 13th Internation Seminar on Paste and Thickened Tailings, PASTE 2010 - R. Jewell, and A. Fourie (Eds.)*, 3-6 May 2010, Toronto, ON. Canada. 2010 Australian Centre for Geomechanics, Perth. pp. 85-98.
- Grabinsky, M., and Simms, P. (2006). Self-desiccation of cemented paste backfill and implications for mine design. In *Sym. of the International Thickened Tailings and Paste, PASTE 2006*, (S. L. R.J. Jewell, Ed.) Limerick, Ireland: Australian Centre for Geomechanics, Perth.
- Grabinsky, M., Bawden, W., Simon, D., and Thompson, B. (2008). In situ properties of cemented paste backfill in an Alimak stope. In *Proceedings of the Canadaian Geotechnical Conference, Edmonton 2008*.
- Grabinsky, M.W., and Bawden, W.F. (2007). In situ measurements of geotechnical design of cemented paste backfill systems. In *Proceedings of Minefill 2007*, 29 April - 2 May, 2007. Paper No. 2456 [CD-ROM].

- Grabinsky, M.W. (2010). In-situ monitoring for ground truthing paste backfill design. In Proceedings of the 13th International Seminar on Paste and Thickened Tailings, PASTE 2010 3-6 May 2010, Toronto ON. PASTE 2010, pp. 85-98
- Grice, T. (1998). Underground mining with backfill. The 2nd Annual Summit - Mine Tailings Disposal Systems, Brisbane., 24-25 November 1998, pp. 1-14.
- Halamickova, P., and Detwiler, R.J. (1995). Water permeability and chloride ion diffusion in Portland cement mortars: Relationship to sand content and critical pore diameter. *Cement and Concrete Research*, 25(4): 790-802.
- Hartman, H. L. (1992). *SME Mining Engineering Handbook*. Society for Mining, Metallurgy, and Exploration, Inc., Vol. 2.
- Harvey, E.N., Barnes, D.K., McElory, W.D., Whiteley, A.H., Pease, D.C., and Cooper, K.W K. (1944). Bubble formations in animal, 1-physical factor. *Journal of Cell Composition and Physiology*, Vol. 24(1): 1-22.
- Hassani, F., and Archibald, J. (1998). *Mine Backfill*, Canadian Institute of Mine, Metallurgy and Petroleum. [CD-ROM]
- Helinski, M., Fahey, M., and Fourie, A. (2007b). Numerical modelling of cemented paste backfill deposition. *Journal of Geotechnical and Geoenvironmental Engineering*, Issue 10: 1308-1319.
- Helinski, M., Fahey, M., and Fourie, A. (2011). Behavior of cemented paste backfill in two mine stopes: measurements and modelling. *Journal of Geotechnical and Geoenvironmental Engineering*, Vol. 137(2): 171-182.
- Helinski, M., Fahey, M., and Fourie, A.B. (2007c). An effective stress approach to modelling mine backfill. In: Proceedings of the 9th International Symposium on Mining with Backfill, 2007 MINEFILL, 29 April - 2 May, 2007, Montreal, QUE. Canada. Paper 29.
- Helinski, M., Fourie, A., Fahey, M., and Ismail, M. (2007a). Assessment of the self-desiccation process in cemented mine backfill. *Canadian Geotechnical Journal*, Vol. 44(2007):1148-1156.
- Helinski, M., Fourie, A.B., and Fahey, M. (2006). Mechanics of early age cemented paste backfill. In S. L. R.J. Jewell (Ed.), *Paste 2006*. Limerick, Ireland: Australian Centre for Geomechanics, Perth. pp. 313-322.
- Hua, C., Acker, P., and Ehlacher, A. (1995). Analyses and models of the autogenous shrinkage of hardening cement paste. *Cement and Concrete Research*, 25(7), 1457-1468.

- Hustrulid, W. A., and Holmberg, R. (1991). Drilling and Blasting, Chapter 5 in the book *Underground Structures Design and Construction*. Elsevier.
- Jayasinghe, P. (2010). Temperature effects on pore water pressure on hydrating cemented paste backfill. EVE 4907 Research Project, Department of Civil and Environmental Engineering, Carleton University.
- Jung, S.J., and Biswas, K. (2002). Review of current high density paste fill and its technology. *Mineral Resource Engineering*, 11(2): 165-182.
- Kesimal, A., Yilmaz, E., Ercikdi, B. (2004). Evaluation of paste backfill mixtures consistin gof sulphide-rich mill tailings and varying cement contents. *Cement and Concrete Research*, 34(2004): 1817-1822.
- Kesimal, A., Yilmaz, E., Ercikdi, B., Alp, I., Deveci, H. (2005). Effect of properties of tailings and binder on the short- and long-term strength and stability of cemented paste backfill. *Materials Letters*, 59(2005): 3703-3709.
- Kim, J.-K., and Lee, C.-S. (1999). Moisture diffusion of concrete considering self-desiccation at early ages. *Cement and Concrete Research*, Issue 29: 1921-1927.
- Krahn, J. and Fredlund, D.G. (1972). On total, matric and osmotic suction. *Soil Science*, 115(5): 339-348.
- Landriault, D. A., and Lidkea, W. (1993). Paste fill and high density slurry fill. In *Proceedings of the International Congress on Mine Design*. Queens University, Kingston, Ontario, Canada, August 1993.
- le Roux, K. (2004). In situ properties and liquefaction potential of cemented paste backfill. PhD thesis, Graduate department of civil engineering, University of Toronto, Canada.
- le Roux, K., Bawden, W.F., and Grabinsky, M.F. (2002a). Comparison of the material properties of in-situ and laboratory prepared cemented paste backfill. Available online: <http://www.civil.engineering.utoronto.ca/assets/civil+engineering+digital+assets/out+put/assets/2002agm.pdf>
- le Roux, K., Bawden, W.F., and Grabinsky, M.F. (2005). Field properties of cemented paste backfill at the Golden Giant mine. *Mining Technology: Trans. of the Institute of Mining and Metallurgy*, Section A, Vol. 114(2):65-80.
- le Roux, K.A., Bawden, W.F., Grabinsky, M.W.F. (2002b). Assessing the interaction between hydration rate and fill rate for a cemented paste backfill. In: *Proceedings of the 55th Canadian Geotechnical and 3rd Joint IAH-CNC Groundwater sepcialty Conferences*. Niagra Falls, Ontario, 20-23 October 2002, pp. 427-432.

- Lee, K.S. (2007). Effects of hysteresis in k-S-P relationships on the performance of mine-waste soil covers. *Geosciences Journal*, Vol. 11(3): 241-247.
- Lei, H.C., Chang, H.W., and Hung, M.J. (1996). Gibson's equation of soil consolidation in convective coordinate and a method for obtaining solutions. In: *Proceedings of the 6th International Offshore and Polar Engineering Conference*, 26 – 31 May, 1996, Los Angeles, USA, pp. 408.
- Leij, F.J., Russell, W.B. and Lesch, S.M. (1996). Closed-form expression for water retention and conductivity data. U.S. Salinity Laboratory, U.S. Dept. of Agri., Agri. Research Services, California. Accessed on August 12, 2009. Retrieved from: www.envsci.rutgers.edu/~gimenez/SoilPhysics/Homework09/Close%20Form%20Equations%20WR%20and%20K.pdf
- Leong, E.C., He, L., and Rahardjo, H. (2002). Factors affecting the filter paper method for total and matric suction measurements. *Geotechnical Testing Journal*, 25(3): 321-332.
- Leong, E.C., Tripathy, S., and Rahardjo, R. (2003). Total suction measurement of unsaturated soils with a device using the chilled-mirror dew-point technique. *Geotechnique*, 53(2):173-182.
- Li, T., Singh, U., Coxon, J., Grice, T.G., and Sainsbury, D. (2002). Development and application of paste fill using drying tailings. *First International Seminar on Deep and High Stress Mining*, Perth, pp. 1-10.
- Marinho, F.A.M, and Chandler, R.J. (1994). Discussion: A new instrument for the measurement of soil moisture suction. *Geotechnique*, Vol. 44(3):551-556.
- Marinho, F.A.M., and Chandler, R.J. (1995). Cavitation and the direct measurement of soil suction. (E. A. (eds.), Ed.) In *Unsaturated Soils Proceeding of the 1st International Conference of Unsaturated Soils*, Paris, Vol. 2: 623-630.
- Marinho, F.A.M., Take, W.A., Tarantino, A. (2008). Measurement of matric suction using tensiometric and axis translation techniques. *Geotechnical and Geological Engineering*, Vol. 26: 615-631.
- Mitchell, R.J. (1989a). Stability of cemented tailings backfill. *Computer and physical modelling in geotechnical engineering*. Balkema, Rotterdam, pp. 501-507.
- Mitchell, R.J. (1989b). Model studies on the stability of confined fills. *Canadian Geotechnical Journal*, Issue 26: 210-216.
- Mitchell, R.J., and Wong, B.C. (1982). Behaviour of cemented tailings sands. *Can. Geotech. J.*, Vol. 19 (1982): 289-295.

- Mongioli, L., and Tarantio, A. (2002). Pore water pressure measurement in unsaturated soils. In Proceedings of International Workshop on "Clay behaviour: Chemo-mechanical coupling", pp. 233-246.
- Mualem, Y. (1976). New model for predicting the hydraulic conductivity of unsaturated porous medium. *Water Resources Research*, Vol. 12: 593-622.
- Mualem, Y. (1978). Hydraulic conductivity of unsaturated porous media: Generalized macroscopic approach. *Water Resources Research*, Vol. 14: 324-334.
- Mualem, Y. (1986). Hydraulic conductivity of unsaturated soils: prediction and formulas. A. K. (Ed.) In: *Methods of Soil Science Analysis, Part 1. Physical and Mineralogical Methods* (2nd Edition), Mualem, pp. 799-823.
- Mualem, Y., and Dagan, G. (1978). Hydraulic conductivity of soils: Unified approach to the statistical models. *Soil Science Society American Journals*, Vol. 42: 392-395.
- Murray, J. W. (2001). Stopes requiring some additional support other than pillars - Undercut-and-fill mining. In B. Richard L. (Ed.), *Underground mining methods handbook SME*. pp. 631-665.
- Nantel, J. (1998). Recent developments and trends in backfill practices in Canada. In Proceedings of the 6th International Symposium on Mining with Backfill, Minefill '98 AIMM, Brisbane. pp. 11-14.
- Narasimhan, T.N. (2005). Central ideas of Buckingham, 1907: A century later. *Vadose Zone Journal*, 4: 434-441.
- Natural Resources Canada. (2011). Important Facts on Canada's Natural Resources (as of October 2011). Accessed on January 22, 2012. Retrieved from: [www.nrcan.gc.ca:http://www.nrcan.gc.ca/sites/www.nrcan.gc.ca/files/files/stat/2012/important-2012-eng.pdf](http://www.nrcan.gc.ca/sites/www.nrcan.gc.ca/files/files/stat/2012/important-2012-eng.pdf)
- Olson, R.E., and Langfelder, L.J. (1965). Pore-water pressures in unsaturated soils. *J. Soil Mech. Found. Div., Proc. Amer. Soc. Civil Eng.*, Vol. 91(4): 127-160.
- Omron (2010). Ultrasonic proximity sensor E4B. Accessed in October 2008. Retrieved from: [www.ia.omron.com:http://www.ia.omron.com/data_pdf/data_sheet/e4b_ds_cs_m1564.pdf](http://www.ia.omron.com/data_pdf/data_sheet/e4b_ds_cs_m1564.pdf)
- Ouellet, S., Bussiere, B.m Mbonimpa, M., Benzaazoua, M., and Aubertin, M. (2006). Reactivity and mineralogical evolution of an underground mine sulphidic cemented paste backfill. *Minerals Engineering*, Vol. 19: 407-419.
- Pan, H., Qing, Y., Pei-yong, L. (2010). Direct and indirect measurement of soil suction in the laboratory. *Electronic Journal of Geotechnical Engineering (EJGE)*, Vol. 15 [2010], Ppr. 10.009.

- Persson, B. (2005). On the temperature effect on self-desiccation of concrete. B.Persson, D.Bentz, and L-O.Nilsson (Eds). Self-desiccation and its importance in concrete technology, Division Building Materials, Lund Institute of Technology, Lund, Sweden. Proceedings of the 4th International Research Seminar, Gaithersburg, Maryland, USA, June 2005, pp. 101 – 124.
- Priestley, D., Fredlund, M, and van Zyl, D. (2011). Modelling consolidation of tailings impoundment in one and two dimension. Tailings and Mine Waste 2011, 6 – 9 November, 20122, Vancouver Canada. Accessed in May 2013, available online: <http://www.infomine.com/library/publications/docs/Priestley2011b.pdf>
- Putzmeister Solid Pumps. (2010). Putzmeister Solid Pumps. Accessed on January 5, 2010. Retrieved from: http://www.pmw.de/cps/rde/xchg/SID-4EBFEBD7-20E11833/pm_online/hs.xsl/9046_ENU_HTML.htm
- Ran, J. (2007). Learning from underground failures - Underground mining case studies. (S. & Eberhardt, Ed.) Rock mechanics: meeting society's challenges and demands Proceedings of the 1st Canada-US Rock Mechanics Symposium, 1(2): 1353-1360.
- Richards, B. (1965). Measurement of the Free Energy of Soil Moisture by the Psychrometric Technique Using Thermistors. In Moisture Equilibria and Moisture changes in Soils beneath Covered areas, A Symp. InPrint: Buttersworth, & Company Ltd, London /UK, pp. 39-46.
- Richards, L. (1931, November 1931). Capillary conduction of liquids through porous mediums. Journal of Applied Physics, Vol.1(1931):318-333.
- Richards, L.A. (1947). Pressure-membrane apparatus - construction and use. Agricultural Engineering, Issue 28: 451-460.
- Ridley, A.M., and Burland, J.B. (1995). Measurement of suction in materials which swell. Applied Mechanics Review, 48(9): 727-732.
- Safe Drinking Water Foundation (SDWF). (2004). Fact sheet: Mining and Water Pollution. Retrieved March 5, 2011, Available online: [www.safewater.org: http://www.safewater.org/PDFS/resourcesknowthefacts/Mining+and+Water+Pollution.pdf](http://www.safewater.org/PDFS/resourcesknowthefacts/Mining+and+Water+Pollution.pdf)
- Sillers, S.W., and Fredlund, D.G. (2001). Statistical assessment of soil-water characteristic curve models for geotechnical engineering. Canadian Geotechnical Journal, 38(2001): 1297-1313.
- Simms, P.H. (2003). A fundamental study of unsaturated flow in compacted clayey soil. Ph.D. Dissertation, Faculty of Graduate studies, University of Western Ontario, London, Ontario, Canada. Page 86 – 87.

- Simms, P., and Grabinsky, M. (2009). Direct measurement of matric suction in triaxial tests on early-age cemented paste backfill. *Can. Geotech. J.*, 46(2009): 93-101.
- Simms, P.H., and Yanful, E.K. (2002). Predicting soil-water characteristic curves of compacted plastic soils from measured pore-size distributions. *Geotechnique*, 52(4):269-278.
- Simms, P.H., and Yanful, E.K. (2004). Estimation of the soil-water characteristic curve of a clayey till using measured pore-size distributions. *ASCE Journal of Environmental Engineering*, 130(8): 847-854.
- Simon, D., and Grabinsky, M.W. (2007). Volumetric water content measurements in cemented paste backfill. In: *Proceedings of The Joint 60th Canadian Geotechnical and 8th IAH-CNC Conferences, October 21 - 24, Ottawa, ON, Canada*. pp. 2222-2230
- Simon, D. (2010). Personal communication, via email.
- Sivankugan, N., Rankine, R. M., Rankine, K. J., and Rankine, K. S. (2004). Geotechnical considerations in mine backfilling in Australia. *Journal of Cleaner Production*, 14 (2006): 1168-1175.
- SoilMoisture Equipment Corporation. (2008). SoilMoisture product details. Retrieved 11 19, 2009. Available online: http://www.soilmoisture.com/prod_details.asp?prod_id=421&cat_id=1
- Stothart, P., Vice-President, Economic Affairs, Mining Association of Canada. (2011). *The Mining Association of Canada: FACTS & FIGURES of the Canadian Mining Industry*. Accessed on January 22, 2013. Retrieved from: www.miningnorth.com: <http://www.miningnorth.com/wp-content/uploads/2012/04/MAC-FactsFigures-2011-English-small.pdf>
- Stone, D.M.R. (1993). The optimization of mix designs for cemented rockfill. In: *Proceedings of the 5th International Symposium on Mining with Backfill, MINEFILL '93, Johannesburg, SA IMM*, pp. 249-253.
- Straskraba, V., and Abel, J. F Jr. (1994). The differences in underground mines dewatering with the application of caving or backfilling mining methods. *Mine Water and Environment*, 13(2), 20-39.
- Take, W.A., and Bolton, M.D. (2003). Tensiometer saturation and the reliable measurement of matric suction. *Geotechnique*, Vol. 53(2): 159-172.
- Take, W.A., and Bolton, M.D. (2004). Discussion: Tensiometer saturation and the reliable measurement of matric suction. *Geotechnique*, Vol. 54(3): 229-232.

- Tarantino, A., and Mongiovi, L. (2001). Experimental procedures and cavitation mechanisms in tensiometer measurements. *Geotechnical Geological Engineering*, Vol. 19(3-4): 189-210.
- The Mining Industry's Weekly Newspaper. (2010). Online Mining Journal: Mining 101, Accessed in January 2010, Retrieved from: <http://www.mining-journal.com/knowledge/Mining-101>.
- Thode, R. (2008). SVFlux Tutorial Manual. (M. Fredlund, Ed.) Saskatoon, Saskatchewan, Canada: SoilVision Systems Ltd.
- Thompson, B.D., Grabinsky, M.W., and Bawden, W.F. (2008). Geomechanical design of cemented paste backfill systems – Progress Report #1 on: Fieldwork results from Kidd Mine and Williams in 2007. Dept. of Civil Engineering, University of Toronto. University of Toronto.
- Thompson, B.D., Grabinsky, M.W., and Bawden, W.F. (2009). Geomechanical design of cemented paste backfill systems – Progress Report #2 on: Fieldwork results from Xstrata Copper Kidd Mine in 2008. Dept. of Civil Engineering, University of Toronto.
- Thompson, B.D., Grabinsky, M.W., Bawden, W.F., and Counter, D.B. (2009). In-situ measurements of cemented paste backfill in long-hole stopes. M. Grassell (Ed.), In: *Proceeding of the 3rd CANUS Rock Mechanics Symposium*, Toronto, May 2009 (ROCKENG09). Paper 4061, pp. 1-10.
- Thompson, B.D., Grabinsky, M.W., and Bawden, W.F. (2010). Monitoring cemented paste backfill barricade performance. In *Proceedings of the 13th International Seminar on Paste and Thickened Tailings, PASTE 2010 3-6 May 2010*, Toronto ON. PASTE 2010 Conference Presentation.
- Thompson, B.D., Grabinsky, M.W., Veenstra, R., and Bawden, W.F. (2011). In situ pressures in cemented paste backfill – a review of field work from 3 different mines. A. Fourie and R.Jewell (Eds.), In: *Proceedings of the 14th International Seminar on Paste & Thickened Tailings*, 5-7 April 2011, Perth Australia, pp. 491-503.
- Uchaipichat, A. (2011). An elasto-plastic deformation model for cemented soils including thermal effect on mechanical behaviour. *Australian Journal of Basic and Applied Science*, Vol. 5(6): 1193-1198
- UMS GmbH Munchen. (2009). User Manual: T5/T5x Pressure transducer tensiometer.
- van Genuchten, M. (1980). A closed-form equation for predicting the hydraulic conductivity of unsaturated soils. *Soil Science Society of America Journal*, 44(1980): 892-898.

- Vanapalli, S.K, Nicotera, M.V, Sharma, R.S. (2008). Axis translation and negative water column techniques for suction control. *Journal of Geotechnical and Geological Engineering*, Vol. 26(6):645-660.
- Vatsala, A., Nova, R., and Srinivasa Murthy, B.R. (2001). Elastoplastic model for cemented soils. *Journal of Geotechnical and Geoenvironmental Engineering*, August 2001, Vol. 127(8): 679-687.
- Veenstra, R. (2010). E-mail correspondence, May 5 2010.
- Verburg, R.B.M. (2001). Use of paste technology for tailings disposal: potential environmental benefits and requirements for geochemical characterization. In: *Proceedings of the International Mine Water Association Symposium Belo Horizonte, Brazil 2001 (IMWA 2001)*, pp. 1 -13.
- Viles, R.F., and Davis, R.T.H. (1989). New material technologies applied in mining with backfill. In: *Innovation in Mining Backfill Technology*, pp. 95-101.
- Wagner, L.E and Ding, D. (1994). Representing aggregate size distributions as modified lognormal distributions. *American Society of Agricultural Engineers*, 37(3):815-821.
- Watson, K. (1966). An instantaneous profile method for determining the hydraulic conductivity of unsaturated porous materials. *Water Resources Research*, 4th Quarter 1966, Vol. 2(3): 709-715.
- Yilmaz, E., Belem, T., Bussiere, B., and Benzaazoua, M. (2008). Consolidation characteristics of early age cemented paste backfill. In *Proceedings of the Annual Canadian Geotechnical Conference, Edmonton Alberta, NRC 2008*, pp.797-804.
- Yilmaz, E., Kesimal, A., and Ericikdi, B. (2003). Strength properties in varying doseages for paste backfill samples. In *Proceedings of the 10th International Conference on tailings and Mine Waste, Balkema, Swets and Zeitlinger, Lisse 12-15 October, Colorado, USA, 2003*, pp. 109-114.
- Yumlu, M., and Guresci, M. (2007a). Paste backfill bulkhead monitoring - A case study from Inmet Caylei Mine, Turkey. In *Proceedings of the 9th International Symposium on Mining with Backfill. Montreal, Quebec, April 2007*.
- Zhang, X.W., Lui, X., Gu, D.X., Zhou, W., Wang, R.L., and Lui, P. (1996). Desorption isotherms of some vegetable. *Journal of the Science of Food and Agriculture*, Issue 70: 303-306.
- Zheng, Q., Durben, D.J., Wolf, G.H., and Angell, C.A. (1991). Liquids at large negative pressures: water at the homogeneous nucleation limit. *Science*, Vo. 254(5033): 829-832.

APPENDICES

APPENDIX A – WILLIAMS AND KIDD TAILINGS [RAW DATA]

A.1 SAMPLE PREPARATIONS AND INITIAL WATER CONTENTS

Table A.1.1 Williams' 3 and 7% Binder specimens prepared for EC calibrations; Test #1 (March 15, 2010)

Specimen	Initial GWC	m_{bowl}	$m_{\text{bowl} + \text{paste}}$	m_{paste}	m_{binder}	m_{FA}	m_{PC}
	%	<i>(RE ± 0.05 g)</i>					
Williams 3%	39.8	277.5	3527.2	3249.7	69.7	34.9	34.9
Williams 7%	39.8	277.5	3621.8	3344.3	167.5	83.7	83.7

Table A.1.2 Confirmatory sample preparations (Initial GWC): Williams' 3 and 7% Binder specimens EC calibrations; Test #1 (March 15, 2010)

Specimen	No.	m_{cup}	$m_{\text{cup} + \text{paste}}$	$m_{\text{oven dried}}$	m_{water}	m_{solids}	GWC
		<i>(RE ± 0.05 g)</i>					
3% binder	1	2.1	49.8	39.8	10	27.7	36.1
	2	2.1	71.5	56.9	14.6	40.2	36.3
	3	2.1	64.2	51.1	13.1	35.9	36.5
					Average GWC = 36.3%		
Specimen	No.	m_{cup}	$m_{\text{cup} + \text{paste}}$	$m_{\text{oven dried}}$	m_{water}	m_{solids}	GWC
		<i>(RE ± 0.05 g)</i>					
7% binder	1	2.1	51.9	41.7	10.2	29.4	34.7
	2	2.1	44.6	35.9	8.7	25.1	34.7
	3	2.1	33.9	27.4	6.5	18.8	34.6
					Average GWC = 34.6%		

Table A.1.3 Williams' 3 and 7% Binder specimens prepared for EC calibrations; Test #2 (April 16, 2010)

Specimen	Initial GWC	m_{bowl}	$m_{bowl+paste}$	m_{paste}	m_{binder}	m_{FA}	m_{PC}
	%	$(RE \pm 0.05 g)$					
Williams 3%	39.9	277.5	3486.5	3209.0	68.8	34.4	34.4
Williams 7% (batch 1)	39.9	277.5	3273.6	2996.1	149.9	74.9	74.9
Williams 7% (batch 2)	39.9	100.4	3526.5	3426.1	171.4	85.7	85.7

Table A.1.4 Confirmatory sample preparations (Initial GWC) Williams' 3 and 7% Binder specimens prepared for EC calibrations; Test #2 (April 16, 2010)

Specimen	No.	m_{cup}	$m_{cup+paste}$	$m_{oven\ dried}$	m_{water}	m_{solids}	GWC
		$(RE \pm 0.05 g)$					
3% binder	1	2.1	49.8	39.7	10.1	27.5	36.7
	2	2.1	52.1	41.5	10.6	28.8	36.8
	3	2.1	56.2	44.7	11.5	31.1	37.0
Average GWC = 36.8%							
Specimen	No.	m_{cup}	$m_{cup+paste}$	$m_{oven\ dried}$	m_{water}	m_{solids}	GWC
		$(RE \pm 0.05 g)$					
7% binder	1	2.1	56.1	44.9	11.2	31.6	35.4
	2	2.1	48.2	38.6	9.6	26.9	35.7
	3	2.1	42.6	34.0	8.6	23.3	36.9
Average GWC = 36.9%							

Table A.1.7 Confirmatory sample prior to Axis translation test on Kidd tailings, no binder (February 10, 2010)

N	m_C	m_{C+P}	m_{OD}	m_W	m_{Solids}	gWC (%)
1	2.1	73.3	58.3	15.0	56.2	26.7
2	2.1	61.4	49.2	12.2	47.1	25.9
3	2.1	91.3	72.8	18.5	70.7	26.2
4	2.1	66.0	53.2	12.8	51.1	25.0
Ave. Gravimetric Water Content (%)			26.0			

Table A.1.5 Trial #1 – Initial conditions (June 4, 2009) of the Axis translation test using Williams 3% binder specimen

Mass (RE +/- 0.05 g)					
$M_{disk, wet}$	$M_{cell, empty}$	$M_{cell + paste}$	M_{paste}	M_{water}	M_{solids}
174.074	5294.4	5727.60	433.20	119.36	313.84
Actual binder to water content - 3% binder specimen					
% Solids (by wt.)			72.45	2.16	1
% Water (by wt.)			27.55	28.15	13
Gravimetric Water Content, %				38.03	

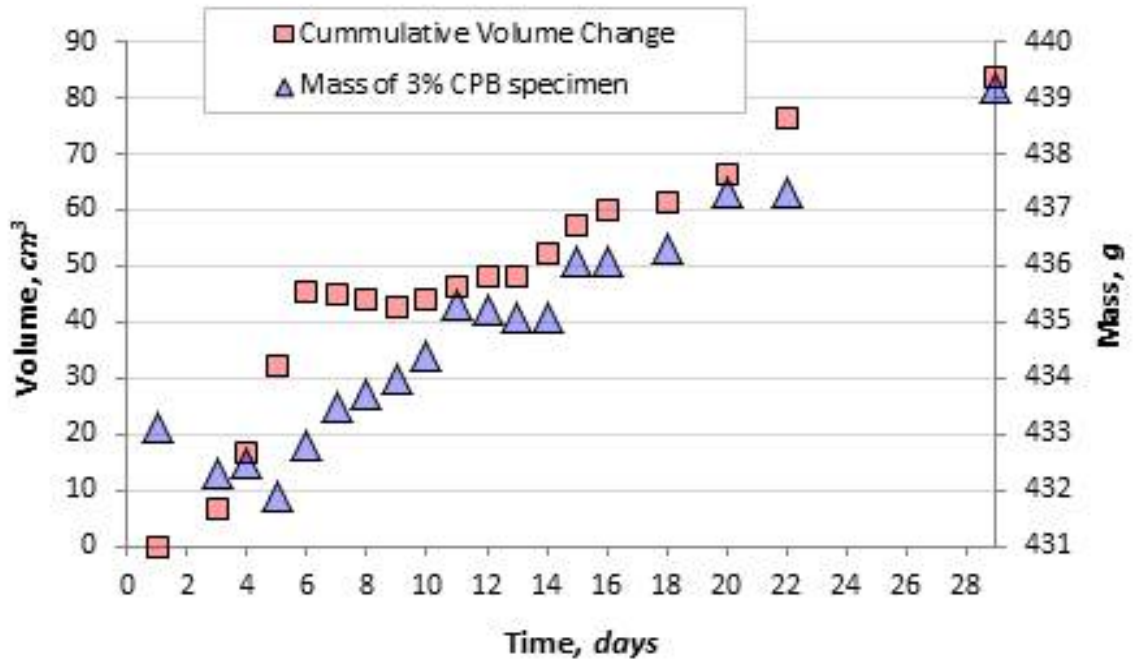


Figure A.1.1 Trial #1 – Change in mass and volume during curing period of 28 days; Williams 3% specimen, cured in pressure plate extractor, where sample swelled due to available water below the porous discs. Uptake of water is due to suction development (balance out pressures).

Table A.1.6 Trial #2 – Initial conditions (November 23, 2009) of the Axis translation test using Williams 3% binder specimen

<i>*Initial Gravimetric Water Content on Day 1 of Post-curing</i>					
<i>**Date: Monday, November 23, 2009 (Day 28)</i>					
<i>Mass (RE +/- 0.005 g)</i>					
<i>M_{crucible}</i>	<i>M_{crucible + CP}</i>	<i>M_{CP}</i>	<i>M_{oven dried}</i>	<i>M_{water}</i>	<i>M_{solids}</i>
56.89	72.75	15.86	68.51	4.24	11.62
<i>gWC (%)</i>		<i>36.49</i>			
<i>Confirmation sample</i>					
<i>Mass (RE +/- 0.005 g)</i>					<i>gWC</i>
<i>M_{cell, empty}</i>	<i>M_{cell + CP}</i>	<i>M_{CP}</i>	<i>M_{water}</i>	<i>M_{solids}</i>	<i>%</i>
5299.8	5599.30	299.50	80.07	219.43	36.49

A.2 PHYSICAL PROPERTIES OF TAILINGS

Table A.2.1 Specific gravity data (Williams tailings)

Test No.	1	2	3	4
$V_{Flask} (mL)$	500	500	500	500
$m_{Flask} + m_w + m_w = m_{BWS}$	707.7	702.3	689.6	685.7
m_{Flask}	187.5	176.9	170.2	129.4
$T (^{\circ}C)$	25	25	25	25
$m_{Flask} + m_w = m_{BW}$	684.9	674.4	667.9	662.8
Flask No.	1	2	3	4
$m_{Flask} + m_s$	223.4	221.0	204.5	165.4
m_s	35.9	44.1	34.3	36.0
$m_w = m_s + m_{BW} - m_{BWS}$	13.1	16.2	12.6	13.1
$\alpha = \rho_{T^{\circ}C} / \rho_{20^{\circ}C}$	1.00043	1.00043	1.00043	1.00043
$G_s = \alpha m_s / m_w$	2.742	2.723	2.723	2.749
Average $G_s \pm 0.005 \text{ g/cm}^3$	2.734			

Table A.2.2 Specific gravity data (Kidd tailings)

Test No.	1	2	3	4
$V_{Flask} (mL)$	500	500	500	500
$m_{Flask} + m_w + m_w = m_{BWS}$	707.7	702.3	689.6	685.7
m_{Flask}	170.3	187.4	129.6	176.8
$T (^{\circ}C)$	25	25	25	25
$m_{Flask} + m_w = m_{BW}$	673.6	680.7	641.4	657.2
Flask No.	1	2	3	4
$m_{Flask} + m_s$	223.1	221.0	204.5	221.2
m_s	52.8	33.6	74.9	44.4
$m_w = m_s + m_{BW} - m_{BWS}$	18.7	12	26.7	15.9
$\alpha = \rho_{T^{\circ}C} / \rho_{20^{\circ}C}$	1.00043	1.00043	1.00043	1.00043
$G_s = \alpha m_s / m_w$	2.825	2.801	2.806	2.794
Average $G_s \pm 0.005 \text{ g/cm}^3$	2.807			

Table A.2.3 Specific gravity data (Kidd - alluvial sand)

Test No.	1	2	3	4
$V_{Flask} (mL)$	500	500	500	500
$m_{Flask} + m_w + m_w = m_{BWS}$	707.7	702.3	689.6	685.7
m_{Flask}	170.4	187.4	129.5	176.7
$T (^{\circ}C)$	25	25	25	25
$m_{Flask} + m_w = m_{BW}$	673.8	680.9	641.6	657.5
Flask No.	1	2	3	4
$m_{Flask} + m_s$	224.1	221.3	205.6	221.6
m_s	53.7	33.9	76.1	44.9
$m_w = m_s + m_{BW} - m_{BWS}$	19.8	12.5	28.1	16.7
$\alpha = \rho_{T^{\circ}C} / \rho_{20^{\circ}C}$	1.00043	1.00043	1.00043	1.00043
$G_s = \alpha m_s / m_w$	2.713	2.713	2.709	2.690
Average $G_s \pm 0.005 g/cm^3$	2.706			

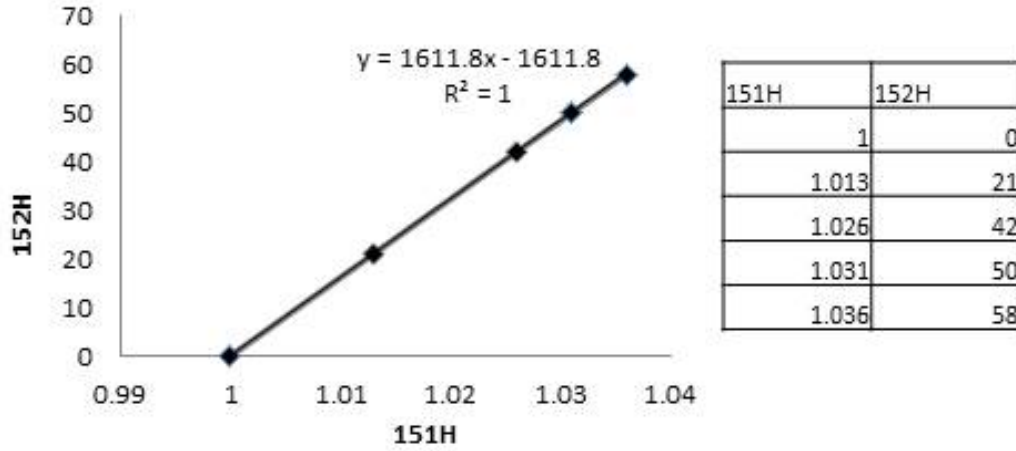


Figure A.2.1 Calibration curve (Hydrometer 151H vs. 152H)

Table A.2.4 Williams PSD for particles smaller than 75 μm

Date	Time of reading	Elapsed time, min	Temp ('C)	Ct	Actual hyd. Reading , Ra (151H)	Actual hyd. Reading , Ra (152H)	Corr.Hyd. Reading , Rc	Act % finer	Hyd. Corr. Only for meniscus, R	L from Table*	L/t	K from Table	D, mm
12-Aug	10:30	0						100.00					0.748
12-Aug								100.00					0.579
12-Aug								100.00					0.375
12-Aug								100.00					0.149
12-Aug		2	23	0.7	1.028	44.3	39.4	78.14	1.028	8.96	4.48000	0.01284	0.027
12-Aug		4	23	0.7	1.024	38.7	33.7	66.94	1.024	9.91	2.47750	0.01284	0.020
12-Aug		8	23	0.7	1.020	31.4	26.5	52.55	1.020	11	1.37500	0.01284	0.015
12-Aug		16	23	0.7	1.016	25.0	20.0	39.76	1.016	12.1	0.75625	0.01284	0.011
12-Aug		30	23	0.7	1.013	21.6	16.7	33.05	1.014	11.5	0.38333	0.01284	0.008
12-Aug	11:30	60	23	0.7	1.013	20.1	15.2	30.17	1.013	12.1	0.20167	0.01284	0.006
12-Aug	12:30	120	23	0.7	1.009	14.5	9.6	18.98	1.009	13.1	0.10917	0.01298	0.004
12-Aug	14:30	240	25	1.3	1.008	12.6	8.2	16.33	1.008	13.7	0.05708	0.01298	0.003
12-Aug	18:40	490	26	1.65	1.007	10.5	6.5	12.87	1.007	14.2	0.02898	0.01298	0.002
13-Aug	7:32	1262	24	1	1.006	9.8	5.2	10.30	1.006	14.4	0.01141	0.01284	0.001
13-Aug	14:35	1685	25	1.3	1.006	9.3	5.0	9.93	1.006	14.7	0.00872	0.01284	0.001
14-Aug	14:40	3130	25	1.3	1.005	8.4	4.0	8.02	1.006	14.7	0.00470	0.01284	0.001
16-Aug	15:45	4635	29	3.05	1.004	6.8	4.2	8.29	1.005	14.7	0.00317	0.01238	0.001

Table A.2.5 Kidd PSD for particles smaller than 75 μm

Date	Elapsed time, min	Temp (°C)	Ct	Actual hyd. Reading , Ra (151H)	Actual hyd. Reading , Ra (152H)	Corr.Hyd. Reading , Rc	Act % finer	Hyd. Corr. Only for meniscus, R	L from Table*	L/t	K from Table	D, mm
25-Feb	0						100.00					0
	0.2	24	0.7	1.0332	53.5	48.6	92.13	1.0335	8.3	41.500	0.01284	0.0827
	0.5	24	0.7	1.0306	49.3	44.4	84.18	1.0309	8.3	16.600	0.01284	0.0523
	1	24	0.7	1.0297	47.9	42.9	81.43	1.03	8.4	8.400	0.01284	0.0372
	1.5	24	0.7	1.0284	45.8	40.8	77.45	1.0287	8.51	5.673	0.01284	0.0306
	2	24	0.7	1.0273	44.0	39.1	74.09	1.0276	9.23	4.615	0.01284	0.0276
	2.2	24	0.7	1.0265	42.7	37.8	71.64	1.0268	9.26	4.209	0.01284	0.0263
	4.2	24	0.7	1.024	38.7	33.7	64.00	1.0243	9.91	2.360	0.01284	0.0197
	7.8	24	0.7	1.0195	31.4	26.5	50.24	1.0198	11	1.410	0.01284	0.0152
	15.8	24	0.7	1.0159	25.6	20.7	39.24	1.0162	12.1	0.766	0.01284	0.0112
	29.5	24	0.7	1.0138	22.2	17.3	32.82	1.0141	11.5	0.390	0.01284	0.0080
	58.9	24	0.7	1.0115	18.5	13.6	25.79	1.0118	12.1	0.205	0.01284	0.0058
	128.7	24	0.7	1.0094	15.2	10.2	19.37	1.0097	13.1	0.102	0.01298	0.0041
	478	25	0.7	1.0081	13.1	8.1	15.39	1.0084	14.2	0.030	0.01298	0.0022
26-Feb	1255	25	0.7	1.0072	11.6	6.7	12.64	1.0075	14.4	0.011	0.01284	0.0014
27-Feb	4137	25	0.7	1.0062	10.0	5.1	9.58	1.0065	14.7	0.004	0.01284	0.0008

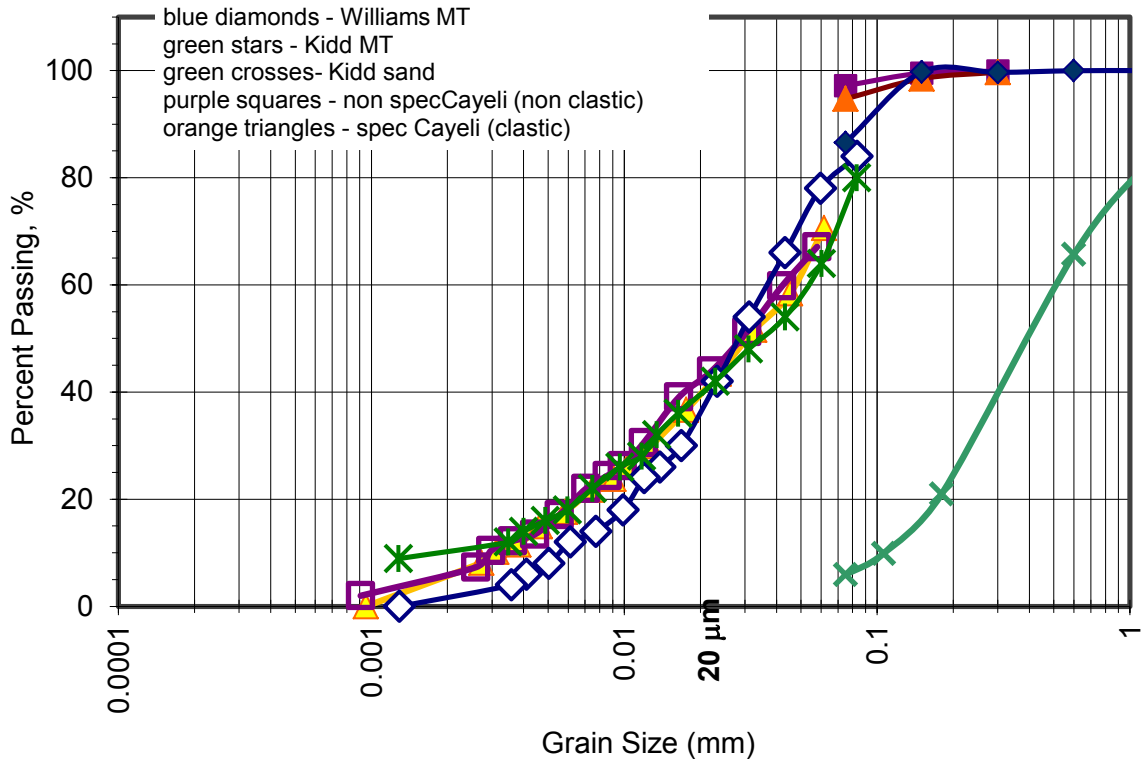


Figure A.2.2 Particle-size distribution curves (University of Toronto)

Table A.2.6 Liquid Limit (Williams)

Liquid Limit Determination					
Can no.	1	2	3	4	5
Mass of wet soil + can	34.5	38.1	36.8	37.5	36.0
Mass of dry soil + can	28.4	31.0	30.2	30.4	29.3
Mass of can	2.1	2.2	2.1	2.1	2.1
Mass of dry soil	26.3	28.8	28.1	28.3	27.2
Mass of moisture	6.1	7.1	6.6	7.1	6.7
Water content, w%	23.19%	24.65%	23.49%	25.09%	24.63%
No. of blows, N	34	23	23	13	10
For 25 no. of blows, w%=	23.91%				

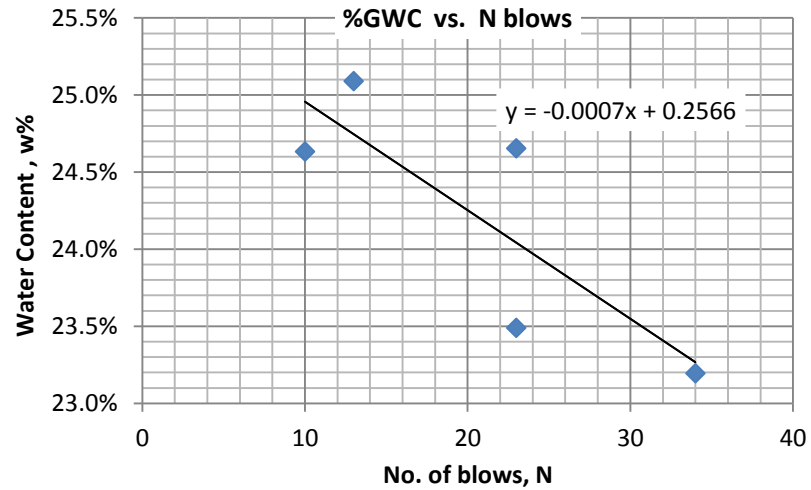


Figure A.2.3 Water content as a function of ‘N’ Blows

Table A.2.7 Plastic Limit (Williams)

Plastic Limit Determination			
Can no.	6	7	8
Mass of wet soil + can	4.9	5.4	5.7
Mass of dry soil + can	4.4	4.8	5.0
Mass of can	2.1	2.1	2.1
Mass of dry soil	2.3	2.7	2.9
Mass of moisture	0.5	0.6	0.7
Water content, w%	21.74%	22.22%	24.14%
Average	22.70%		

Table A.2.8 Atterberg Limits (Williams)

Result Summary	
Flow index, Fi	-2.35
Liquid Limit	23.9%
Plastic Limit	22.7%
Plastic Index, Ip	1.2%

Table A.2.9 Shrinkage Limit Test (Williams)

<p>Shrinkage Limit Test</p> <p>Williams Tailings</p> <p>$\rho_{\text{water}} = 1.0 \text{ g/mL}$</p> <p>$\rho_{\text{wax}} = 0.845 \text{ g/mL}$</p>		<p>Trial1</p> <table border="1" style="width: 100%; border-collapse: collapse;"> <thead> <tr> <th>Sample</th> <th>Md (g)</th> <th>Vd (mL)</th> <th>Mwsd (g)</th> <th>Ms (g)</th> <th>W%</th> <th>Mb (g)</th> <th>Mbw (g)</th> <th>Mbws (g)</th> <th>Ms+w (g)</th> <th>Vwax (mL)</th> </tr> </thead> <tbody> <tr> <td>1</td> <td>13.7</td> <td>39.68</td> <td>87.7</td> <td>56.9</td> <td>30.1</td> <td>117.8</td> <td>314.1</td> <td>338.4</td> <td>61.4</td> <td>5.33</td> </tr> <tr> <td>2</td> <td>10.8</td> <td>40.82</td> <td>83.7</td> <td>55.9</td> <td>30.4</td> <td>117.8</td> <td>314.4</td> <td>338.3</td> <td>59.6</td> <td>4.38</td> </tr> <tr> <td>3</td> <td>10.5</td> <td>41.33</td> <td>85.2</td> <td>56.6</td> <td>32.0</td> <td>117.8</td> <td>315.1</td> <td>339.5</td> <td>59.6</td> <td>3.55</td> </tr> </tbody> </table>									Sample	Md (g)	Vd (mL)	Mwsd (g)	Ms (g)	W%	Mb (g)	Mbw (g)	Mbws (g)	Ms+w (g)	Vwax (mL)	1	13.7	39.68	87.7	56.9	30.1	117.8	314.1	338.4	61.4	5.33	2	10.8	40.82	83.7	55.9	30.4	117.8	314.4	338.3	59.6	4.38	3	10.5	41.33	85.2	56.6	32.0	117.8	315.1	339.5	59.6	3.55				
Sample	Md (g)	Vd (mL)	Mwsd (g)	Ms (g)	W%	Mb (g)	Mbw (g)	Mbws (g)	Ms+w (g)	Vwax (mL)																																																
1	13.7	39.68	87.7	56.9	30.1	117.8	314.1	338.4	61.4	5.33																																																
2	10.8	40.82	83.7	55.9	30.4	117.8	314.4	338.3	59.6	4.38																																																
3	10.5	41.33	85.2	56.6	32.0	117.8	315.1	339.5	59.6	3.55																																																
		<p>Trial2</p> <table border="1" style="width: 100%; border-collapse: collapse;"> <thead> <tr> <th>Sample</th> <th>Md (g)</th> <th>Vd (mL)</th> <th>Mwsd (g)</th> <th>Ms (g)</th> <th>W%</th> <th>Mb (g)</th> <th>Mbw (g)</th> <th>Mbws (g)</th> <th>Ms+w (g)</th> <th>Vwax (mL)</th> </tr> </thead> <tbody> <tr> <td>1</td> <td>13.7</td> <td>39.68</td> <td>87.7</td> <td>56.9</td> <td>30.1</td> <td>117.8</td> <td>315.8</td> <td>340.5</td> <td>61.4</td> <td>5.33</td> </tr> <tr> <td>2</td> <td>10.8</td> <td>40.82</td> <td>83.7</td> <td>55.9</td> <td>30.4</td> <td>117.8</td> <td>313.3</td> <td>339</td> <td>59.6</td> <td>4.38</td> </tr> <tr> <td>3</td> <td>10.5</td> <td>41.33</td> <td>85.2</td> <td>56.6</td> <td>32.0</td> <td>117.8</td> <td>315.8</td> <td>338.9</td> <td>59.6</td> <td>3.55</td> </tr> </tbody> </table>									Sample	Md (g)	Vd (mL)	Mwsd (g)	Ms (g)	W%	Mb (g)	Mbw (g)	Mbws (g)	Ms+w (g)	Vwax (mL)	1	13.7	39.68	87.7	56.9	30.1	117.8	315.8	340.5	61.4	5.33	2	10.8	40.82	83.7	55.9	30.4	117.8	313.3	339	59.6	4.38	3	10.5	41.33	85.2	56.6	32.0	117.8	315.8	338.9	59.6	3.55				
Sample	Md (g)	Vd (mL)	Mwsd (g)	Ms (g)	W%	Mb (g)	Mbw (g)	Mbws (g)	Ms+w (g)	Vwax (mL)																																																
1	13.7	39.68	87.7	56.9	30.1	117.8	315.8	340.5	61.4	5.33																																																
2	10.8	40.82	83.7	55.9	30.4	117.8	313.3	339	59.6	4.38																																																
3	10.5	41.33	85.2	56.6	32.0	117.8	315.8	338.9	59.6	3.55																																																
		<p>Results for Shrinkage Limit</p> <table border="1" style="width: 100%; border-collapse: collapse;"> <thead> <tr> <th colspan="4" style="text-align: center;"><i>trial 1</i></th> <th colspan="4" style="text-align: center;"><i>trial 2</i></th> </tr> <tr> <th>Sample</th> <th>Vt (mL)</th> <th>Vf (mL)</th> <th>Ws (%)</th> <th>Sample</th> <th>Vt (mL)</th> <th>Vf (mL)</th> <th>Ws (%)</th> </tr> </thead> <tbody> <tr> <td>1</td> <td>37.10</td> <td>31.77</td> <td>16.2</td> <td>1</td> <td>36.70</td> <td>31.37</td> <td>15.5</td> </tr> <tr> <td>2</td> <td>35.70</td> <td>31.32</td> <td>13.4</td> <td>2</td> <td>33.90</td> <td>29.52</td> <td>10.2</td> </tr> <tr> <td>3</td> <td>35.20</td> <td>31.65</td> <td>14.9</td> <td>3</td> <td>36.50</td> <td>32.95</td> <td>17.2</td> </tr> <tr> <td colspan="3"></td> <td style="text-align: center;">44.5</td> <td colspan="3"></td> <td style="text-align: center;">42.8</td> </tr> </tbody> </table>									<i>trial 1</i>				<i>trial 2</i>				Sample	Vt (mL)	Vf (mL)	Ws (%)	Sample	Vt (mL)	Vf (mL)	Ws (%)	1	37.10	31.77	16.2	1	36.70	31.37	15.5	2	35.70	31.32	13.4	2	33.90	29.52	10.2	3	35.20	31.65	14.9	3	36.50	32.95	17.2				44.5				42.8
<i>trial 1</i>				<i>trial 2</i>																																																						
Sample	Vt (mL)	Vf (mL)	Ws (%)	Sample	Vt (mL)	Vf (mL)	Ws (%)																																																			
1	37.10	31.77	16.2	1	36.70	31.37	15.5																																																			
2	35.70	31.32	13.4	2	33.90	29.52	10.2																																																			
3	35.20	31.65	14.9	3	36.50	32.95	17.2																																																			
			44.5				42.8																																																			
<p>Md: mass dish</p> <p>Vd: volume dish</p> <p>Mwsd: mass of wet soil + dish</p> <p>Ms: mass of dry soil, no dish</p> <p>Mb: mass of beaker</p> <p>Mbw: mass of beaker +water to the mark</p> <p>Mbws: mass of beaker +water to the mark + soil cake with wax coat</p> <p>Ms+w: mass of dry soil cake + wax coat</p> <p>Vt: volume of water displaced by wax coated soil cake</p> <p>Vf: volume of displaced water - volume of wax coat (thus, gives volume of dry soil cake)</p> <p>Ws: shrinkage limit in percent water content</p>		<table border="1" style="width: 100%; border-collapse: collapse;"> <tr> <td colspan="2">Trial 1 Average:</td> <td>Ws1 =</td> <td>14.8</td> <td>%</td> </tr> <tr> <td colspan="2">Trial 2 Average:</td> <td>Ws2 =</td> <td>14.3</td> <td>%</td> </tr> <tr> <td colspan="2">Total Average Shrinkage Limit:</td> <td></td> <td>14.5</td> <td>%</td> </tr> </table>									Trial 1 Average:		Ws1 =	14.8	%	Trial 2 Average:		Ws2 =	14.3	%	Total Average Shrinkage Limit:			14.5	%																																	
Trial 1 Average:		Ws1 =	14.8	%																																																						
Trial 2 Average:		Ws2 =	14.3	%																																																						
Total Average Shrinkage Limit:			14.5	%																																																						

A.3 CALIBRATION DATA

Table A.3.1 Proximity displacement sensor calibrated at 17.27 volts – vertical displacement (mm) as a function of output current (mV).

Displacement	Current
<i>(RE ± 0.05 mm)</i>	<i>(RE ± 0.05 mV)</i>
135.0	19.07
118.0	16.81
98.0	14.30
87.0	12.85
70.0	10.69
55.5	8.75
41.0	6.82
30.5	5.53
23.5	4.48
19.0	4.05

Table A.3.2 Calibrations for EC-5 and 10HS sensors, used with Williams tailings

Em50_PS 5766 records Time	Port 1 (raw) 10HS m³/m³ VWC	Port 2 (raw) EC-5 m³/m³ VWC	Em50_PS 5766 records Time	Port 1 (raw) 10HS m³/m³ VWC	Port 2 (raw) EC-5 m³/m³ VWC
1/30/10 15:06	666	522	1/30/10 16:39	887	709
1/30/10 15:07	666	522	1/30/10 16:40	887	709
1/30/10 15:08	666	523	1/30/10 16:41	887	709
1/30/10 15:09	666	523	1/30/10 16:42	887	710
1/30/10 15:10	665	523	1/30/10 16:52	1106	849
1/30/10 15:11	665	523	1/30/10 16:53	1107	849
1/30/10 15:12	667	523	1/30/10 16:54	1107	849
1/30/10 15:13	667	522	1/30/10 16:55	1107	850
1/30/10 15:14	667	523	1/30/10 16:56	1108	850
1/30/10 15:34	683	543	1/30/10 16:57	1107	850
1/30/10 15:35	684	544	1/30/10 16:58	1107	850
1/30/10 15:36	684	544	1/30/10 17:07	1369	958
1/30/10 15:37	684	545	1/30/10 17:08	1368	958
1/30/10 15:38	684	545	1/30/10 17:09	1368	958
1/30/10 15:39	684	545	1/30/10 17:10	1367	959
1/30/10 15:40	684	545	1/30/10 17:11	1367	958
1/30/10 15:41	684	545	1/30/10 17:12	1367	958
1/30/10 15:42	684	544	1/30/10 17:13	1367	958
1/30/10 15:43	684	544	1/30/10 17:14	1367	958
1/30/10 15:44	684	544	1/30/10 17:15	1366	958
1/30/10 15:45	683	544	1/30/10 17:16	1366	957

Em50_PS	Port 1 (raw)	Port 2 (raw)	Em50_PS	Port 1 (raw)	Port 2 (raw)
5766 records	10HS	EC-5	5766 records	10HS	EC-5
Time	m ³ /m ³ VWC	m ³ /m ³ VWC	Time	m ³ /m ³ VWC	m ³ /m ³ VWC
1/30/10 15:55	694	551	1/30/10 17:17	1366	957
1/30/10 15:56	694	551	1/30/10 17:18	1366	957
1/30/10 15:57	695	551	1/30/10 17:19	1366	957
1/30/10 15:58	694	551	1/30/10 17:20	1366	957
1/30/10 15:59	695	552	1/30/10 17:21	1366	957
1/30/10 16:00	695	552	1/30/10 17:22	1366	957
1/30/10 16:01	695	552	1/30/10 17:23	1366	957
1/30/10 16:02	695	552	1/30/10 17:24	1366	957
1/30/10 16:03	694	552	1/30/10 17:25	1366	956
1/30/10 16:04	694	552	1/30/10 17:26	1366	957
1/30/10 16:05	695	552	1/30/10 17:32	1375	991
1/30/10 16:14	760	614	1/30/10 17:33	1380	992
1/30/10 16:15	760	614	1/30/10 17:34	1378	993
1/30/10 16:16	760	614	1/30/10 17:35	1378	992
1/30/10 16:17	760	614	1/30/10 17:36	1378	993
1/30/10 16:18	760	614	1/30/10 17:37	1377	990
1/30/10 16:19	760	614	1/30/10 17:38	1378	991
1/30/10 16:20	761	614	1/30/10 17:39	1378	993
1/30/10 16:21	761	614	1/30/10 17:40	1378	992
1/30/10 16:32	886	709	1/30/10 17:41	1377	993
1/30/10 16:33	886	709	1/30/10 17:42	1378	993
1/30/10 16:34	886	709	1/30/10 17:43	1377	993
1/30/10 16:35	886	709	1/30/10 17:44	1376	993

Table A.3.3 Test #1 (March 15, 2010): Water content measurements for Williams 3% and 7% binder specimens

% Binder	Date	<i>RE ± 0.05 g</i>					%	<i>± 0.05 g</i>	<i>± 0.005 mm</i>			<i>cm³</i>		%
		<i>m_c</i>	<i>m_{c+CPB}</i>	<i>m_{OD}</i>	<i>m_W</i>	<i>m_S</i>	θ_G	<i>M_{total sample}</i>	ϕ_i	<i>h_{void}</i>	<i>h_{sample}</i>	<i>V_{total void}</i>	<i>V_{total sample}</i>	θ_V
3% Binder Specimen (10HS Sensor)	14-Mar-10	2.1	32.9	24.4	8.5	22.3	38.12	596.94	76.65	151.10	71.65	696.88	330.45	49.85
	15-Mar-10	2.1	27.5	20.7	6.8	18.6	36.56	583.10	76.65	79.45	71.65	366.43	330.45	47.24
	16-Mar-10	2.1	19.1	15.2	3.9	13.1	29.77	576.60	76.15	83.45	67.65	379.87	307.95	42.95
	17-Mar-10	2.1	20.7	16.6	4.1	14.5	28.28	558.70	75.65	84.70	66.40	380.51	298.30	41.29
	18-Mar-10	2.1	20.9	16.7	4.2	14.6	28.77	541.70	75.40	84.80	66.30	378.45	295.89	40.90
	19-Mar-10	2.1	26.8	21.4	5.4	19.3	27.98	529.70	75.40	84.85	66.25	378.67	295.66	39.17
	20-Mar-10	2.1	27.0	21.7	5.3	19.6	27.04	517.70	75.45	84.90	66.20	379.40	295.83	37.25
	21-Mar-10	2.1	34.4	27.6	6.8	25.5	26.67	506.40	75.45	84.90	66.20	379.40	295.83	36.04
	22-Mar-10	2.1	21.9	17.8	4.1	15.7	26.11	491.70	75.45	84.95	66.15	379.62	295.61	34.44
	25-Mar-10	2.1	29.4	24.3	5.1	22.2	22.97	470.80	75.45	85.00	66.10	379.85	295.39	29.78
	27-Mar-10	2.1	45.0	40.5	4.5	38.4	11.72	461.70	76.40	85.10	66.00	389.93	302.41	16.01
	10-Apr-10	2.1	61.8	55.8	6.0	53.7	11.17	442.9	76.40	85.30	65.80	390.85	301.50	14.76
7% Binder Specimen (EC-5 Sensor)	14-Mar-10	2.1	25.3	18.9	6.4	16.8	38.10	990.03	76.65	151.10	116.90	696.88	539.15	50.66
	15-Mar-10	2.1	18.4	14.2	4.2	12.1	34.71	985.20	76.65	34.20	116.90	157.73	539.15	47.08
	16-Mar-10	2.1	20.5	16.3	4.2	14.2	29.58	974.60	76.65	34.20	116.90	157.73	539.15	41.26
	17-Mar-10	2.1	25.2	20.0	5.2	17.9	29.05	953.90	76.65	34.20	116.90	157.73	539.15	39.83
	18-Mar-10	2.1	22.7	18.1	4.6	16.0	28.75	934.50	76.65	34.50	116.60	159.12	537.76	38.80
	19-Mar-10	2.1	15.8	12.8	3.0	10.7	28.04	921.10	76.40	34.65	116.45	158.77	533.58	37.80
	20-Mar-10	2.1	25.8	20.8	5.0	18.7	26.74	908.40	76.40	34.70	116.40	159.00	533.35	35.93
	21-Mar-10	2.1	21.7	17.7	4.0	15.6	25.64	895.20	76.40	34.75	116.35	159.22	533.12	34.27
	22-Mar-10	2.1	26.7	21.6	5.1	19.5	26.15	880.60	76.40	34.75	116.35	159.22	533.12	34.24
	25-Mar-10	2.1	31.0	25.8	5.2	23.7	21.94	858.60	76.40	34.75	116.35	159.22	533.12	28.98
	27-Mar-10	2.1	40.5	34.9	5.6	32.8	17.07	843.10	76.40	34.80	116.30	159.45	532.89	23.07
	10-Apr-10	2.1	77.6	69.6	8.0	67.5	11.85	799.00	76.40	35.10	116.00	160.83	531.51	15.93

Table A.3.4a Test #2 (April 16, 2010): Water content measurements for Williams 3% binder specimens to calibrate the EC-5 sensor

CPB	Date	m_{C+CPB}	m_{CPB}	hi	ϕ_{in}	Volume	m_C	m_{C+CPB}	m_{OD}	m_W	m_S	θ_G	θ_V
	dd-mm-yy	$\pm 0.05 g$		$\pm 0.005mm$		$\pm 0.005 cm^3$	$\pm 0.00005 g$					$\pm 0.005 \%$	
3 % Binder (EC-5 Sensor)	16-Apr-10	76	0	151.25	76.68	698.47	NA	NA	NA	NA	NA	NA	NA
	16-Apr-10	76	877	151.25	76.68	504.05	2.05	28.53	21.39	7.13	19.34	36.88	46.87
	17-Apr-10	952.6	876.6	109.15	76.68	504.05	2.04	29.58	22.29	7.29	20.25	35.99	46.03
	18-Apr-10	919.4	843.4	101.5	74.98	448.17	2.04	30.23	24.28	5.96	22.24	26.78	39.75
	18-Apr-10	919.4	843.4	101.5	74.98	448.17	2.08	34.45	27.72	6.73	25.64	26.25	39.12
	19-Apr-10	916.1	840.1	101.2	73.28	426.82	2.12	33.99	28.02	5.98	25.89	23.09	36.92
	19-Apr-10	916.1	840.1	101.2	73.28	426.82	2.06	22.44	18.61	3.83	16.56	23.12	36.96
	20-Apr-10	910.8	834.8	100.3	73.03	420.14	2.03	31.34	27.50	3.84	25.46	15.08	26.03
	20-Apr-10	910.8	834.8	100.3	73.03	420.14	2.05	23.80	20.69	3.11	18.64	16.69	28.42
	22-Apr-10	889.9	813.9	100.15	72.28	410.94	2.04	42.87	38.19	4.68	36.15	12.94	22.70
	22-Apr-10	889.9	813.9	100.15	72.28	410.94	2.04	49.99	44.69	5.30	42.65	12.42	21.88
	23-Apr-10	882.2	806.2	99.95	70.58	391.05	2.08	56.99	51.90	5.09	49.83	10.21	19.10
	23-Apr-10	882.2	806.2	99.95	70.58	391.05	2.03	38.62	34.98	3.64	32.94	11.06	20.53
	24-Apr-10	865.9	789.9	99.35	70.58	388.71	2.01	54.84	50.24	4.60	48.23	9.55	17.71
	24-Apr-10	865.9	789.9	99.35	70.58	388.71	2.09	42.71	39.23	3.48	37.14	9.37	17.40
	25-Apr-10	857.1	781.1	99.1	70.58	387.73	2.11	70.77	65.99	4.78	63.88	7.48	14.02
	25-Apr-10	857.1	781.1	99.1	70.58	387.73	2.01	30.29	28.33	1.97	26.32	7.48	14.01
	26-Apr-10	845.3	769.3	98.8	70.58	386.55	2.04	66.27	63.37	2.90	61.34	4.72	8.98
26-Apr-10	845.3	769.3	98.8	70.58	386.55	2.03	68.40	65.58	2.82	63.55	4.44	8.46	

Table A.3.4b Test #2 (April 16,2010): Water content measurements for Williams 7% binder specimens to calibrate the 10HS sensor

CPB	Date	m _{C+CPB}	m _{CPB}	hi	φ _{in}	Volume	m _C	m _{C+CPB}	m _{OD}	m _W	m _S	θ _G	θ _V
	dd-mm-yy	± 0.05 g		± 0.005mm		± 0.005 cm ³	± 0.00005 g					± 0.05 %	
7 % Binder (10HS Sensor)	16-Apr-10	76	0	151.25	76.44	694.11	NA	NA	NA	NA	NA	NA	NA
	16-Apr-10	800	724	91.45	76.44	419.68	2.11	21.87	16.64	5.22	14.53	35.95	45.62
	17-Apr-10	800	724	91.45	76.44	419.68	2.04	32.10	24.64	7.46	22.60	33.02	42.82
	18-Apr-10	770.3	694.3	85.85	75.84	387.82	2.08	30.60	25.30	5.31	23.22	22.87	33.32
	18-Apr-10	770.3	694.3	85.85	75.84	387.82	2.01	32.57	26.73	5.85	24.72	23.65	34.24
	19-Apr-10	767.2	691.2	84.90	75.84	383.53	2.03	43.18	36.71	6.47	34.68	18.67	28.35
	19-Apr-10	767.2	691.2	84.70	75.84	382.62	2.03	27.93	23.80	4.13	21.77	18.99	28.82
	20-Apr-10	762.3	686.3	84.60	75.59	379.65	2.05	23.81	21.71	2.10	19.66	10.67	17.43
	20-Apr-10	762.3	686.3	83.40	75.59	374.27	2.08	48.14	42.94	5.20	40.85	12.74	20.71
	22-Apr-10	743.6	667.6	85.20	75.59	382.35	2.04	76.65	69.81	6.84	67.77	10.10	16.01
	22-Apr-10	743.6	667.6	83.00	75.59	372.47	2.08	56.67	51.70	4.96	49.62	10.00	16.29
	23-Apr-10	736.8	660.8	84.80	75.59	380.55	2.02	51.94	48.44	3.50	46.42	7.54	12.17
	23-Apr-10	736.8	660.8	82.60	75.59	370.68	2.10	35.70	33.31	2.39	31.21	7.64	12.66
	24-Apr-10	723.0	647	84.50	75.59	379.21	2.03	43.51	41.48	2.02	39.46	5.13	8.32
24-Apr-10	723.0	647	82.30	75.59	369.33	2.06	49.60	47.33	2.28	45.27	5.03	8.38	

* Refer to Appendix C – CD containing additional data

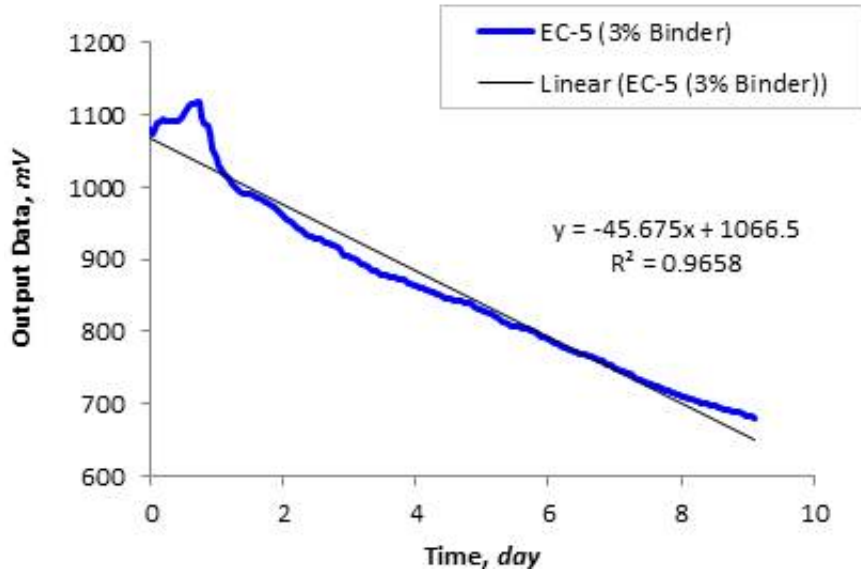


Figure A.3.1 EC-5 sensor calibrated for 3% binder material (Test #2): Output data as a function of time

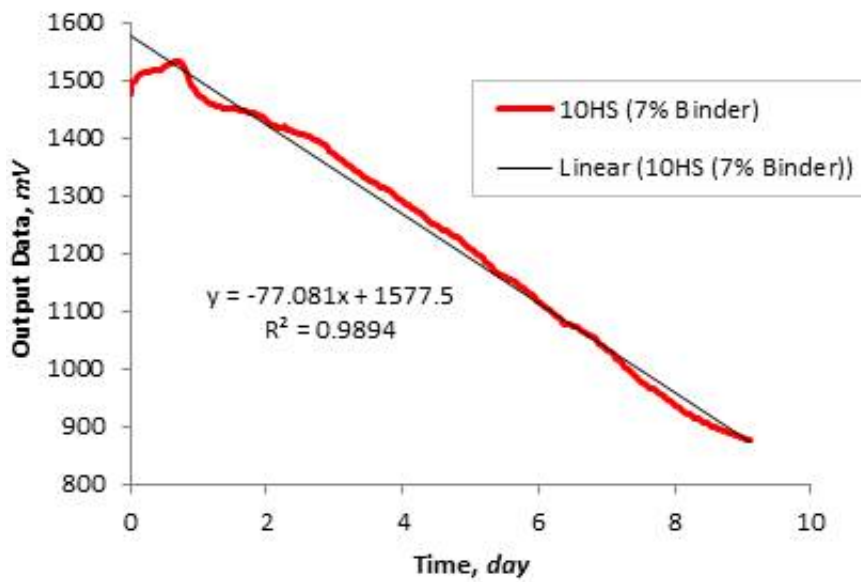


Figure A.2.2 10HS sensor calibrated for 7% binder material (Test #2): Output data as a function of time

Table A.3.5 Measured parameters for the 5 bar and 15 bar ceramic porous discs

5 bar (500 kPa) Porous Disc						
Conditions	L <i>(RE± 0.005 mm)</i>	d	m_{disk}	m_w <i>(RE± 0.05 g)</i>	Δm_w	ψ <i>(kPa)</i>
Initial	10.55	79.25	171.6	98.6	--	--
Final	10.55	79.25	171.6	6.8	91.8	200
15 bar (1500 kPa) Porous Disc						
Initial	10.55	79.25	174.1	56.2	--	--
Final	10.55	79.25	174.1	48.7	7.5	450

A.4 WATER-RETENTION CURVES

Table A.4.1 Williams results using a 5 bar AEV porous ceramic disc with the axis translation technique, with measurements of volume changes

Matric Suction	M_{paste}	M_{solids}	M_{water}	V_{paste}	V_{solids}	V_{voids}	V_v/V_s	GWC	VWC	Deg. of Sat
<i>(kPa)</i>	<i>(RE ± 0.05g)</i>			<i>(cm³)</i>			<i>(cm³/cm³)</i>	<i>(%)</i>		
Initial	653.0	472.89	180.11	369.77	172.97	196.80	1.14	38.09	48.71	100.00
0	621.5	472.89	148.61	333.75	172.97	160.78	0.93	31.42	44.53	100.00
30	577.2	472.89	104.31	272.91	172.97	99.94	0.58	22.06	38.22	100.00
50	577.8	472.89	104.91	270.80	172.97	97.83	0.57	22.18	38.74	100.00
90	543.1	472.89	70.21	266.82	172.97	93.85	0.54	14.85	26.31	74.81
130	522.4	472.89	49.51	264.00	172.97	91.03	0.53	10.47	18.75	54.38
190	507.2	472.89	34.31	251.99	172.97	79.02	0.46	7.25	13.61	43.41
250	499.2	472.89	26.31	251.99	172.97	79.02	0.46	5.56	10.44	33.29
320	493.9	472.89	21.01	251.99	172.97	79.02	0.46	4.44	8.34	26.58

Table A.4.2 Total suction measurement range for Williams water-retention curve containing no binder

Total Suction	GWC	VWC	S=Vw/Vv	Void Ratio
(kPa)	(%)			(cm ³ /cm ³)
1150	3.06	5.13	17.95	0.46
1220	2.97	4.67	17.42	0.46
1670	2.50	4.35	14.66	0.46
2140	1.81	4.48	10.63	0.46
4160	1.25	3.20	7.32	0.46
7905	0.60	1.55	3.50	0.46
90540	0.15	0.46	0.88	0.46
133830	0.21	0.59	1.25	0.46
141190	0.12	0.36	0.73	0.46
149560	0.12	0.29	0.72	0.46

Table A.4.3 Volumetric strain data for post-hydrated Williams (Trial #1) containing 3% binder

<i>i</i>	Matric Suction (kPa)	Change in V _{Voids} (cm ³)	Volumetric Strain (cm ³ /cm ³)	Cumulative Strain	$m_v = \frac{\delta \varepsilon_v}{\delta(u_a - u_w)}$
1	0.00	0.00	0.000	0.000	0.0
2	40.00	3.02	0.015	0.015	0.0004
3	80.00	1.07	0.005	0.020	0.0001
4	100.00	0.29	0.001	0.022	0.0000
5	180.00	1.40	0.007	0.029	0.0000
6	300.00	10.95	0.054	0.083	0.0002

Table A.4.4 Williams post-hydration (Trial #1) results using a 15 bar AEV porous ceramic disc with the axis translation technique, with measurements of volume change

Date	Time	Ψ_m	M_{cell}	$M_{cell + paste}$	M_{CP}	M_{water}	M_{solids}	V_{Paste}	V_{voids}	V_{solids}	θ_g	θ_v	S	Void Ratio
		kPa	Mass (RE +/- 0.005 g)					cm ³			%		cm ³ /cm ³	
3-Jul-09	17:30	0	5294.4	5667.8	373.4	99.5	273.9	201.1	100.9	100.2	36.3	49.5	0.0	1.01
6-Jul-09	16:30	40	5294.4	5663.1	368.7	94.8	273.9	198.0	97.8	100.2	34.6	47.8	96.8	0.98
9-Jul-09	17:45	80	5294.4	5662.9	368.5	94.6	273.9	197.0	96.8	100.2	34.5	48.0	97.7	0.97
11-Jul-09	16:20	100	5294.4	5662.6	368.2	94.3	273.9	196.7	96.5	100.2	34.4	47.9	97.7	0.96
13-Jul-09	13:20	180	5294.4	5657.6	363.2	89.3	273.9	195.3	95.1	100.2	32.6	45.7	93.9	0.95
16-Jul-09	15:20	300	5294.4	5654.4	360.0	86.1	273.9	184.3	84.1	100.2	31.4	46.7	102.3	0.84

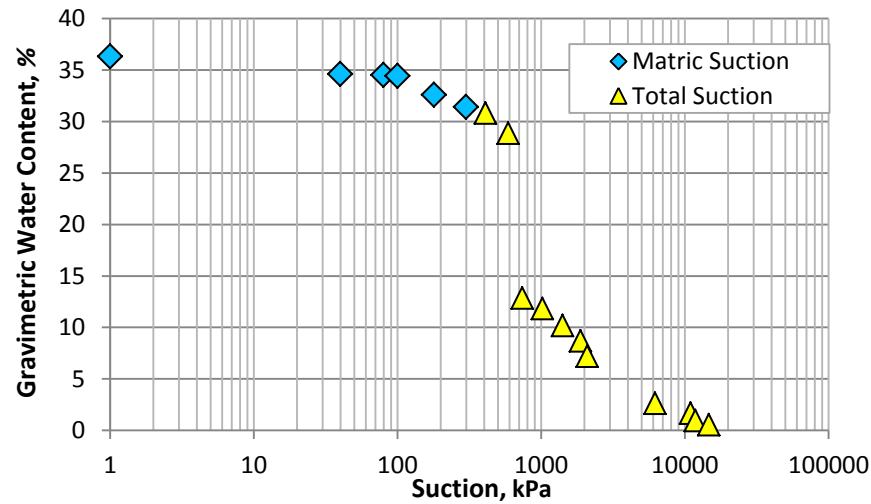


Figure A.4.1 Williams post-WRC (Trial #1) in terms of gravimetric water content, only

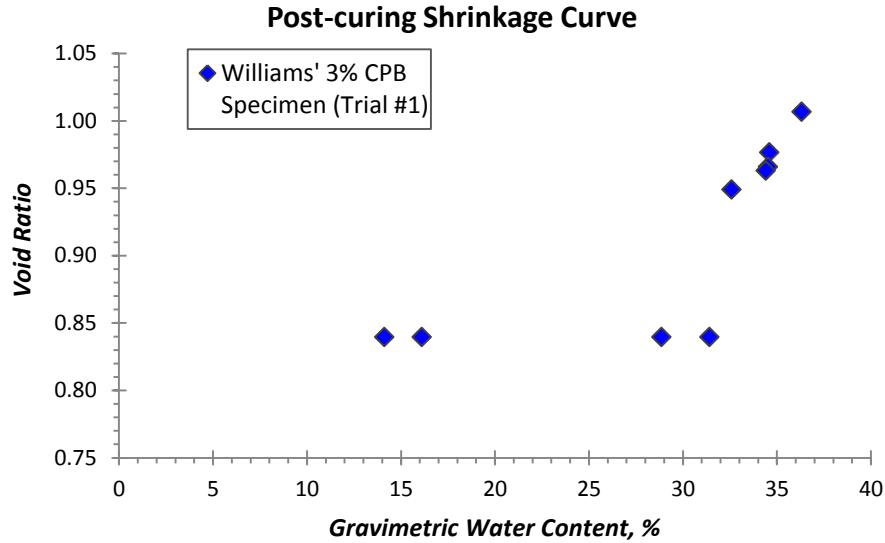


Figure A.4.2 Shrinkage curve for post-hydrated Williams 3% binder (Trial #1)

Table A.4.5 Williams post-hydration (Trial #2) results using a 15 bar AEV porous ceramic disc with the axis translation technique, with measurements of volume change

Matric Suction	M_{paste}	M_{water}	M_{solids}	V_{paste}	V_{solids}	V_{voids}	V_v/V_s	GWC	VWC	Deg. of Saturation
(kPa)	(RE ± 0.05g)			(cm ³)			(cm ³ /cm ³)	(%)		
0	299.50	80.07	219.43	159.88	80.26	79.62	0.99	36.49	50.08	100.00
80	297.00	77.57	219.43	157.32	80.26	77.06	0.96	35.35	49.31	100.00
120	295.10	75.67	219.43	155.87	80.26	75.61	0.94	34.48	48.55	100.00
150	286.70	67.27	219.43	154.54	80.26	74.28	0.93	30.66	43.53	90.57
170	276.80	57.37	219.43	152.79	80.26	72.53	0.90	26.14	37.55	79.09
200	271.90	52.47	219.43	152.66	80.26	72.40	0.90	23.91	34.37	72.47
250	265.90	46.47	219.43	151.08	80.26	70.82	0.88	21.18	30.76	65.61
300	254.80	35.37	219.43	150.31	80.26	70.05	0.87	16.12	23.53	50.49
350	248.60	29.17	219.43	149.98	80.26	69.72	0.87	13.29	19.45	41.84
420	245.00	25.57	219.43	149.94	80.26	69.68	0.87	11.65	17.05	36.69
460	243.40	23.97	219.43	149.94	80.26	69.68	0.87	10.92	15.99	34.40
560	241.60	22.17	219.43	149.94	80.26	69.68	0.87	10.10	14.78	31.81

Table A.4.6 Total suction measurement range for post-hydrated Williams (Trial #2) water-retention curve containing 3% binder

Total Suction	GWC	VWC	S=Vw/Vv	Void Ratio
(kPa)	(%)			(cm ³ /cm ³)
980	7.17	10.48	22.53	0.87
1020	7.06	10.32	22.19	0.87
1060	6.91	10.10	21.71	0.87
1420	6.59	9.63	20.71	0.87
1870	6.25	9.14	19.65	0.87
2080	6.03	8.82	18.96	0.87
3920	4.39	6.42	13.79	0.87
6781	2.19	3.20	6.88	0.87
25723	0.23	0.34	0.72	0.87
26820	0.21	0.31	0.66	0.87
157230	0.11	0.16	0.35	0.87
168260	0.00	0.00	0.00	0.87

Table A.4.7 Kidd tailings results using a 5 bar porous ceramic disc with the axis translation technique, with measurements of volume change

Matric Suction	M _{paste}	M _{water}	M _{solids}	V _{paste}	V _{Solids}	V _{Voids}	Void Ratio	GWC	VWC	S
(kPa)	(RE ± 0.05 g)			(cm ³)			(cm ³ /cm ³)	(%)		
Initial	397.5	80.8	313.8	NA	121.1	NA	NA	25.74	NA	NA
0	336.3	60.5	275.8	156.1	106.5	49.6	0.47	21.92	38.74	100.00
30	324.0	48.2	275.8	149.6	106.5	43.1	0.41	17.46	32.19	100.00
50	315.4	39.6	275.8	144.6	106.5	38.1	0.36	14.34	27.36	99.35
90	305.7	29.9	275.8	143.8	106.5	37.3	0.35	10.82	20.76	76.75
120	299.7	23.9	275.8	142.9	106.5	36.4	0.34	8.65	16.70	62.89
150	296.1	20.3	275.8	142.1	106.5	35.6	0.33	7.34	14.26	54.51
180	294.2	18.4	275.8	142.0	106.5	35.5	0.33	6.66	12.93	49.49
230	292.3	16.5	275.8	141.4	106.5	34.9	0.33	5.97	11.64	45.08

Table A.4.8 Kidd 2.2% binder specimen results using a 15 bar porous ceramic disc with the axis translation technique, with measurements of volume change

Matric Suction	M_{paste}	M_{water}	M_{solids}	V_{paste}	V_{Solids}	V_{Voids}	Void Ratio	GWC	VWC	Deg. of Saturation
<i>(kPa)</i>	<i>(RE ± 0.05 g)</i>			<i>(cm³)</i>			<i>(cm³/cm³)</i>	<i>(%)</i>		
0	372.2	61.59	310.61	179.34	119.92	59.42	0.50	19.83	34.34	103.65
80	370.4	59.79	310.61	177.62	119.92	57.70	0.48	19.25	33.66	103.62
110	368.6	57.99	310.61	177.14	119.92	57.22	0.48	18.67	32.74	101.34
140	367.6	56.99	310.61	176.46	119.92	56.54	0.47	18.35	32.30	100.79
160	363.7	53.09	310.61	175.14	119.92	55.22	0.46	17.09	30.31	96.14
190	359.9	49.29	310.61	174.48	119.92	54.56	0.46	15.87	28.25	90.34
210	357.3	46.69	310.61	174.46	119.92	54.54	0.45	15.03	26.76	85.60
240	353.9	43.29	310.61	174.46	119.92	54.54	0.45	13.94	24.81	79.37
280	351	40.39	310.61	174.46	119.92	54.54	0.45	13.00	23.15	74.05
300	348.9	38.29	310.61	174.46	119.92	54.54	0.45	12.33	21.95	70.20
360	346.1	35.49	310.61	174.46	119.92	54.54	0.45	11.43	20.34	65.07
440	341.4	30.79	310.61	174.46	119.92	54.54	0.45	9.91	17.65	56.45
540	338.5	27.89	310.61	174.46	119.92	54.54	0.45	8.86	15.99	51.13

A.5 MERCURY INTRUSION POROSIMETRY

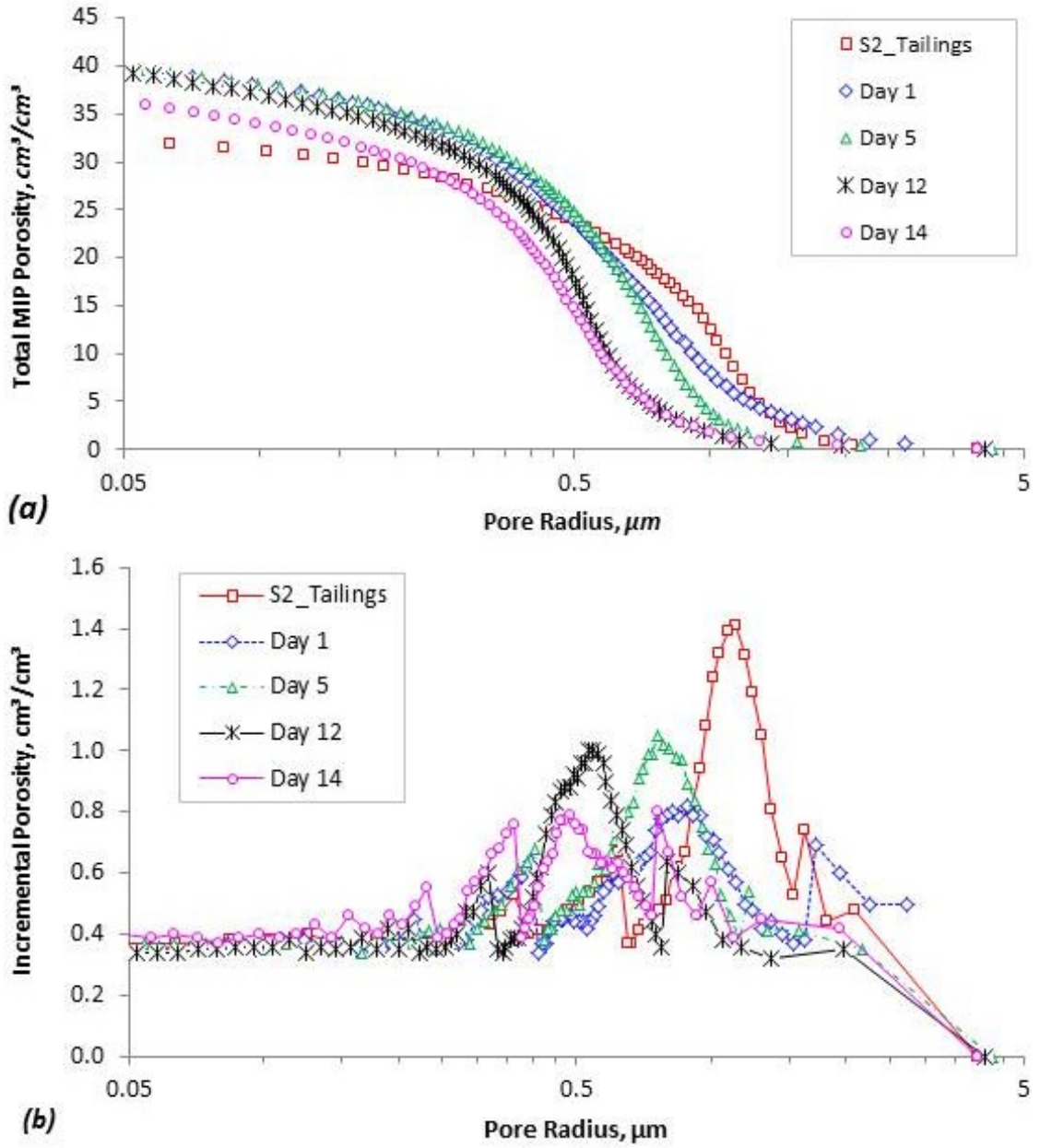


Figure. A.5.1 7% binder: (a) total MIP porosity, and (b) incremental porosity as a function of pore radius

A.6 CHEMICAL ANALYSES

Table A.6.1 Mineralogy of Williams' tailings and 3% binder paste material

Client: Carleton University - Env. Engineering Lab 2432 C.J. Mackenzie Bldg., 1125 Colonel By Dr. Ottawa, ON K1S 5B6			Report Number: 1112500 Date: 2011-07-15 Date Submitted: 2011-06-10		
INVOICE: Carleton University Chain of Custody Number: 143424					
LAB ID:			887433	887434	887435
Sample Date:			2011-06-10	2011-06-10	2011-06-10
Sample ID:			Williams' Filter Cake	3% binder (Post- hydration_Column)	3% binder (Pre- hydration)
PARAMETER	UNITS	MRL			
Hydrogen Sulphide (total sulphate)	mg/kg	5	14	12	30
pH			8.1	8.5	10.2
Sulphate	%	0.01	0.32	1.03	0.53
Calcium	ug/g	100	18800	20400	23300
Magnesium	ug/g	100	9300	9400	9200
Iron	ug/g	5	17900	18500	19100

Table A.6.2 Williams mine water chemistry

Client: Carleton University - Env. Eng. Lab 2432 C.J. Mackenzie Bldg., 1125 Colonel By Dr. Ottawa, ON K1S 5B6			Report Number: 1112499 2011-06- 27 Date: 2011-06- 10 Date Submitted: 10				
INVOICE: Carleton University Chain of Custody Number: 143424			matrix - water				
LAB ID:			887428	887429	887430	887431	887432
Sample Date:			6/10/11	6/10/11	6/10/11	6/10/11	6/10/11
Sample ID:			Plug pour	Main_1	Main_2	Main_3	Processed Mine H2O
PARAMETER	UNITS	MRL					
Alkalinity as CaCO ₃	mg/L	5	78	59	25	177	88
Conductivity	uS/cm	5	5960	5280	5990	6120	3250
pH			8.02	7.77	7.25	7.80	7.41
Total Dissolved Solids (COND - CALC)	mg/L	1	3870	3430	3890	3980	2110
CO ₃ as CaCO ₃	mg/L	1	N/A-PH	N/A-PH	N/A-PH	N/A-PH	N/A-PH

APPENDIX B – ÇAYELI TAILINGS [EXPERIMENTAL RESULTS]

The following test results of Çayeli tailings with and without binder were obtained from Jayasinghe (2010).

B.1 PHYSICAL PROPERTIES OF ÇAYELI TAILINGS

Table B.1.1 Specific gravity and Atterberg Limits for non-spec Çayeli tailings

Specific Gravity <i>g/cm³</i>	Liquid Limit	Plastic Limit <i>% GWC</i>	Shrinkage Limit
2.35*	14.5	13.8	8.99

*The SG was reported as 4.86 g/cm³, which is closer to the value obtained by Dragana Simon (2010), for non-spec / clastic tailings.

The PSD (Figure B.1.1) of the non-spec Çayeli tailings were determined using the BrightWELL Particle Counter DPA4100 from BrightWELL Technologies Incorporated. 1.0 grams of air dried tailings were used at a dilution factor of 1/10⁶ mL.

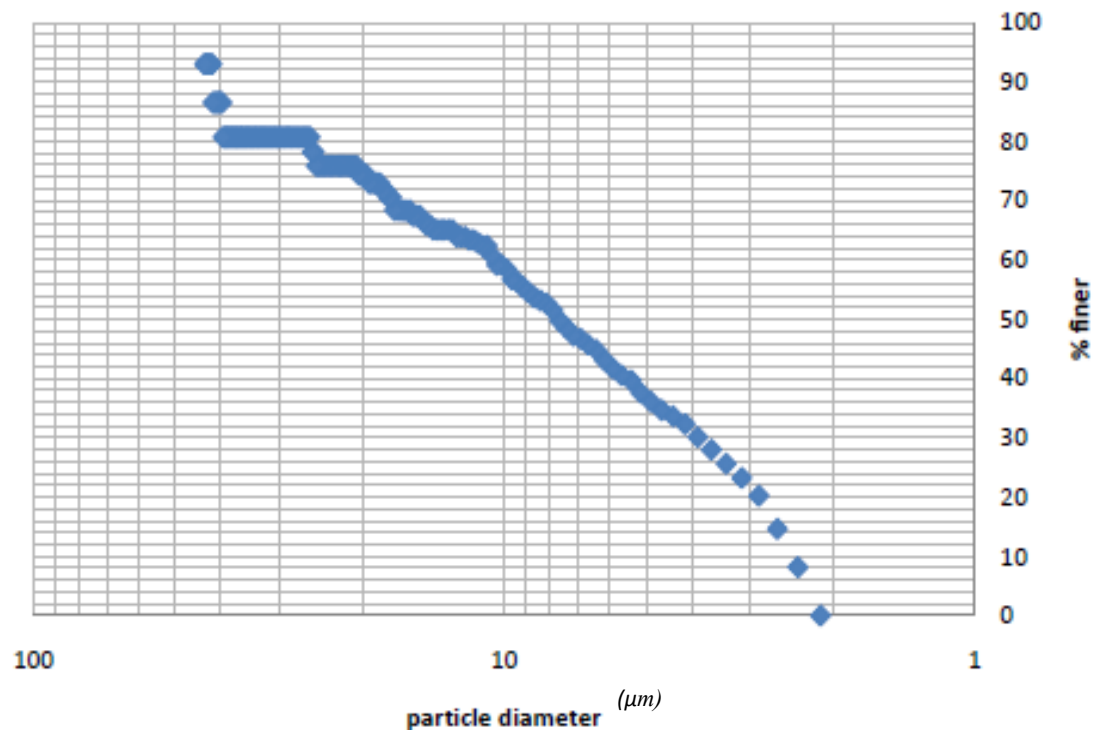


Figure B.1.1 Particle size-distribution of non-spec Çayeli tailings

B.2 SELF-DESICCATION – HEAT TESTS

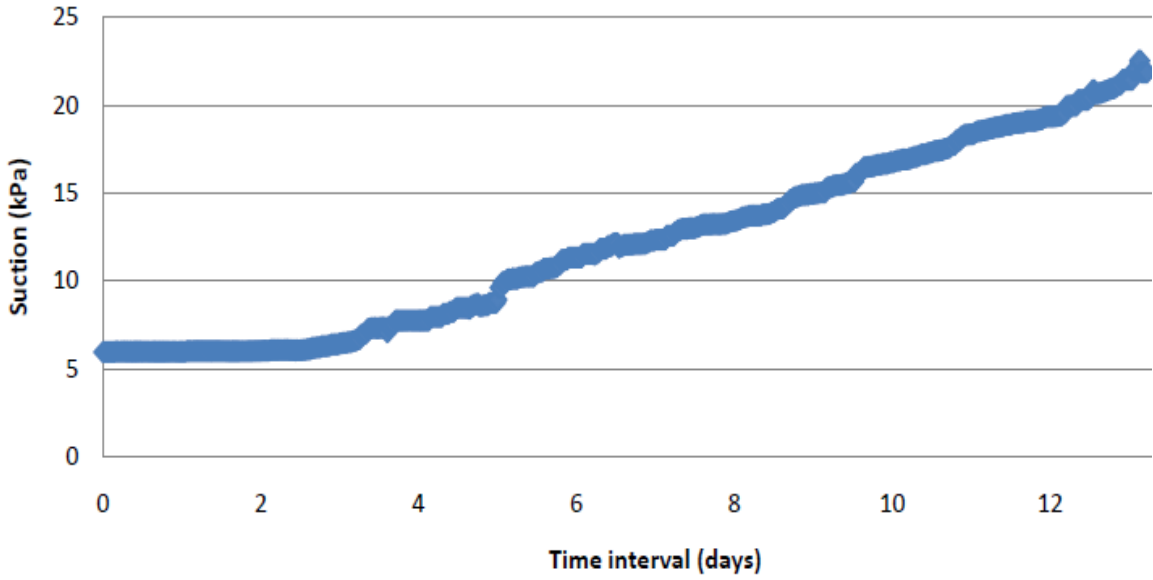


Figure B.2.1 Çayeli 4.5% binder: rate of self-desiccation at ambient temperature of 24 °C

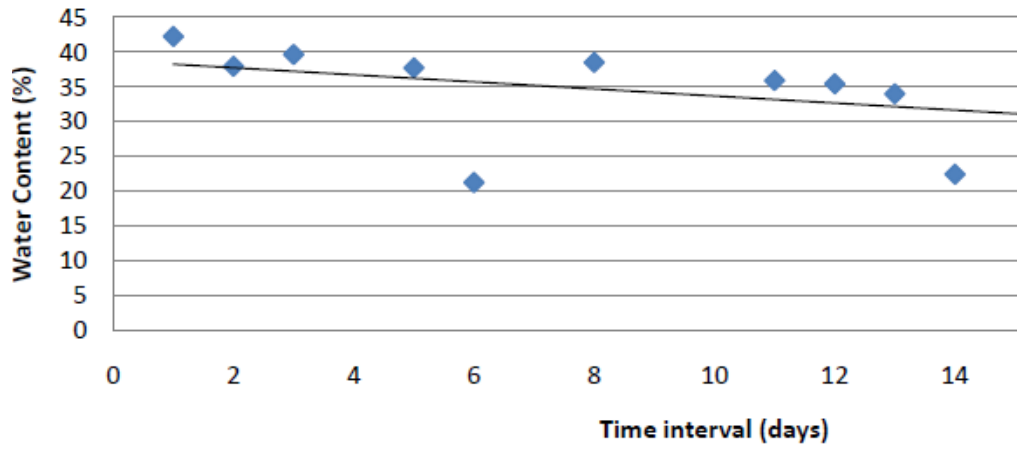


Figure B.2.2 Çayeli 4.5% binder: rate of water removal (GWC) at ambient temperature of 24 °C

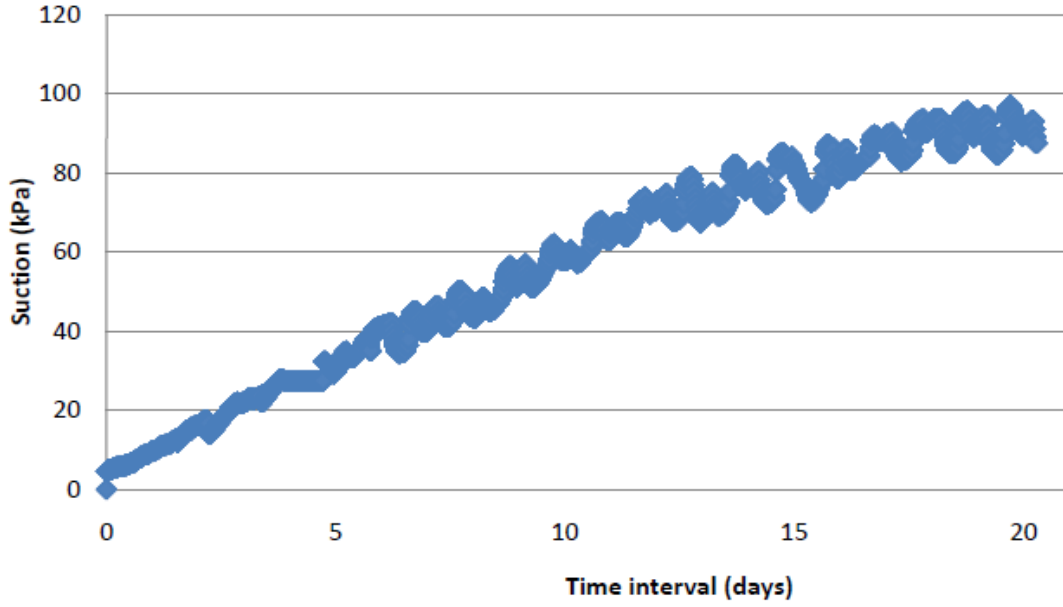


Figure B.2.3 Çayeli 8.5% binder: rate of self-desiccation at ambient temperature of 24 °C

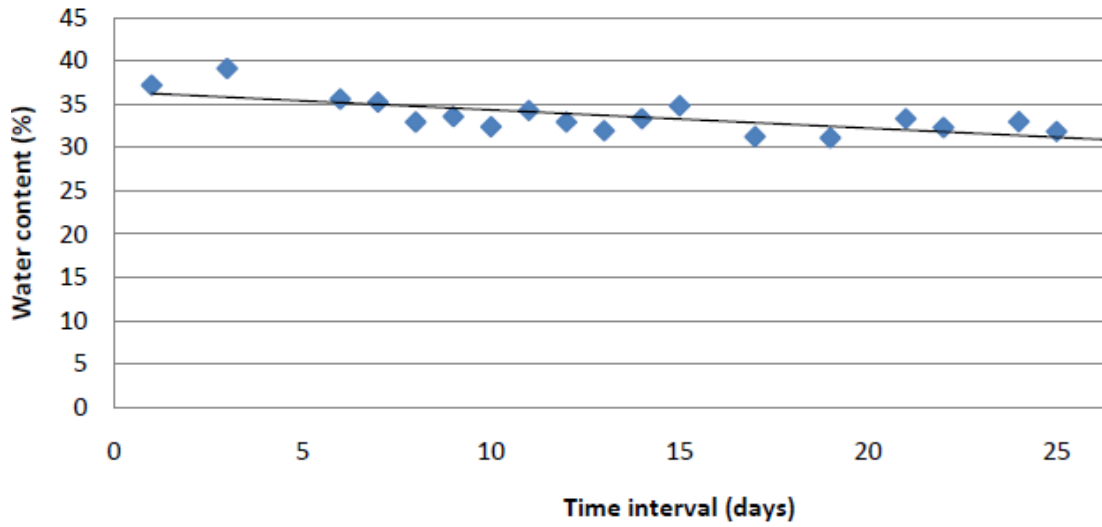


Figure B.2.4 Çayeli 8.5% binder: rate of water removal at ambient temperature of 24 °C

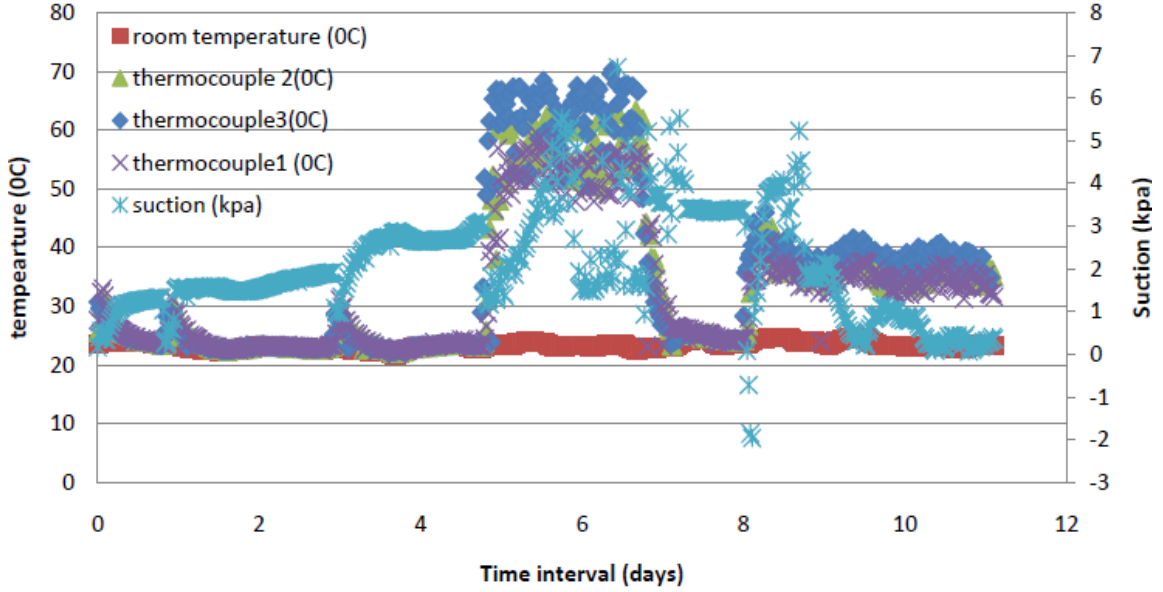


Figure B.2.5 Çayeli 4.5% binder: rate of self-desiccation at an external temperature of 40°C

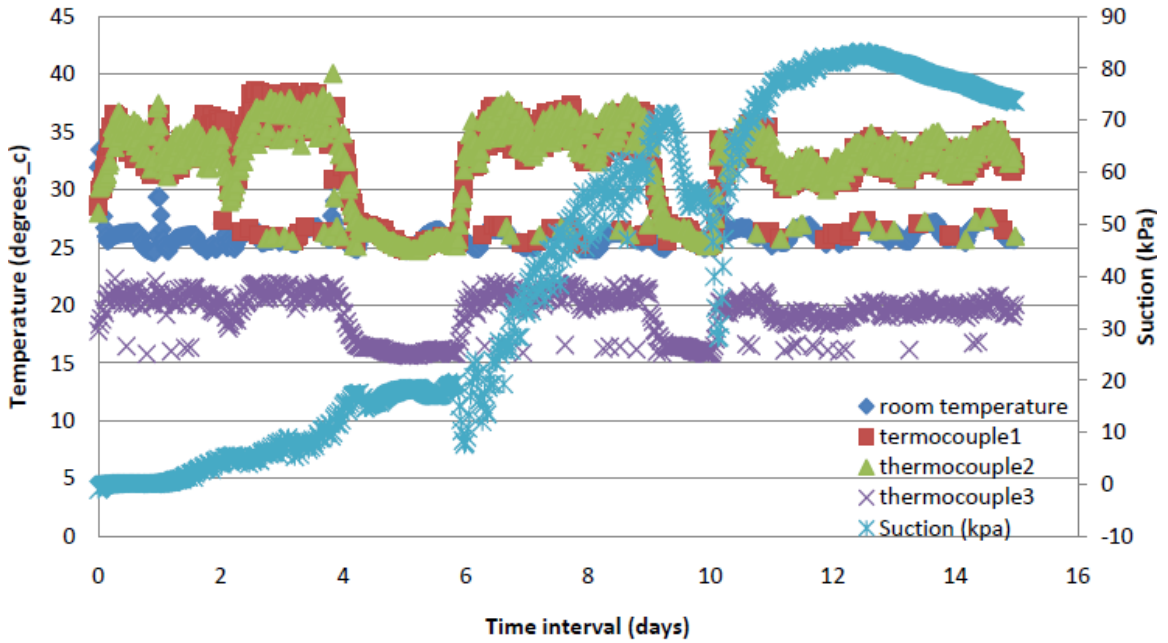


Figure B.2.5 Çayeli 8.5% binder: rate of self-desiccation at an external temperature of 40°C

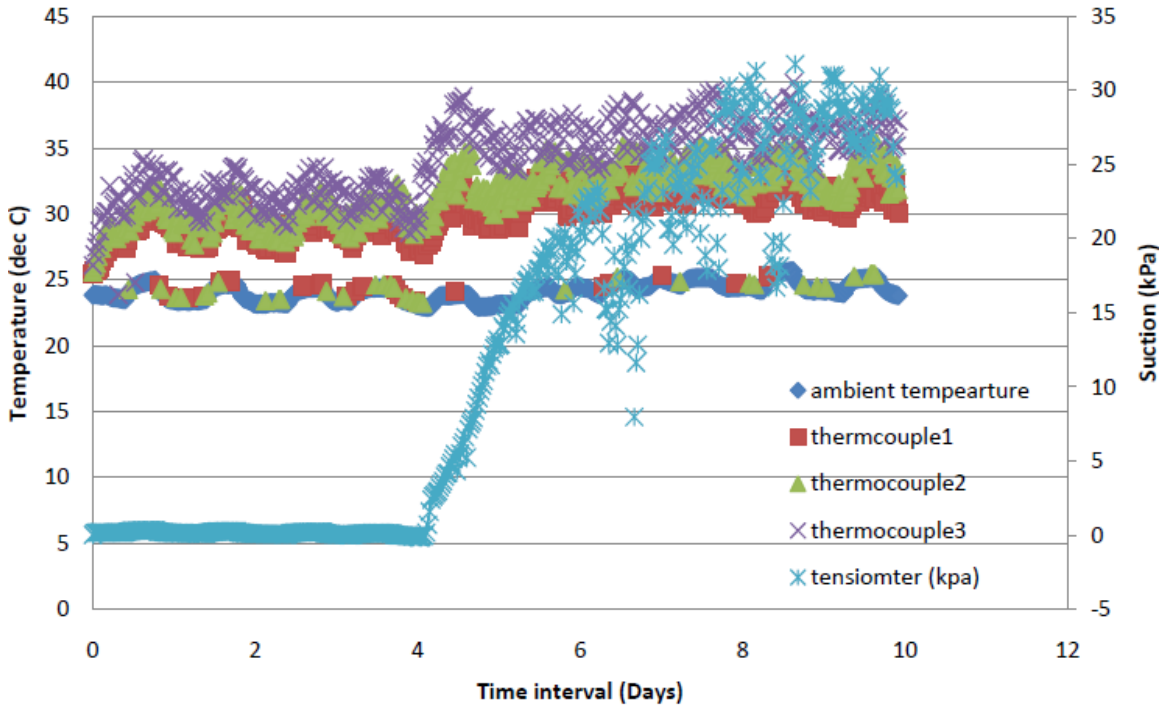


Figure B.2.6 Çayeli 8.5% binder: rate of self-desiccation at an external temperature of 50°C

B.3 PRE- AND POST- WATER-RETENTION CURVE

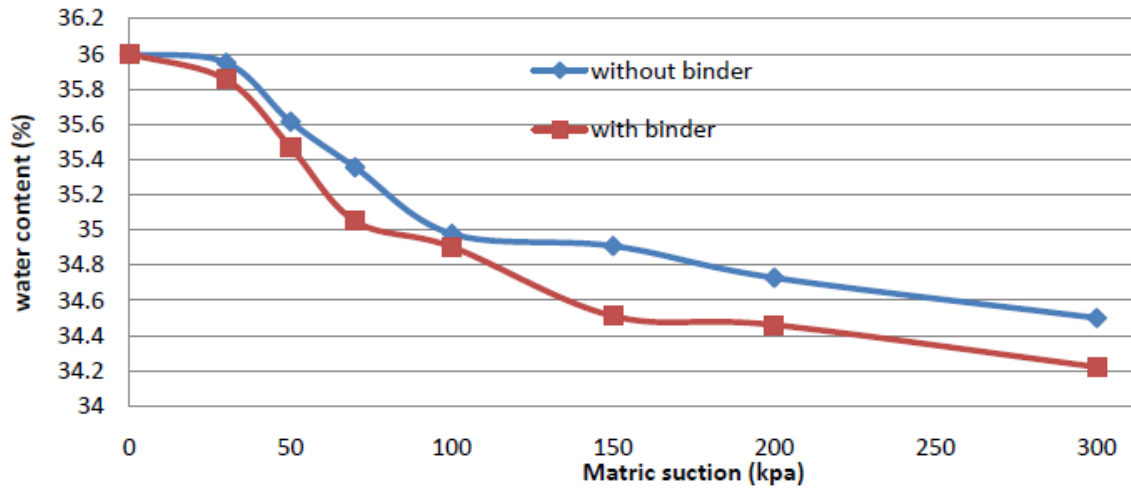


Figure B.3.1 Çayeli pre- and post- water retention curve containing 4.5% binder (post-hydration)

APPENDIX C – NUMERICAL MODELLING [DATA]

C.1 MODELLING ‘INPUTS’

Table C.1.1 3% binder sink data

Curing Time	Date	m _c	m _{c + CPB}	m _{OD}	m _w	m _s	GWC	Ms'	Mw'	VWC = GWC(ρ _b / ρ _w)	Average time	Sink	Sink	Sink (.15m layer)	Sink (.30m layer)
(day)	(dd-mm-yy)	<i>(RE ± 0.05 g)</i>					(%)	<i>(kg)</i>		<i>(m³/m³)</i>		<i>per day</i>	<i>per day</i>	<i>m/day</i>	<i>m/day</i>
0	3-Mar-10	2.1	16.1	12.4	3.7	10.3	0.359	121.68	43.71	0.486	0.000	0.022	-0.0217	-0.0033	0.0065
1	4-Mar-10	2.1	15.8	12.3	3.5	10.2	0.343	123.13	42.25	0.464	0.500	0.022	-0.0217	-0.0033	0.0065
4	18-Mar-10	2.1	24.9	19.4	5.5	17.3	0.318	125.49	39.90	0.430	2.476	0.012	-0.0116	-0.0017	0.0035
5	19-Mar-10	2.1	19.2	15.1	4.1	13.0	0.315	125.73	39.65	0.426	4.403	0.004	-0.0038	-0.0006	0.0011
6	20-Mar-10	2.1	15.5	12.3	3.2	10.2	0.314	125.89	39.50	0.424	5.354	0.002	-0.0022	-0.0003	0.0007
7	21-Mar-10	2.1	12.0	9.6	2.4	7.5	0.313	125.93	39.46	0.424	6.323	0.001	-0.0006	-0.0001	0.0002
11	14-Mar-10	2.1	20.9	16.4	4.5	14.3	0.313	125.97	39.41	0.423	8.917	0.000	-0.0001	0.0000	0.0000
12	15-Mar-10	2.1	18.5	14.6	3.9	12.5	0.312	126.06	39.33	0.422	11.474	0.001	-0.0014	-0.0002	0.0004
13	16-Mar-10	2.0	13.8	11.0	2.8	9.0	0.311	126.14	39.24	0.421	12.345	0.001	-0.0014	-0.0002	0.0004
14	17-Mar-10	2.1	17.3	13.7	3.6	11.6	0.310	126.22	39.17	0.420	13.316	0.001	-0.0010	-0.0001	0.0003
15	18-Mar-10	2.1	13.5	10.8	2.7	8.7	0.310	126.22	39.17	0.420	14.399	0.000	0.0000	0.0000	0.0000
16	19-Mar-10	2.1	20.6	16.2	4.4	14.1	0.309	126.32	39.06	0.418	15.403	0.002	-0.0017	-0.0003	0.0005
17	20-Mar-10	2.1	10.7	8.7	2.0	6.6	0.309	126.34	39.05	0.418	16.354	0.000	-0.0002	0.0000	0.0001
18	21-Mar-10	2.1	19.4	15.3	4.1	13.2	0.308	126.41	38.98	0.417	17.323	0.001	-0.0011	-0.0002	0.0003
22	25-Mar-10	2.1	25.0	19.6	5.4	17.5	0.306	126.66	38.72	0.413	19.800	0.001	-0.0009	-0.0001	0.0003
24	27-Mar-10	2.1	23.8	18.7	5.1	16.6	0.305	126.69	38.69	0.413	22.953	0.000	-0.0002	0.0000	0.0001
29	1-Apr-10	2.1	75.7	58.5	17.2	56.4	0.305	126.68	38.70	0.413	26.465	0.000	0.0000	0.0000	0.0000

Table C.1.2 Initial conditions / Final conditions

Modelling Layers	Depth (R1+R2) (m)	Initial Condition (R1) (m)	Final Condition (R1) (m)	Initial Condition (R2) (m)
Plug	0.142	0.008	-10.98	N/A
Main_1	0.430	0.012	10.92	-10.98
Main_2	0.718	0.012	-9.72	-10.92
Main_3	1.006	0.012	-9.17	-9.72

Table C.1.3 Plug layer: experimental drainage rates and bottom boundary condition data

Timestamp <i>mm/dd/yy</i>	Mass of water <i>g</i>	Cumulative outflow <i>m³</i>	Time (days) <i>days</i>	Instantaneous Flux rate <i>m³/day/m²</i>
10/1/2010 7:38	0	0.000000	0.0000	0.0000
10/1/2010 7:41	107.1	-0.000107	0.0021	-0.00460
10/1/2010 7:44	128.6	-0.000129	0.0042	-0.00276
10/1/2010 7:47	149.2	-0.000149	0.0063	-0.00214
10/1/2010 7:50	169.8	-0.000170	0.0084	-0.00183
10/1/2010 7:53	190.4	-0.000190	0.0104	-0.00164
10/1/2010 7:56	212.5	-0.000213	0.0125	-0.00153
10/1/2010 7:59	226.8	-0.000227	0.0146	-0.00140
10/1/2010 8:02	240.2	-0.000240	0.0167	-0.00129
10/1/2010 8:05	253.6	-0.000254	0.0188	-0.00122
10/1/2010 8:08	267.0	-0.000267	0.0209	-0.00115
10/1/2010 8:11	280.4	-0.000280	0.0230	-0.00110
10/1/2010 8:14	293.8	-0.000294	0.0250	-0.00106
10/1/2010 8:17	307.2	-0.000307	0.0271	-0.00102
10/1/2010 8:20	320.6	-0.000321	0.0292	-0.00099
10/1/2010 8:23	334.9	-0.000335	0.0313	-0.00096
10/1/2010 8:26	349.2	-0.000349	0.0334	-0.00094
10/1/2010 8:29	363.5	-0.000364	0.0355	-0.00092
10/1/2010 8:32	375.3	-0.000375	0.0376	-0.00090
10/1/2010 8:35	389.8	-0.000390	0.0396	-0.00088
10/1/2010 8:38	404.3	-0.000404	0.0417	-0.00087
10/1/2010 8:41	418.8	-0.000419	0.0438	-0.00086
10/1/2010 8:44	433.3	-0.000433	0.0459	-0.00085
10/1/2010 8:47	447.8	-0.000448	0.0480	-0.00084
10/1/2010 8:50	462.3	-0.000462	0.0501	-0.00083

10/1/2010 8:53	476.8	-0.000477	0.0522	-0.00082
10/1/2010 8:56	491.3	-0.000491	0.0542	-0.00082
10/1/2010 8:59	505.8	-0.000506	0.0563	-0.00081
10/1/2010 9:02	520.3	-0.000520	0.0584	-0.00080
10/1/2010 9:05	534.8	-0.000535	0.0605	-0.00080
10/1/2010 9:08	549.5	-0.000550	0.0626	-0.00079
10/1/2010 9:12	555.8	-0.000556	0.0647	-0.00077
10/1/2010 9:15	562.1	-0.000562	0.0668	-0.00076
10/1/2010 9:18	568.4	-0.000568	0.0688	-0.00074
10/1/2010 9:21	574.7	-0.000575	0.0709	-0.00073
10/1/2010 9:24	581.0	-0.000581	0.0730	-0.00072
10/1/2010 9:27	587.3	-0.000587	0.0751	-0.00070
10/1/2010 9:30	593.6	-0.000594	0.0772	-0.00069
10/1/2010 9:33	599.9	-0.000600	0.0793	-0.00068
10/1/2010 9:36	606.2	-0.000606	0.0814	-0.00067
10/1/2010 9:39	612.5	-0.000613	0.0834	-0.00066
10/1/2010 9:42	618.8	-0.000619	0.0855	-0.00065
10/1/2010 9:45	625.1	-0.000625	0.0876	-0.00064
10/1/2010 9:48	631.4	-0.000631	0.0897	-0.00063
10/1/2010 9:51	637.7	-0.000638	0.0918	-0.00063
10/1/2010 9:54	644.0	-0.000644	0.0939	-0.00062
10/1/2010 9:57	650.3	-0.000650	0.0960	-0.00061
10/1/2010 10:00	656.6	-0.000657	0.0980	-0.00060
10/1/2010 10:03	662.9	-0.000663	0.1001	-0.00060
10/1/2010 10:06	669.2	-0.000669	0.1022	-0.00059
10/1/2010 10:09	675.5	-0.000676	0.1043	-0.00058
10/1/2010 10:12	681.8	-0.000682	0.1064	-0.00058
10/1/2010 10:15	688.1	-0.000688	0.1085	-0.00057
10/1/2010 10:18	694.4	-0.000694	0.1106	-0.00057
10/1/2010 10:21	700.0	-0.000700	0.1126	-0.00056
10/1/2010 10:24	706.0	-0.000706	0.1147	-0.00055
10/1/2010 10:27	711.6	-0.000712	0.1168	-0.00055
10/1/2010 10:30	717.0	-0.000717	0.1189	-0.00054
10/1/2010 10:33	722.6	-0.000723	0.1210	-0.00054
10/1/2010 10:36	727.9	-0.000728	0.1231	-0.00053
10/1/2010 10:39	733.4	-0.000733	0.1252	-0.00053
10/1/2010 10:42	738.7	-0.000739	0.1272	-0.00052
10/1/2010 10:45	743.8	-0.000744	0.1293	-0.00052
10/1/2010 10:48	748.7	-0.000749	0.1314	-0.00051
10/1/2010 10:51	753.4	-0.000753	0.1335	-0.00051

10/1/2010 10:54	758.1	-0.000758	0.1356	-0.00050
10/1/2010 10:57	762.8	-0.000763	0.1377	-0.00050
10/1/2010 11:00	767.0	-0.000767	0.1397	-0.00049
10/1/2010 11:03	771.0	-0.000771	0.1418	-0.00049
10/1/2010 11:06	774.9	-0.000775	0.1439	-0.00048
10/1/2010 11:09	778.6	-0.000779	0.1460	-0.00048
10/1/2010 11:12	781.8	-0.000782	0.1481	-0.00048
10/1/2010 11:15	784.8	-0.000785	0.1502	-0.00047
10/1/2010 11:18	787.5	-0.000788	0.1523	-0.00047
10/1/2010 11:21	789.8	-0.000790	0.1543	-0.00046
10/1/2010 11:24	792.0	-0.000792	0.1564	-0.00046
10/1/2010 11:27	793.5	-0.000794	0.1585	-0.00045
10/1/2010 11:30	795.2	-0.000795	0.1606	-0.00045
10/1/2010 11:33	796.8	-0.000797	0.1627	-0.00044
10/1/2010 11:36	797.8	-0.000798	0.1648	-0.00044
10/1/2010 11:39	798.5	-0.000799	0.1669	-0.00043
10/1/2010 11:42	798.9	-0.000799	0.1689	-0.00043
10/1/2010 11:45	799.4	-0.000799	0.1710	-0.00042
10/1/2010 11:48	799.8	-0.000800	0.1731	-0.00042
10/1/2010 11:51	800.0	-0.000800	0.1752	-0.00041
10/1/2010 11:54	800.2	-0.000800	0.1773	-0.00041
10/1/2010 11:57	800.2	-0.000800	0.1794	-0.00040
10/1/2010 12:00	800.2	-0.000800	0.1814	-0.00040
10/1/2010 12:03	800.3	-0.000800	0.1835	-0.00039
10/1/2010 12:06	800.5	-0.000801	0.1856	-0.00039
10/1/2010 12:09	800.5	-0.000801	0.1877	-0.00038
10/1/2010 12:12	800.5	-0.000801	0.1898	-0.00038
10/1/2010 12:15	800.5	-0.000801	0.1919	-0.00038
10/1/2010 12:18	800.5	-0.000801	0.1946	-0.00037

Table C.1.4 Main_1 layer: experimental drainage rates and bottom boundary condition data

Timestamp	Mass of water	Cumulative outflow	Time (days)	Instantaneous Flux rate
<i>mm/dd/yy</i>	<i>g</i>	<i>m³</i>	<i>days</i>	<i>m³/day/m²</i>
10/21/2010 23:41	0	0.000000	0.0000	0.00000
NA	35.2	-0.000035	0.0021	-0.00151
NA	69.5	-0.000070	0.0042	-0.00149
NA	102.9	-0.000103	0.0063	-0.00148

NA	135.4	-0.000135	0.0084	-0.00146
NA	167.2	-0.000167	0.0104	-0.00144
NA	198.2	-0.000198	0.0125	-0.00142
NA	228.4	-0.000228	0.0146	-0.00141
NA	258.1	-0.000258	0.0167	-0.00139
NA	286.8	-0.000287	0.0188	-0.00137
NA	314.9	-0.000315	0.0209	-0.00136
NA	342.2	-0.000342	0.0230	-0.00134
NA	368.8	-0.000369	0.0250	-0.00133
NA	394.9	-0.000395	0.0271	-0.00131
NA	420.1	-0.000420	0.0292	-0.00129
NA	444.7	-0.000445	0.0313	-0.00128
NA	468.7	-0.000469	0.0334	-0.00126
NA	492.1	-0.000492	0.0355	-0.00125
NA	514.8	-0.000515	0.0376	-0.00123
NA	536.9	-0.000537	0.0396	-0.00122
NA	558.4	-0.000558	0.0417	-0.00120
NA	579.3	-0.000579	0.0438	-0.00119
NA	599.6	-0.000600	0.0459	-0.00118
NA	619.5	-0.000619	0.0480	-0.00116
NA	638.6	-0.000639	0.0501	-0.00115
NA	657.3	-0.000657	0.0522	-0.00113
NA	675.4	-0.000675	0.0542	-0.00112
NA	693.1	-0.000693	0.0563	-0.00111
NA	710.2	-0.000710	0.0584	-0.00109
NA	726.8	-0.000727	0.0605	-0.00108
NA	742.8	-0.000743	0.0626	-0.00107
NA	758.5	-0.000759	0.0647	-0.00106
NA	773.7	-0.000774	0.0668	-0.00104
NA	788.3	-0.000788	0.0688	-0.00103
NA	802.6	-0.000803	0.0709	-0.00102
NA	816.4	-0.000816	0.0730	-0.00101
NA	829.8	-0.000830	0.0751	-0.00099
NA	842.7	-0.000843	0.0772	-0.00098
NA	855.2	-0.000855	0.0793	-0.00097
NA	867.4	-0.000867	0.0814	-0.00096
NA	879.1	-0.000879	0.0834	-0.00095
NA	890.5	-0.000890	0.0855	-0.00094
NA	901.5	-0.000901	0.0876	-0.00093
NA	912.1	-0.000912	0.0897	-0.00092

NA	922.3	-0.000922	0.0918	-0.00090
NA	932.3	-0.000932	0.0939	-0.00089
NA	941.8	-0.000942	0.0960	-0.00088
NA	951.0	-0.000951	0.0980	-0.00087
NA	960.0	-0.000960	0.1001	-0.00086
NA	968.5	-0.000969	0.1022	-0.00085
NA	976.8	-0.000977	0.1043	-0.00084
NA	984.9	-0.000985	0.1064	-0.00083
NA	992.6	-0.000993	0.1085	-0.00082
NA	1000.0	-0.001000	0.1106	-0.00081
NA	1007.1	-0.001007	0.1126	-0.00080
NA	1014.0	-0.001014	0.1147	-0.00080
NA	1020.6	-0.001021	0.1168	-0.00079
NA	1027.0	-0.001027	0.1189	-0.00078
NA	1033.2	-0.001033	0.1210	-0.00077
NA	1039.0	-0.001039	0.1231	-0.00076
NA	1044.7	-0.001045	0.1252	-0.00075
NA	1050.1	-0.001050	0.1272	-0.00074
NA	1055.3	-0.001055	0.1293	-0.00073
NA	1060.3	-0.001060	0.1314	-0.00073
NA	1065.2	-0.001065	0.1335	-0.00072
NA	1069.8	-0.001070	0.1356	-0.00071
NA	1074.2	-0.001074	0.1377	-0.00070
NA	1078.4	-0.001078	0.1397	-0.00069
NA	1082.4	-0.001082	0.1418	-0.00069
NA	1086.3	-0.001086	0.1439	-0.00068
NA	1090.0	-0.001090	0.1460	-0.00067
NA	1093.6	-0.001094	0.1481	-0.00066
NA	1097.0	-0.001097	0.1502	-0.00066
NA	1100.2	-0.001100	0.1523	-0.00065
NA	1103.3	-0.001103	0.1543	-0.00064
NA	1106.3	-0.001106	0.1564	-0.00064
NA	1109.1	-0.001109	0.1585	-0.00063
NA	1111.8	-0.001112	0.1606	-0.00062
NA	1114.4	-0.001114	0.1627	-0.00062
NA	1116.8	-0.001117	0.1648	-0.00061
NA	1119.2	-0.001119	0.1669	-0.00060
NA	1121.4	-0.001121	0.1689	-0.00060
NA	1123.5	-0.001124	0.1710	-0.00059
NA	1125.6	-0.001126	0.1731	-0.00059

NA	1127.5	-0.001127	0.1752	-0.00058
NA	1129.3	-0.001129	0.1773	-0.00057
NA	1131.1	-0.001131	0.1794	-0.00057
NA	1132.7	-0.001133	0.1814	-0.00056
NA	1134.3	-0.001134	0.1835	-0.00056
NA	1135.8	-0.001136	0.1856	-0.00055
NA	1137.2	-0.001137	0.1877	-0.00055
NA	1138.6	-0.001139	0.1898	-0.00054
NA	1139.9	-0.001140	0.1919	-0.00053
NA	1141.1	-0.001141	0.1940	-0.00053
NA	1142.3	-0.001142	0.1961	-0.00052
NA	1143.4	-0.001143	0.1982	-0.00052
NA	1144.4	-0.001144	0.2003	-0.00051
NA	1145.4	-0.001145	0.2023	-0.00051
NA	1146.4	-0.001146	0.2044	-0.00050
NA	1147.3	-0.001147	0.2065	-0.00050
NA	1148.2	-0.001148	0.2086	-0.00050
NA	1149.0	-0.001149	0.2107	-0.00049
NA	1149.8	-0.001150	0.2128	-0.00049
NA	1150.5	-0.001151	0.2149	-0.00048
NA	1151.2	-0.001151	0.2170	-0.00048
NA	1151.9	-0.001152	0.2191	-0.00047
NA	1152.5	-0.001153	0.2212	-0.00047
10/21/2010 23:44	1159.4	-0.001159	0.2917	-0.00036

Table C.1.5 Main_2 layer: experimental drainage rates and bottom boundary condition data

Timestamp	Mass of water	Cumulative outflow	Time (days)	Instantaneous Flux rate
<i>mm/dd/yy</i>	<i>g</i>	<i>m³</i>	<i>days</i>	<i>m³/day/m²</i>
11/19/2010 1:47	0	0.000000	0.0000	0.0000
11/19/2010 1:48	0.2	0.000000	0.0007	-0.00003
11/19/2010 1:49	3.7	-0.000004	0.0014	-0.00024
11/19/2010 1:50	7.2	-0.000007	0.0021	-0.00031
11/19/2010 1:51	10.7	-0.000011	0.0028	-0.00035
11/19/2010 1:52	14.1	-0.000014	0.0035	-0.00036
11/19/2010 1:53	17.6	-0.000018	0.0042	-0.00038
11/19/2010 1:54	20.8	-0.000021	0.0049	-0.00038
11/19/2010 1:55	23.8	-0.000024	0.0056	-0.00038
11/19/2010 1:56	27	-0.000027	0.0063	-0.00039

11/19/2010 1:57	30.2	-0.000030	0.0070	-0.00039
11/19/2010 1:58	33.4	-0.000033	0.0077	-0.00039
11/19/2010 1:59	36.6	-0.000037	0.0084	-0.00039
11/19/2010 2:00	39.7	-0.000040	0.0091	-0.00039
11/19/2010 2:01	42.9	-0.000043	0.0098	-0.00040
11/19/2010 2:02	46	-0.000046	0.0105	-0.00040
11/19/2010 2:03	49.1	-0.000049	0.0112	-0.00040
11/19/2010 2:04	52.1	-0.000052	0.0119	-0.00040
11/19/2010 2:05	55.1	-0.000055	0.0125	-0.00040
11/19/2010 2:06	58	-0.000058	0.0132	-0.00039
11/19/2010 2:07	61	-0.000061	0.0139	-0.00039
11/19/2010 2:08	63.9	-0.000064	0.0146	-0.00039
11/19/2010 2:09	66.8	-0.000067	0.0153	-0.00039
11/19/2010 2:10	69.7	-0.000070	0.0160	-0.00039
11/19/2010 2:11	72.5	-0.000073	0.0167	-0.00039
11/19/2010 2:12	75.4	-0.000075	0.0174	-0.00039
11/19/2010 2:13	78.2	-0.000078	0.0181	-0.00039
11/19/2010 2:14	81	-0.000081	0.0188	-0.00039
11/19/2010 2:15	83.7	-0.000084	0.0195	-0.00039
11/19/2010 2:16	86.4	-0.000086	0.0202	-0.00038
11/19/2010 2:17	89	-0.000089	0.0209	-0.00038
11/19/2010 2:18	91.7	-0.000092	0.0216	-0.00038
11/19/2010 2:19	94.4	-0.000094	0.0223	-0.00038
11/19/2010 2:20	97.1	-0.000097	0.0230	-0.00038
11/19/2010 2:21	99.7	-0.000100	0.0237	-0.00038
11/19/2010 2:22	102.4	-0.000102	0.0244	-0.00038
11/19/2010 2:23	104.9	-0.000105	0.0251	-0.00038
11/19/2010 2:24	107.5	-0.000108	0.0258	-0.00038
11/19/2010 2:25	110.2	-0.000110	0.0265	-0.00037
11/19/2010 2:26	113	-0.000113	0.0272	-0.00037
11/19/2010 2:27	115.7	-0.000116	0.0279	-0.00037
11/19/2010 2:28	118.2	-0.000118	0.0286	-0.00037
11/19/2010 2:29	120.8	-0.000121	0.0293	-0.00037
11/19/2010 2:30	123.2	-0.000123	0.0300	-0.00037
11/19/2010 2:31	125.5	-0.000126	0.0307	-0.00037
11/19/2010 2:32	127.7	-0.000128	0.0314	-0.00037
11/19/2010 2:33	130	-0.000130	0.0321	-0.00036
11/19/2010 2:34	132.4	-0.000132	0.0328	-0.00036
11/19/2010 2:35	134.7	-0.000135	0.0335	-0.00036
11/19/2010 2:36	137	-0.000137	0.0342	-0.00036

11/19/2010 2:37	139.4	-0.000139	0.0349	-0.00036
11/19/2010 2:38	141.8	-0.000142	0.0356	-0.00036
11/19/2010 2:39	144.1	-0.000144	0.0362	-0.00036
11/19/2010 2:40	146.3	-0.000146	0.0369	-0.00036
11/19/2010 2:41	148.5	-0.000149	0.0377	-0.00035
11/19/2010 2:42	150.7	-0.000151	0.0383	-0.00035
11/19/2010 2:43	152.9	-0.000153	0.0390	-0.00035
11/19/2010 2:44	155.1	-0.000155	0.0397	-0.00035
11/19/2010 2:45	157.1	-0.000157	0.0404	-0.00035
11/19/2010 2:46	159.3	-0.000159	0.0411	-0.00035
11/19/2010 2:47	161.5	-0.000162	0.0418	-0.00035
11/19/2010 2:48	163.5	-0.000164	0.0425	-0.00035
11/19/2010 2:49	165.6	-0.000166	0.0432	-0.00034
11/19/2010 2:50	167.7	-0.000168	0.0439	-0.00034
11/19/2010 2:51	169.8	-0.000170	0.0446	-0.00034
11/19/2010 2:52	171.8	-0.000172	0.0453	-0.00034
11/19/2010 2:53	173.9	-0.000174	0.0460	-0.00034
11/19/2010 2:54	175.9	-0.000176	0.0467	-0.00034
11/19/2010 2:55	177.9	-0.000178	0.0474	-0.00034
11/19/2010 2:56	179.9	-0.000180	0.0481	-0.00034
11/19/2010 2:57	181.8	-0.000182	0.0488	-0.00034
11/19/2010 2:58	183.8	-0.000184	0.0495	-0.00033
11/19/2010 2:59	185.8	-0.000186	0.0502	-0.00033
11/19/2010 3:00	187.7	-0.000188	0.0509	-0.00033
11/19/2010 3:01	189.7	-0.000190	0.0516	-0.00033
11/19/2010 3:02	191.5	-0.000192	0.0523	-0.00033
11/19/2010 3:03	193.5	-0.000194	0.0530	-0.00033
11/19/2010 3:04	195.3	-0.000195	0.0537	-0.00033
11/19/2010 3:05	197.1	-0.000197	0.0544	-0.00033
11/19/2010 3:06	199	-0.000199	0.0551	-0.00033
11/19/2010 3:07	200.9	-0.000201	0.0558	-0.00032
11/19/2010 3:08	202.7	-0.000203	0.0565	-0.00032
11/19/2010 3:09	204.9	-0.000205	0.0572	-0.00032
11/19/2010 3:10	206.9	-0.000207	0.0579	-0.00032
11/19/2010 3:11	208.7	-0.000209	0.0586	-0.00032
11/19/2010 3:12	210.5	-0.000211	0.0593	-0.00032
11/19/2010 3:13	212.3	-0.000212	0.0600	-0.00032
11/19/2010 3:14	213.9	-0.000214	0.0606	-0.00032
11/19/2010 3:15	215.4	-0.000215	0.0613	-0.00032
11/19/2010 3:16	217.1	-0.000217	0.0620	-0.00031

11/19/2010 3:17	218.8	-0.000219	0.0627	-0.00031
11/19/2010 3:18	220.6	-0.000221	0.0634	-0.00031
11/19/2010 3:19	222.3	-0.000222	0.0641	-0.00031
11/19/2010 3:20	224	-0.000224	0.0648	-0.00031
11/19/2010 3:21	225.7	-0.000226	0.0655	-0.00031
11/19/2010 3:22	227.3	-0.000227	0.0662	-0.00031
11/19/2010 3:23	229	-0.000229	0.0669	-0.00031
11/19/2010 3:24	230.7	-0.000231	0.0676	-0.00031
11/19/2010 3:25	232.4	-0.000232	0.0683	-0.00031
11/19/2010 3:26	234.1	-0.000234	0.0690	-0.00031
11/19/2010 3:27	235.8	-0.000236	0.0697	-0.00030
11/19/2010 3:28	237.4	-0.000237	0.0704	-0.00030
11/19/2010 3:29	239	-0.000239	0.0711	-0.00030
11/19/2010 3:30	240.6	-0.000241	0.0718	-0.00030
11/19/2010 3:31	242.4	-0.000242	0.0725	-0.00030
11/19/2010 3:32	244.1	-0.000244	0.0732	-0.00030
11/19/2010 3:33	245.6	-0.000246	0.0739	-0.00030
11/19/2010 3:34	247.3	-0.000247	0.0746	-0.00030
11/19/2010 3:35	248.9	-0.000249	0.0753	-0.00030
11/19/2010 3:36	250.5	-0.000251	0.0760	-0.00030
11/19/2010 3:37	252.2	-0.000252	0.0767	-0.00030
11/19/2010 3:38	253.8	-0.000254	0.0774	-0.00030
11/19/2010 3:39	255.4	-0.000255	0.0781	-0.00029
11/19/2010 3:40	257	-0.000257	0.0788	-0.00029
11/19/2010 3:41	258.6	-0.000259	0.0795	-0.00029
11/19/2010 3:42	260.5	-0.000261	0.0802	-0.00029
11/19/2010 3:43	262.2	-0.000262	0.0809	-0.00029
11/19/2010 3:44	263.9	-0.000264	0.0816	-0.00029
11/19/2010 3:45	265.5	-0.000266	0.0823	-0.00029
11/19/2010 3:46	267.2	-0.000267	0.0830	-0.00029
11/19/2010 3:47	268.7	-0.000269	0.0837	-0.00029
11/19/2010 3:48	270.1	-0.000270	0.0844	-0.00029
11/19/2010 3:49	271.5	-0.000272	0.0851	-0.00029
11/19/2010 3:50	273.1	-0.000273	0.0858	-0.00029
11/19/2010 3:51	274.6	-0.000275	0.0865	-0.00029
11/19/2010 3:52	276.2	-0.000276	0.0872	-0.00029
11/19/2010 3:53	277.9	-0.000278	0.0878	-0.00028
11/19/2010 3:54	279.4	-0.000279	0.0885	-0.00028
11/19/2010 3:55	281	-0.000281	0.0892	-0.00028
11/19/2010 3:56	282.6	-0.000283	0.0899	-0.00028

11/19/2010 3:57	284.1	-0.000284	0.0906	-0.00028
11/19/2010 3:58	285.7	-0.000286	0.0913	-0.00028
11/19/2010 3:59	287.3	-0.000287	0.0920	-0.00028
11/19/2010 4:00	288.9	-0.000289	0.0927	-0.00028
11/19/2010 4:01	290.5	-0.000291	0.0934	-0.00028
11/19/2010 4:02	292	-0.000292	0.0941	-0.00028
11/19/2010 4:03	293.6	-0.000294	0.0948	-0.00028
11/19/2010 4:04	295.2	-0.000295	0.0955	-0.00028
11/19/2010 4:05	296.7	-0.000297	0.0962	-0.00028
11/19/2010 4:06	298.2	-0.000298	0.0969	-0.00028
11/19/2010 4:07	299.8	-0.000300	0.0976	-0.00028
11/19/2010 4:08	301.4	-0.000301	0.0983	-0.00028
11/19/2010 4:09	303	-0.000303	0.0990	-0.00028
11/19/2010 4:10	304.6	-0.000305	0.0997	-0.00027
11/19/2010 4:11	306.1	-0.000306	0.1004	-0.00027
11/19/2010 4:12	307.7	-0.000308	0.1011	-0.00027
11/19/2010 4:13	309.2	-0.000309	0.1018	-0.00027
11/19/2010 4:14	310.8	-0.000311	0.1025	-0.00027
11/19/2010 4:15	312.3	-0.000312	0.1032	-0.00027
11/19/2010 4:16	313.9	-0.000314	0.1039	-0.00027
11/19/2010 4:17	315.5	-0.000316	0.1046	-0.00027
11/19/2010 4:18	317.1	-0.000317	0.1053	-0.00027
11/19/2010 4:19	318.7	-0.000319	0.1060	-0.00027
11/19/2010 4:20	320.2	-0.000320	0.1067	-0.00027
11/19/2010 4:21	322	-0.000322	0.1074	-0.00027
11/19/2010 4:22	323.7	-0.000324	0.1081	-0.00027
11/19/2010 4:23	325.2	-0.000325	0.1088	-0.00027
11/19/2010 4:24	326.8	-0.000327	0.1095	-0.00027
11/19/2010 4:25	328.4	-0.000328	0.1102	-0.00027
11/19/2010 4:26	330	-0.000330	0.1109	-0.00027
11/19/2010 4:27	331.3	-0.000331	0.1116	-0.00027
11/19/2010 4:28	332.6	-0.000333	0.1123	-0.00027
11/19/2010 4:29	334.1	-0.000334	0.1130	-0.00027
11/19/2010 4:30	335.6	-0.000336	0.1137	-0.00027
11/19/2010 4:31	337.1	-0.000337	0.1144	-0.00027
11/19/2010 4:32	338.5	-0.000339	0.1151	-0.00026
11/19/2010 4:33	340	-0.000340	0.1158	-0.00026
11/19/2010 4:34	341.4	-0.000341	0.1164	-0.00026
11/19/2010 4:35	342.9	-0.000343	0.1171	-0.00026
11/19/2010 4:36	344.3	-0.000344	0.1178	-0.00026

11/19/2010 4:37	345.8	-0.000346	0.1185	-0.00026
11/19/2010 4:38	347.2	-0.000347	0.1192	-0.00026
11/19/2010 4:39	348.7	-0.000349	0.1199	-0.00026
11/19/2010 4:40	350.2	-0.000350	0.1206	-0.00026
11/19/2010 4:41	351.6	-0.000352	0.1213	-0.00026
11/19/2010 4:42	353.1	-0.000353	0.1220	-0.00026
11/19/2010 4:43	354.5	-0.000355	0.1227	-0.00026
11/19/2010 4:44	356	-0.000356	0.1234	-0.00026
11/19/2010 4:45	357.5	-0.000358	0.1241	-0.00026
11/19/2010 4:46	359	-0.000359	0.1248	-0.00026
11/19/2010 4:47	360.5	-0.000361	0.1255	-0.00026
11/19/2010 4:48	362	-0.000362	0.1262	-0.00026
11/19/2010 4:49	363.5	-0.000364	0.1269	-0.00026
11/19/2010 4:50	365	-0.000365	0.1276	-0.00026
11/19/2010 4:51	366.5	-0.000367	0.1283	-0.00026
11/19/2010 4:52	368	-0.000368	0.1290	-0.00026
11/19/2010 4:54	369.4	-0.000369	0.1297	-0.00026
11/19/2010 4:55	370.9	-0.000371	0.1304	-0.00026
11/19/2010 4:56	372.4	-0.000372	0.1311	-0.00026
11/19/2010 4:57	373.7	-0.000374	0.1318	-0.00026
11/19/2010 4:58	375.2	-0.000375	0.1325	-0.00025
11/19/2010 4:59	376.7	-0.000377	0.1332	-0.00025
11/19/2010 5:00	378.1	-0.000378	0.1339	-0.00025
11/19/2010 5:01	379.5	-0.000380	0.1346	-0.00025
11/19/2010 5:02	380.9	-0.000381	0.1353	-0.00025
11/19/2010 5:03	382.3	-0.000382	0.1360	-0.00025
11/19/2010 5:04	383.6	-0.000384	0.1367	-0.00025
11/19/2010 5:05	385	-0.000385	0.1374	-0.00025
11/19/2010 5:06	386.4	-0.000386	0.1381	-0.00025
11/19/2010 5:07	388	-0.000388	0.1387	-0.00025
11/19/2010 5:08	389.7	-0.000390	0.1395	-0.00025
11/19/2010 5:09	391.2	-0.000391	0.1402	-0.00025
11/19/2010 5:10	392.7	-0.000393	0.1408	-0.00025
11/19/2010 5:11	394.1	-0.000394	0.1416	-0.00025
11/19/2010 5:12	395.5	-0.000396	0.1422	-0.00025
11/19/2010 5:13	396.8	-0.000397	0.1429	-0.00025
11/19/2010 5:14	398.1	-0.000398	0.1436	-0.00025
11/19/2010 5:15	399.4	-0.000399	0.1443	-0.00025
11/19/2010 5:16	400.7	-0.000401	0.1450	-0.00025
11/19/2010 5:17	402.2	-0.000402	0.1457	-0.00025

11/19/2010 5:18	403.5	-0.000404	0.1464	-0.00025
11/19/2010 5:19	404.9	-0.000405	0.1471	-0.00025
11/19/2010 5:20	406.2	-0.000406	0.1478	-0.00025
11/19/2010 5:21	407.6	-0.000408	0.1485	-0.00025
11/19/2010 5:22	409	-0.000409	0.1492	-0.00025
11/19/2010 5:23	410.3	-0.000410	0.1499	-0.00025
11/19/2010 5:24	411.8	-0.000412	0.1506	-0.00025
11/19/2010 5:25	413.2	-0.000413	0.1513	-0.00025
11/19/2010 5:26	414.6	-0.000415	0.1520	-0.00025
11/19/2010 5:27	416	-0.000416	0.1527	-0.00025
11/19/2010 5:28	417.3	-0.000417	0.1534	-0.00024
11/19/2010 5:29	418.7	-0.000419	0.1541	-0.00024
11/19/2010 5:30	420.1	-0.000420	0.1548	-0.00024
11/19/2010 5:31	421.6	-0.000422	0.1555	-0.00024
11/19/2010 5:32	423	-0.000423	0.1562	-0.00024
11/19/2010 5:33	424.4	-0.000424	0.1569	-0.00024
11/19/2010 5:34	425.7	-0.000426	0.1576	-0.00024
11/19/2010 5:35	427.1	-0.000427	0.1583	-0.00024
11/19/2010 5:36	428.4	-0.000428	0.1590	-0.00024
11/19/2010 5:37	429.8	-0.000430	0.1597	-0.00024
11/19/2010 5:38	431.3	-0.000431	0.1604	-0.00024
11/19/2010 5:39	432.6	-0.000433	0.1611	-0.00024
11/19/2010 5:40	434	-0.000434	0.1618	-0.00024
11/19/2010 5:41	435.4	-0.000435	0.1625	-0.00024
11/19/2010 5:42	436.7	-0.000437	0.1632	-0.00024
11/19/2010 5:43	438.1	-0.000438	0.1639	-0.00024
11/19/2010 5:44	439.5	-0.000440	0.1645	-0.00024
11/19/2010 5:45	440.9	-0.000441	0.1653	-0.00024
11/19/2010 5:46	442.3	-0.000442	0.1659	-0.00024
11/19/2010 5:47	443.8	-0.000444	0.1666	-0.00024
11/19/2010 5:48	445.3	-0.000445	0.1673	-0.00024
11/19/2010 5:49	446.7	-0.000447	0.1680	-0.00024
11/19/2010 5:50	448.1	-0.000448	0.1687	-0.00024
11/19/2010 5:51	449.5	-0.000450	0.1694	-0.00024
11/19/2010 5:52	450.9	-0.000451	0.1701	-0.00024
11/19/2010 5:53	452	-0.000452	0.1708	-0.00024
11/19/2010 5:54	453.3	-0.000453	0.1715	-0.00024
11/19/2010 5:55	454.5	-0.000455	0.1722	-0.00024
11/19/2010 5:56	455.9	-0.000456	0.1729	-0.00024
11/19/2010 5:57	457.2	-0.000457	0.1736	-0.00024

11/19/2010 5:58	458.5	-0.000459	0.1743	-0.00024
11/19/2010 5:59	459.9	-0.000460	0.1750	-0.00024
11/19/2010 6:00	461.1	-0.000461	0.1757	-0.00024
11/19/2010 6:01	462.5	-0.000463	0.1764	-0.00024
11/19/2010 6:02	463.8	-0.000464	0.1771	-0.00024
11/19/2010 6:03	465.1	-0.000465	0.1778	-0.00024
11/19/2010 6:04	466.4	-0.000466	0.1785	-0.00024
11/19/2010 6:05	467.7	-0.000468	0.1792	-0.00023
11/19/2010 6:06	469	-0.000469	0.1799	-0.00023
11/19/2010 6:07	470.3	-0.000470	0.1806	-0.00023
11/19/2010 6:08	471.6	-0.000472	0.1813	-0.00023
11/19/2010 6:09	472.8	-0.000473	0.1820	-0.00023
11/19/2010 6:10	474.1	-0.000474	0.1827	-0.00023
11/19/2010 6:11	475.4	-0.000475	0.1834	-0.00023
11/19/2010 6:12	476.6	-0.000477	0.1841	-0.00023
11/19/2010 6:13	477.8	-0.000478	0.1848	-0.00023
11/19/2010 6:14	479.1	-0.000479	0.1855	-0.00023
11/19/2010 6:15	480.2	-0.000480	0.1862	-0.00023
11/19/2010 6:16	481.5	-0.000482	0.1869	-0.00023
11/19/2010 6:17	482.7	-0.000483	0.1876	-0.00023
11/19/2010 6:18	483.9	-0.000484	0.1883	-0.00023
11/19/2010 6:19	485	-0.000485	0.1889	-0.00023
11/19/2010 6:20	486.2	-0.000486	0.1897	-0.00023
11/19/2010 6:21	487.3	-0.000487	0.1903	-0.00023
11/19/2010 6:22	488.5	-0.000489	0.1910	-0.00023
11/19/2010 6:23	489.6	-0.000490	0.1917	-0.00023
11/19/2010 6:24	490.6	-0.000491	0.1924	-0.00023
11/19/2010 6:25	491.8	-0.000492	0.1931	-0.00023
11/19/2010 6:26	493.1	-0.000493	0.1938	-0.00023
11/19/2010 6:27	494.2	-0.000494	0.1945	-0.00023
11/19/2010 6:28	495.2	-0.000495	0.1952	-0.00023
11/19/2010 6:29	496.2	-0.000496	0.1959	-0.00023
11/19/2010 6:30	497.2	-0.000497	0.1966	-0.00023
11/19/2010 6:31	498	-0.000498	0.1973	-0.00023
11/19/2010 6:32	498.8	-0.000499	0.1980	-0.00023
11/19/2010 6:33	499.7	-0.000500	0.1987	-0.00023
11/19/2010 6:34	500.6	-0.000501	0.1994	-0.00023
11/19/2010 6:35	501.6	-0.000502	0.2001	-0.00023
11/19/2010 6:36	502.4	-0.000502	0.2008	-0.00023
11/19/2010 6:37	503.4	-0.000503	0.2015	-0.00022

11/19/2010 6:38	504.3	-0.000504	0.2022	-0.00022
11/19/2010 6:39	505.3	-0.000505	0.2029	-0.00022
11/19/2010 6:40	506.2	-0.000506	0.2036	-0.00022
11/19/2010 6:41	507.2	-0.000507	0.2043	-0.00022
11/19/2010 6:42	508.2	-0.000508	0.2050	-0.00022
11/19/2010 6:43	509.1	-0.000509	0.2057	-0.00022
11/19/2010 6:44	510.1	-0.000510	0.2064	-0.00022
11/19/2010 6:45	510.9	-0.000511	0.2071	-0.00022
11/19/2010 6:46	511.9	-0.000512	0.2078	-0.00022
11/19/2010 6:47	513	-0.000513	0.2085	-0.00022
11/19/2010 6:48	513.8	-0.000514	0.2092	-0.00022
11/19/2010 6:49	514.6	-0.000515	0.2099	-0.00022
11/19/2010 6:50	515.3	-0.000515	0.2106	-0.00022
11/19/2010 6:51	516.1	-0.000516	0.2113	-0.00022
11/19/2010 6:52	516.9	-0.000517	0.2120	-0.00022
11/19/2010 6:53	517.7	-0.000518	0.2127	-0.00022
11/19/2010 6:54	518.5	-0.000519	0.2134	-0.00022
11/19/2010 6:55	519.2	-0.000519	0.2141	-0.00022
11/19/2010 6:56	519.9	-0.000520	0.2148	-0.00022
11/19/2010 6:57	520.6	-0.000521	0.2155	-0.00022
11/19/2010 6:58	521.4	-0.000521	0.2161	-0.00022
11/19/2010 6:59	522.1	-0.000522	0.2168	-0.00022
11/19/2010 7:00	522.8	-0.000523	0.2175	-0.00022
11/19/2010 7:01	523.5	-0.000524	0.2182	-0.00022
11/19/2010 7:02	524.2	-0.000524	0.2189	-0.00022
11/19/2010 7:03	524.9	-0.000525	0.2196	-0.00022
11/19/2010 7:04	525.5	-0.000526	0.2203	-0.00021
11/19/2010 7:05	526.3	-0.000526	0.2210	-0.00021
11/19/2010 7:06	527	-0.000527	0.2217	-0.00021
11/19/2010 7:07	527.8	-0.000528	0.2224	-0.00021
11/19/2010 7:08	528.5	-0.000529	0.2231	-0.00021
11/19/2010 7:09	529.2	-0.000529	0.2238	-0.00021
11/19/2010 7:10	529.8	-0.000530	0.2245	-0.00021
11/19/2010 7:11	530.5	-0.000531	0.2252	-0.00021
11/19/2010 7:12	531.1	-0.000531	0.2259	-0.00021
11/19/2010 7:13	531.8	-0.000532	0.2266	-0.00021
11/19/2010 7:14	532.4	-0.000532	0.2273	-0.00021
11/19/2010 7:15	533	-0.000533	0.2280	-0.00021
11/19/2010 7:16	533.6	-0.000534	0.2287	-0.00021
11/19/2010 7:17	534.3	-0.000534	0.2294	-0.00021

11/19/2010 7:18	534.9	-0.000535	0.2301	-0.00021
11/19/2010 7:19	535.6	-0.000536	0.2308	-0.00021
11/19/2010 7:20	536.2	-0.000536	0.2315	-0.00021
11/19/2010 7:21	536.9	-0.000537	0.2322	-0.00021
11/19/2010 7:22	537.4	-0.000537	0.2329	-0.00021
11/19/2010 7:23	538	-0.000538	0.2336	-0.00021
11/19/2010 7:24	538.6	-0.000539	0.2343	-0.00021
11/19/2010 7:25	539.3	-0.000539	0.2350	-0.00021
11/19/2010 7:26	539.8	-0.000540	0.2357	-0.00021
11/19/2010 7:27	540.4	-0.000540	0.2364	-0.00021
11/19/2010 7:28	540.9	-0.000541	0.2370	-0.00021
11/19/2010 7:29	541.3	-0.000541	0.2377	-0.00020
11/19/2010 7:30	541.9	-0.000542	0.2384	-0.00020
11/19/2010 7:31	542.3	-0.000542	0.2391	-0.00020
11/19/2010 7:32	542.8	-0.000543	0.2398	-0.00020
11/19/2010 7:33	543.3	-0.000543	0.2405	-0.00020
11/19/2010 7:34	543.7	-0.000544	0.2412	-0.00020
11/19/2010 7:35	544.1	-0.000544	0.2419	-0.00020
11/19/2010 7:36	544.6	-0.000545	0.2426	-0.00020
11/19/2010 7:37	545.1	-0.000545	0.2433	-0.00020
11/19/2010 7:38	545.4	-0.000545	0.2440	-0.00020
11/19/2010 7:39	545.8	-0.000546	0.2447	-0.00020
11/19/2010 7:40	546.1	-0.000546	0.2454	-0.00020
11/19/2010 7:41	546.5	-0.000547	0.2461	-0.00020
11/19/2010 7:42	546.8	-0.000547	0.2468	-0.00020
11/19/2010 7:43	547.1	-0.000547	0.2475	-0.00020
11/19/2010 7:44	547.4	-0.000547	0.2482	-0.00020
11/19/2010 7:45	547.6	-0.000548	0.2489	-0.00020
11/19/2010 7:46	548	-0.000548	0.2496	-0.00020
11/19/2010 7:47	548.3	-0.000548	0.2503	-0.00020
11/19/2010 7:48	548.5	-0.000549	0.2510	-0.00020
11/19/2010 7:49	548.8	-0.000549	0.2517	-0.00020
11/19/2010 7:50	549	-0.000549	0.2524	-0.00020
11/19/2010 7:51	549.3	-0.000549	0.2531	-0.00020
11/19/2010 7:52	549.6	-0.000550	0.2538	-0.00019
11/19/2010 7:53	549.9	-0.000550	0.2545	-0.00019
11/19/2010 7:54	550.2	-0.000550	0.2552	-0.00019
11/19/2010 7:55	550.4	-0.000550	0.2559	-0.00019
11/19/2010 7:56	550.7	-0.000551	0.2566	-0.00019
11/19/2010 7:57	551	-0.000551	0.2573	-0.00019

11/19/2010 7:58	551.2	-0.000551	0.2580	-0.00019
11/19/2010 7:59	551.5	-0.000552	0.2587	-0.00019
11/19/2010 8:00	551.8	-0.000552	0.2594	-0.00019
11/19/2010 8:01	551.9	-0.000552	0.2600	-0.00019
11/19/2010 8:02	552.1	-0.000552	0.2607	-0.00019
11/19/2010 8:03	552.2	-0.000552	0.2614	-0.00019
11/19/2010 8:04	552.5	-0.000553	0.2621	-0.00019
11/19/2010 8:05	552.6	-0.000553	0.2628	-0.00019
11/19/2010 8:06	552.8	-0.000553	0.2635	-0.00019
11/19/2010 8:07	553	-0.000553	0.2642	-0.00019
11/19/2010 8:08	553.1	-0.000553	0.2649	-0.00019
11/19/2010 8:09	553.3	-0.000553	0.2656	-0.00019
11/19/2010 8:10	553.4	-0.000553	0.2663	-0.00019
11/19/2010 8:11	553.6	-0.000554	0.2670	-0.00019
11/19/2010 8:12	553.7	-0.000554	0.2677	-0.00019
11/19/2010 8:13	553.8	-0.000554	0.2684	-0.00019
11/19/2010 8:14	554.1	-0.000554	0.2691	-0.00019
11/19/2010 8:15	554.2	-0.000554	0.2698	-0.00018
11/19/2010 8:16	554.4	-0.000554	0.2705	-0.00018
11/19/2010 8:17	554.5	-0.000555	0.2712	-0.00018
11/19/2010 8:18	554.7	-0.000555	0.2719	-0.00018
11/19/2010 8:19	554.9	-0.000555	0.2726	-0.00018
11/19/2010 8:20	555	-0.000555	0.2733	-0.00018
11/19/2010 8:21	555.2	-0.000555	0.2740	-0.00018
11/19/2010 8:22	555.4	-0.000555	0.2747	-0.00018
11/19/2010 8:23	555.4	-0.000555	0.2754	-0.00018
11/19/2010 8:24	555.6	-0.000556	0.2761	-0.00018
11/19/2010 8:25	555.8	-0.000556	0.2768	-0.00018
11/19/2010 8:26	555.9	-0.000556	0.2775	-0.00018
11/19/2010 8:27	556	-0.000556	0.2782	-0.00018
11/19/2010 8:28	556.1	-0.000556	0.2789	-0.00018
11/19/2010 8:29	556.3	-0.000556	0.2796	-0.00018
11/19/2010 8:30	556.4	-0.000556	0.2803	-0.00018
11/19/2010 8:31	556.7	-0.000557	0.2810	-0.00018
11/19/2010 8:32	556.9	-0.000557	0.2817	-0.00018
11/19/2010 8:33	557	-0.000557	0.2824	-0.00018
11/19/2010 8:34	557.1	-0.000557	0.2831	-0.00018
11/19/2010 8:35	557.2	-0.000557	0.2838	-0.00018
11/19/2010 8:36	557.3	-0.000557	0.2845	-0.00018
11/19/2010 8:37	557.4	-0.000557	0.2852	-0.00018

11/19/2010 8:38	557.6	-0.000558	0.2858	-0.00018
11/19/2010 8:39	557.7	-0.000558	0.2866	-0.00018
11/19/2010 8:40	557.8	-0.000558	0.2872	-0.00017
11/19/2010 8:41	557.9	-0.000558	0.2879	-0.00017
11/19/2010 8:42	558.1	-0.000558	0.2886	-0.00017
11/19/2010 8:43	558.1	-0.000558	0.2893	-0.00017
11/19/2010 8:44	558.2	-0.000558	0.2900	-0.00017
11/19/2010 8:45	558.4	-0.000558	0.2907	-0.00017
11/19/2010 8:46	558.4	-0.000558	0.2914	-0.00017
11/19/2010 8:47	558.5	-0.000559	0.2921	-0.00017
11/19/2010 8:48	558.6	-0.000559	0.2928	-0.00017
11/19/2010 8:49	558.8	-0.000559	0.2935	-0.00017
11/19/2010 8:50	558.9	-0.000559	0.2942	-0.00017
11/19/2010 8:51	559	-0.000559	0.2949	-0.00017
11/19/2010 8:52	559.2	-0.000559	0.2956	-0.00017
11/19/2010 8:53	559.3	-0.000559	0.2963	-0.00017
11/19/2010 8:54	559.4	-0.000559	0.2970	-0.00017
11/19/2010 8:55	559.5	-0.000560	0.2977	-0.00017
11/19/2010 8:56	559.6	-0.000560	0.2984	-0.00017
11/19/2010 8:57	559.7	-0.000560	0.2991	-0.00017
11/19/2010 8:58	559.7	-0.000560	0.2998	-0.00017
11/19/2010 8:59	559.8	-0.000560	0.3005	-0.00017
11/19/2010 9:00	559.8	-0.000560	0.3012	-0.00017
11/19/2010 9:01	560	-0.000560	0.3019	-0.00017
11/19/2010 9:02	559.9	-0.000560	0.3026	-0.00017
11/19/2010 9:03	559.9	-0.000560	0.3033	-0.00017
11/19/2010 9:04	559.9	-0.000560	0.3040	-0.00017
11/19/2010 9:05	560.1	-0.000560	0.3047	-0.00017
11/19/2010 9:06	560.1	-0.000560	0.3054	-0.00017
11/19/2010 9:07	560.1	-0.000560	0.3061	-0.00016
11/19/2010 9:09	560.2	-0.000560	0.3068	-0.00016
11/19/2010 9:10	560.3	-0.000560	0.3075	-0.00016
11/19/2010 9:11	560.3	-0.000560	0.3082	-0.00016
11/19/2010 9:12	560.4	-0.000560	0.3089	-0.00016
11/19/2010 9:13	560.4	-0.000560	0.3095	-0.00016
11/19/2010 9:14	560.5	-0.000561	0.3102	-0.00016
11/19/2010 9:15	560.6	-0.000561	0.3109	-0.00016
11/19/2010 9:16	560.7	-0.000561	0.3116	-0.00016
11/19/2010 9:17	560.7	-0.000561	0.3123	-0.00016
11/19/2010 9:18	560.7	-0.000561	0.3130	-0.00016

11/19/2010 9:19	560.7	-0.000561	0.3137	-0.00016
11/19/2010 9:20	560.7	-0.000561	0.3144	-0.00016
11/19/2010 9:21	560.7	-0.000561	0.3151	-0.00016
11/19/2010 9:22	560.8	-0.000561	0.3158	-0.00016
11/19/2010 9:23	560.8	-0.000561	0.3165	-0.00016
11/19/2010 9:24	560.8	-0.000561	0.3172	-0.00016
11/19/2010 9:25	560.9	-0.000561	0.3179	-0.00016
11/19/2010 9:26	560.9	-0.000561	0.3186	-0.00016
11/19/2010 9:27	560.9	-0.000561	0.3193	-0.00016
11/19/2010 9:28	561	-0.000561	0.3200	-0.00016
11/19/2010 9:29	561	-0.000561	0.3207	-0.00016
11/19/2010 9:30	561	-0.000561	0.3214	-0.00016
11/19/2010 9:31	561	-0.000561	0.3221	-0.00016
11/19/2010 9:32	561.1	-0.000561	0.3228	-0.00016
11/19/2010 9:33	561.2	-0.000561	0.3235	-0.00016
11/19/2010 9:34	561.2	-0.000561	0.3242	-0.00016
11/19/2010 9:35	561.3	-0.000561	0.3249	-0.00016
11/19/2010 9:36	561.2	-0.000561	0.3256	-0.00016
11/19/2010 9:37	561.3	-0.000561	0.3263	-0.00015
11/19/2010 9:38	561.3	-0.000561	0.3270	-0.00015
11/19/2010 9:39	561.3	-0.000561	0.3277	-0.00015
11/19/2010 9:40	561.3	-0.000561	0.3284	-0.00015
11/19/2010 9:41	561.3	-0.000561	0.3291	-0.00015
11/19/2010 9:42	561.3	-0.000561	0.3298	-0.00015
11/19/2010 9:43	561.3	-0.000561	0.3305	-0.00015
11/19/2010 9:44	561.3	-0.000561	0.3312	-0.00015
11/19/2010 9:45	561.3	-0.000561	0.3319	-0.00015
11/19/2010 9:46	561.4	-0.000561	0.3326	-0.00015
11/19/2010 9:47	561.4	-0.000561	0.3333	-0.00015
11/19/2010 9:48	561.4	-0.000561	0.3339	-0.00015
11/19/2010 9:49	561.4	-0.000561	0.3346	-0.00015
11/19/2010 9:50	561.4	-0.000561	0.3353	-0.00015
11/19/2010 9:51	561.5	-0.000562	0.3360	-0.00015
11/19/2010 9:52	561.5	-0.000562	0.3367	-0.00015
11/19/2010 9:53	561.4	-0.000561	0.3374	-0.00015
11/19/2010 9:54	561.5	-0.000562	0.3381	-0.00015
11/19/2010 9:55	561.5	-0.000562	0.3388	-0.00015
11/19/2010 9:56	561.6	-0.000562	0.3395	-0.00015
11/19/2010 9:57	561.7	-0.000562	0.3402	-0.00015
11/19/2010 9:58	561.6	-0.000562	0.3409	-0.00015

11/19/2010 9:59	561.7	-0.000562	0.3416	-0.00015
11/19/2010 10:00	561.7	-0.000562	0.3423	-0.00015
11/19/2010 10:01	561.7	-0.000562	0.3430	-0.00015
11/19/2010 10:02	561.7	-0.000562	0.3437	-0.00015
11/19/2010 10:03	561.7	-0.000562	0.3444	-0.00015
11/19/2010 10:04	561.7	-0.000562	0.3451	-0.00015
11/19/2010 10:05	561.8	-0.000562	0.3458	-0.00015
11/19/2010 10:06	561.8	-0.000562	0.3465	-0.00015
11/19/2010 10:07	561.8	-0.000562	0.3472	-0.00015
11/19/2010 10:08	561.8	-0.000562	0.3479	-0.00015
11/19/2010 10:09	561.8	-0.000562	0.3486	-0.00015
11/19/2010 10:10	561.8	-0.000562	0.4658	-0.00011

Table C.1.6 Main_3 layer: experimental drainage rates and bottom boundary condition data

Timestamp	Mass of water	Cumulative outflow	Time (days)	Instantaneous Flux rate
<i>mm/dd/yy</i>	<i>g</i>	<i>m³</i>	<i>days</i>	<i>m³/day/m²</i>
12/20/2010 23:56	0.000	0.000000	0.000	0.0000
12/20/2010 23:59	0.000	0.000000	0.002	0.0000
12/21/2010 0:02	0.000	0.000000	0.004	0.0000
12/21/2010 0:05	0.000	0.000000	0.006	0.0000
12/21/2010 0:06	0.000	0.000000	0.007	0.0000
12/21/2010 0:07	0.000	0.000000	0.008	0.0000
12/21/2010 0:08	0.000	0.000000	0.008	0.0000
12/21/2010 0:09	0.000	0.000000	0.009	0.0000
12/21/2010 0:10	0.000	0.000000	0.010	0.0000
12/21/2010 0:11	0.000	0.000000	0.010	0.0000
12/21/2010 0:12	0.000	0.000000	0.011	0.0000
12/21/2010 0:13	0.000	0.000000	0.012	0.0000
12/21/2010 0:14	0.000	0.000000	0.012	0.0000
12/21/2010 0:15	0.000	0.000000	0.013	0.0000
12/21/2010 0:16	0.000	0.000000	0.014	0.0000
12/21/2010 0:17	0.000	0.000000	0.015	0.0000
12/21/2010 0:18	0.000	0.000000	0.015	0.0000
12/21/2010 0:19	0.000	0.000000	0.016	0.0000
12/21/2010 0:20	0.000	0.000000	0.017	0.0000
12/21/2010 0:21	0.000	0.000000	0.017	0.0000

12/21/2010 0:22	0.000	0.000000	0.018	0.0000
12/21/2010 0:22	0.000	0.000000	0.019	0.0000
12/21/2010 0:22	0.000	0.000000	0.019	0.0000
12/21/2010 0:23	0.000	0.000000	0.019	0.0000
12/21/2010 0:24	0.000	0.000000	0.019	0.0000
12/21/2010 0:25	0.000	0.000000	0.020	0.0000
12/21/2010 0:26	0.000	0.000000	0.021	0.0000
12/21/2010 0:27	0.000	0.000000	0.022	0.0000
12/21/2010 0:28	0.000	0.000000	0.022	0.0000
12/21/2010 0:29	0.000	0.000000	0.023	0.0000
12/21/2010 0:30	0.000	0.000000	0.024	0.0000
12/21/2010 0:31	0.000	0.000000	0.024	0.0000
12/21/2010 0:32	0.000	0.000000	0.025	0.0000
12/21/2010 0:33	0.000	0.000000	0.026	0.0000
12/21/2010 0:34	0.000	0.000000	0.026	0.0000
12/21/2010 0:35	0.000	0.000000	0.027	0.0000
12/21/2010 0:36	0.000	0.000000	0.028	0.0000
12/21/2010 0:37	0.000	0.000000	0.028	0.0000
12/21/2010 0:38	0.000	0.000000	0.029	0.0000
12/21/2010 0:39	0.000	0.000000	0.030	0.0000
12/21/2010 0:40	0.000	0.000000	0.031	0.0000
12/21/2010 0:41	0.000	0.000000	0.031	0.0000
12/21/2010 0:42	0.000	0.000000	0.032	0.0000
12/21/2010 0:43	0.000	0.000000	0.033	0.0000
12/21/2010 0:44	0.000	0.000000	0.033	0.0000
12/21/2010 0:45	0.000	0.000000	0.034	0.0000
12/21/2010 0:46	0.000	0.000000	0.035	0.0000
12/21/2010 0:47	0.000	0.000000	0.035	0.0000
12/21/2010 0:48	0.000	0.000000	0.036	0.0000
12/21/2010 0:49	0.000	0.000000	0.037	0.0000
12/21/2010 0:50	0.000	0.000000	0.038	0.0000
12/21/2010 0:51	0.000	0.000000	0.038	0.0000
12/21/2010 0:52	0.000	0.000000	0.039	0.0000
12/21/2010 0:53	0.000	0.000000	0.040	0.0000
12/21/2010 0:54	0.000	0.000000	0.040	0.0000
12/21/2010 0:55	0.000	0.000000	0.041	0.0000
12/21/2010 0:56	0.000	0.000000	0.042	0.0000
12/21/2010 0:57	0.000	0.000000	0.042	0.0000
12/21/2010 0:58	0.000	0.000000	0.043	0.0000
12/21/2010 0:59	0.000	0.000000	0.044	0.0000

12/21/2010 1:00	0.000	0.000000	0.044	0.0000
12/21/2010 1:01	0.000	0.000000	0.045	0.0000
12/21/2010 1:02	0.000	0.000000	0.046	0.0000
12/21/2010 1:03	0.000	0.000000	0.047	0.0000
12/21/2010 1:04	0.000	0.000000	0.047	0.0000
12/21/2010 1:05	0.000	0.000000	0.048	0.0000
12/21/2010 1:06	0.000	0.000000	0.049	0.0000
12/21/2010 1:07	0.000	0.000000	0.049	0.0000
12/21/2010 1:08	0.000	0.000000	0.050	0.0000
12/21/2010 1:09	0.000	0.000000	0.051	0.0000
12/21/2010 1:10	0.000	0.000000	0.051	0.0000
12/21/2010 1:11	0.000	0.000000	0.052	0.0000
12/21/2010 1:12	0.000	0.000000	0.053	0.0000
12/21/2010 1:13	0.000	0.000000	0.054	0.0000
12/21/2010 1:14	0.000	0.000000	0.054	0.0000
12/21/2010 1:15	0.000	0.000000	0.055	0.0000
12/21/2010 1:16	0.000	0.000000	0.056	0.0000
12/21/2010 1:17	0.000	0.000000	0.056	0.0000
12/21/2010 1:18	0.000	0.000000	0.057	0.0000
12/21/2010 1:19	0.000	0.000000	0.058	0.0000
12/21/2010 1:20	0.000	0.000000	0.058	0.0000
12/21/2010 1:21	0.000	0.000000	0.059	0.0000
12/21/2010 1:22	0.000	0.000000	0.060	0.0000
12/21/2010 1:23	0.000	0.000000	0.061	0.0000
12/21/2010 1:24	0.000	0.000000	0.061	0.0000
12/21/2010 1:25	0.000	0.000000	0.062	0.0000
12/21/2010 1:26	0.000	0.000000	0.063	0.0000
12/21/2010 1:27	0.000	0.000000	0.063	0.0000
12/21/2010 1:28	0.000	0.000000	0.064	0.0000
12/21/2010 1:29	0.000	0.000000	0.065	0.0000
12/21/2010 1:30	0.000	0.000000	0.065	0.0000
12/21/2010 1:31	0.000	0.000000	0.066	0.0000
12/21/2010 1:32	0.000	0.000000	0.067	0.0000
12/21/2010 1:33	0.000	0.000000	0.067	0.0000
12/21/2010 1:34	0.000	0.000000	0.068	0.0000
12/21/2010 1:35	0.000	0.000000	0.069	0.0000
12/21/2010 1:36	0.000	0.000000	0.070	0.0000
12/21/2010 1:37	0.000	0.000000	0.070	0.0000
12/21/2010 1:38	0.000	0.000000	0.071	0.0000
12/21/2010 1:39	0.000	0.000000	0.072	0.0000

12/21/2010 1:40	0.000	0.000000	0.072	0.0000
12/21/2010 1:41	0.000	0.000000	0.073	0.0000
12/21/2010 1:42	0.000	0.000000	0.074	0.0000
12/21/2010 1:43	0.000	0.000000	0.074	0.0000
12/21/2010 1:44	0.000	0.000000	0.075	0.0000
12/21/2010 1:45	0.000	0.000000	0.076	0.0000
12/21/2010 1:46	0.000	0.000000	0.077	0.0000
12/21/2010 1:47	0.000	0.000000	0.077	0.0000
12/21/2010 1:48	0.000	0.000000	0.078	0.0000
12/21/2010 1:49	0.000	0.000000	0.079	0.0000
12/21/2010 1:50	0.000	0.000000	0.079	0.0000
12/21/2010 1:51	0.000	0.000000	0.080	0.0000
12/21/2010 1:52	0.000	0.000000	0.081	0.0000
12/21/2010 1:53	0.000	0.000000	0.081	0.0000
12/21/2010 1:54	0.000	0.000000	0.082	0.0000
12/21/2010 1:55	0.000	0.000000	0.083	0.0000
12/21/2010 1:56	0.000	0.000000	0.083	0.0000
12/21/2010 1:57	0.000	0.000000	0.084	0.0000
12/21/2010 1:58	0.000	0.000000	0.085	0.0000
12/21/2010 1:59	0.000	0.000000	0.086	0.0000
12/21/2010 2:00	0.000	0.000000	0.086	0.0000
12/21/2010 2:01	0.000	0.000000	0.087	0.0000
12/21/2010 2:02	0.000	0.000000	0.088	0.0000
12/21/2010 2:03	0.000	0.000000	0.088	0.0000
12/21/2010 2:04	0.000	0.000000	0.089	0.0000
12/21/2010 2:05	0.000	0.000000	0.090	0.0000
12/21/2010 2:06	0.000	0.000000	0.090	0.0000
12/21/2010 2:07	0.000	0.000000	0.091	0.0000
12/21/2010 2:08	0.000	0.000000	0.092	0.0000
12/21/2010 2:09	0.000	0.000000	0.093	0.0000
12/21/2010 2:10	0.000	0.000000	0.093	0.0000
12/21/2010 2:11	0.000	0.000000	0.094	0.0000
12/21/2010 2:12	0.000	0.000000	0.095	0.0000
12/21/2010 2:13	0.000	0.000000	0.095	0.0000
12/21/2010 2:14	0.000	0.000000	0.096	0.0000
12/21/2010 2:15	0.000	0.000000	0.097	0.0000
12/21/2010 2:16	0.000	0.000000	0.097	0.0000
12/21/2010 2:17	0.000	0.000000	0.098	0.0000
12/21/2010 2:18	0.000	0.000000	0.099	0.0000
12/21/2010 2:19	0.000	0.000000	0.099	0.0000

12/21/2010 2:20	0.000	0.000000	0.100	0.0000
12/21/2010 2:21	0.000	0.000000	0.101	0.0000
12/21/2010 2:22	0.000	0.000000	0.102	0.0000
12/21/2010 2:23	0.000	0.000000	0.102	0.0000
12/21/2010 2:24	0.000	0.000000	0.103	0.0000
12/21/2010 2:25	0.000	0.000000	0.104	0.0000
12/21/2010 2:26	0.000	0.000000	0.104	0.0000
12/21/2010 2:27	1.100	-0.000001	0.105	0.00000
12/21/2010 2:28	2.600	-0.000003	0.106	0.00000
12/21/2010 2:29	4.200	-0.000004	0.106	0.00000
12/21/2010 2:30	5.700	-0.000006	0.107	0.00000
12/21/2010 2:31	7.300	-0.000007	0.108	-0.00001
12/21/2010 2:32	8.900	-0.000009	0.109	-0.00001
12/21/2010 2:33	10.400	-0.000010	0.109	-0.00001
12/21/2010 2:34	12.200	-0.000012	0.110	-0.00001
12/21/2010 2:35	13.900	-0.000014	0.111	-0.00001
12/21/2010 2:36	15.500	-0.000016	0.111	-0.00001
12/21/2010 2:37	17.000	-0.000017	0.112	-0.00001
12/21/2010 2:38	18.500	-0.000019	0.113	-0.00001
12/21/2010 2:39	20.000	-0.000020	0.113	-0.00002
12/21/2010 2:40	21.200	-0.000021	0.114	-0.00002
12/21/2010 2:41	22.500	-0.000023	0.115	-0.00002
12/21/2010 2:42	23.800	-0.000024	0.115	-0.00002
12/21/2010 2:43	25.300	-0.000025	0.116	-0.00002
12/21/2010 2:44	26.700	-0.000027	0.117	-0.00002
12/21/2010 2:45	28.100	-0.000028	0.118	-0.00002
12/21/2010 2:46	29.600	-0.000030	0.118	-0.00002
12/21/2010 2:47	31.000	-0.000031	0.119	-0.00002
12/21/2010 2:48	32.400	-0.000032	0.120	-0.00002
12/21/2010 2:49	33.800	-0.000034	0.120	-0.00003
12/21/2010 2:50	35.200	-0.000035	0.121	-0.00003
12/21/2010 2:51	36.600	-0.000037	0.122	-0.00003
12/21/2010 2:52	38.000	-0.000038	0.122	-0.00003
12/21/2010 2:53	39.400	-0.000039	0.123	-0.00003
12/21/2010 2:54	40.700	-0.000041	0.124	-0.00003
12/21/2010 2:55	42.100	-0.000042	0.125	-0.00003
12/21/2010 2:56	43.500	-0.000044	0.125	-0.00003
12/21/2010 2:57	44.900	-0.000045	0.126	-0.00003
12/21/2010 2:58	46.400	-0.000046	0.127	-0.00003
12/21/2010 2:59	47.600	-0.000048	0.127	-0.00003

12/21/2010 3:00	48.800	-0.000049	0.128	-0.00003
12/21/2010 3:01	48.200	-0.000048	0.129	-0.00003
12/21/2010 3:02	49.000	-0.000049	0.129	-0.00003
12/21/2010 3:03	50.300	-0.000050	0.130	-0.00003
12/21/2010 3:04	51.500	-0.000052	0.131	-0.00004
12/21/2010 3:05	52.700	-0.000053	0.131	-0.00004
12/21/2010 3:06	53.900	-0.000054	0.132	-0.00004
12/21/2010 3:07	55.000	-0.000055	0.133	-0.00004
12/21/2010 3:08	56.200	-0.000056	0.134	-0.00004
12/21/2010 3:09	57.300	-0.000057	0.134	-0.00004
12/21/2010 3:10	58.600	-0.000059	0.135	-0.00004
12/21/2010 3:11	59.800	-0.000060	0.136	-0.00004
12/21/2010 3:12	61.100	-0.000061	0.136	-0.00004
12/21/2010 3:13	62.400	-0.000062	0.137	-0.00004
12/21/2010 3:14	63.600	-0.000064	0.138	-0.00004
12/21/2010 3:15	64.900	-0.000065	0.138	-0.00004
12/21/2010 3:16	66.100	-0.000066	0.139	-0.00004
12/21/2010 3:17	67.300	-0.000067	0.140	-0.00004
12/21/2010 3:18	68.500	-0.000069	0.141	-0.00004
12/21/2010 3:19	69.900	-0.000070	0.141	-0.00004
12/21/2010 3:20	71.100	-0.000071	0.142	-0.00005
12/21/2010 3:21	72.400	-0.000072	0.143	-0.00005
12/21/2010 3:22	73.600	-0.000074	0.143	-0.00005
12/21/2010 3:23	74.700	-0.000075	0.144	-0.00005
12/21/2010 3:24	76.000	-0.000076	0.145	-0.00005
12/21/2010 3:25	77.200	-0.000077	0.145	-0.00005
12/21/2010 3:26	78.500	-0.000079	0.146	-0.00005
12/21/2010 3:27	79.900	-0.000080	0.147	-0.00005
12/21/2010 3:28	81.000	-0.000081	0.147	-0.00005
12/21/2010 3:29	82.200	-0.000082	0.148	-0.00005
12/21/2010 3:30	83.400	-0.000083	0.149	-0.00005
12/21/2010 3:31	84.600	-0.000085	0.150	-0.00005
12/21/2010 3:32	85.700	-0.000086	0.150	-0.00005
12/21/2010 3:33	86.500	-0.000087	0.151	-0.00005
12/21/2010 3:34	87.600	-0.000088	0.152	-0.00005
12/21/2010 3:35	88.700	-0.000089	0.152	-0.00005
12/21/2010 3:36	89.600	-0.000090	0.153	-0.00005
12/21/2010 3:37	90.800	-0.000091	0.154	-0.00005
12/21/2010 3:38	91.700	-0.000092	0.154	-0.00005
12/21/2010 3:39	92.800	-0.000093	0.155	-0.00005

12/21/2010 3:40	93.900	-0.000094	0.156	-0.00005
12/21/2010 3:41	95.000	-0.000095	0.157	-0.00005
12/21/2010 3:42	96.100	-0.000096	0.157	-0.00006
12/21/2010 3:43	97.200	-0.000097	0.158	-0.00006
12/21/2010 3:44	98.300	-0.000098	0.159	-0.00006
12/21/2010 3:45	99.400	-0.000099	0.159	-0.00006
12/21/2010 3:46	100.500	-0.000101	0.160	-0.00006
12/21/2010 3:47	101.600	-0.000102	0.161	-0.00006
12/21/2010 3:48	102.600	-0.000103	0.161	-0.00006
12/21/2010 3:49	103.700	-0.000104	0.162	-0.00006
12/21/2010 3:50	104.800	-0.000105	0.163	-0.00006
12/21/2010 3:51	105.800	-0.000106	0.163	-0.00006
12/21/2010 3:52	106.800	-0.000107	0.164	-0.00006
12/21/2010 3:53	108.000	-0.000108	0.165	-0.00006
12/21/2010 3:54	109.200	-0.000109	0.166	-0.00006
12/21/2010 3:55	110.300	-0.000110	0.166	-0.00006
12/21/2010 3:56	111.500	-0.000112	0.167	-0.00006
12/21/2010 3:57	112.400	-0.000112	0.168	-0.00006
12/21/2010 3:58	113.400	-0.000113	0.168	-0.00006
12/21/2010 3:59	114.400	-0.000114	0.169	-0.00006
12/21/2010 4:00	115.200	-0.000115	0.170	-0.00006
12/21/2010 4:01	116.100	-0.000116	0.170	-0.00006
12/21/2010 4:02	117.000	-0.000117	0.171	-0.00006
12/21/2010 4:03	118.000	-0.000118	0.172	-0.00006
12/21/2010 4:04	119.000	-0.000119	0.173	-0.00006
12/21/2010 4:05	120.000	-0.000120	0.173	-0.00006
12/21/2010 4:06	121.000	-0.000121	0.174	-0.00006
12/21/2010 4:07	122.000	-0.000122	0.175	-0.00006
12/21/2010 4:08	123.100	-0.000123	0.175	-0.00006
12/21/2010 4:09	124.000	-0.000124	0.176	-0.00006
12/21/2010 4:10	125.100	-0.000125	0.177	-0.00006
12/21/2010 4:11	126.100	-0.000126	0.177	-0.00006
12/21/2010 4:12	127.000	-0.000127	0.178	-0.00006
12/21/2010 4:13	128.100	-0.000128	0.179	-0.00006
12/21/2010 4:14	129.100	-0.000129	0.180	-0.00006
12/21/2010 4:15	130.100	-0.000130	0.180	-0.00006
12/21/2010 4:16	131.100	-0.000131	0.181	-0.00007
12/21/2010 4:17	132.100	-0.000132	0.182	-0.00007
12/21/2010 4:18	133.200	-0.000133	0.182	-0.00007
12/21/2010 4:19	134.100	-0.000134	0.183	-0.00007

12/21/2010 4:20	135.000	-0.000135	0.184	-0.00007
12/21/2010 4:21	136.100	-0.000136	0.184	-0.00007
12/21/2010 4:22	137.300	-0.000137	0.185	-0.00007
12/21/2010 4:23	138.400	-0.000138	0.186	-0.00007
12/21/2010 4:24	139.300	-0.000139	0.186	-0.00007
12/21/2010 4:25	140.400	-0.000140	0.187	-0.00007
12/21/2010 4:26	141.400	-0.000141	0.188	-0.00007
12/21/2010 4:27	142.300	-0.000142	0.189	-0.00007
12/21/2010 4:28	143.100	-0.000143	0.189	-0.00007
12/21/2010 4:29	144.000	-0.000144	0.190	-0.00007
12/21/2010 4:30	144.900	-0.000145	0.191	-0.00007
12/21/2010 4:31	145.800	-0.000146	0.191	-0.00007
12/21/2010 4:32	146.800	-0.000147	0.192	-0.00007
12/21/2010 4:33	147.900	-0.000148	0.193	-0.00007
12/21/2010 4:34	148.800	-0.000149	0.193	-0.00007
12/21/2010 4:35	149.800	-0.000150	0.194	-0.00007
12/21/2010 4:36	150.700	-0.000151	0.195	-0.00007
12/21/2010 4:37	151.700	-0.000152	0.196	-0.00007
12/21/2010 4:38	152.500	-0.000153	0.196	-0.00007
12/21/2010 4:39	153.500	-0.000154	0.197	-0.00007
12/21/2010 4:40	154.500	-0.000155	0.198	-0.00007
12/21/2010 4:41	155.400	-0.000155	0.198	-0.00007
12/21/2010 4:42	156.300	-0.000156	0.199	-0.00007
12/21/2010 4:43	157.200	-0.000157	0.200	-0.00007
12/21/2010 4:44	158.100	-0.000158	0.200	-0.00007
12/21/2010 4:45	159.100	-0.000159	0.201	-0.00007
12/21/2010 4:46	160.100	-0.000160	0.202	-0.00007
12/21/2010 4:47	161.000	-0.000161	0.202	-0.00007
12/21/2010 4:48	162.000	-0.000162	0.203	-0.00007
12/21/2010 4:49	162.900	-0.000163	0.204	-0.00007
12/21/2010 4:50	164.100	-0.000164	0.205	-0.00007
12/21/2010 4:51	165.200	-0.000165	0.205	-0.00007
12/21/2010 4:52	166.100	-0.000166	0.206	-0.00007
12/21/2010 4:53	167.100	-0.000167	0.207	-0.00007
12/21/2010 4:54	168.000	-0.000168	0.207	-0.00007
12/21/2010 4:55	169.000	-0.000169	0.208	-0.00007
12/21/2010 4:56	169.700	-0.000170	0.209	-0.00007
12/21/2010 4:57	170.500	-0.000171	0.209	-0.00007
12/21/2010 4:58	171.400	-0.000171	0.210	-0.00007
12/21/2010 4:59	172.300	-0.000172	0.211	-0.00007

12/21/2010 5:00	173.200	-0.000173	0.212	-0.00007
12/21/2010 5:01	174.100	-0.000174	0.212	-0.00007
12/21/2010 5:02	175.200	-0.000175	0.213	-0.00007
12/21/2010 5:03	176.200	-0.000176	0.214	-0.00007
12/21/2010 5:04	177.100	-0.000177	0.214	-0.00007
12/21/2010 5:05	178.000	-0.000178	0.215	-0.00007
12/21/2010 5:06	178.900	-0.000179	0.216	-0.00007
12/21/2010 5:07	179.900	-0.000180	0.216	-0.00007
12/21/2010 5:08	180.800	-0.000181	0.217	-0.00007
12/21/2010 5:09	181.800	-0.000182	0.218	-0.00008
12/21/2010 5:10	182.700	-0.000183	0.218	-0.00008
12/21/2010 5:11	183.600	-0.000184	0.219	-0.00008
12/21/2010 5:12	184.600	-0.000185	0.220	-0.00008
12/21/2010 5:13	185.500	-0.000186	0.221	-0.00008
12/21/2010 5:14	186.400	-0.000186	0.221	-0.00008
12/21/2010 5:15	187.300	-0.000187	0.222	-0.00008
12/21/2010 5:16	188.500	-0.000189	0.223	-0.00008
12/21/2010 5:17	189.500	-0.000190	0.223	-0.00008
12/21/2010 5:18	190.500	-0.000191	0.224	-0.00008
12/21/2010 5:19	191.500	-0.000192	0.225	-0.00008
12/21/2010 5:20	192.400	-0.000192	0.225	-0.00008
12/21/2010 5:21	193.400	-0.000193	0.226	-0.00008
12/21/2010 5:22	194.300	-0.000194	0.227	-0.00008
12/21/2010 5:23	195.000	-0.000195	0.228	-0.00008
12/21/2010 5:24	195.900	-0.000196	0.228	-0.00008
12/21/2010 5:25	196.800	-0.000197	0.229	-0.00008
12/21/2010 5:26	197.700	-0.000198	0.230	-0.00008
12/21/2010 5:27	198.400	-0.000198	0.230	-0.00008
12/21/2010 5:28	199.500	-0.000200	0.231	-0.00008
12/21/2010 5:29	200.300	-0.000200	0.232	-0.00008
12/21/2010 5:30	201.400	-0.000201	0.232	-0.00008
12/21/2010 5:31	202.200	-0.000202	0.233	-0.00008
12/21/2010 5:32	203.100	-0.000203	0.234	-0.00008
12/21/2010 5:33	204.100	-0.000204	0.234	-0.00008
12/21/2010 5:34	205.000	-0.000205	0.235	-0.00008
12/21/2010 5:35	205.900	-0.000206	0.236	-0.00008
12/21/2010 5:36	206.800	-0.000207	0.237	-0.00008
12/21/2010 5:37	207.800	-0.000208	0.237	-0.00008
12/21/2010 5:38	208.700	-0.000209	0.238	-0.00008
12/21/2010 5:39	209.700	-0.000210	0.239	-0.00008

12/21/2010 5:40	210.600	-0.000211	0.239	-0.00008
12/21/2010 5:41	211.500	-0.000212	0.240	-0.00008
12/21/2010 5:42	212.400	-0.000212	0.241	-0.00008
12/21/2010 5:43	213.300	-0.000213	0.241	-0.00008
12/21/2010 5:44	214.400	-0.000214	0.242	-0.00008
12/21/2010 5:45	215.600	-0.000216	0.243	-0.00008
12/21/2010 5:46	216.600	-0.000217	0.244	-0.00008
12/21/2010 5:47	217.500	-0.000218	0.244	-0.00008
12/21/2010 5:48	218.400	-0.000218	0.245	-0.00008
12/21/2010 5:49	219.200	-0.000219	0.246	-0.00008
12/21/2010 5:50	220.100	-0.000220	0.246	-0.00008
12/21/2010 5:51	220.700	-0.000221	0.247	-0.00008
12/21/2010 5:52	221.600	-0.000222	0.248	-0.00008
12/21/2010 5:53	222.500	-0.000223	0.248	-0.00008
12/21/2010 5:54	223.400	-0.000223	0.249	-0.00008
12/21/2010 5:55	224.400	-0.000224	0.250	-0.00008
12/21/2010 5:56	225.200	-0.000225	0.250	-0.00008
12/21/2010 5:57	226.200	-0.000226	0.251	-0.00008
12/21/2010 5:58	227.000	-0.000227	0.252	-0.00008
12/21/2010 5:59	228.000	-0.000228	0.253	-0.00008
12/21/2010 6:00	228.800	-0.000229	0.253	-0.00008
12/21/2010 6:01	229.700	-0.000230	0.254	-0.00008
12/21/2010 6:02	230.600	-0.000231	0.255	-0.00008
12/21/2010 6:03	231.400	-0.000231	0.255	-0.00008
12/21/2010 6:04	232.400	-0.000232	0.256	-0.00008
12/21/2010 6:05	233.300	-0.000233	0.257	-0.00008
12/21/2010 6:06	234.300	-0.000234	0.257	-0.00008
12/21/2010 6:07	235.200	-0.000235	0.258	-0.00008
12/21/2010 6:08	236.100	-0.000236	0.259	-0.00008
12/21/2010 6:09	237.100	-0.000237	0.260	-0.00008
12/21/2010 6:10	237.900	-0.000238	0.260	-0.00008
12/21/2010 6:11	239.100	-0.000239	0.261	-0.00008
12/21/2010 6:12	240.000	-0.000240	0.262	-0.00008
12/21/2010 6:13	240.900	-0.000241	0.262	-0.00008
12/21/2010 6:14	241.900	-0.000242	0.263	-0.00008
12/21/2010 6:15	242.700	-0.000243	0.264	-0.00008
12/21/2010 6:16	243.600	-0.000244	0.264	-0.00008
12/21/2010 6:17	244.400	-0.000244	0.265	-0.00008
12/21/2010 6:18	245.100	-0.000245	0.266	-0.00008
12/21/2010 6:19	245.900	-0.000246	0.266	-0.00008

12/21/2010 6:20	246.800	-0.000247	0.267	-0.00008
12/21/2010 6:21	247.800	-0.000248	0.268	-0.00008
12/21/2010 6:22	248.600	-0.000249	0.269	-0.00008
12/21/2010 6:23	249.500	-0.000250	0.269	-0.00008
12/21/2010 6:24	250.400	-0.000250	0.270	-0.00008
12/21/2010 6:25	251.300	-0.000251	0.271	-0.00008
12/21/2010 6:26	252.200	-0.000252	0.271	-0.00008
12/21/2010 6:27	253.000	-0.000253	0.272	-0.00008
12/21/2010 6:28	253.900	-0.000254	0.273	-0.00008
12/21/2010 6:29	254.800	-0.000255	0.273	-0.00008
12/21/2010 6:30	255.600	-0.000256	0.274	-0.00008
12/21/2010 6:31	256.600	-0.000257	0.275	-0.00008
12/21/2010 6:32	257.500	-0.000258	0.276	-0.00008
12/21/2010 6:33	258.400	-0.000258	0.276	-0.00008
12/21/2010 6:34	259.300	-0.000259	0.277	-0.00008
12/21/2010 6:35	260.100	-0.000260	0.278	-0.00008
12/21/2010 6:36	261.000	-0.000261	0.278	-0.00008
12/21/2010 6:37	262.000	-0.000262	0.279	-0.00008
12/21/2010 6:38	262.800	-0.000263	0.280	-0.00008
12/21/2010 6:39	263.800	-0.000264	0.280	-0.00008
12/21/2010 6:40	264.700	-0.000265	0.281	-0.00008
12/21/2010 6:41	265.700	-0.000266	0.282	-0.00008
12/21/2010 6:42	266.600	-0.000267	0.283	-0.00008
12/21/2010 6:43	267.500	-0.000268	0.283	-0.00009
12/21/2010 6:44	268.200	-0.000268	0.284	-0.00009
12/21/2010 6:45	268.900	-0.000269	0.285	-0.00009
12/21/2010 6:46	269.700	-0.000270	0.285	-0.00009
12/21/2010 6:47	270.600	-0.000271	0.286	-0.00009
12/21/2010 6:48	271.500	-0.000272	0.287	-0.00009
12/21/2010 6:49	272.300	-0.000272	0.287	-0.00009
12/21/2010 6:50	273.100	-0.000273	0.288	-0.00009
12/21/2010 6:51	274.000	-0.000274	0.289	-0.00009
12/21/2010 6:52	274.900	-0.000275	0.289	-0.00009
12/21/2010 6:53	275.700	-0.000276	0.290	-0.00009
12/21/2010 6:54	276.500	-0.000277	0.291	-0.00009
12/21/2010 6:55	277.500	-0.000278	0.292	-0.00009
12/21/2010 6:56	278.300	-0.000278	0.292	-0.00009
12/21/2010 6:57	279.300	-0.000279	0.293	-0.00009
12/21/2010 6:58	280.200	-0.000280	0.294	-0.00009
12/21/2010 6:59	281.100	-0.000281	0.294	-0.00009

12/21/2010 7:00	282.000	-0.000282	0.295	-0.00009
12/21/2010 7:01	282.900	-0.000283	0.296	-0.00009
12/21/2010 7:02	283.900	-0.000284	0.296	-0.00009
12/21/2010 7:03	284.800	-0.000285	0.297	-0.00009
12/21/2010 7:04	285.700	-0.000286	0.298	-0.00009
12/21/2010 7:05	286.600	-0.000287	0.299	-0.00009
12/21/2010 7:06	287.500	-0.000288	0.299	-0.00009
12/21/2010 7:07	288.400	-0.000288	0.300	-0.00009
12/21/2010 7:08	289.200	-0.000289	0.301	-0.00009
12/21/2010 7:09	290.100	-0.000290	0.301	-0.00009
12/21/2010 7:10	291.100	-0.000291	0.302	-0.00009
12/21/2010 7:11	291.900	-0.000292	0.303	-0.00009
12/21/2010 7:12	292.900	-0.000293	0.303	-0.00009
12/21/2010 7:13	293.800	-0.000294	0.304	-0.00009
12/21/2010 7:14	294.700	-0.000295	0.305	-0.00009
12/21/2010 7:15	295.700	-0.000296	0.305	-0.00009
12/21/2010 7:16	296.600	-0.000297	0.306	-0.00009
12/21/2010 7:17	297.500	-0.000298	0.307	-0.00009
12/21/2010 7:18	298.400	-0.000298	0.308	-0.00009
12/21/2010 7:19	299.300	-0.000299	0.308	-0.00009
12/21/2010 7:20	300.200	-0.000300	0.309	-0.00009
12/21/2010 7:21	301.100	-0.000301	0.310	-0.00009
12/21/2010 7:22	302.000	-0.000302	0.310	-0.00009
12/21/2010 7:23	302.900	-0.000303	0.311	-0.00009
12/21/2010 7:24	303.700	-0.000304	0.312	-0.00009
12/21/2010 7:25	304.600	-0.000305	0.312	-0.00009
12/21/2010 7:26	305.500	-0.000306	0.313	-0.00009
12/21/2010 7:27	306.400	-0.000306	0.314	-0.00009
12/21/2010 7:28	307.400	-0.000307	0.315	-0.00009
12/21/2010 7:29	308.300	-0.000308	0.315	-0.00009
12/21/2010 7:30	309.100	-0.000309	0.316	-0.00009
12/21/2010 7:31	310.100	-0.000310	0.317	-0.00009
12/21/2010 7:32	310.900	-0.000311	0.317	-0.00009
12/21/2010 7:33	311.900	-0.000312	0.318	-0.00009
12/21/2010 7:34	312.900	-0.000313	0.319	-0.00009
12/21/2010 7:35	313.800	-0.000314	0.319	-0.00009
12/21/2010 7:36	314.700	-0.000315	0.320	-0.00009
12/21/2010 7:38	315.500	-0.000316	0.321	-0.00009
12/21/2010 7:39	316.400	-0.000316	0.321	-0.00009
12/21/2010 7:40	317.200	-0.000317	0.322	-0.00009

12/21/2010 7:41	318.100	-0.000318	0.323	-0.00009
12/21/2010 7:42	319.100	-0.000319	0.324	-0.00009
12/21/2010 7:43	319.900	-0.000320	0.324	-0.00009
12/21/2010 7:44	320.800	-0.000321	0.325	-0.00009
12/21/2010 7:45	321.600	-0.000322	0.326	-0.00009
12/21/2010 7:46	322.600	-0.000323	0.326	-0.00009
12/21/2010 7:47	323.500	-0.000324	0.327	-0.00009
12/21/2010 7:48	324.300	-0.000324	0.328	-0.00009
12/21/2010 7:49	325.200	-0.000325	0.328	-0.00009
12/21/2010 7:50	326.100	-0.000326	0.329	-0.00009
12/21/2010 7:51	326.900	-0.000327	0.330	-0.00009
12/21/2010 7:52	327.800	-0.000328	0.331	-0.00009
12/21/2010 7:53	328.700	-0.000329	0.331	-0.00009
12/21/2010 7:54	329.600	-0.000330	0.332	-0.00009
12/21/2010 7:55	330.500	-0.000331	0.333	-0.00009
12/21/2010 7:56	331.400	-0.000331	0.333	-0.00009
12/21/2010 7:57	332.300	-0.000332	0.334	-0.00009
12/21/2010 7:58	333.200	-0.000333	0.335	-0.00009
12/21/2010 7:59	334.000	-0.000334	0.335	-0.00009
12/21/2010 8:00	334.900	-0.000335	0.336	-0.00009
12/21/2010 8:01	335.800	-0.000336	0.337	-0.00009
12/21/2010 8:02	336.600	-0.000337	0.337	-0.00009
12/21/2010 8:03	337.400	-0.000337	0.338	-0.00009
12/21/2010 8:04	338.200	-0.000338	0.339	-0.00009
12/21/2010 8:05	339.000	-0.000339	0.340	-0.00009
12/21/2010 8:06	339.900	-0.000340	0.340	-0.00009
12/21/2010 8:07	340.900	-0.000341	0.341	-0.00009
12/21/2010 8:08	341.700	-0.000342	0.342	-0.00009
12/21/2010 8:09	342.600	-0.000343	0.342	-0.00009
12/21/2010 8:10	343.500	-0.000344	0.343	-0.00009
12/21/2010 8:11	344.300	-0.000344	0.344	-0.00009
12/21/2010 8:12	345.200	-0.000345	0.344	-0.00009
12/21/2010 8:13	346.100	-0.000346	0.345	-0.00009
12/21/2010 8:14	346.900	-0.000347	0.346	-0.00009
12/21/2010 8:15	347.900	-0.000348	0.347	-0.00009
12/21/2010 8:16	348.700	-0.000349	0.347	-0.00009
12/21/2010 8:17	349.500	-0.000350	0.348	-0.00009
12/21/2010 8:18	350.400	-0.000350	0.349	-0.00009
12/21/2010 8:19	351.200	-0.000351	0.349	-0.00009
12/21/2010 8:20	352.100	-0.000352	0.350	-0.00009

12/21/2010 8:21	352.900	-0.000353	0.351	-0.00009
12/21/2010 8:22	353.800	-0.000354	0.351	-0.00009
12/21/2010 8:23	354.700	-0.000355	0.352	-0.00009
12/21/2010 8:24	355.500	-0.000356	0.353	-0.00009
12/21/2010 8:25	356.400	-0.000356	0.353	-0.00009
12/21/2010 8:26	357.200	-0.000357	0.354	-0.00009
12/21/2010 8:27	358.100	-0.000358	0.355	-0.00009
12/21/2010 8:28	358.900	-0.000359	0.356	-0.00009
12/21/2010 8:29	359.800	-0.000360	0.356	-0.00009
12/21/2010 8:30	360.600	-0.000361	0.357	-0.00009
12/21/2010 8:31	361.500	-0.000362	0.358	-0.00009
12/21/2010 8:32	362.400	-0.000362	0.358	-0.00009
12/21/2010 8:33	363.200	-0.000363	0.359	-0.00009
12/21/2010 8:34	364.200	-0.000364	0.360	-0.00009
12/21/2010 8:35	365.100	-0.000365	0.360	-0.00009
12/21/2010 8:36	365.900	-0.000366	0.361	-0.00009
12/21/2010 8:37	366.800	-0.000367	0.362	-0.00009
12/21/2010 8:38	367.600	-0.000368	0.363	-0.00009
12/21/2010 8:39	368.500	-0.000369	0.363	-0.00009
12/21/2010 8:40	369.300	-0.000369	0.364	-0.00009
12/21/2010 8:41	370.100	-0.000370	0.365	-0.00009
12/21/2010 8:42	370.900	-0.000371	0.365	-0.00009
12/21/2010 8:43	371.800	-0.000372	0.366	-0.00009
12/21/2010 8:44	372.700	-0.000373	0.367	-0.00009
12/21/2010 8:45	373.500	-0.000374	0.367	-0.00009
12/21/2010 8:46	374.300	-0.000374	0.368	-0.00009
12/21/2010 8:47	375.200	-0.000375	0.369	-0.00009
12/21/2010 8:48	375.900	-0.000376	0.370	-0.00009
12/21/2010 8:49	376.800	-0.000377	0.370	-0.00009
12/21/2010 8:50	377.600	-0.000378	0.371	-0.00009
12/21/2010 8:51	378.400	-0.000378	0.372	-0.00009
12/21/2010 8:52	379.200	-0.000379	0.372	-0.00009
12/21/2010 8:53	379.900	-0.000380	0.373	-0.00009
12/21/2010 8:54	380.900	-0.000381	0.374	-0.00009
12/21/2010 8:55	381.600	-0.000382	0.374	-0.00009
12/21/2010 8:56	382.400	-0.000382	0.375	-0.00009
12/21/2010 8:57	383.200	-0.000383	0.376	-0.00009
12/21/2010 8:58	384.000	-0.000384	0.376	-0.00009
12/21/2010 8:59	384.800	-0.000385	0.377	-0.00009
12/21/2010 9:00	385.700	-0.000386	0.378	-0.00009

12/21/2010 9:01	386.500	-0.000387	0.379	-0.00009
12/21/2010 9:02	387.400	-0.000387	0.379	-0.00009
12/21/2010 9:03	388.300	-0.000388	0.380	-0.00009
12/21/2010 9:04	389.100	-0.000389	0.381	-0.00009
12/21/2010 9:05	389.800	-0.000390	0.381	-0.00009
12/21/2010 9:06	390.600	-0.000391	0.382	-0.00009
12/21/2010 9:07	391.500	-0.000392	0.383	-0.00009
12/21/2010 9:08	392.300	-0.000392	0.383	-0.00009
12/21/2010 9:09	393.200	-0.000393	0.384	-0.00009
12/21/2010 9:10	394.000	-0.000394	0.385	-0.00009
12/21/2010 9:11	394.800	-0.000395	0.386	-0.00009
12/21/2010 9:12	395.600	-0.000396	0.386	-0.00009
12/21/2010 9:13	396.400	-0.000396	0.387	-0.00009
12/21/2010 9:14	397.200	-0.000397	0.388	-0.00009
12/21/2010 9:15	398.000	-0.000398	0.388	-0.00009
12/21/2010 9:16	398.800	-0.000399	0.389	-0.00009
12/21/2010 9:17	399.600	-0.000400	0.390	-0.00009
12/21/2010 9:18	400.400	-0.000400	0.390	-0.00009
12/21/2010 9:19	401.200	-0.000401	0.391	-0.00009
12/21/2010 9:20	402.000	-0.000402	0.392	-0.00009
12/21/2010 9:21	402.800	-0.000403	0.392	-0.00009
12/21/2010 9:22	403.600	-0.000404	0.393	-0.00009
12/21/2010 9:23	404.400	-0.000404	0.394	-0.00009
12/21/2010 9:24	405.200	-0.000405	0.395	-0.00009
12/21/2010 9:25	406.000	-0.000406	0.395	-0.00009
12/21/2010 9:26	406.800	-0.000407	0.396	-0.00009
12/21/2010 9:27	407.600	-0.000408	0.397	-0.00009
12/21/2010 9:28	408.400	-0.000408	0.397	-0.00009
12/21/2010 9:29	409.200	-0.000409	0.398	-0.00009
12/21/2010 9:30	409.900	-0.000410	0.399	-0.00009
12/21/2010 9:31	410.900	-0.000411	0.399	-0.00009
12/21/2010 9:32	411.600	-0.000412	0.400	-0.00009
12/21/2010 9:33	412.400	-0.000412	0.401	-0.00009
12/21/2010 9:34	413.200	-0.000413	0.402	-0.00009
12/21/2010 9:35	413.900	-0.000414	0.402	-0.00009
12/21/2010 9:36	414.700	-0.000415	0.403	-0.00009
12/21/2010 9:37	415.400	-0.000415	0.404	-0.00009
12/21/2010 9:38	416.200	-0.000416	0.404	-0.00009
12/21/2010 9:39	416.900	-0.000417	0.405	-0.00009
12/21/2010 9:40	417.700	-0.000418	0.406	-0.00009

12/21/2010 9:41	418.400	-0.000418	0.406	-0.00009
12/21/2010 9:42	419.200	-0.000419	0.407	-0.00009
12/21/2010 9:43	420.000	-0.000420	0.408	-0.00009
12/21/2010 9:44	420.800	-0.000421	0.408	-0.00009
12/21/2010 9:45	421.600	-0.000422	0.409	-0.00009
12/21/2010 9:46	422.300	-0.000422	0.410	-0.00009
12/21/2010 9:47	423.100	-0.000423	0.411	-0.00009
12/21/2010 9:48	423.900	-0.000424	0.411	-0.00009
12/21/2010 9:49	424.600	-0.000425	0.412	-0.00009
12/21/2010 9:50	425.500	-0.000426	0.413	-0.00009
12/21/2010 9:51	426.100	-0.000426	0.413	-0.00009
12/21/2010 9:52	426.900	-0.000427	0.414	-0.00009
12/21/2010 9:53	427.600	-0.000428	0.415	-0.00009
12/21/2010 9:54	428.300	-0.000428	0.415	-0.00009
12/21/2010 9:55	429.100	-0.000429	0.416	-0.00009
12/21/2010 9:56	429.800	-0.000430	0.417	-0.00009
12/21/2010 9:57	430.600	-0.000431	0.418	-0.00009
12/21/2010 9:58	431.300	-0.000431	0.418	-0.00009
12/21/2010 9:59	432.000	-0.000432	0.419	-0.00009
12/21/2010 10:00	432.600	-0.000433	0.420	-0.00009
12/21/2010 10:01	433.400	-0.000433	0.420	-0.00009
12/21/2010 10:02	434.000	-0.000434	0.421	-0.00009
12/21/2010 10:03	434.800	-0.000435	0.422	-0.00009
12/21/2010 10:04	435.400	-0.000435	0.422	-0.00009
12/21/2010 10:05	436.100	-0.000436	0.423	-0.00009
12/21/2010 10:06	436.800	-0.000437	0.424	-0.00009
12/21/2010 10:07	437.500	-0.000438	0.424	-0.00009
12/21/2010 10:08	438.200	-0.000438	0.425	-0.00009
12/21/2010 10:09	438.800	-0.000439	0.426	-0.00009
12/21/2010 10:10	439.400	-0.000439	0.427	-0.00009
12/21/2010 10:11	440.100	-0.000440	0.427	-0.00009
12/21/2010 10:12	440.700	-0.000441	0.428	-0.00009
12/21/2010 10:13	441.400	-0.000441	0.429	-0.00009
12/21/2010 10:14	442.100	-0.000442	0.429	-0.00009
12/21/2010 10:15	442.800	-0.000443	0.430	-0.00009
12/21/2010 10:16	443.300	-0.000443	0.431	-0.00009
12/21/2010 10:17	443.900	-0.000444	0.431	-0.00009
12/21/2010 10:18	444.400	-0.000444	0.432	-0.00009
12/21/2010 10:19	445.100	-0.000445	0.433	-0.00009
12/21/2010 10:20	445.700	-0.000446	0.434	-0.00009

12/21/2010 10:21	446.200	-0.000446	0.434	-0.00009
12/21/2010 10:22	446.800	-0.000447	0.435	-0.00009
12/21/2010 10:23	447.300	-0.000447	0.436	-0.00009
12/21/2010 10:24	447.900	-0.000448	0.436	-0.00009
12/21/2010 10:25	448.400	-0.000448	0.437	-0.00009
12/21/2010 10:26	449.000	-0.000449	0.438	-0.00009
12/21/2010 10:27	449.500	-0.000450	0.438	-0.00009
12/21/2010 10:28	450.100	-0.000450	0.439	-0.00009
12/21/2010 10:29	450.600	-0.000451	0.440	-0.00009
12/21/2010 10:30	451.100	-0.000451	0.440	-0.00009
12/21/2010 10:31	451.600	-0.000452	0.441	-0.00009
12/21/2010 10:32	452.100	-0.000452	0.442	-0.00009
12/21/2010 10:33	452.700	-0.000453	0.443	-0.00009
12/21/2010 10:34	453.200	-0.000453	0.443	-0.00009
12/21/2010 10:35	453.700	-0.000454	0.444	-0.00009
12/21/2010 10:36	454.100	-0.000454	0.445	-0.00009
12/21/2010 10:37	454.600	-0.000455	0.445	-0.00009
12/21/2010 10:38	455.100	-0.000455	0.446	-0.00009
12/21/2010 10:39	455.600	-0.000456	0.447	-0.00009
12/21/2010 10:40	456.200	-0.000456	0.447	-0.00009
12/21/2010 10:41	456.700	-0.000457	0.448	-0.00009
12/21/2010 10:42	457.100	-0.000457	0.449	-0.00009
12/21/2010 10:43	457.500	-0.000458	0.450	-0.00009
12/21/2010 10:44	458.000	-0.000458	0.450	-0.00009
12/21/2010 10:45	458.400	-0.000458	0.451	-0.00009
12/21/2010 10:46	458.900	-0.000459	0.452	-0.00009
12/21/2010 10:47	459.400	-0.000459	0.452	-0.00009
12/21/2010 10:48	459.800	-0.000460	0.453	-0.00009
12/21/2010 10:49	460.200	-0.000460	0.454	-0.00009
12/21/2010 10:50	460.700	-0.000461	0.454	-0.00009
12/21/2010 10:51	461.100	-0.000461	0.455	-0.00009
12/21/2010 10:52	461.500	-0.000462	0.456	-0.00009
12/21/2010 10:53	461.900	-0.000462	0.456	-0.00009
12/21/2010 10:54	462.400	-0.000462	0.457	-0.00009
12/21/2010 10:55	462.800	-0.000463	0.458	-0.00009
12/21/2010 10:56	463.200	-0.000463	0.459	-0.00009
12/21/2010 10:57	463.600	-0.000464	0.459	-0.00009
12/21/2010 10:58	463.900	-0.000464	0.460	-0.00009
12/21/2010 10:59	464.200	-0.000464	0.461	-0.00009
12/21/2010 11:00	464.700	-0.000465	0.461	-0.00009

12/21/2010 11:01	465.000	-0.000465	0.462	-0.00009
12/21/2010 11:02	465.300	-0.000465	0.463	-0.00009
12/21/2010 11:03	465.600	-0.000466	0.463	-0.00009
12/21/2010 11:04	466.000	-0.000466	0.464	-0.00009
12/21/2010 11:05	466.400	-0.000466	0.465	-0.00009
12/21/2010 11:06	466.700	-0.000467	0.466	-0.00009
12/21/2010 11:07	467.000	-0.000467	0.466	-0.00009
12/21/2010 11:08	467.400	-0.000467	0.467	-0.00009
12/21/2010 11:09	467.800	-0.000468	0.468	-0.00009
12/21/2010 11:10	468.100	-0.000468	0.468	-0.00009
12/21/2010 11:11	468.400	-0.000468	0.469	-0.00009
12/21/2010 11:12	468.700	-0.000469	0.470	-0.00009
12/21/2010 11:13	469.000	-0.000469	0.470	-0.00009
12/21/2010 11:14	469.300	-0.000469	0.471	-0.00009
12/21/2010 11:15	469.600	-0.000470	0.472	-0.00009
12/21/2010 11:16	469.900	-0.000470	0.472	-0.00009
12/21/2010 11:17	470.200	-0.000470	0.473	-0.00009
12/21/2010 11:18	470.500	-0.000471	0.474	-0.00009
12/21/2010 11:19	470.800	-0.000471	0.475	-0.00009
12/21/2010 11:20	471.000	-0.000471	0.475	-0.00009
12/21/2010 11:21	471.300	-0.000471	0.476	-0.00009
12/21/2010 11:22	471.600	-0.000472	0.477	-0.00009
12/21/2010 11:23	471.900	-0.000472	0.477	-0.00009
12/21/2010 11:24	472.100	-0.000472	0.478	-0.00009
12/21/2010 11:25	472.300	-0.000472	0.479	-0.00009
12/21/2010 11:26	472.600	-0.000473	0.479	-0.00009
12/21/2010 11:27	472.900	-0.000473	0.480	-0.00009
12/21/2010 11:28	473.200	-0.000473	0.481	-0.00009
12/21/2010 11:29	473.500	-0.000474	0.482	-0.00009
12/21/2010 11:30	473.800	-0.000474	0.482	-0.00009
12/21/2010 11:31	474.000	-0.000474	0.483	-0.00009
12/21/2010 11:32	474.300	-0.000474	0.484	-0.00009
12/21/2010 11:33	474.500	-0.000475	0.484	-0.00009
12/21/2010 11:34	474.800	-0.000475	0.485	-0.00009
12/21/2010 11:35	475.000	-0.000475	0.486	-0.00009
12/21/2010 11:36	475.200	-0.000475	0.486	-0.00009
12/21/2010 11:37	475.500	-0.000476	0.487	-0.00009
12/21/2010 11:38	475.800	-0.000476	0.488	-0.00009
12/21/2010 11:39	476.000	-0.000476	0.489	-0.00009
12/21/2010 11:40	476.300	-0.000476	0.489	-0.00009

12/21/2010 11:41	476.600	-0.000477	0.490	-0.00009
12/21/2010 11:42	476.800	-0.000477	0.491	-0.00009
12/21/2010 11:43	477.000	-0.000477	0.491	-0.00009
12/21/2010 11:44	477.300	-0.000477	0.492	-0.00009
12/21/2010 11:45	477.500	-0.000478	0.493	-0.00009
12/21/2010 11:46	477.700	-0.000478	0.493	-0.00009
12/21/2010 11:47	478.000	-0.000478	0.494	-0.00009
12/21/2010 11:48	478.200	-0.000478	0.495	-0.00009
12/21/2010 11:49	478.400	-0.000478	0.495	-0.00009
12/21/2010 11:50	478.700	-0.000479	0.496	-0.00009
12/21/2010 11:51	478.800	-0.000479	0.497	-0.00009
12/21/2010 11:52	479.000	-0.000479	0.498	-0.00009
12/21/2010 11:53	479.100	-0.000479	0.498	-0.00009
12/21/2010 11:54	479.300	-0.000479	0.499	-0.00009
12/21/2010 11:55	479.500	-0.000480	0.500	-0.00009
12/21/2010 11:56	479.700	-0.000480	0.500	-0.00009
12/21/2010 11:57	479.900	-0.000480	0.501	-0.00009
12/21/2010 11:58	480.100	-0.000480	0.502	-0.00009
12/21/2010 11:59	480.200	-0.000480	0.502	-0.00009
12/21/2010 12:00	480.400	-0.000480	0.503	-0.00009
12/21/2010 12:01	480.600	-0.000481	0.504	-0.00009
12/21/2010 12:02	480.800	-0.000481	0.505	-0.00009
12/21/2010 12:03	480.900	-0.000481	0.505	-0.00009
12/21/2010 12:04	481.100	-0.000481	0.506	-0.00009
12/21/2010 12:05	481.200	-0.000481	0.507	-0.00009
12/21/2010 12:06	481.400	-0.000481	0.507	-0.00009
12/21/2010 12:07	481.600	-0.000482	0.508	-0.00009
12/21/2010 12:08	481.700	-0.000482	0.509	-0.00009
12/21/2010 12:09	481.900	-0.000482	0.509	-0.00009
12/21/2010 12:10	482.000	-0.000482	0.510	-0.00009
12/21/2010 12:11	482.200	-0.000482	0.511	-0.00008
12/21/2010 12:12	482.400	-0.000482	0.511	-0.00008
12/21/2010 12:13	482.600	-0.000483	0.512	-0.00008
12/21/2010 12:14	482.700	-0.000483	0.513	-0.00008
12/21/2010 12:15	482.700	-0.000483	0.514	-0.00008
12/21/2010 12:16	482.900	-0.000483	0.514	-0.00008
12/21/2010 12:17	483.000	-0.000483	0.515	-0.00008
12/21/2010 12:18	483.100	-0.000483	0.516	-0.00008
12/21/2010 12:19	483.300	-0.000483	0.516	-0.00008
12/21/2010 12:20	483.400	-0.000483	0.517	-0.00008

12/21/2010 12:21	483.500	-0.000484	0.518	-0.00008
12/21/2010 12:22	483.700	-0.000484	0.518	-0.00008
12/21/2010 12:23	483.800	-0.000484	0.519	-0.00008
12/21/2010 12:24	484.000	-0.000484	0.520	-0.00008
12/21/2010 12:25	484.200	-0.000484	0.521	-0.00008
12/21/2010 12:26	484.400	-0.000484	0.521	-0.00008
12/21/2010 12:27	484.500	-0.000485	0.522	-0.00008
12/21/2010 12:28	484.600	-0.000485	0.523	-0.00008
12/21/2010 12:29	484.700	-0.000485	0.523	-0.00008
12/21/2010 12:30	484.800	-0.000485	0.524	-0.00008
12/21/2010 12:31	484.900	-0.000485	0.525	-0.00008
12/21/2010 12:32	485.100	-0.000485	0.525	-0.00008
12/21/2010 12:33	485.300	-0.000485	0.526	-0.00008
12/21/2010 12:34	485.500	-0.000486	0.527	-0.00008
12/21/2010 12:35	485.700	-0.000486	0.527	-0.00008
12/21/2010 12:36	485.700	-0.000486	0.528	-0.00008
12/21/2010 12:37	485.800	-0.000486	0.529	-0.00008
12/21/2010 12:38	486.100	-0.000486	0.530	-0.00008
12/21/2010 12:39	486.100	-0.000486	0.530	-0.00008
12/21/2010 12:40	486.200	-0.000486	0.531	-0.00008
12/21/2010 12:41	486.400	-0.000486	0.532	-0.00008
12/21/2010 12:42	486.500	-0.000487	0.532	-0.00008
12/21/2010 12:43	486.600	-0.000487	0.533	-0.00008
12/21/2010 12:44	486.800	-0.000487	0.534	-0.00008
12/21/2010 12:45	486.900	-0.000487	0.534	-0.00008
12/21/2010 12:46	487.000	-0.000487	0.535	-0.00008
12/21/2010 12:47	487.100	-0.000487	0.536	-0.00008
12/21/2010 12:48	487.200	-0.000487	0.537	-0.00008
12/21/2010 12:49	487.400	-0.000487	0.537	-0.00008
12/21/2010 12:50	487.500	-0.000488	0.538	-0.00008
12/21/2010 12:51	487.700	-0.000488	0.539	-0.00008
12/21/2010 12:52	487.700	-0.000488	0.539	-0.00008
12/21/2010 12:53	488.000	-0.000488	0.540	-0.00008
12/21/2010 12:54	488.100	-0.000488	0.541	-0.00008
12/21/2010 12:55	488.100	-0.000488	0.541	-0.00008
12/21/2010 12:56	488.200	-0.000488	0.542	-0.00008
12/21/2010 12:57	488.400	-0.000488	0.543	-0.00008
12/21/2010 12:58	488.400	-0.000488	0.543	-0.00008
12/21/2010 12:59	488.500	-0.000489	0.544	-0.00008
12/21/2010 13:00	488.600	-0.000489	0.545	-0.00008

12/21/2010 13:01	488.700	-0.000489	0.546	-0.00008
12/21/2010 13:02	488.700	-0.000489	0.546	-0.00008
12/21/2010 13:03	488.700	-0.000489	0.547	-0.00008
12/21/2010 13:04	488.900	-0.000489	0.548	-0.00008
12/21/2010 13:05	489.000	-0.000489	0.548	-0.00008
12/21/2010 13:06	489.100	-0.000489	0.549	-0.00008
12/21/2010 13:07	489.200	-0.000489	0.550	-0.00008
12/21/2010 13:08	489.200	-0.000489	0.550	-0.00008
12/21/2010 13:09	489.300	-0.000489	0.551	-0.00008
12/21/2010 13:10	489.400	-0.000489	0.552	-0.00008
12/21/2010 13:11	489.600	-0.000490	0.553	-0.00008
12/21/2010 13:12	489.500	-0.000490	0.553	-0.00008
12/21/2010 13:13	489.600	-0.000490	0.554	-0.00008
12/21/2010 13:14	489.700	-0.000490	0.555	-0.00008
12/21/2010 13:15	489.800	-0.000490	0.555	-0.00008
12/21/2010 13:16	489.900	-0.000490	0.556	-0.00008
12/21/2010 13:17	490.000	-0.000490	0.557	-0.00008
12/21/2010 13:18	490.000	-0.000490	0.557	-0.00008
12/21/2010 13:19	490.100	-0.000490	0.558	-0.00008
12/21/2010 13:20	490.200	-0.000490	0.559	-0.00008
12/21/2010 13:21	490.300	-0.000490	0.559	-0.00008
12/21/2010 13:22	490.400	-0.000490	0.560	-0.00008
12/21/2010 13:23	490.500	-0.000491	0.561	-0.00008
12/21/2010 13:24	490.600	-0.000491	0.562	-0.00008
12/21/2010 13:25	490.700	-0.000491	0.562	-0.00008
12/21/2010 13:26	490.700	-0.000491	0.563	-0.00008
12/21/2010 13:27	490.800	-0.000491	0.564	-0.00008
12/21/2010 13:28	490.900	-0.000491	0.564	-0.00008
12/21/2010 13:29	491.000	-0.000491	0.565	-0.00008
12/21/2010 13:30	491.000	-0.000491	0.566	-0.00008
12/21/2010 13:31	491.100	-0.000491	0.566	-0.00008
12/21/2010 13:32	491.100	-0.000491	0.567	-0.00008
12/21/2010 13:33	491.200	-0.000491	0.568	-0.00008
12/21/2010 13:34	491.300	-0.000491	0.569	-0.00008
12/21/2010 13:35	491.300	-0.000491	0.569	-0.00008
12/21/2010 13:36	491.300	-0.000491	0.570	-0.00008
12/21/2010 13:37	491.300	-0.000491	0.571	-0.00008
12/21/2010 13:38	491.400	-0.000491	0.571	-0.00008
12/21/2010 13:39	491.500	-0.000492	0.572	-0.00008
12/21/2010 13:40	491.600	-0.000492	0.573	-0.00008

12/21/2010 13:41	491.600	-0.000492	0.573	-0.00008
12/21/2010 13:42	491.600	-0.000492	0.574	-0.00008
12/21/2010 13:43	491.700	-0.000492	0.575	-0.00008
12/21/2010 13:44	491.800	-0.000492	0.575	-0.00008
12/21/2010 13:45	491.900	-0.000492	0.576	-0.00008
12/21/2010 13:46	491.900	-0.000492	0.577	-0.00008
12/21/2010 13:47	491.900	-0.000492	0.578	-0.00008
12/21/2010 13:48	492.000	-0.000492	0.578	-0.00008
12/21/2010 13:49	492.100	-0.000492	0.579	-0.00008
12/21/2010 13:50	492.100	-0.000492	0.580	-0.00008
12/21/2010 13:51	492.200	-0.000492	0.580	-0.00008
12/21/2010 13:52	492.200	-0.000492	0.581	-0.00008
12/21/2010 13:53	492.200	-0.000492	0.582	-0.00008
12/21/2010 13:54	492.200	-0.000492	0.582	-0.00008
12/21/2010 13:55	492.300	-0.000492	0.583	-0.00008
12/21/2010 13:56	492.400	-0.000492	0.584	-0.00008
12/21/2010 13:57	492.300	-0.000492	0.585	-0.00008
12/21/2010 13:58	492.400	-0.000492	0.585	-0.00008
12/21/2010 13:59	492.400	-0.000492	0.586	-0.00008
12/21/2010 14:00	492.500	-0.000493	0.587	-0.00008
12/21/2010 14:01	492.500	-0.000493	0.587	-0.00008
12/21/2010 14:02	492.500	-0.000493	0.588	-0.00008
12/21/2010 14:03	492.600	-0.000493	0.589	-0.00008
12/21/2010 14:04	492.600	-0.000493	0.589	-0.00008
12/21/2010 14:05	492.600	-0.000493	0.590	-0.00008
12/21/2010 14:06	492.600	-0.000493	0.591	-0.00008
12/21/2010 14:07	492.700	-0.000493	0.591	-0.00007
12/21/2010 14:08	492.700	-0.000493	0.592	-0.00007
12/21/2010 14:09	492.700	-0.000493	0.593	-0.00007
12/21/2010 14:10	492.700	-0.000493	0.594	-0.00007
12/21/2010 14:11	492.700	-0.000493	0.594	-0.00007
12/21/2010 14:12	492.700	-0.000493	0.595	-0.00007
12/21/2010 14:13	492.800	-0.000493	0.596	-0.00007
12/21/2010 14:14	492.700	-0.000493	0.596	-0.00007
12/21/2010 14:15	492.800	-0.000493	0.597	-0.00007
12/21/2010 14:16	492.900	-0.000493	0.598	-0.00007
12/21/2010 14:17	493.000	-0.000493	0.598	-0.00007
12/21/2010 14:18	493.000	-0.000493	0.599	-0.00007
12/21/2010 14:19	493.000	-0.000493	0.600	-0.00007
12/21/2010 14:20	493.000	-0.000493	0.601	-0.00007

12/21/2010 14:21	493.000	-0.000493	0.601	-0.00007
12/21/2010 14:22	493.000	-0.000493	0.602	-0.00007
12/21/2010 14:23	493.000	-0.000493	0.603	-0.00007
12/21/2010 14:24	493.000	-0.000493	0.603	-0.00007
12/21/2010 14:25	493.000	-0.000493	0.604	-0.00007
12/21/2010 14:26	493.000	-0.000493	0.605	-0.00007
12/21/2010 14:27	493.100	-0.000493	0.605	-0.00007
12/21/2010 14:28	493.100	-0.000493	0.606	-0.00007
12/21/2010 14:29	493.200	-0.000493	0.607	-0.00007
12/21/2010 14:32	493.300	-0.000493	0.609	-0.00007
12/21/2010 14:33	493.300	-0.000493	0.610	-0.00007
12/21/2010 14:34	493.300	-0.000493	0.610	-0.00007
12/21/2010 14:35	493.300	-0.000493	0.611	-0.00007
12/21/2010 14:36	493.400	-0.000493	0.612	-0.00007
12/21/2010 14:37	493.400	-0.000493	0.612	-0.00007
12/21/2010 14:38	493.400	-0.000493	0.613	-0.00007
12/21/2010 14:39	493.400	-0.000493	0.614	-0.00007
12/21/2010 14:40	493.400	-0.000493	0.614	-0.00007
12/21/2010 14:41	493.400	-0.000493	0.615	-0.00007
12/21/2010 14:42	493.400	-0.000493	0.616	-0.00007
12/21/2010 14:43	493.400	-0.000493	0.617	-0.00007
12/21/2010 14:44	493.400	-0.000493	0.617	-0.00007
12/21/2010 14:45	493.600	-0.000494	0.618	-0.00007
12/21/2010 14:46	493.500	-0.000494	0.619	-0.00007
12/21/2010 14:47	493.500	-0.000494	0.619	-0.00007
12/21/2010 14:48	493.600	-0.000494	0.620	-0.00007
12/21/2010 14:49	493.600	-0.000494	0.621	-0.00007
12/21/2010 14:50	493.700	-0.000494	0.621	-0.00007
12/21/2010 14:51	493.600	-0.000494	0.622	-0.00007
12/21/2010 14:52	493.600	-0.000494	0.623	-0.00007
12/21/2010 14:53	493.700	-0.000494	0.624	-0.00007
12/21/2010 14:54	493.700	-0.000494	0.624	-0.00007
12/21/2010 14:55	493.700	-0.000494	0.625	-0.00007
12/21/2010 14:56	493.800	-0.000494	0.626	-0.00007
12/21/2010 14:57	493.700	-0.000494	0.626	-0.00007
12/21/2010 14:58	493.700	-0.000494	0.627	-0.00007
12/21/2010 14:59	493.700	-0.000494	0.628	-0.00007
12/21/2010 15:00	493.800	-0.000494	0.628	-0.00007
12/21/2010 15:01	493.800	-0.000494	0.629	-0.00007
12/21/2010 15:02	493.700	-0.000494	0.630	-0.00007

12/21/2010 15:03	493.800	-0.000494	0.630	-0.00007
12/21/2010 15:04	493.800	-0.000494	0.631	-0.00007
12/21/2010 15:05	493.800	-0.000494	0.632	-0.00007
12/21/2010 15:06	493.800	-0.000494	0.633	-0.00007
12/21/2010 15:07	493.900	-0.000494	0.633	-0.00007
12/21/2010 15:08	493.900	-0.000494	0.634	-0.00007
12/21/2010 15:09	493.900	-0.000494	0.635	-0.00007
12/21/2010 15:10	494.000	-0.000494	0.635	-0.00007
12/21/2010 15:11	493.900	-0.000494	0.636	-0.00007
12/21/2010 15:13	493.900	-0.000494	0.637	-0.00007
12/21/2010 15:14	493.900	-0.000494	0.637	-0.00007
12/21/2010 15:15	493.800	-0.000494	0.638	-0.00007
12/21/2010 15:16	493.900	-0.000494	0.639	-0.00007
12/21/2010 15:17	493.800	-0.000494	0.640	-0.00007
12/21/2010 15:18	493.800	-0.000494	0.640	-0.00007
12/21/2010 15:19	493.800	-0.000494	0.641	-0.00007
12/21/2010 15:20	493.900	-0.000494	0.642	-0.00007
12/21/2010 15:21	494.000	-0.000494	0.642	-0.00007
12/21/2010 15:22	494.100	-0.000494	0.643	-0.00007
12/21/2010 15:23	494.100	-0.000494	0.644	-0.00007
12/21/2010 15:24	494.000	-0.000494	0.644	-0.00007
12/21/2010 15:25	494.100	-0.000494	0.645	-0.00007
12/21/2010 15:26	494.000	-0.000494	0.646	-0.00007
12/21/2010 15:27	494.100	-0.000494	0.647	-0.00007
12/21/2010 15:28	494.200	-0.000494	0.647	-0.00007
12/21/2010 15:29	494.100	-0.000494	0.648	-0.00007
12/21/2010 15:30	494.200	-0.000494	0.649	-0.00007
12/21/2010 15:31	494.200	-0.000494	0.649	-0.00007
12/21/2010 15:32	494.200	-0.000494	0.650	-0.00007
12/21/2010 15:33	494.200	-0.000494	0.651	-0.00007
12/21/2010 15:34	494.200	-0.000494	0.651	-0.00007
12/21/2010 15:35	494.100	-0.000494	0.652	-0.00007
12/21/2010 15:36	494.200	-0.000494	0.653	-0.00007
12/21/2010 15:37	494.200	-0.000494	0.653	-0.00007
12/21/2010 15:38	494.200	-0.000494	0.654	-0.00007
12/21/2010 15:39	494.200	-0.000494	0.655	-0.00007
12/21/2010 15:40	494.200	-0.000494	0.656	-0.00007
12/21/2010 15:41	494.300	-0.000494	0.656	-0.00007
12/21/2010 15:42	494.300	-0.000494	0.657	-0.00007
12/21/2010 15:43	494.300	-0.000494	0.658	-0.00007

12/21/2010 15:44	494.300	-0.000494	0.658	-0.00007
12/21/2010 15:45	494.400	-0.000494	0.659	-0.00007
12/21/2010 15:46	494.300	-0.000494	0.660	-0.00007
12/21/2010 15:47	494.400	-0.000494	0.660	-0.00007
12/21/2010 15:48	494.400	-0.000494	0.661	-0.00007
12/21/2010 15:49	494.400	-0.000494	0.662	-0.00007
12/21/2010 15:50	494.400	-0.000494	0.663	-0.00007
12/21/2010 15:51	494.500	-0.000495	0.663	-0.00007
12/21/2010 15:52	494.500	-0.000495	0.664	-0.00007
12/21/2010 15:53	494.600	-0.000495	0.665	-0.00007
12/21/2010 15:54	494.600	-0.000495	0.665	-0.00007
12/21/2010 15:55	494.500	-0.000495	0.666	-0.00007
12/21/2010 15:56	494.600	-0.000495	0.667	-0.00007
12/21/2010 15:57	494.600	-0.000495	0.667	-0.00007
12/21/2010 15:58	494.600	-0.000495	0.668	-0.00007
12/21/2010 15:59	494.600	-0.000495	0.669	-0.00007
12/21/2010 16:00	494.600	-0.000495	0.669	-0.00007
12/21/2010 16:01	494.500	-0.000495	0.670	-0.00007
12/21/2010 16:02	494.500	-0.000495	0.671	-0.00007
12/21/2010 16:03	494.500	-0.000495	0.672	-0.00007
12/21/2010 16:04	494.500	-0.000495	0.672	-0.00007
12/21/2010 16:05	494.500	-0.000495	0.673	-0.00007
12/21/2010 16:06	494.600	-0.000495	0.674	-0.00007
12/21/2010 16:07	494.500	-0.000495	0.674	-0.00007
12/21/2010 16:08	494.400	-0.000494	0.675	-0.00007
12/21/2010 16:09	494.500	-0.000495	0.676	-0.00007
12/21/2010 16:10	494.600	-0.000495	0.676	-0.00007
12/21/2010 16:11	494.600	-0.000495	0.677	-0.00007
12/21/2010 16:12	494.700	-0.000495	0.678	-0.00007
12/21/2010 16:13	494.700	-0.000495	0.679	-0.00007
12/21/2010 16:14	494.700	-0.000495	0.679	-0.00007
12/21/2010 16:15	494.700	-0.000495	0.680	-0.00007
12/21/2010 16:16	494.700	-0.000495	0.681	-0.00007
12/21/2010 16:17	494.700	-0.000495	0.681	-0.00007
12/21/2010 16:18	494.700	-0.000495	0.682	-0.00007

APPENDIX D – SUPPORTING FILES [COMPACT DISC]

D.1 DESCRIPTION AND CONTENTS OF CD

This CD contains the experimental data from Phases I, II, III and Phase IV as well as the numerical modelling files – SVFlux files (*.svm). There are 5 folders, which contain Excel files of both the experimental and numerical data. A list of each folder and subfolders are as follows:

PHASE I_Calibrations

- 1) ECH2O EC Sensors

PHASE II_ Pre- and Post- WRCs

- 1) Williams Tailings >> pre and post hydration >> trials 1 and 2
- 2) Kidd Tailings >> pre and post hydration

PHASE III_Paste Hydration

- 1) Self-desiccation:
 - (i) Williams Paste >> trials 1 and 2
 - (ii) Kidd Paste >> trials 1 and 2
- 2) MIP Results:
 - (i) Williams 3% Binder [* .red and * .xls Formats]
 - (ii) Williams 7% Binder [* .red and * .xls Formats]

PHASE IV_Column Test Results

- 1) PICTURES_Column
- 2) Suction and Moisture Profiles

NUMERICAL MODELLING

- 1) Column Results
- 2) SVFlux Files

D.2 ACCOMPANIED CD

GLOSSARY

Absolute pressure	Zero-referenced against a perfect vacuum, which is equal to gauge pressure plus atmospheric pressure
Acid mine drainage	Oxidation by-product of acid generating tailings to mobilize in water, resulting in high concentrations of dissolved metals and a pH less than 3
Admixtures	Chemical additives such as, antifreeze compounds and accelerators are sometimes added to change the physical and chemical properties of cement pastes and mortars, respectively
Air entry pressure	An air pressure required to introduce air into and through the pores of a saturated porous disc/plate
Air entry value	A suction required to introduce air into and through the pores of a saturated porous media (i.e. soil specimen)
Axis translation	Principle stating that a matric suction can be applied to a soil by controlling the pore-air pressure and the pore-water pressure so that the difference between the pore pressures equals to the desired matric suction
Barricade	A construction wall whose purpose is to retain backfill within a mined-out stope. Can be constructed out of timber, concrete, brick and shotcrete
Binder	Refers to an adhesive combined with admixtures, such as fly ash, bottom ash, slag and accelerants (i.e. calcium chloride)
Blast-furnace slag	Also called ground granulated blast-furnace slag (GGBFS) is a by-product of iron processing through blast-furnace. Non-metallic portion of this process or molten slag is drenched and cooled to form granular, which is then grounded to a suitable fineness
Bulkhead	A constructed barrier that separates sections of a mine where no external loads are applied. Typically used for ventilation purposes
Cavitation nuclei	Presence of tiny gas bubbles rupturing in the liquid water phase under tension.
Cement	The adhesive or binder reagent consisting of a lime base (i.e. chalk), heated at temperatures 600 degrees Celsius plus

Cemented paste backfill	Material made up of dewatered tailings made into a filter cake (approximately 75-80% weight by solids), processes water and a binding agent. Used in underground fill
Critical pore diameter	The maximum continuous pore radius, corresponding to the largest fraction of interconnecting pores. It can also be defined as the smallest pore at which significant intruded mercury volume can be detected
Concrete	A particulate composite of stone and sand, held together by an adhesive (cemented paste)
Cross-cut	A horizontal or nearly horizontal underground opening that is driven to intersect an ore body
Degree of saturation	Ratio of the volume of water in a given soil or rock mass, to the total volume of intergranular pore space (voids)
Dip	An angle at which an ore deposit is inclined from the horizontal
Differential pressure	A pressure gradient, which is equal to the difference in pressure from one point to another
Drift	A horizontal underground tunnel that follows a vein or ore body
Drilling and Blasting	Process of using a drill to create long, narrow cylindrical holes in the rock, and filling these holes with explosives which are then detonated to fragment the rock
Elevation head	Elevation energy that is equal to the elevation of the point of above a datum
Electrical capacitance sensor	A tool used to infer the volumetric water content of an unsaturated soil through measurement of the capacitance of a sensor embedded within the soil specimen
Fill Fence	Specific type of barricade consisting of an anchored rebar skeleton and shotcrete
Footwall	A wall or rock under the ore deposit
Gage Pressure	Zero-referenced against ambient air pressure, which is equal to absolute pressure minus atmospheric pressure. Negative signs are usually omitted
Gravimetric water content	Ratio of the mass of water contained in the pore spaces of soil or rock to the mass of solid particles

Hanging wall	A wall or rock above an ore deposit
Hydraulic binders	Binders or cements that set and harden by reacting chemically with water, which is composed primarily of hydraulic calcium silicates
Hydraulic conductivity	The coefficient of proportionality between the water discharge velocity under laminar flow conditions through a unit cross-section area of a porous medium under a unit hydraulic gradient and standard temperature conditions (20°C). Also referred to as the water permeability
Hydraulic conductivity function	A relationship between the hydraulic conductivity and the matric suction, volumetric water content, or degree of saturation
Hydraulic fill	Deslimed mill tailings slurry, primarily composed of the coarser fractions, while the slimes are rejected to surface impoundments. It is a highly permeable backfill containing high water content (approximately 60-70% solids by weight)
Hydraulic gradient	The change in total hydraulic head per unit distance in the direction of fluid flow
Hydrostatic pressure	Pressure exerted by a fluid at equilibrium (at rest) due to the force of gravity; the height of a liquid column of uniform density is directly proportional to the hydrostatic pressure
Internal Stresses	Total stresses and hydraulic stresses
Liquefaction	A process by which water-saturated sediments temporarily loses strength and acts as a fluid (ground subsidence)
Level / sub-levels	A system of horizontal underground working that is connected to the shaft. It forms the basis for excavation of the ore above or below
Load	A measured applied force, in N or kN
Man-way	An underground opening that is intended for personnel access and communication
Matric suction	Difference between the pore-air pressure and the pore-water pressure, also referred to as the matric potential, capillary suction and capillary potential. It is the negative gauge pressure, relative to an external gas pressure acting on the soil water.
Mine safety	Integrity of the mine workings as a whole or in part

Mortar	A bonding agent that is used to integrate masonry walls. As per ASTM C270, mortars consist of either Type I (Type 10), Type II (Type 20), or Type III (Type 30) Portland Cement, or hydrated lime (Type S) mixed with sand and water
Nucleation	Refer to cavitation
Newtonian fluid	A fluid whose stress versus strain curve is linear, such that the flow rate and strain rate is independent of viscosity.
Non-Newtonian fluid	A fluid whose stress and strain curve is non-linear, such that the flow rate and strain rate is dependent upon viscosity
Optimize recovery	80% or greater recovery of geological reserves
Optimize stope sequencing	Minimize schedule required to achieve full mine production
Ore	A metallic mineral deposit that can be extracted from host rock for monetary profit under existing economic conditions
Ore pillars	Ore masses that are left behind to provide ground support
Osmotic suction	Negative gauge pressure derived from the measurement of the vapour pressure of water in equilibrium with a solution identical in composition with the soil water, relative to the vapour pressure of water in equilibrium with free pure water. It is also referred to as osmotic potential
Paste	High density tailings that are dewatered and have more than 70% solids by wt.
Paste fill	Refer to <i>cemented paste backfill</i>
Porous disc/plate	A plate made of ceramic or other porous material that can transmit water and has an air-entry pressure exceeding the highest matric suction to be applied during a test
Portland cement	A controlled mixture of chalk and clay fired in a kiln at a temperature of 1500 degrees Celsius to yield a Portland cement
Pre-production development	Mining from the top-down versus bottom-up mining
Pressure	Force per unit area. Measured in kPa or MPa
Pressure head	The height of a column of static water that can be supported by the static pressure at that point

Pressure chamber	A sealed vessel used to apply an air pressure or vacuum on a specimen and/or device
Sand fill	A non-homogenous backfill mixture containing approximately 50 to 70% tailings and water
Shaft	A vertical or inclined underground opening through which a mine is worked
Shotcrete	Concrete that is pneumatically sprayed onto a surface; consists of Portland Cement
Shrinkage limit	The water content at which no further loss of moisture will result in any more volume reduction
Soil-water characteristic curve	Refer to <i>water-retention curve</i>
Stope	An underground excavation from that is made by removing ore from the surrounding rock
Stope development	Minimize selective extraction mining versus bulk mining
Stope turn-around cycle	Time / cycle from drilling, loading blasting, backfilling, setting and hardening
Sublimation	The process of directly transforming from the solid phase to the gaseous phase without passing through an intermediate liquid phase
Sublevel	A system of horizontal underground workings. Normally, sublevels are used only within stoping areas where they are required for the ore production
Subsidence	A sinking or lowering of the Earth's surface
Strain	Total deformation of an element in terms of the elements original length. Units are dimensionless
Stress	Internal resistance offered by a unit area of a material from which a member is made to an externally applied load. Measured in kPa or MPa
Tensiometer / Pressure transducer	A tool to measure the matric suction in soil by measuring the negative water pressure in a water reservoir in equilibrium with a soil via saturated porous interface (e.g., tip/cup)

Threshold diameter	the minimum fraction of interconnecting pores, which represents the pore-size above which there is comparatively little mercury intrusion, and below where the main intrusion occurs
Time domain reflectometer	A tool used to infer the volumetric water content of an unsaturated soil through measurement of the travel time of an electromagnetic pulse through a metallic shielded rod embedded within a soil
Total head	Sum of the pressure head, elevation head and velocity head; also referred to as the hydraulic head
Total suction	Negative gauge pressure derived from both matric suction and osmotic suction, also referred to as the total soil potential
Velocity head	The height of the kinetic energy of the liquid, capable of lifting said liquid
Volumetric water content	Ratio of the volume of water contained in the pore spaces of soil or rock to the total volume of soil and/or rock
Volumetric flow rate	Volume of water flow rate through a porous media / soil specimen; also referred to as water flow rate
Wall rock	A wall in which the ore deposit is enclosed
Waste rock	Barren rock or the rock of too low a grade to be mined economically
Water discharge velocity	Rate of discharge of water through a porous media per unit area perpendicular to the direction of flow; also referred to as the hydraulic conductivity
Water flow rate	The volumetric flow rate of flow of water through a porous media / soil specimen; also referred to as volumetric flow rate
Water permeability	Refer to <i>hydraulic conductivity</i>
Water-retention curve	A graph of suction (matric or total) versus water content (gravimetric or volumetric) or saturation. The water-retention curve is also referred to as the soil-water characteristic curve and the capillary pressure curve
Winze	A vertical or inclined underground opening that is driven downward from one level to another level or from the surface to a level

PUBLICATION

Hydraulic Responses in Cemented Paste Backfill During and After Hydration

M. Witteman, *Department of Civil and Environmental Engineering, Carleton University, Canada*¹

P. Simms, *Department of Civil and Environmental Engineering, Carleton University, Ottawa, Canada*²

Abstract

The distribution of pore-pressures in mine stopes may have important implications to the design of cemented paste backfill (CPB) systems. Self-weight consolidation after filling is inherently problematic when pore-water pressures begin to develop. However, during cement hydration, self-desiccation begins to occur and consequently, suction can develop within stopes, depending upon adopted mine strategies, such as filling rate and % water to binder content. Tracking the evolution and quantifying the hydraulic behaviour in cemented paste is rather difficult because of the complexity of the hydrating material. The current study investigates and attempts to capture CPB's transient responses during and after cement hydration through a series of self-desiccation and axis translation tests. Self-desiccation tests are conducted on cemented paste specimens containing 0, 3, 5 and 7% wt. binder material. The water-retention properties of the material are measured without binder, and after 28 days of hydration. This data is then used to approximately model the dissipation of pore-water pressures measured at the bottom of a stope during curing of a plug pour. The approach shows promise. Significance and future improvement to the proposed methodology are discussed.

¹ Corresponding author: mwittema@connect.carleton.ca

² Corresponding author: Paul_Simms@carleton.ca

1 Introduction and Background

Cemented paste backfill (CPB) is a relatively recent form of backfilling – a material made up of a mixture of wet tailings (70-85% wt solids), binding agent (3-7% wt) and process water. CPB technology has gained popularity around the world, as it increases ore recovery while providing a disposal option for a significant fraction of the tailings. However, the state of practice is highly conservative, as CPB is a complex material and little data is available on field performance.

CPB technology involves filling underground voids (stopes) with cemented paste material. Depending upon mining procedures, underground voids may vary in height – up to 100 meters tall. At the bottom of an open stope, a structural barricade is placed to contain the fill. It is not uncommon that mining operations employ CPB mixtures containing fine particle size distributions with rates that often result in more than 10m vertical rise per day (le Roux, 2004). The combination of particle size distribution and fill rates have important ramifications upon adopted mining strategies. While mining operations tend to vary from site to site, a rapid rate of rise will increase the total stresses that are subjected onto a stope fill and hence, increase the level of risk of a barricade failure. The rate of consolidation and strength gain in CPB is critical for sequencing removal of adjacent pillars of ore (Belem et al., 2001; Li et al., 2005; and Grabinsky and Bawden, 2007). Furthermore, ample strength must be maintain in filled stopes to allow for subsequent pillar removal while avoiding liquefaction of premature CPB from free standing exposure to nearby blasting of surrounding rock mass. Currently, the strength of CPB is evaluated through unconfined compressive strength (UCS) tests performed on laboratory-cured specimens (e.g. Belem et al., 2004; Belem and Benzaazoua, 2008; and among others). However, UCS tests provide limited information on its properties as it does not account for consolidation, drainage and hydration affects on the stress and strength distributions throughout the stope (Simms and Grabinsky, 2009). Therefore, it is necessary to assess how CPB's mechanical and hydraulic properties evolve over time as it hydrates.

Self-weight consolidation occurs immediately upon deposition of fill, generating excess pore-water pressure. However, self-desiccation due to cement hydration can significantly reduce excess pore-pressures. Self-desiccation is a known phenomenon in cement hydration (Hua et al., 1995; Kim and Lee, 1999; and Acker, 2004), where the total volume of unhydrated constituents is greater than the total hydrated volume. This change in volume or shrinkage per se, occurs when water in pore-air desaturates, producing a capillary depression between the liquid-vapor water phase, causing the solid matrix to contract or go under compression to balance capillary tension at the liquid-vapor boundary (Acker, 2004). Thus, the process of hydration has the combined effect of reducing the total volume of the water phase; increasing the water retention properties; and increasing strength and stiffness of the solid phase.

Evidence of self-desiccation has been observed in CPB; for example, Grabinsky and Simms (2006) observed significant generation of matric suctions (i.e. 100 kPa during the 6th day of curing) in sealed laboratory specimens contain 5% binder material.

Furthermore, they examined in situ samples that were representative of highest binder to lowest fill rate, and found that under such conditions, the rate of hydration effectively suppressed excess pore-water pressure development due to self-weight consolidation. Helinski et al. (2007) and Fourie et al. (2006) conducted laboratory experiments on saturated CPB samples to assess the effects of hydration on consolidated sample and found that its contribution significantly reduced excess pore-water pressures. They also identified the rapid stiffening of CPB with hydration as being very important to dissipation of excess pore-water pressure (PWP) by self-weight desiccation. One aspect that has not been studied as of yet, is tracking the evolution of CPB's hydraulic behaviour under negative pore-water pressures (matric suction), where CPB stopes are potentially unsaturated due to self-desiccation and drainage, which is the focus of this work.

The remainder of the paper presents (i) a numerical methodology to track and predict the evolution of pore-pressure distribution during and after cement hydration; (ii) some initial test results to demonstrate the affects self-desiccation and drainage; and (iii) field measurements of pore-water pressure dissipation, which are compared with generic numerical modeling that incorporates the above data.

2 Methodology for predicting pore-water pressure due to drainage and self-desiccation as unsaturated

As with any unsaturated porous material, the relevant properties governing flow are the water-retention curve (WRC), also referred to as the soil-water characteristic curve (SWCC), the saturated hydraulic conductivity, the unsaturated hydraulic conductivity function, and its compressibility when the pore-water pressure is positive. These properties can be used in the 1-D unsaturated flow equation to predict the dissipation of pore-pressure or generation of matric suction, with the addition of a sink term to account for removal of water due to inequality between the loss of water volume and the volume of generated hydration products. The 1-D unsaturated flow equation may be stated as:

$$S \frac{\partial(\psi)}{\partial t} = \frac{\partial}{\partial z} [K(\psi)] \frac{\partial h_z}{\partial z} - \text{sink term} \quad (1)$$

where, S is the specific storage (the slope of the water-retention curve in the negative pore-pressure range, or the compressibility (m_v) in the positive pore-pressure range), $K(\psi)$ is the unsaturated hydraulic conductivity as a function of matric suction, and h_z is the total head.

In CPB, the use of Equation 1 is complicated by the evolution in the material properties due to hydration. There are presently no published techniques to measure the complete evolving water retention characteristics of hydrating materials, in part because most techniques rely on achieving a steady state condition, which is not possible when the material's properties are constantly evolving. We can, however, measure the WRC without binder, and with binder once hydration has almost

ceased. This will give us upper and lower bounds on the water retention behaviour of CPB. The following experiments were designed to generate the WRC data as well as the necessary information to formulate a sink term.

3 Materials and Methods

The experimental tests included (1) Self desiccation tests: Monitoring of matric suction generation in sealed samples of CPB samples containing 3%, 5%, and 7% binder, with replicate sealed samples destructively tested at different times for gravimetric water content (GWC) to evaluate water consumption by hydration; and (2) axis translation tests to measure (i) the WRC of a CPB sample containing 3% binder material after 28 days, and (ii) a WRC of a sample without binder. These results were then used as inputs for a 1-D transient, unsaturated flow model to evaluate pore-pressure distributions within a generic stope. Further discussion on the numerical modelling simulation is presented in Section 4 of this paper.

3.1 Materials and Devices

Tailings from the Williams gold mine (Ontario, Canada) were used. The binder content for typical William mine CPB is 3% by mass of solid tailings particles. The binder material is made up of equal parts by mass of Portland cement (PC) and fly ash (FA). Filter cake, process water, and binder shipped in separate containers were received from the mine. The gravimetric water content of each sample was brought to $39 \pm 0.5\%$ of tailings solid particles before addition of the binder. A house-hold electric mixer was used to mix the tailings, water and binder materials for 1 minute.

Matric suction and total suction were directly and indirectly measured, respectively. The T5x pressure transducers / tensiometers from Umwelt-Monitoring-Systeme (UMS), Germany were used to measure the matric suction during hydration. The T5x is capable of measuring pore-water pressures up to 100 kPa and suctions up to 250 kPa and in some instances, up to 400 kPa (UMS, 2009). A volumetric pressure plate extractor, the SWC – 150, Fredlund SWCC Device, from GCTS Testing Systems, Arizona, USA, was used for WRC determination by axis translation. The volumetric pressure plate extractor cell was equipped with a high AEV ceramic disc of 15 bar (1500 kPa). The cell was connected to a pressurized air supply, in which nitrogen gas was used. Total suctions were indirectly measured using the WP4 – DewPoint PotentiaMeter, (psychrometer) from Decagon Devices, WA, USA. This device can measure suctions from 0 to – 300 MPa with an accuracy of ± 0.1 MPa from 0 to -10 MPa, and $\pm 1\%$ from -10 to -300 MPa. The WP4 uses the chilled-mirror dew point technique to measure the total suction of a sample. In this type of instrument, a small sample (< 50 g) is equilibrated with the headspace of a sealed chamber that contains a mirror and a means of detecting condensation on the mirror. At equilibrium, the relative humidity of the air in the chamber is the same as the relative humidity of the sample (Decagon Devices, 2007). Table 1, is brief summary of the measuring devices used in this study.

Table 1 **Devices and performance specifications**

Measuring Devices	Parameter	Range	Accuracy
Direct Measurement			
T5x tensiometer	Matric suction	250 kPa to -100 kPa	+/-0.5 kPa
Axis translation cell	Matric suction	0 to 1500 kPa	--
Indirect Measurement			
WP4 - psychrometer	Total suction	0 to 300 MPa	+/-1.0%

3.2 Methodology

3.2.1 Self-desiccation in CPB Specimens

CPB specimens containing 0, 3, 5 and 7% binder material were prepared and poured into concrete curing containers. The T5xs were inserted in the paste material and covered with plastic wrap to prevent water loss from evaporation. Matric suction measurements were recorded every 5 minutes for the first 48 hours and at every 10 minutes thereafter for 28 days. Some release of bleed water typically occurred within the first hour of setting for all three binder specimens, while the control (non-cemented paste) settled for over 24 hours. Water that pooled onto the surface from settling was removed with a syringe. Water contents before and after release of bleed water are shown in Table 2.

Replicate samples were prepared without tensiometers, in order to sample for gravimetric water content over time to track hydration by change in the solids to water ratio.

Table 2 **CPB recipe for 3, 5 and 7% binder specimens**

Mass (RE of +/- 0.005g)	3 % Binder Specimen	5 % Binder Specimen	7 % Binder Specimen
M_{paste}	1068.16	1025.19	1034.76
M_{solids}	766.64	735.80	742.67
M_{water}	301.52	289.39	292.09
$M_{\text{evaporable water (removed)}}$	23.25	13.59	9.12
Initial Water Content* (%)	39% / 28%		
M_{PC}	11.50	18.39	25.99
M_{FA}	11.50	18.39	25.99
M'_{paste}^+	1091.16	1061.98	1086.75
M'_{solids}^+	789.64	772.59	794.66
M'_{water}	278.27	275.80	282.97
%solids	72.37	72.75	73.12
%water	25.50	25.97	26.04
Final Water Content* (%)	35% / 25.5%	36% / 26%	35.6% / 26%

* GWCs of CPB, based on geotechnical (M_w/M_s) and mining process (M_w/M_{paste}) calculations, respectively.

* Includes the amount of PC and FA added.

3.2.2 Axis translation Technique on Fully Hydrated CPB

The axis-translation tests follow standard methods (Hilf, 1956); except that volume change is estimated at each stage by removing the cell's top after equilibration and taking vertical displacement measurements using a non-contact displacement sensor.

To ensure that contact between the specimen and ceramic disc was maintained, the sample was poured into the cell, sealed from any moisture loss and cured with zero gauge air pressure (i.e. without applied air pressure). During this time, weight and volume changes were recorded and measured during the 28 days of curing. On Day 29, the axis-translation test was initiated. Measurements were not recorded after 300 kPa, because the sample exploded inside the pressurized cell at 400 kPa. Another approach was taken to measure the remaining portion of the SWCC. The specimen was allowed to dry and total suction and gravimetric water contents were obtained by sampling the larger specimen at various times.

The WRC of the non-cemented sample was obtained using axis-translation for matric suctions less than 1000 kPa, while simultaneous sampling for total suction and gravimetric water content analyses of a drying sample was used to obtain higher values.

3.2 Experimental Results

3.2.1 Self-desiccation Tests

The sample test results are presented in Fi. There is a strong correlation between the amount of binder and the rate of suction generation. All the data exhibit a transformation in rate of suction generation in the range of 110-120 kPa. One might suspect cavitation in the tensiometers as the cause, but these sensors generally show a very sharp drop in suction subsequent to cavitation. The transformation may be because the AEV of the hydrating material is exceeded, and so the rate of suction to water removal is changing; or possibly the pace of hydration is slowing.

Matric suctions were observed in the non-cemented (control) sample after Day 9. This indicates that some evaporation does occur within the sealed samples, though the 0 % binder sample would be the most susceptible to evaporation as it had the largest air-space in its container, as it experienced the most settling.

Figure 2 shows the decrease in gravimetric water content in eight (8) replicate sealed samples with 3% binder, each oven-dried (at 98 °C) at the times shown. As there is no significant water loss from these measurements, as checked by weighing, the change in gravimetric water content is due to the change in water to solids ratio due to hydration. The relatively linear shape of the plot will allow us to assume a constant rate of water removal (sink term) in our numerical simulations. However, the constant rate at which water is removed eventually decreases as the 'available water' becomes limited as the hydration progresses.

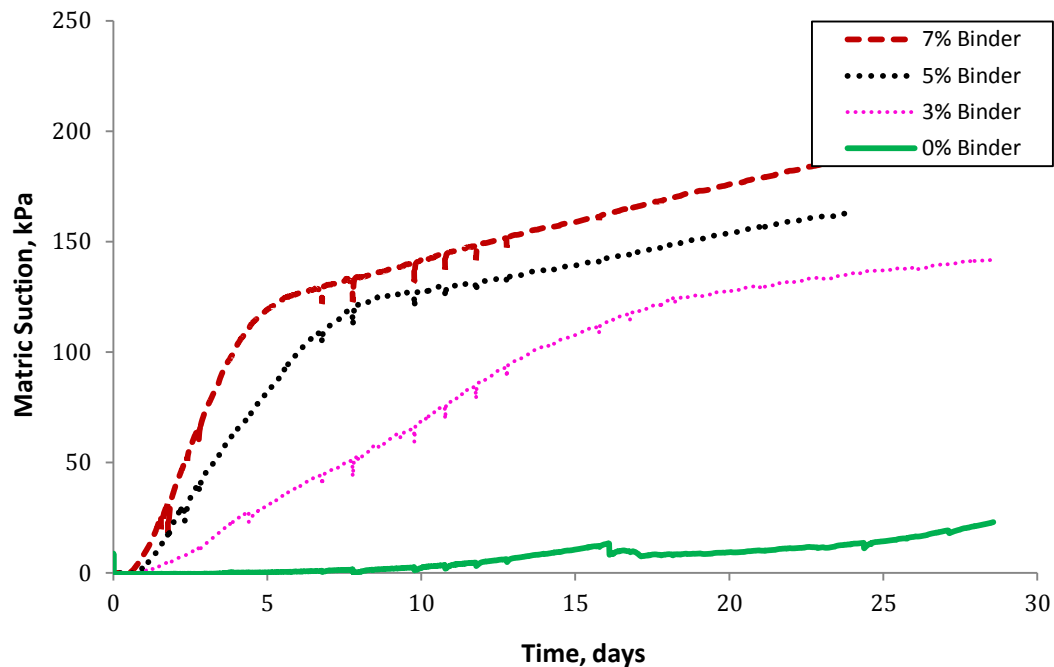


Figure 1 Induced matrix suction during paste hydration in sealed samples

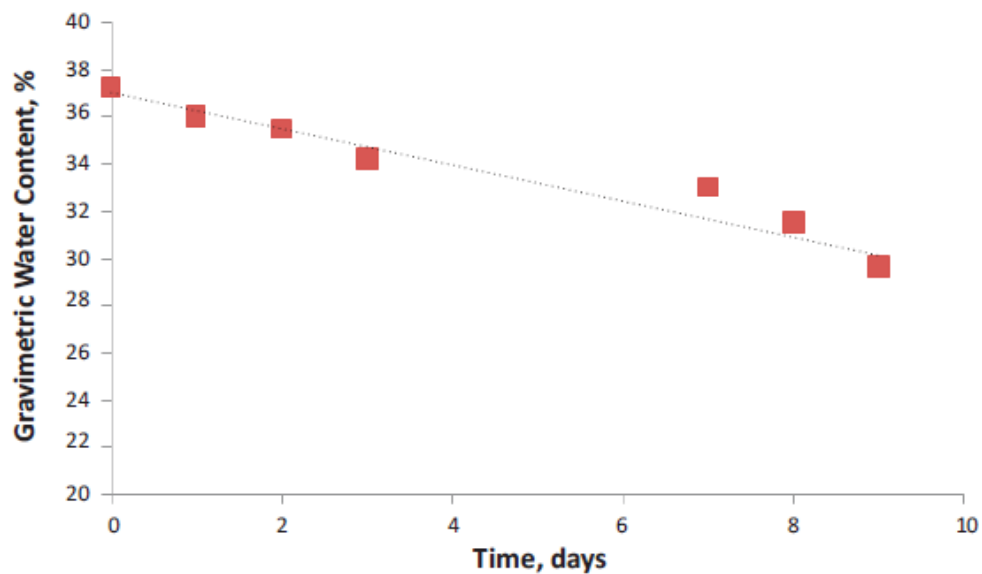


Figure 2 Gravimetric water content of replicate sealed samples with 3% binder, showing increase in solids to water ratio due to formation of hydration products

3.2.2 Water Retention Curves

The WRC for the fully hydrated 3% CPB specimen and the uncemented specimen are compared in Figure 3. The prominent differences between the two curves are the slope before the air-entry value (AEV), and the AEV itself. The AEV for the CPB sample is ~ 150 kPa, and ~ 40 kPa for the uncemented tailings (the decrease in water content $> 23\%$ GWC) is almost concurrent with shrinkage. In other words, the change in volume of water is roughly equal to the change in volume of voids for water contents $> 23\%$, as is expected in porous materials drying from a water content above their shrinkage limit. The slope of the fully hydrated specimen's WRC before the AEV is quite flat. As discussed in Simms and Grabinsky (2009), the flatness of the curve allows for significant generation of matric suctions by relatively small consumption of water due to hydration. The slope of the WRC before the AEV correlates to stiffness: the stiffer the material, the more resistant it is to dewatering by squeezing from matric suction. Figure 4 presents volumetric strain measurements made before the AEV for the CPB 3% binder specimen.

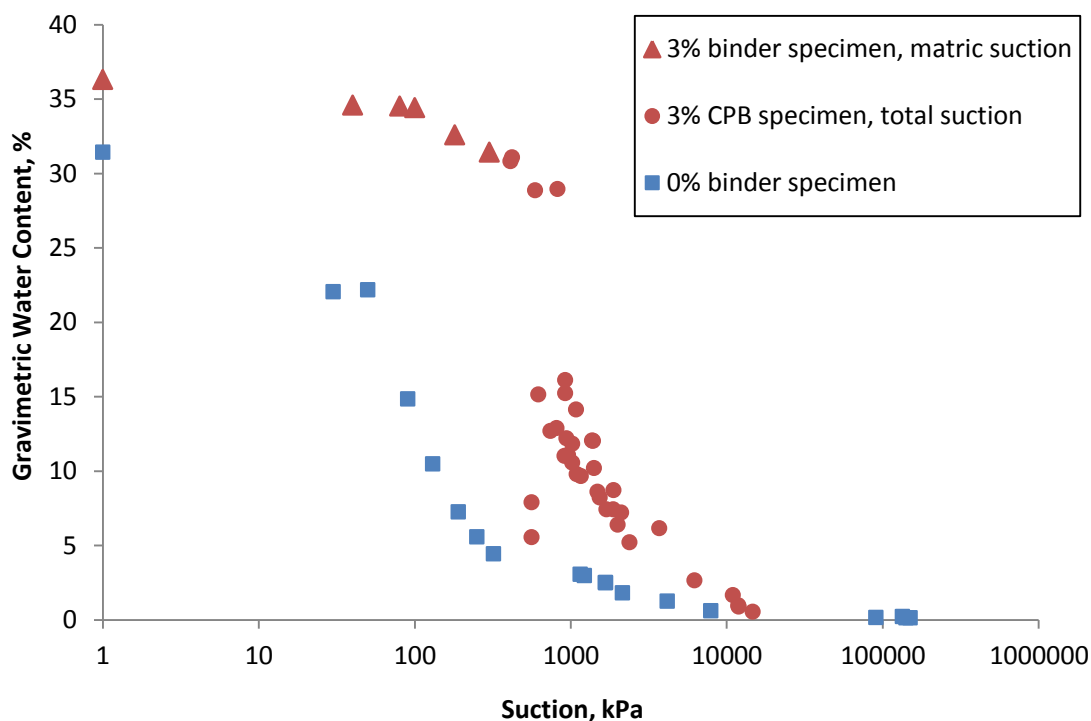


Figure 3 Pre and post-curing WRC for 3% binder specimen

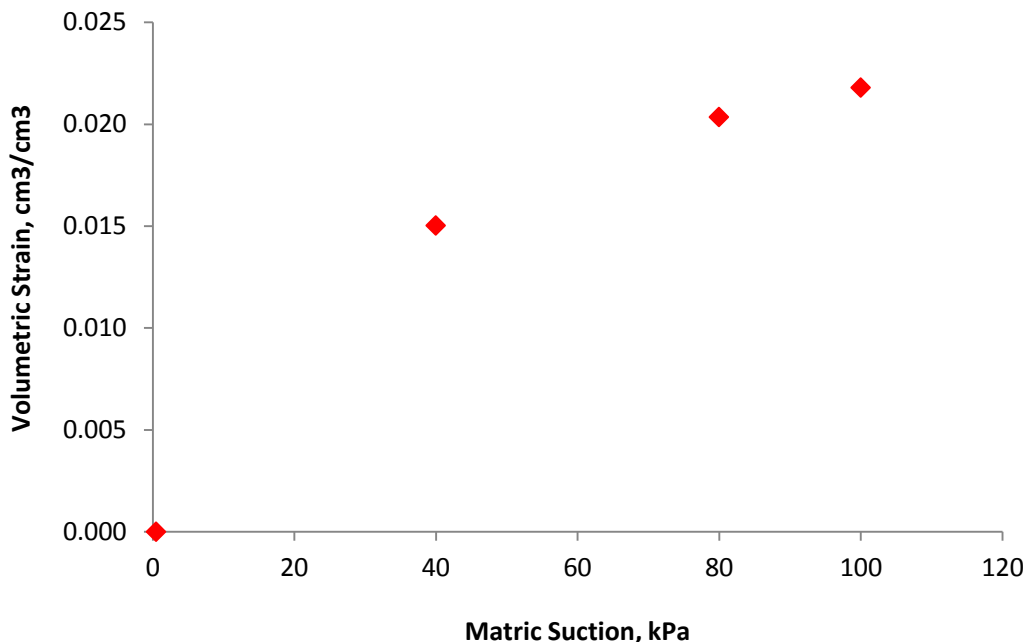


Figure 4 Volumetric strain and matric suction measured in axis-translation test of 3% binder CPB specimen after curing

4 Unsaturated Flow Modeling

4.1 Numerical Simulation Methodology

The authors attempted to simulate pore-pressure dissipation and matric suction generation measured at the Williams Gold mine in northern Ontario during and immediately after a plug pour, near the barricade at the bottom of the stope (Grabinsky and Bawden 2007). The geometry of the stope and the location of the pore-water pressure sensors are shown in Figure 5. The 8 m height was filled with 24 hours and the paste submerged the barricade by 20 hours.

Equation 1 is solved using the finite element unsaturated flow software SVFlux, which automatically optimizes time-stepping and mesh geometry. Since it is not known how the relevant properties evolve with time, several analyses have been performed, alternately using the WRC, compressibility (0.07 or 0.007) and hydraulic conductivity of the tailings (1×10^{-7} m/s or 1×10^{-8} m/s) of either the tailings without binder or of the tailings with 3% binder after 28 days of curing. We have modeled an instantaneously placed 5 m thick layer of CPB for 20 hours. We assumed an initial hydrostatic PWP distribution, but assumed only half density, to account for the slow pour. The bottom boundary condition was set to a constant head of 0 – this is conservative and will underestimate drainage. The sink term in Equation 1 was determined by the rate of water removal observed during self-desiccation for the 3% binder specimen during the first two days, using the data shown in Figure 2.

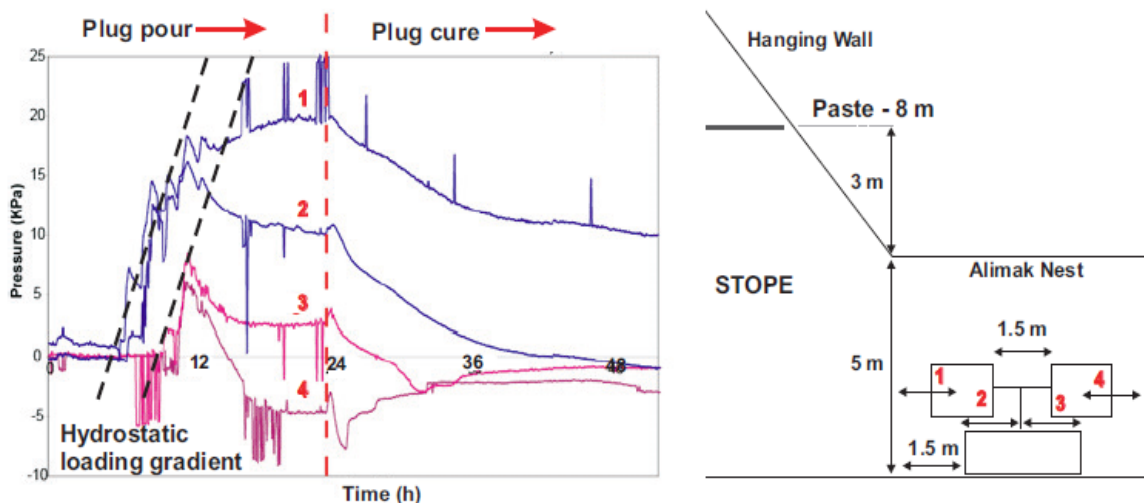


Figure 5 Geometry of simulated stope, field measurements of stress, and PWP during the plug pour

4.2 Generic Modeling Results

The results are presented in Figures 6 and 7, which explore the sensitivity of numerical simulations to the different parameters: WRC of the non-cemented or post-curing tailings, compressibility, and the sink term. Certainly the magnitude of the drawdown reported in the field can be simulated. As the compressibility decreases, and if the WRC of the cemented sample is used, the pore-pressures are then dissipated at a greater rate, as it takes only a relatively small amount of water removal (either due to drainage or self-desiccation) to dissipate PWP or generate suction.

Figure 7 illustrates an important point with respect to the relative importance of drainage and self-desiccation in alleviating pore-pressures. While the post-curing simulation with sink generates the most negative pore-water pressures, the post-curing simulation without a sink generates the least: this is due to the lower saturated hydraulic conductivity of this material, which reduces the amount of drainage.

This case is a good target for this kind of modeling. Temperatures were not elevated in this mine, though in some mines the rise in temperature due to hydration can be significant enough to affect the hydraulic properties of the CPB. This case has also relatively low total stresses. In deeper stopes with a fast rate of filling, the total stress may be sufficient to compress the pore matrix of the CPB and alter its water retention characteristics. This effect, however, may be suppressed in many mines by the increase in stiffness. Compression of the CPB will naturally result in further excess PWP generation, though arching effects must also be taken into account in the field.

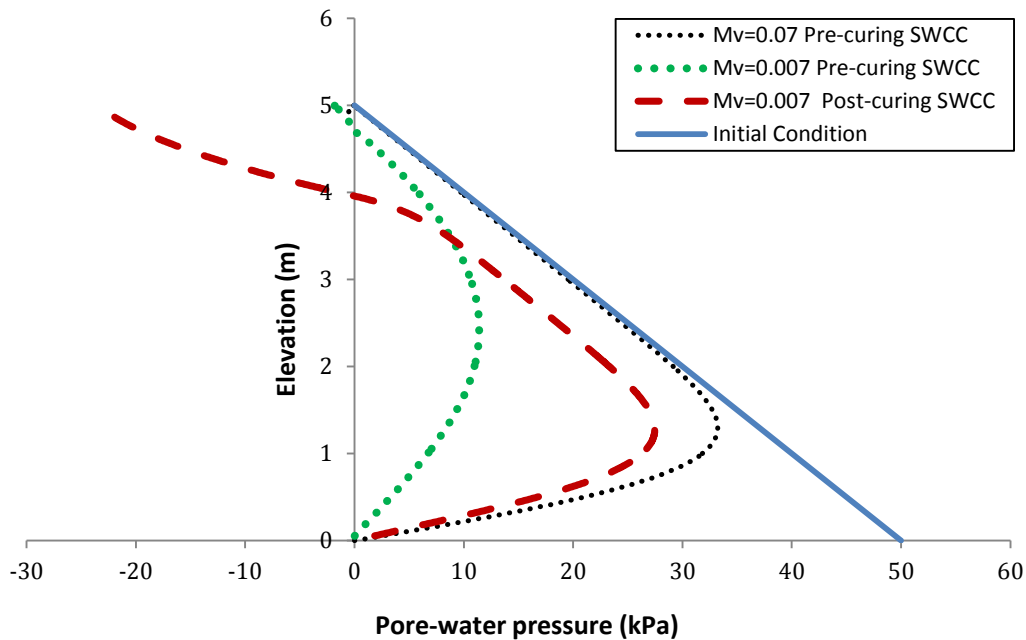


Figure 6 Simulations of pore-water pressure drawdown after 20 hours, varying compressibility and the WRC

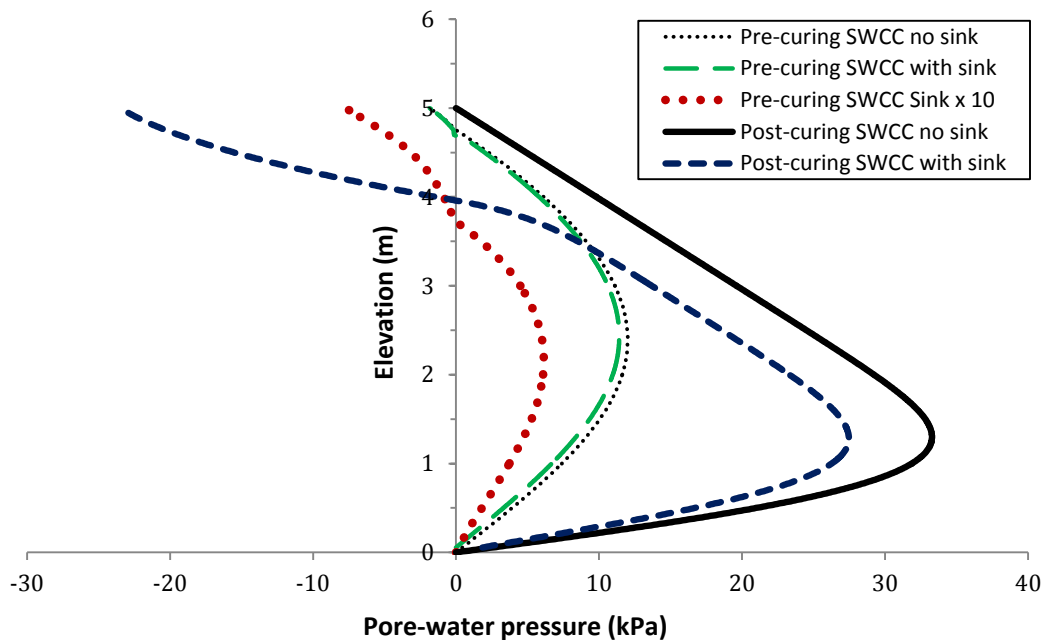


Figure 7 Simulations of pore-water pressure drawdown after 20 hours, showing the relative contributions of drainage and hydration

5 Conclusions and Future Work

This work has established a framework to simulate pore-pressure drawdown by both drainage and self-desiccation in CPB in the context of unsaturated flow modeling. Ongoing work is focusing on (i) tracking the evolution of the WRC and saturated hydraulic conductivity over time by analyzing the evolution of pore-size distribution, (ii) incorporating transient compressibility obtained by bender element tests (such as those undertaken by Helinski et al. 2007) into the modeling, and (iii) studying the effects of temperature and total stress on the water retention properties of the material. This work forms part of a larger study incorporating field measurements from three mines using varied stope deposition schemes. Measurements of PWP and suction in these stopes will serve as validation and calibration data for the modeling approach shown in this paper. Whereas the dissipation of pore-water pressure is crucial to optimizing backfill placement, this research would also apply to surface deposition schemes incorporating layers of CPB. The effect of self-desiccation on drying and potential desaturation of surrounding tailings would be very important to the performance of the whole stack.

Acknowledgements

This research is part of a larger collaborative research project on Cemented Paste Backfill involving three universities, headed by the University of Toronto. Financial support for the project was provided by Barrick Gold Corporation, Xstrata Copper Canada, and Inmet Mining Corporation, as well as by the Natural Sciences and Engineering Research Council Canada (NSERC).

References

- Acker, P. (2004). Swelling, shrinking and creep: a mechanical approach to cement hydration. *Materials and Structures / Concret Science and Engineering* , 37, pp. 237-243.
- Belem, T., Bussiere, B., and Benzaazoua, M. (2001). The effect of microstructural evolution on the physical properties of paste backfill. (R. a. A.A. Balkema, Ed.) In *Proceedings of Tailing and Mine Waste '01*, 16-19 January 2001, Fort Collins, Colo. , pp. 365-374.
- Belem, T., Harvey, A., Simon, R., and Aubertin, M. (2004). Measurement and prediction of internal stresses in an underground opening during its filling with cemented fill. (V. a. Ed.), 28-30 September 2004. In *Proceedings of the 5th International Symp. on Ground Support in Mining and Underground Construction* , pp. 619-630.
- Belem, T., and Benzaazoua, M. (2008). Design and application of underground mine paste backfill technology. *Geotechnical and Geological Engineering* , 26 (2008), 147-174.
- Decagon Devices, Inc. (2007). Operator's manual for models WP4 and WP4-T, Dewpoint PotentiaMeter.
- Fourie, A., Helinski, M., and Fahey, M. (2006). Filling the gap - a geomechanics perspective. *Anustralian Centre for Geomechanics* , 26, pp. 1-4.

- Fredlund, D.G., and Rahardjo, H. (1993). Soil mechanics for unsaturated soils. Department of civil engineering, University of Saskatchewan, and School of civil and structural engineering, Nanyang Technological University: Wiley-Interscience.
- Grabinsky, M., and Simms, P. (2006). Self-desiccation of cemented paste backfill and implications for mine design. (S. L. R.J. Jewell, Ed.). In Proceedings of Paste and Thickend Tailings'06, Limerick, Ireland: Australian Centre for Geomechanics, Perth.
- Grabinsky, M.W., and Bawden, W.F. (2007). In situ measurements of geomechanical design of cemented paste backfill systems. In Proceedings of Minefill 2007, April 29 – May 2, 2007. (Paper No. 2456), [CD-ROM].
- Helinski, M., Fourie, M., Fahey, M., Ismail, M. (2007). Assessment of the self-desiccation process in cemented mine backfills. Canadian Geotechnical Journal, 44, pp. 1148-1156.
- Hilf, J. W. (1956). An investigation of pore-water pressure in compacted cohesive soil. Ph.D. thesis, Technical Memorandum 654, U.S. Department of the Interior Bureau of Reclamation, Denver, Colorado.
- Hua, C., Acker, P., and Ehrlacher, A. (1995). Analyses and models of the autogenous shrinkage of hardening cement paste. Cement and Concrete Research, 25 (7), pp. 1457-1468.
- Kim, J.-K., and Lee, C.-S. (1999). Moisture diffusion of concrete considering self-desiccation at early ages. Cement and Concrete Research, 29, pp. 1921-1927.
- Le Roux, K. (2004). In situ properties and liquefaction potential of cemented paste backfill. PhD thesis, Graduate department of civil engineering, University of Toronto, Canada.
- Li, L., Aubertin, M., and Belem, T. (2005). Formulation of a three dimensional analytical solution to evaluate stresses in backfilled vertical narrow openings. Canadian Geotechnical Journal, 42, pp. 1705-1717.
- Simms, P., and Grabinsky, M. (2009). Direct measurement of matric suction in triaxial tests on early-age cemented paste backfill. Canadian Geotechnical Journal, 46, pp. 93-101.
- T.K., G.E., and M.A. (2009). User Manual: T5/T5x pressure transducer tensiometer. UMS GmbH Munchen.